Dielectric Characterization

Using a Wideband Dielectric Filled Cavity (WDFC)

by

Mohammad Ali Saed

Dissertation submitted to the Faculty of the

Virginia Polytechnic Institute and State University

in partial fulfillment of the requirements for the degree of

Doctor of Philosophy

in

Electrical Engineering

APPROVED:

Sedki M. Riad, Chairman	Ioannis M. Besieris
Gary S. Brown	William A. Davis
Aicha Elshabini-Riad	Ronald D. Riess

November 13, 1987

Blacksburg, Virginia

Dielectric Characterization

Using a Wideband Dielectric Filled Cavity (WDFC)

by

Mohammad Ali Saed

Sedki M. Riad, Chairman

Electrical Engineering

(ABSTRACT)

This dissertation summarizes the research performed towards the development, analysis, and testing of two new sample configurations used for characterizing dielectric materials over a wide band of frequencies. In the two configurations, a cylindrical cavity completely filled with a sample of the dielectric material of interest is used. The two configurations are the following:

1. The cylindrical cavity is adapted to the end of a transmission line and the reflection coefficient is measured. The complex permittivity of the dielectric sample is then derived from the measured reflection coefficient information.

2. The cylindrical cavity is placed between two transmission lines. The complex permittivity of the dielectric material can be computed from either the measured reflection coefficient or the measured transmission coefficient.

The full field analysis of these configurations is carried out and the solution is obtained using the method of moments. Computer simulation experiments are performed to test the sensitivity of these techniques and predict their performance. Actual experiments on some dielectric materials with known dielectric properties are performed for

verification. The first configuration is also used to characterize two thick film dielectric materials.

These configurations proved to provide solutions to the many problems with the conventional configurations found in the literature.

Acknowledgements

The author would like to thank Dr. Sedki M. Riad for his invaluable help, support, and continuous guidance throughout this work.

Sincere thanks are due to the members of the advisory committee, Dr. I. M. Besieris, Dr. G. S. Brown, Dr. W. A. Davis, Dr. A. Elshabini-Riad, and Dr. R. D. Riess, for their assistance and valuable comments. The author is specially grateful to Dr. W. A. Davis for the numerous discussions regarding the field analysis and computational techniques in this work. Special thanks are also due to Dr. A. Elshabini-Riad for her great help and assistance in the area of thick film technology.

The author is indebted to   and his wife,   , for their dear friendship and encouragement. The author is also thankful to   ,

            , and   for their great friendship.

The author would like to express his deep gratitude and appreciation to his parents,

            , and to his brothers and sisters for their love, affection, and unlimited support.

TABLE OF CONTENTS

Chapter 1

INTRODUCTION

A dielectric material is characterized by measuring its relative complex permittivity, $\varepsilon^*_r(j\omega)$, which is a function of frequency, over the frequency band of interest. The basic concept used in dielectric characterization is to place a sample of the dielectric material in some convenient electrical component structure and measure the impedance of this structure. By properly selecting this structure, accurate and convenient relations between the structure impedance and the material properties can be established.

At low frequencies (kHz - MHz), the typical structure used for dielectric characterization is the parallel plate capacitor, where the dielectric is to fill the space between two parallel conducting plates. The relationship between the capacitor impedance, $Z(j\omega)$, and the complex relative permittivity, $\varepsilon^*_r(j\omega)$, of the dielectric is given by:

$$Z(j\omega) = \frac{1}{j\omega\varepsilon_o\varepsilon^*_r(j\omega)}\frac{t}{A}$$

where t, , A, , ε_o denote the dielectric thickness, the capacitor area and the permittivity of free space, respectively.

For higher frequencies reaching into the microwave region, transmission lines and cavity structures are more appropriate to use for the dielectric characterization problem. Typical approaches at high frequencies as found in the literature include measuring the reflections of a dielectric filled section of a transmission line or the resonance and/or quality factor of a cavity containing a sample of the dielectric. The measurements may

be performed in either the time domain or the frequency domain. Relationships between the measured quantities and the material's dielectric constant need to be known to enable the computation of $\varepsilon^*_r(j\omega)$.

In this research, a cylindrical dielectric filled cavity to be used for dielectric characterization over a wide range of frequencies is developed. The abbreviation WDFC (Wideband Dielectric Filled Cavity) will be used to refer to this structure. This structure proved to provide solutions to the many problems with the conventional configurations found in the literature. Two configurations are investigated:

1. The WDFC is adapted to the end of a transmission line and the reflection coefficient, $S_{11}(j\omega)$, is measured. The complex permittivity is then derived from the measured reflection coefficient information.

2. The WDFC is placed between two transmission lines. This arrangement enables the measurement of the reflection coefficient, $S_{11}(j\omega)$ as well as the transmission coefficient, $S_{21}(j\omega)$. Ideally, the availability of both $S_{11}(j\omega)$ and $S_{21}(j\omega)$ should enable the computation of the relative complex permeability, μ^*_r, in addition to the permittivity. However, this was difficult to achieve because of the insensitivity of the reflection and transmission coefficients to variations in the permeability, as will be discussed in Chapter 4. Therefore, it was assumed that dielectric materials are nonmagnetic, i.e. $\mu^*_r = 1$.

The full field analysis of these configurations is carried out and the solution is obtained using the method of moments. Furthermore, the results of computer simulation experiments and actual experiments performed on some dielectric materials are also presented.

The next chapter, Chapter 2, summarizes the time domain and frequency domain dielectric characterization techniques investigated in the literature over the frequency range 50 MHz - 15 GHz. In Chapter 3, the concept of the configuration adapting the WDFC to the end of a transmission line is introduced and a field analysis establishing the relationship between $\varepsilon^*_r(j\omega)$ and the reflection coefficient, $S_{11}(j\omega)$, is detailed. The results of computer simulation experiments performed to test the sensitivity of the technique to various parameters of the WDFC and to predict its performance are also presented. In addition, the experimental setup, verification experiments, and results of experiments on two thick film dielectric materials, DuPont 5704 and DuPont PCM dielectric, are presented. Chapter 4 presents the concept and field analysis of the arrangement placing the WDFC between two transmission lines. The results of computer simulation experiments, performed for the same purposes stated earlier, are presented. Moreover, the results of actual experiments performed on known dielectric materials are provided for verification. Finally, Chapter 5 provides a summary of this work as well as a discussion of the results.

Chapter 2

LITERATURE SURVEY OF

DIELECTRIC CHARACTERIZATION IN THE

FREQUENCY RANGE (50 MHz - 15 GHz)

The following two subsections present a brief summary of the time domain and frequency domain measurement techniques investigated in the literature. This survey is mainly concerned with the use of transmission line techniques in measuring dielectric material properties in the frequency range 50 MHz to 15 GHz.

2.1 Time Domain Techniques:

Since about 1969 time domain methods (or sometimes referred to as transient methods) have been introduced in dielectric spectroscopy at high frequencies. These methods are based on the use of the Time Domain Spectroscopy, TDS, techniques in characterizing a discontinuity caused by a dielectric sample located in a transmission line environment. The concept of a TDS system is to propagate a train of suitably generated wideband pulses with a fairly fast transition (transition duration can be as fast as 30 ps in available TDS systems) in a reference line and observe the reflected and/or transmitted waveforms. The waveforms in the line are to be measured using a sampling oscilloscope interfaced to a data acquisition system. Using adequate signal processing involving the Fourier transformation, the complex permittivity of the dielectric sample located in the

line may be determined over a wide range of frequencies ($\sim$ 100 KHz - $\sim$ 10 GHz). As demonstrated in figure 2.1, a dielectric sample is either inserted in or attached to the end of the line. The resultant voltage waveform $v(t)$ at the front surface of the sample is the sum of the incident pulse $v_o(t)$ and the ensuing reflections $v_r(t)$, $v(t) = v_o(t) + v_r(t)$, with a transmitted signal $v_t(t)$ behind the sample. The relation between $v_r(t)$ and $v_t(t)$ to $v(t)$ is then dictated by the response characteristics of the sample, propagation in the sample and boundary conditions.
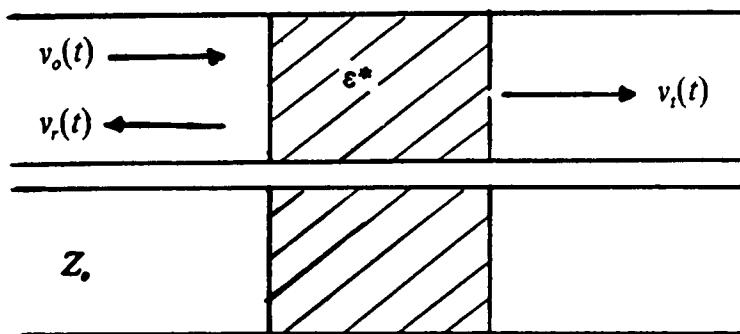
Figure 2.1: Dielectric sample located in a transmission line.

The following is a summary of the TDS techniques investigated in the literature as of July 1987. This summary is classified according to sample configuration used. It is assumed that the material of interest is linear, nonmagnetic ($\mu_r{}^* = 1$) and has no free charges ($\sigma = 0$) unless otherwise stated. The following configurations are considered:

1. Sample inserted in a matched coaxial line.

    •   Direct reflection method.

    •   Transmission methods.

- Total reflection methods.

- Combined total reflection - transmission methods.

- Combined transmission coefficient ratio and direct TDR method.

2. Sample placed at the end of a coaxial line.

- The sample is backed by a short circuit.

- The sample is terminated with an open circuit.

3. Lumped capacitance method.

4. Other methods.

- Sample located at the end of a coaxial line line which opens into a circular waveguide.

- Difference methods.

- Using a dipole probe.

2.1.1 Sample Inserted in a Matched Coaxial Line :

The sample is placed in a coaxial line which is terminated by its characteristic impedance. This configuration has been investigated extensively. The methods of analysis are summarized as follows:

(1) Direct Reflection Method:

For this method, only the reflection of the incident voltage step against the first air-dielectric interface is taken into account, figure 2.2. Therefore, the reflected time domain decay has to be virtually complete before reflections from the end of the sample reach the sampler. Theoretically, this means that the length of the sample should be infinite.
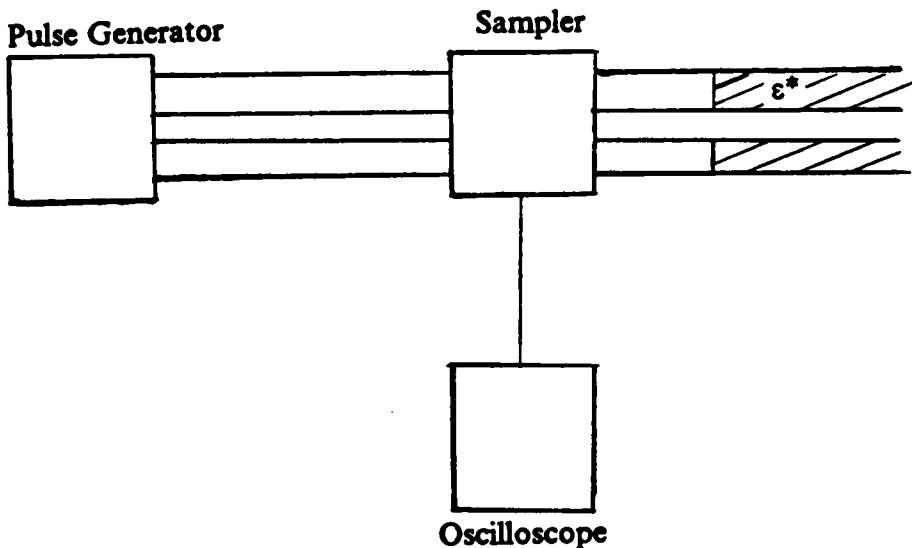
Figure 2.2: Direct reflection method.

Fellner-Feldegg [1] was the first to investigate this case for Debye dielectrics where the complex permittivity can be modeled in the form

$$\overset{*}{\varepsilon_r}(j\omega) = \varepsilon_{r_\infty} + \frac{\varepsilon_{r_o} - \varepsilon_{r_\infty}}{1 - j\omega\tau} \, , \tag{2.1}$$

ε_{r_o}, ε_{r_∞} are the static and high frequency relative permittivities and τ is the relaxation time. The reflection coefficient $\rho(j\omega)$ is related to $\varepsilon_r{}^*(j\omega)$ as follows [2]:

$$\rho(j\omega) = \frac{1 - \sqrt{\varepsilon_r^*(j\omega)}}{1 + \sqrt{\varepsilon_r^*(j\omega)}} = \frac{V_r(j\omega)}{V_o(j\omega)} \qquad (2.2)$$

or,

$$\varepsilon_r^*(j\omega) = \left[\frac{1 - \rho(j\omega)}{1 + \rho(j\omega)}\right]^2 . \qquad (2.3)$$

Equation (2.3) can be used to evaluate the complex permittivity. The major drawback of the direct reflection method lies in the imprecision in time reference determination [3]. This is particularly serious for materials having relaxation frequencies in the microwave region. Therefore, the high frequency limit of this method hardly exceeds 3 GHz [2]. Also, very long samples may be required to obtain sufficiently low frequencies [20].

(2) Transmission Methods:

The experimental set-up for this method is shown in figure 2.3 where the sample is placed between the pulse generator and the sampler.
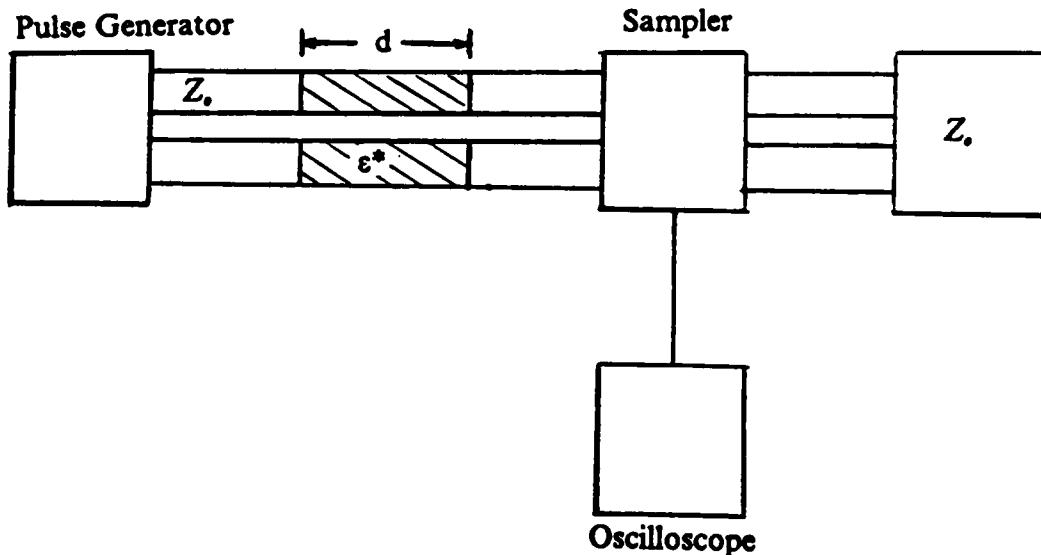
Figure 2.3: Transmission methods.

The transmission coefficient $T(j\omega)$ is given by [20]

$$T(j\omega) = \frac{V_t(j\omega)}{V_o(j\omega)} = \frac{(1 - \rho^2)\exp\{-(j\omega d/c)(\sqrt{\varepsilon_r^*} - 1)\}}{1 - \rho^2\exp\{-(2j\omega d/c)\sqrt{\varepsilon_r^*}\}} \qquad (2.4)$$

where the reflection coefficient ρ is given by (2), d is the sample length, and c is the speed of light. The evaluation of ε_r^* from (2.4) can be done by numerical methods.

This method has not been used extensively; the principal reason is that proper time referencing to establish a common zero of time for the two signals, incident and transmitted, is hard to establish with sufficient accuracy unless further circuitry or other means are introduced to provide some sort of time reference marker. Gestblom and Noreland [5] described a method for determining $\varepsilon_r^*(j\omega)$ using the linear dependence of the attenuation coefficient $\alpha(j\omega) = Re\{j\omega d(\sqrt{\varepsilon_r^*(j\omega)} - 1)/c\}$ and the phase coefficient $\beta(j\omega) = Im\{j\omega d(\sqrt{\varepsilon_r^*(j\omega)} - 1)/c\}$.

The use of only the first signal before arrival of internal reflections in the sample (Direct Transmission) can also be useful. In this case, the transmission coefficient $T(j\omega)$ simplifies to

$$T(j\omega) = \frac{4\sqrt{\varepsilon_r^*(j\omega)}}{[1 + \sqrt{\varepsilon_r^*(j\omega)}]^2}\exp\{-j(\omega d/c)\sqrt{\varepsilon_r^*(j\omega)}\} . \qquad (2.5)$$

Again, numerical methods are needed to evaluate ε_r^* . This also has not been investigated in the literature in detail.

To reduce the effect of time referencing problems involved in the mentioned transmission methods, a technique called Transmission Coefficient Ratio (TCR) was intro-

duced [3]. Two samples of different lengths d_1, d_2 are used. The ratio of their transmission coefficient is evaluated as

$$\frac{T_1(j\omega)}{T_2(j\omega)} = \exp\{j[\omega(d_1 - d_2)/c]\sqrt{\varepsilon_r^*(j\omega)}\}\,. \tag{2.6}$$

Expressing the ratio T_1/T_2 in terms of its amplitude, $B(j\omega)$, and its phase, $\psi(j\omega)$, $\varepsilon_r^*(j\omega)$ can be solved in a closed form. The result is [2]

$$\varepsilon_r^*(j\omega) = \frac{c^2}{\omega^2(l_1 - l_2)^2}[\psi^2(j\omega) - (lnB(j\omega))^2 + 2j\psi(j\omega)lnB(j\omega)] \tag{2.7}$$

where

$$\frac{T_1(j\omega)}{T_2(j\omega)} = B(j\omega)\exp[j\psi(j\omega)]\,. \tag{2.8}$$

The TCR method has the advantage that it produces very large phase shifts $(500° - 1000°)$[1] and therefore it is much less sensitive to timing errors. However, it has the disadvantage that it has a small bandwidth (less than 2 GHz).

(3) Total Reflection Methods:

In these methods, all reflections from the dielectric sample (figure 2.2) are taken into account. The reflection coefficient $R(j\omega)$ is given by

$$R(j\omega) = \frac{V_r(j\omega)}{V_o(j\omega)} = \rho(j\omega)\frac{1 - \exp\{-(2d/c)j\omega\sqrt{\varepsilon_r^*(j\omega)}\}}{1 - \rho^2(j\omega)\exp\{-(2d/c)j\omega\sqrt{\varepsilon_r^*(j\omega)}\}}\,. \tag{2.9}$$

---

[1]   When the phase is made continuous.

The term $\varepsilon_r^*(j\omega)$ can be evaluated exactly from (2.9) by using numerical methods. However, dealing with approximate analytical solutions is necessary for the following reasons [9]:

1. To determine the feasibility of a direct time-domain interpretation of the step response in terms of the dielectric response functions.

2. To develop simple analytical solutions, convenient for producing accurate starting values for the iterative procedure. These solutions become a necessity when the experimental Fourier spectrum is noisy, and/or when conductivity processes are involved. Then convergence is bad and the procedure may easily iterate to a wrong solution.

3. To develop simple solutions accurate enough to replace the numerical procedure. This is especially advantageous for a rapid analysis of experiments, e.g. by means of a small computer.

The approximate solutions may be obtained by the following three different approaches:

(i) Taylor series expansion of the exponentials in (2.9) and truncation of the series. This has been introduced by Fellner-Feldegg [6] where they used the first term of the series only and obtained

$$R(j\omega) \cong j(\frac{\omega l}{2c})[d - \varepsilon_r^*(j\omega)] . \qquad (2.10)$$

This has been called the thin cell method. Gemert [7] presented a rigorous mathematical analysis for the thin cell method. He derived restrictions on the thickness of the sample for three common permittivity relations: Debye, Cole-Cole and Davidson-Cole relations. He also showed using the thin cell relation for Debye materials that the relaxation time

found experimentally is always larger than the actual time constant τ. Springett and Bose [8] derived the theoretical time response for the pulse reflected from a thin dielectric sample which is assumed to have a distribution of relaxation times, taking into account the finite rise time of the applied pulse. The thin cell formula is valid in the limit $d \to 0$. Therefore, it is inadequate for many experimental circumstances. Better results are obtained by Cole [11], [20] where he considered the input admittance of the dielectric section as a four-terminal network terminated by the characteristic impedance of the line. His result

$$\overset{*}{\varepsilon_r}(j\omega) - 1 = \frac{2c}{d} \left\{ \frac{V_r(j\omega)/[j\omega V_o(j\omega)]}{1 - j\omega[V_r(j\omega)/j\omega V_o(j\omega)]} \right\} \left\{ x(j\omega) \cot[x(j\omega)] + j\frac{\omega d}{c} \right\} \quad (2.11)$$

where $x(j\omega) = \omega d \sqrt{\varepsilon_r^*(j\omega)} / c$. Although (2.11) is transcendental, ε_r^* can be evaluated simply for $\omega d |\varepsilon_r^*|^{1/2}/c < 1$. The simplicity in evaluation arises from the fact that the complicating factor $x \cot x$ has the limiting value unity for $x < < 1$ and the series expansion

$$x \cot x = 1 - \left(\frac{\omega d}{c}\right)^2 \frac{\overset{*}{\varepsilon_r}}{3} - \left(\frac{\omega d}{c}\right)^4 \frac{\overset{*2}{\varepsilon_r}}{45} + \cdots \quad (2.12)$$

is valid for $|x| < \pi$ and rapidly convergent for $|x| < 1$. As a result (2.11) can be solved rapidly by iteration [11]. An upper frequency limit on the usefulness of this method is dictated by (2.11) and (2.12). The term $x \cot x$ has a zero at $x = \omega d \sqrt{\varepsilon_r^*}/c = \pi/2$, corresponding to a sample one-quarter wavelength long and $x \cot x$ changing rapidly near this point, making calculated values of ε_r^* extremely sensitive to small errors in the evaluation of $V_r(j\omega)/[j\omega V_o(j\omega)]$. Instead of a Taylor series expansion of $R(j\omega)$, Claasen and Gemert [9] obtained a new approximation by the expansion of $1/R(j\omega)$. Their result is

$$R(j\omega) \cong j\frac{\omega d}{2c} \quad \frac{1 - \varepsilon_r^*}{1 + j(\frac{\omega d}{2c})[1 + \varepsilon_r^*] + \frac{4}{3}[j(\frac{\omega d}{2c})]^2 \varepsilon_r^*} \quad , \quad d << \lambda/\sqrt{|\varepsilon_r^*|} \quad (2.13)$$

This result applies only when $\omega < \pi c/(d\sqrt{|\varepsilon_r^*|})$.

(ii) Modelling of the transmission line structure by the means of lumped elements and solving ε_r^* from the network equations. Gemert [12] used this approach and obtained the following approximation:

$$R(j\omega) \cong j(\frac{\omega d}{2c}) \frac{1 - \varepsilon_r^* + (\frac{j\omega d}{2c})^2 \varepsilon_r^*}{1 + j\frac{\omega d}{2c}[1 + \varepsilon_r^*] + (\frac{j\omega d}{2c})^2 [2 + j\frac{\omega d}{2c}] \varepsilon_r^*} \quad (2.14)$$

Equation (2.14) is valid for $d << \lambda/\sqrt{|\varepsilon_r^*|}$. For small values of $\omega l/2c$, (2.14) reduces to

$$R(j\omega) \cong j(\frac{\omega d}{2c}) \frac{1 - \varepsilon_r^*}{1 + j\frac{\omega d}{2c}[1 + \varepsilon_r^*]} \quad (2.15)$$

and

$$\varepsilon_r^* \cong \frac{j(\frac{\omega d}{2c})[1 - R(j\omega)] - R(j\omega)}{j(\frac{\omega d}{2c})[1 + R(j\omega)]} . \quad (2.16)$$

Gemert reported good results in the frequency range 100 KHz to 2 GHz in most circumstances. However, the results are as not as reliable as those reported by Cole, equation (2.11), or those obtained using (2.13). Also, an important disadvantage is that the reflection coefficient does not tend to zero as $\varepsilon_r^* \rightarrow 1$. Other lumped element models were proposed by Claasen and Gemert [9]. These are the T ladder or the π ladder models shown in figure 2.4. Although the formulas derived do not have the disadvantage of the

previous model, $R(j\omega)$ tends to zero as $\varepsilon_r^* \to 1$, the results obtained are less accurate than those obtained using (2.12).

(iii) Evaluation of the dielectric response by real time analysis. This method was introduced by Cole [10] where he evaluated the dielectric response function from the time integral and self convolution of the reflections, taking into account the finite amplitude of the reflection in a second-order approximation and the finite rise time of the incident pulse. This analysis was extended by Chahine and Bose [13] by considering third-order approximation. However, the resulting formulas involve multiple convolutions and time derivatives which are unattractive for numerical calculations. Therefore, working with frequency domain formulas such as equation (2.11) is more useful. Later, Chahine and Bose [27] compared this method with the frequency-domain analysis and they discussed the limitations of each.

(a) T - ladder model

$$Z_T = Z_o \sqrt{1 - (\frac{\omega d}{2C})^2}$$

(b) π ladder model

$$Z_\pi = \frac{Z_o}{\sqrt{1 - (\frac{\omega d}{2}C)^2}}$$
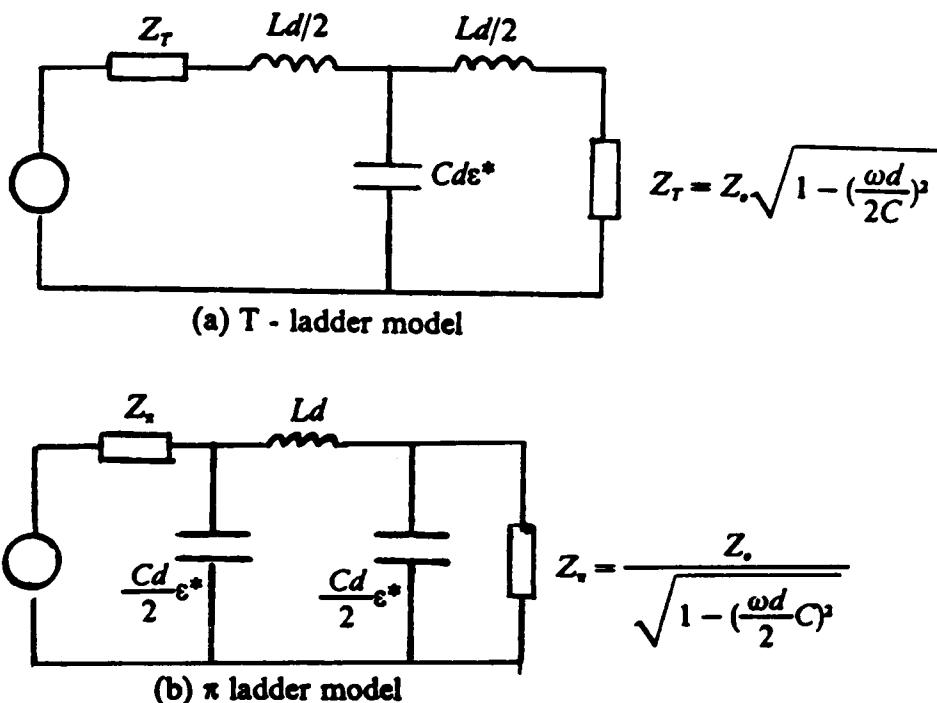
Figure 2.4: Lumped element models.

(4) Combined Total Reflection-Transmission Methods:

In 1970, Nicolson and Ross [15] introduced a new method to measure simultaneously the relative complex permeability $\mu_r^*(j\omega)$ and the relative complex permittivity $\varepsilon_r^*(j\omega)$. Their method is based upon the measurement of the totally reflected voltage waveform and of the totally transmitted voltage waveform of a sample of material inserted in a coaxial line. The scattering coefficients $S_{11}(j\omega)$ and $S_{21}(j\omega)$ can be obtained from the Fourier analysis of the reflected, transmitted, and reference waveforms. For $\mu_r^* \neq 1$, $S_{11}(j\omega)$ and $S_{21}(j\omega)$ are given by

$$S_{11}(j\omega) = \rho(j\omega)\frac{1 - \exp\{-(2d/c)j\omega\sqrt{\varepsilon_r^*\mu_r^*}\}}{1 - \rho^2(j\omega)\exp\{-(2d/c)j\omega\sqrt{\varepsilon_r^*\mu_r^*}\}} \tag{2.17}$$

$$S_{21}(j\omega) = [1 - \rho^2(j\omega)]\frac{\exp\{-(d/c)j\omega\sqrt{\varepsilon_r^*\mu_r^*}\}}{1 - \rho^2(j\omega)\exp\{-(2d/c)j\omega\sqrt{\varepsilon_r^*\mu_r^*}\}}, \tag{2.18}$$

where

$$\rho(j\omega) = \frac{\sqrt{\mu_r^*(j\omega)} - \sqrt{\varepsilon_r^*(j\omega)}}{\sqrt{\mu_r^*(j\omega)} + \sqrt{\varepsilon_r^*(j\omega)}} \tag{2.19}$$

Nicolson and Ross derived closed form solutions for ε_r^* and μ_r^* from equations (2.17) and (2.18). Their result is:

$$\mu_r^* = \sqrt{c_1 c_2} \tag{2.20}$$

$$\varepsilon_r^* = \sqrt{c_1/c_2}, \tag{2.21}$$

where

$$c_1 = \frac{\mu_r^*}{\varepsilon_r^*} = \left[\frac{1 + \rho(j\omega)}{1 - \rho(j\omega)}\right]^2 \tag{2.22}$$

$$c_2 = \overset{*}{\mu_r}\overset{*}{\varepsilon_r} = -\left[(c/\omega d)\ln(z^{-1}(j\omega))\right]^2 \tag{2.23}$$

and z is the transmission coefficient given by

$$z(j\omega) = \exp\{-j(\omega d/c)\sqrt{\overset{*}{\varepsilon_r}\overset{*}{\mu_r}}\}. \tag{2.24}$$

The quantities $z(j\omega)$ and $\rho(j\omega)$ can be evaluated from $S_{11}(j\omega)$ and $S_{21}(j\omega)$ [15]. They applied this method on a sample of teflon and obtained good results in the frequency range 0.4-9.6 GHz. In 1974, Cronson, et al, [16] described a method to extend the upper frequency limit obtained by Nicolson and Ross up to 16 GHz. The main feature of their method is the use of a 400-ps wide pulse waveform that furnishes the necessary spectral amplitude in the 9-16 GHz frequency band. The waveform was generated by differentiating the fast step produced by a step-recovery diode (SRD) using a series capacitor in a transmission line as a simple high pass filter. Stuchly and Matuszewski [17] used the same principle of Nicolson and Ross assuming the material is nonmagnetic. The result is

$$\overset{*}{\varepsilon_r} = \frac{[1 - S_{11}(j\omega)]^2 - S_{21}^2(j\omega)}{[1 + S_{11}(j\omega)]^2 - S_{21}^2(j\omega)}. \tag{2.25}$$

They also gave an empirical formula for the normalized sample length l/λ which gives minimum experimental uncertainty:

$$\frac{d}{\lambda} = \frac{1}{4|\overset{*}{\varepsilon_r}|^{1/2}} \tag{2.26}$$

which they claim is satisfactory for the majority of practical applications.

(5) Combined TCR and direct TDR Method:

· Since the direct TDR method has a large bandwidth but is very sensitive to timing errors, and the TCR has a small bandwidth but very insensitive to timing errors, combining both methods should yield optimum results. This method was first described in [3] where the permittivity of H_2O at $5°C$ was evaluated. Good results were obtained up to 15 GHz. Later, Suggett [18] used this method which permitted time referencing to better than 0.08 ps. He used the TCR method to obtain smooth ε_r^* data in the frequency range 100 MHz-2 GHz which are extremely reliable. The coefficient $\rho(j\omega)$ was evaluated for this data and then superimposed upon the $\rho(j\omega)$ data determined experimentally by direct TDR method. Then ε_r^* is evaluated from the final $\rho(j\omega)$ data.

2.1.2 Sample Placed at the End of a Coaxial Line:

In this case, the sample is placed at the end of the line backed by either a short or an open circuit termination. The following discusses both arrangements.

(1) The sample is backed by a short circuit:

Several authors [2], [14], [19], [20] have investigated this arrangement. It is concluded that useful results can be obtained only over a band of frequencies with a lower limit. This is apparent from the expression obtained by Cole [20]

$$1 = \frac{c}{l} \frac{[S(j\omega)/2j\omega V_o(j\omega)]}{1 - j\omega[S(j\omega)/2j\omega V_o(j\omega)]} x \cot x \qquad (2.27)$$

where $S(j\omega)$ is the Fourier transform of S(t) which is the difference between the waveforms reflected of a short circuit placed once in front of the sample and once behind the sample, and $x = \omega d\sqrt{\varepsilon_r^*}/c$. Thus, ε_r^* appears only in the function $x \cot x$ and at low

frequencies the expression becomes independent of ε_r^* since $x \cot x \cong 1$. Bottreau, et al, [19] proposed a method where two samples are needed, one twice as long as the other, both terminated with a short circuit. Still, their method suffered from the low frequency limit. Using the measurements obtained from the two samples the complex permittivity is evaluated without the need for iteration or approximation. They reported results of ε_r^* of some alcohols in the frequency range 60 MHz-3 GHz.

(2) The sample is terminated with an open circuit:

Cole [11], [14], [20] investigated this case. The expression he obtained is

$$\varepsilon_r^*(j\omega) = \frac{c}{j\omega d} \left[\frac{P(j\omega)}{2V_o(j\omega) - P(j\omega)} \right] x \cot x \qquad (2.28)$$

where $P(j\omega) = V_o(j\omega) + V_r(j\omega)$. Let's compare this equation (2.28) with (2.11), the case where the sample is inserted in a matched line. The open circuit results in a larger response for a given sample length, by a factor of 4 at low frequencies. However, both solutions share the same problem of becoming impractical for $|x|$ near $\pi/2$ as discussed before. Since an ideal open circuit is impossible to realize exactly, corrections for finite stray capacitance at the end of the line has to be made as discussed in [14]. Another disadvantage is that for materials with high permittivities (~ 80) the maximum length of the sample at high frequencies (above 1 GHz) must be very small (1-2 mm) for satisfactory results. Despite this, Cole concludes that this case, sample termination with an open circuit, yields better results than both the short circuit termination and the case of a sample inserted in a matched line.

2.1.3 Lumped Capacitance Method:

In this arrangement, a small shunt capacitor terminating a coaxial line is used as a sample holder as shown in figure 2.5. This method was proposed by Iskander and Stuchly [21]. The reflection coefficient is approximately

$$\rho(j\omega) = |\rho|e^{-j\theta} = \frac{1 - j\omega C_o Z_o \varepsilon_r^*}{1 + j\omega C_o Z_o \varepsilon_r^*} \tag{2.29}$$

where C_o is the shunt capacitance of the empty sample holder. The complex permittivity can be calculated from (2.29) in closed form [21]. The result is

$$\varepsilon'_r(j\omega) = \frac{2|\rho| \sin \theta}{\omega C_o Z_o(|\rho|^2 + 2|\rho| \cos \theta + 1)} \tag{2.30}$$

and

$$\varepsilon_r''(j\omega) = \frac{1 - |\rho|^2}{\omega C_o Z_o(|\rho|^2 + 2|\rho| \cos \theta + 1)} \tag{2.31}$$
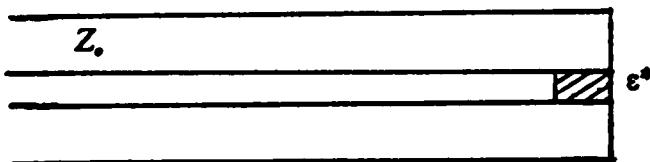
Figure 2.5: Lumped capacitance method.

Stuchly, et al, [22] applied this method on some alcohols and they reported good results in the frequency range 0.1-10 GHz. Further analysis was carried out in [23]. Later, Iskander and Stuchly [30] provided theoretical analysis for the fringing field effect in this method. As a result a term C_f/C_o, where C_f is the fringing field capacitance, should be

subtracted from the right-hand side of equation (2.30) while equation (2.31) remains unchanged assuming that the introduction of the test dielectric to the sample holder (the capacitor) causes only small variations in the fringe field capacitance [31]. C_o and C_f are given by [31]

$$C_o = \frac{\pi a^2}{4d} \varepsilon_o \qquad (2.32)$$

$$C_f = 2a\varepsilon_o \ln(\frac{b-a}{2d}) \qquad (2.33)$$

provided that $\lambda >> b-a$ and $d << b-a$ where λ is the wavelength, ε_o is the permittivity of free space, d is the sample thickness, and a and b are the inner and outer radius of the line respectively. Parisien and Stuchly [28] described a system which uses a microcomputer to control the experimental procedure as well as perform data processing and output. They did not take into account the fringing field effect.

2.1.4 Other Methods:

(1) Sample located at the end of a coaxial line which opens into a circular waveguide:

This configuration is shown in figure 2.6.
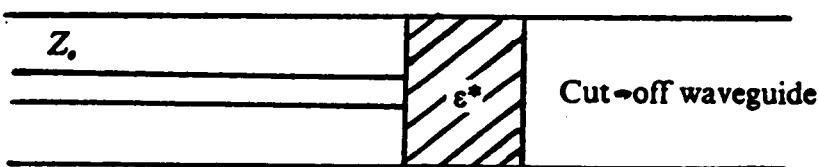
Figure 2.6: Sample terminating a coaxial line which opens into a circular waveguide.

The waveguide is operating below cut-off. Stuchly, et al, [24] used this arrangement to provide theoretical analysis, uncertainty evaluation, and experimental results for plant leaves. The expression they derived is

$$\overset{*}{\varepsilon_r}(j\omega) = \frac{\lambda}{2\pi d/\lambda} \left\{ \frac{1-\rho}{(2\pi d/\lambda)(1-\rho)+j(1+\rho)} - \omega Z_o C_T \right\} \tag{2.34}$$

where C_T is the fringe field capacitance and d is the sample thickness. C_T can be calculated as described in [32] or evaluated experimentally. Good results were obtained for plant leaves [24] in the frequency range $\sim$ 100 MHz-8 GHz.

(2) Difference method:

This method is used for measurements of small differences between an unknown material and a reference material to get more accurate results than if they were analyzed separately. Cole [25] proposed the method for the permittivity measurements of liquids. The expression he derived is:

$$\varepsilon_x - \varepsilon_s = \varepsilon_s \left\{ \frac{R_s - R_x}{V_o - R_s} \right\} \frac{\left\{ 1 + j\omega(d\varepsilon_s/cf_s) - \frac{1}{3}(\frac{\omega d}{c})^2 \varepsilon_s \right\}}{\left\{ 1 - j\omega(d\varepsilon_s/cf_s)(\frac{R_s - R_x}{V_o - R_s}) \right\}} \tag{2.35}$$

where V_o, R_s, R_x are the Fourier transform of the incident pulse, signal reflected from the reference sample, and signal reflected from the unknown sample, respectively. The terms f_x and f_s are the respective values of $x\coth x$ for the unknown and reference samples. He obtained satisfactory results for dilute solutions with small dispersion (small relaxation processes) in the frequency range 1 MHz to several GHz. Chahine and Bose [26] applied this method to water/oil emulsions

(3) Using a Dipole Probe :

· Recently, Bose et al [29] developed (qualitatively) and tested a new method to allow permittivity measurements of biological substances *in vitro* or *in vivo* . The configuration used is shown in figure 2.7. They used the formulas of the total reflection configuration with open termination discussed earlier. They tested their method on beef muscle and fat and they obtained good results up to about 2 GHz.
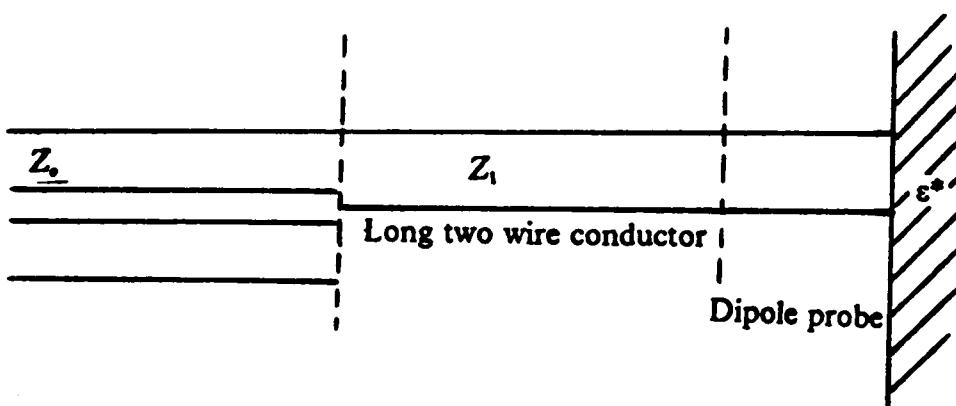
Figure 2.7: Dipole probe arrangement.

2.2 Frequency Domain Transmission Line Techniques:

Time domain techniques offer broad bandwidth at the cost of resolution. Also, the accuracy of the results reduces rapidly for frequencies above 10 GHz because of the insufficient spectral amplitude of the pulse generated by tunnel diodes beyond that frequency. Therefore, for more accurate measurements one still turns to the frequency domain, particularly for low loss materials. The following is a summary of the techniques investigated in the literature:

2.2.1 Methods Involving The Measurement of Voltage Standing Wave in a Line Terminated by a Section Filled with Dielectric:

The general configuration is shown in figure (2.8). The dielectric under test is contained in a section of a line or a waveguide terminated with an impedance. A signal generated by an oscillator at the frequency of measurement passes to the dielectric filled section via a slotted line from which a signal proportional to the electric field is obtained by a probe passing through a slot in the outer conductor. Thus, the voltage standing wave ratio (S) can be measured.
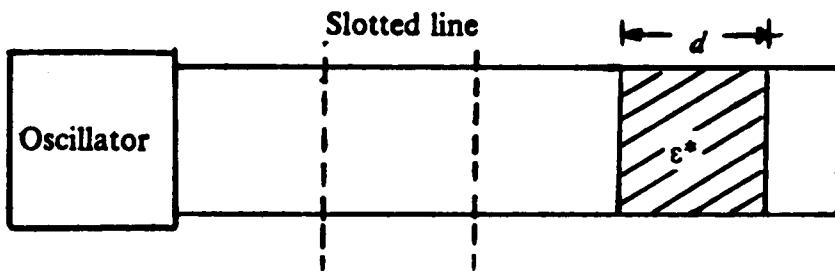
Figure 2.8: Methods involving the measurement of VSWR.

The following cases are considered:

(1) The Dielctric Filled Section is Terminated with a Short Circuit:

One of the most commonly used techniques is that of Roberts and Van Hippel [40] where they terminated the dielectric filled section with a short circuit. The expression they obtained is

$$\frac{\tanh(\gamma_d d)}{\gamma_d d} = \frac{(S - j\tan(2\pi x/\lambda_g))}{j(2\pi d/\lambda_g)(1 - jS\tan(2\pi x/\lambda_g))} \qquad (2.36)$$

where γ_d is the propagation coefficient in the dielectric filled section, λ_s is the wavelength in the air filled waveguide, x is the distance of the voltage minimum from the air-dielectric interface, d is the length of the dielectric filled section and, S is the voltage standing wave ratio, VSWR. The values on the right hand side of equation (2.36) are measured; hence γ_d can be evaluated using the charts prepared by Von Hippel [33]. The term γ_d can be written as $\gamma_d = \alpha_d + j\beta_d$ where α_d is the attenuation coefficient and β_d is the phase change coefficient in the dielectric filled section. Assuming loss free line, ε'_r and ε''_r are given by

$$\varepsilon'_r = (\frac{\lambda_o}{2\pi})^2 (\beta_d^2 - \alpha_d^2)^{1/2} \qquad (2.37)$$

$$\varepsilon''_r = (\frac{\lambda_o}{2\pi})^2 2\alpha_d\beta_d \qquad (2.38)$$

where λ_o is the wavelength of free space propagation. Williams [41] described an experimental procedure for liquids in the frequency range 250-920 MHz using the method of Roberts and Hippel with a coaxial line instead of a waveguide. Dakin and Works [42] simplified the expression in (2.36) assuming $\alpha_d d$ and S are small. The expressions they obtained may be used for loss angles less than 0.1. Their result is

$$\frac{\tanh(\beta_d d)}{\beta_d d} \cong - \lambda_g \frac{\tan(2\pi x/\lambda_g)}{2\pi d} \qquad (2.39)$$

and

$$\alpha_d d \cong \frac{(\beta_d d)^2 \lambda_g}{2\pi d} \frac{S[1 + \tan^2(2\pi x/\lambda_g)]}{[\beta_d d(1 + \tan^2(\beta_d d)) - \tan(\beta_d d)]} \cdot \qquad (2.40)$$

Corfield, et al, [43] have simplified the above expressions further by using a coaxial line with an adjustable short-circuiting piston, the dielectric liquid being supported on a thin

insulating membrane. Using this arrangement, measurements were taken for dielectric sample lengths which are integral multiples of $\lambda_d/2$ (λ_d is the wavelength in the dielectric filled section). If the sample length is $m\lambda_d/2$, then ε'_r and $\tan \delta$ are given by

$$\varepsilon'_r = (\frac{m\lambda}{2d})^2 \tag{2.41}$$

and

$$\tan \delta = \frac{\Delta x}{d} . \tag{2.42}$$

where λ is the wavelength in the air filled line and Δx is the distance between the points on either side of a voltage minimum where the voltage is $\sqrt{2}\,|V_{min}|$ (then S is given by $\pi\Delta x/\lambda$). Bennett and Calderwood [44] have introduced a method of computation to allow the experimental procedure (coaxial line with the short circuiting piston) to be used with liquids having higher values of $\tan \delta$. The expression they obtained is

$$\frac{\lambda Z_{in}}{dz_o} = \frac{\tanh[j2\pi\{\varepsilon'_r(d/\lambda)^2 - j\varepsilon_r''(d/\lambda)^2\}^{1/2}]}{[\varepsilon'_r(d/\lambda)^2 - j\varepsilon_r''(d/\lambda)^2]^{1/2}} \tag{2.43}$$

where Z_{in} is the impedance at liquid-air interface (which is purely resistive for $d = m\lambda_d/2$). They provided charts from which ε'_r and ε_r'' may be determined. Brydon and Hepplestone [45] described a modification of the short-circuit method (method of Roberts and Von Hippel) to enable it to be used with ceramics at high temperature. They used a cylindrical waveguide with a 1 cm long circular specimen. They measured the permittivity at 9375 MHz over a temperature range $20° - 700°c$.

Clarricoats [46] has developed methods of measurement where the dielectric sample does not fill the whole cross section of the waveguide. The sample is in the form of a slab which is mounted in a rectangular waveguide either on the waveguide axis or in

contact with the side wall. The slab contacts a fixed short circuit plate. The advantage of his method is that the slab need not have a specific length. Also, the thickness can lie within quite a wide range. Correction is made to take account of the difference between the slab height and that of the waveguide. The method has the disadvantage that ε_r'' cannot be determined with high accuracy when the dielectric has a very low loss tangent. Also, the frequency of measurement depends on the width of the waveguide.

(2) Variable Length Methods:

Fatuzzo and Mason [47] described a method in which the length of the dielectric sample is varied. The position of the standing wave minima is recorded as the length of the sample is increased. Loon and Finsey [48] described a method for the permittivity measurement of liquids in the frequency range 5-150 GHz. Their method is based on obtaining a large number of data points, each point corresponds to a measurement of the power reflected from a variable length dielectric cell. The length of the cell is varied by a short-circuit plunger. Then, by fitting an analytical curve to the data points using a least squares criterion, the wave propagation constant is determined which yields the value of the complex permittivity.

2.2.2 Sample Inserted in a Coaxial Line or a Waveguide:

Weir [49] used a computer controlled network analyzer to measure the permittivity and the permeability of a dielectric sample inserted in a waveguide. From the measured reflection (S_{11}) and transmission (S_{21}) coefficients, ε_r^* and μ_r^* may be computed. The reflection coefficient at the air-dielectric interface (ρ) may be found from S_{11} and S_{21} as

$$\rho = \zeta \pm \sqrt{\zeta^2 - 1} \qquad (2.44)$$

where

$$\zeta = \frac{S_{11} - S_{21} + 1}{2S_{11}} \ .$$ (2.45)

The propagation factor $P = e^{-\gamma d}$ can, in turn, be found from S_{11}, S_{21} and ρ as

$$P = \frac{S_{11} + S_{21} - \rho}{1 - (S_{11} + S_{21})\rho} \ .$$ (2.46)

Then, the complex permittivity and complex permeability can be determined from P and ρ; defining Λ such that

$$\frac{1}{\Lambda^2} = (\frac{\dot{\varepsilon}_r \dot{\mu}_r}{\lambda_o^2} - \frac{1}{\lambda_c^2}) = -\{\frac{1}{2\pi l} \ln(\frac{1}{P})\}^2$$ (2.47)

where λ_c is the cutoff wavelength of the guide ($\lambda_c = \infty$ for TEM transmission lines), and $Re(\frac{1}{\Lambda}) = \frac{1}{\lambda_s}$. Then

$$\dot{\mu}_r = \frac{1 + \rho}{\Lambda(1 - \rho)\sqrt{\frac{1}{\lambda_o^2} - \frac{1}{\lambda_c^2}}}$$ (2.48)
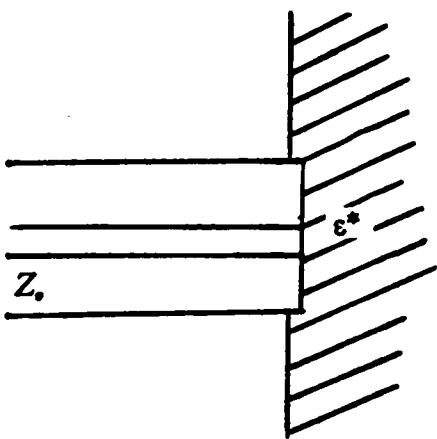
and ε_r^* may then be determined from (2.47). Phase ambiguity is involved in (2.47) because the logarithm of P (complex quantity) is equal to the angle of the complex value plus $2\pi n$, where n is equal to the integer of (d/λ_s) . A method is described to resolve the ambiguity. He applied this method on teflon and absorber, Emerson and Cuming Eccosorb SF-5.5.

2.2.3 Using an Open-Ended Coaxial Line:
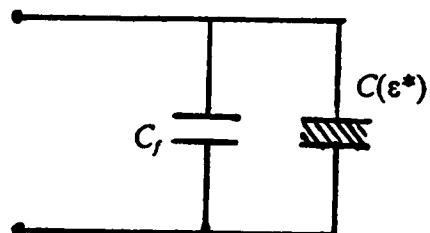
Stuchly, et al, [50], [51] analyzed this arrangement (figure 2.9a). It is assumed that the sample simulates a slab which is infinite in size. They used a computer-controlled network analyzer to measure the reflection coefficient at frequencies from 10 MHz to 1 GHz. They modeled the configuration by an equivalent circuit (figure 2.9b) which consists of two elements, a lossy capacitor $C(\varepsilon_r{}^*) = C_o\varepsilon_r{}^*$ (where C_o is the capacitance when the line is in air) and a capacitor C_f which accounts for fringing field. The expression they obtained is

$$\varepsilon_r^{\bullet} = \frac{1 - S_{11}}{j\omega Z_o C_o(1 + S_{11})} - \frac{C_f}{C_o} . \qquad (2.49)$$

The capacitances C_f and C_o are determined experimentally. They used this method for the permittivity measurement of biological tissues. The importance of this method stems from the ability of using it to carry out the measurements in vivo.

(a) Configuration   (b) Equivalent circuit

Figure 2.9: A coaxial line terminated by an infinite dielectric slab and its equivalent circuit.

2.2.4 Other Methods:

Buchanan and Grant [52] described an apparatus, figure 2.10, that can be used for permittivity measurement of liquids.
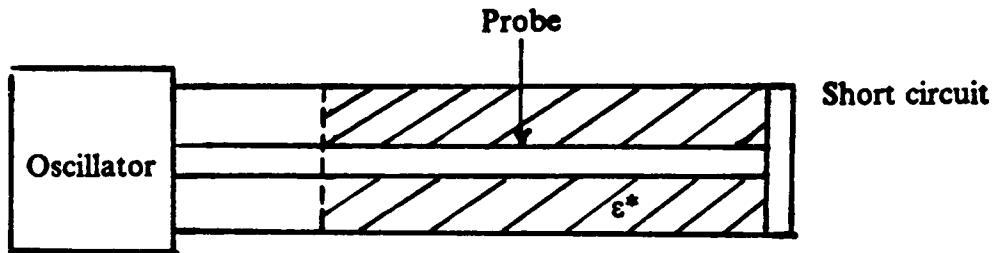
Figure 2.10: Buchanan and Grant arrangement.

A short circuited coaxial line filled with the dielectric is used. A probe is attached to the center conductor to measure the voltage. They used a bridge circuit (figure 2.11) to measure the phase.
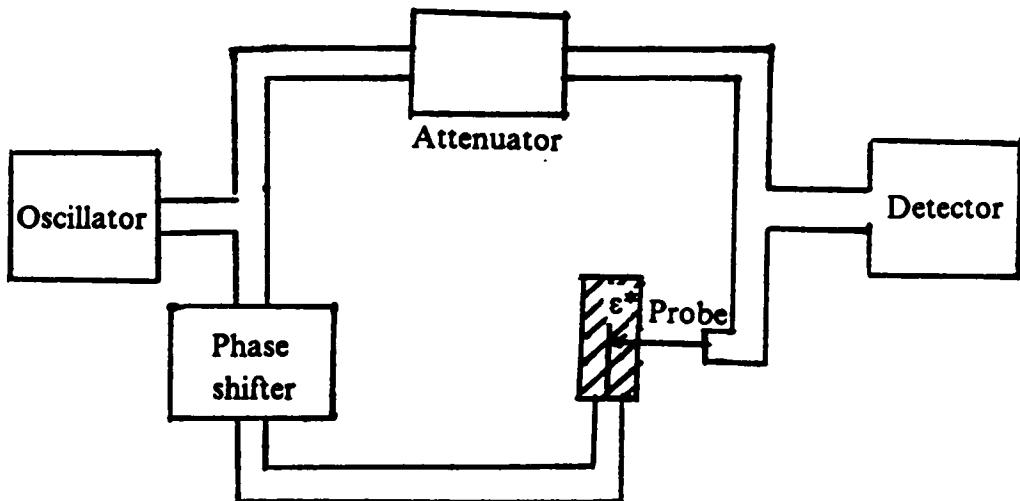
Figure 2.11: Bridge circuit used to measure phase changes.

If measurement of the voltage is made at distances d and 2d from the short circuit, then α_d and β_d are given by

$$\cos 2\alpha_d d = \frac{r^2}{4} + \{(1 - \frac{r^2}{4})^2 + r^2 \sin^2\theta\}^{1/2} \qquad (2.50)$$

and

$$\cos 2\beta_d d = \frac{r^2}{4} - \{(1 + \frac{r^2}{4})^2 + r^2 \sin^2\theta\}^{1/2} \qquad (2.51)$$

where r is the ratio of the magnitudes of the induced voltages and θ is the phase difference. Then ε_r^* may be calculated from α_d and β_d as in (2.37) and (2.38). More recently, Lighthart [53] described an experimental set-up where he used a single moded cylindrical waveguide filled with dielectric and terminated with either a load or a moving short. This enables the comparison between transmission-reflection and short-circuited line methods. He used a network analyzer to measure the scattering coefficients for a set of frequencies. In his analysis he used the mutual dependence of the scattering parameters (S_{11} and S_{21}) to reduce the uncertainty.

The methods discussed in section 2.1 (the time domain methods) which derives the permittivity from the global reflection coefficient (S_{11}) and the global transmission coefficient (S_{21}) are also used in the frequency domain where the measurement is done using a network analyzer.

2.3 Conclusion:

In this chapter, a summary of the time-domain and frequency-domain dielectric characterization techniques investigated in the literature was presented. The frequency range of interest was 50 MHz - 15 GHz. The wideband transmission line techniques

were emphasized. The presented techniques suffered from several drawbacks which are severe when used to characterize thick film materials. Consequently, new sample configurations are needed to minimize those problems and, hence, characterize dielectric materials more accurately.

Chapter 3

WIDEBAND DIELECTRIC FILLED CAVITY

ADAPTED TO THE END OF

A TRANSMISSION LINE

This chapter presents the concept, analysis, and computer simulation, as well as experimental results of a wideband dielectric filled cavity (WDFC) adapted to the end of a transmission line. The concept of the WDFC is presented in section 3.1. In section 3.2, the full field analysis of the proposed configuration is carried out assuming that the material is linear and nonmagnetic. It is further assumed that the conductors of the transmission line and the conductor walls of the cavity are lossless. The results of computer simulation experiments performed to test the sensitivity of the technique to various parameters, and to predict its performance are presented in section 3.3. The time-domain measurement technique is described in section 3.4. Section 3.5 presents the results of some experiments performed in both the time domain and frequency domain [60]. Some of these experiments were performed using materials of known characteristics for verification purposes. The other experiments were performed for the characterization of two types of thick film dielectric materials: the DuPont 5704 thick film dielectric paste and the DuPont PCM dielectric. Finally, a conclusion is provided in section 3.6.

3.1 Concept:

One of the most widely used sample configurations, as was shown in Chapter 2, is the dielectric sample inserted in a precision coaxial air line. This procedure has several disadvantages. First, the sample must be precisely cut to fit in between the inner and outer conductors of the air line. This is impossible to achieve perfectly, thus, the resulting air gaps between the sample and the line's conductors can lead to significant errors in the measured relative complex permittivity. Secondly, when dealing with solid dielectric materials like ceramics, the shaped sample may still have rough edges, consequently, inserting it in the line scratches the inner and outer conductors of the air line, thus degrading its quality and performance. Finally, the typical analysis of such configuration was carried out using equivalent lumped circuit elements, and hence, higher order modes generated due to the presence of the sample in the line have been neglected.

To avoid these drawbacks, a new sample configuration is proposed. The proposed configuration is shown in figure (3.1) where a cavity like sample holder is attached to the end of a transmission line. In this configuration, there is no need to cut or shape the sample precisely to fit in an existing structure, rather, the cavity walls can be molded or deposited on a cylindrically shaped sample. This procedure of depositing the conductor on the dielectric sample results in the elimination of any possible air gaps. This is particularly well suited for thick film materials where the dielectric layer along with the sample holder walls can be printed on a ceramic substrate. The dielectric properties can be derived from the measured reflection coefficient. The reflection coefficient can be measured using either a time-domain or a frequency-domain set-up. It is measured directly in a frequency-domain set-up while Fourier transformation is needed if the measurement is performed in the time domain. The functional relationship between the reflection coefficient and the complex permittivity of the dielectric sample is established

by carrying out a full field analysis of the proposed structure. This is presented in the next section.
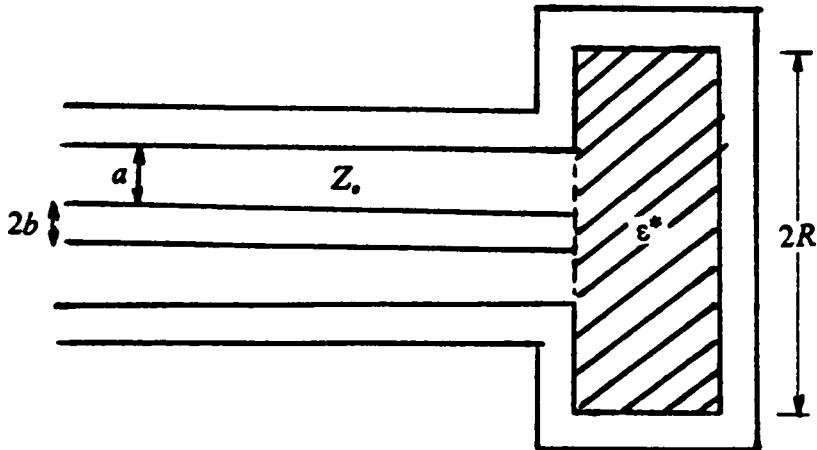
Figure 3.1: Proposed sample configuration.

3.2 Analysis of the proposed structure:

The analysis of the problem, assuming that the permittivity is known and the reflection coefficient, $S_{11}(j\omega)$, is unknown, is first presented in section 3.2.1. Section 3.2.2 describes the inverse process, in other words, determining ε^* knowing the reflection coefficient, $S_{11}(j\omega)$, which is our goal.

3.2.1 Derivation of $S_{11}(j\omega)$ Given ε^*:

Using the equivalence principle [59], figure (3.1) can be modeled as shown in figure (3.2) where region (a) is the transmission line region and region (b) is the cavity region. The aperture is replaced by a perfect electric conductor on top of which an equivalent magnetic current source M is imposed. To ensure the continuity of the electric field, the

equivalent magnetic current source in region (b) is the negative of that in region (a) (M in region (a) and $-M$ in region (b)). The current M is solved for by satisfying the continuity of the magnetic field across the aperture. Therefore, we have to derive expressions for the magnetic fields in region (a) and region (b).
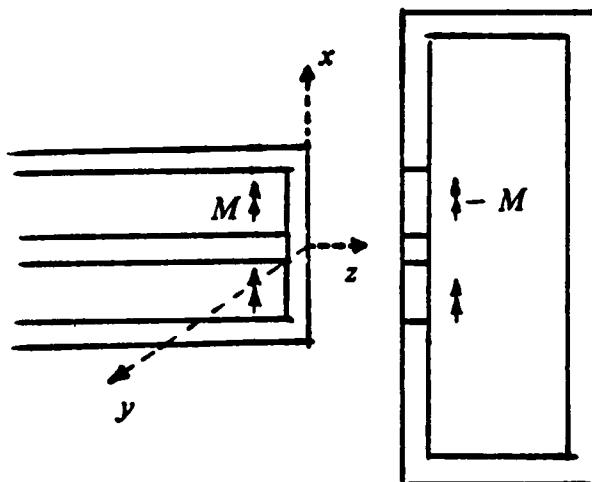
Figure 3.2: The equivalent problem.

Let H^a denote the magnetic field in region (a) and H^b denote the magnetic field in region (b) . Then H^a is given by

$$H^a = H^i + H^r + H^a(M) \tag{3.1}$$

where H^i, H^r are the incident and the reflected magnetic fields, respectively, and $H^a(M)$ is that due to the equivalent source M . Note that $H^a_t(M)$ should be computed with a conductor covering the aperture. The magnetic field in region (b) is

$$H^b = H^b(-M) = -H^b(M) \tag{3.2}$$

The last equality is a consequence of the linearity of H^b. Let the subscript t denote tangential component over the aperture. The true solution is obtained when the

tangential component of the magnetic field over the aperture in region (a) (H_t^a) equals the similar component in region (b) (H_t^b), giving

$$H_t^a \equiv H^a|_{z=0} = H_t^b \equiv H^b|_{z=0} \qquad (3.3)$$

Hence,

$$H_t^a(M) + H_t^b(M) = - H_t^i - H_t^r = -2H_t^i \qquad (3.4)$$

because $H^i|_{z=0} = H^r|_{z=0}$. Equation (3.4) is the exact equation for determining M . Expressions for the fields components in equation (3.4) in terms of M are obtained by solving the Helmoltz scalar equation and applying the boundary conditions [59]. Helmoltz equation is

$$\nabla^2 \Psi + K^2 \Psi = 0 \qquad (3.5)$$

where $K = \omega \sqrt{\varepsilon \mu}$. Our structure is axially symmetric, therefore the only higher order modes generated are the TM_{on} modes (no angular variation). These modes are given by

$$E_\rho = \frac{1}{j\omega\varepsilon} \frac{\partial^2 \Psi}{\partial z \partial \rho} \qquad (3.6)$$

$$E_z = \frac{1}{j\omega\varepsilon} (K^2 + \frac{\partial^2}{\partial z^2})\Psi \qquad (3.7)$$

$$H_\phi = - \frac{\partial \Psi}{\partial \rho} \qquad (3.8)$$

$$E_\phi = H_\rho = H_z = 0 \ . \qquad (3.9)$$

The following two subsections present the derivation of the magnetic fields components in the two regions:

(1) The Transmission Line Region (Region (a)):

The incident field is the TEM mode only. This is given by

$$H^I = \frac{1}{\eta_o \sqrt{2\pi \ln(a/b)}} \frac{1}{\rho} e^{-jK_o z} u_\phi \tag{3.10}$$

where $\eta_o = \sqrt{\frac{\mu_o}{\varepsilon_o}}$ is the intrinsic impedance. Note that the above expression is normalized such that the incident power is unity.

The scalar function Ψ^a appropriate for the derivation of $H^a_z(M)$ is the following:

$$\Psi^a = (B_o + C_o \ln \rho)e^{jK_o z} + \sum_{n=1}^{\infty} \left[B_n J_o(K^a_{\rho_n}\rho) + C_n N_o(K^a_{\rho_n}\rho) \right] e^{jK^a_{z_n} z} \tag{3.11}$$

where J_o and N_o denote zeroth order Bessel functions of the first and second kind, respectively. The separation equation is

$$(K^a_{z_n})^2 + (K^a_{\rho_n})^2 = K_o^2 = \omega^2 \varepsilon_o \mu_o . \tag{3.12}$$

The constants B_n and C_n which can be evaluated by applying the boundary conditions. The first boundary condition is that the tangential component of the electric field equals zero at the inner and outer conductors of the transmission line, i.e. at $\rho = b$ and at $\rho = a$. Therefore, for $n > 0$

$$B_n J_o(K^a_{\rho_n}a) + C_n N_o(K^a_{\rho_n}a) = 0 \tag{3.13}$$

$$B_n J_o(K^a_{\rho_n}b) + C_n N_o(K^a_{\rho_n}b) = 0 . \tag{3.14}$$

Using equations (3.13) and (3.14) and introducing the constants D_n :

$$B_n = D_n N_o(K^a_{\rho_n}b) \tag{3.15}$$

and

$$C_n = - D_n J_o(K^a_{\rho_n} b) \tag{3.16}$$

with $K^a_{\rho_n}$ such that

$$N_o(K^a_{\rho_n} b) J_o(K^a_{\rho_n} a) - J_o(K^a_{\rho_n} b) N_o(K^a_{\rho_n} a) = 0 \ . \tag{3.17}$$

Let x^a_n denote the solution of the standard form

$$N_o(x) J_o(\lambda x) - J_o(x) N_o(\lambda x) = 0 \tag{3.18}$$

where $\lambda = \dfrac{a}{b}$, then

$$K^a_{\rho_n} = \frac{x^a_n}{b} \quad , \quad n > 0 \ . \tag{3.19}$$

Therefore, using equations (3.11), (3.15) and (3.16),

$$\Psi^a = (B_o + C_o \ln \rho) e^{jK_o z} + \sum_{n=1}^{\infty} D_n \big[N_o(K^a_{\rho_n} b) J_o(K^a_{\rho_n} \rho) - J_o(K^a_{\rho_n} b) N_o(K^a_{\rho_n} \rho) \big] e^{jK^a_{z_n} z} \ . \tag{3.20}$$

The transversal electric and magnetic fields can be computed from equations (3.6), (3.8) and (3.20). The result takes the form

$$E^a_\rho(M) = \frac{A_o}{\rho} e^{jK_o z} + \sum_{n=1}^{\infty} A_n f_n(\rho) e^{jK^a_{z_n} z} \quad \text{and} \tag{3.21}$$

$$H^a_\phi(M) = - \frac{A_o}{\eta_o \rho} e^{jK_o z} - \sum_{n=1}^{\infty} \frac{A_n}{\eta_n} f_n(\rho) e^{jK^a_{z_n} z} \tag{3.22}$$

chapter 3

where

$$f_n(\rho) = J_o(K^a_{\rho_n}b)N_1(K^a_{\rho_n}\rho) - N_o(K^a_{\rho_n}b)J_1(K^a_{\rho_n}\rho) \ , \tag{3.23}$$

J_1 and N_1 being the first order Bessel functions of the first and second kind, respectively. and $A_o = \eta_o C_o, \quad A_n = \dfrac{K^o_{\rho_n}K^o_{z_n}D_n}{\omega\varepsilon_o}$, η_o is the intrinsic impedance, η_n is given by

$$\eta_n = \frac{K^a_{z_n}}{\omega\varepsilon_o} \tag{3.24}$$

$f_n(\rho)$ is orthogonal to $f_m(\rho)$. For computational convenience let's normalize $f_n(\rho)$ for unity power and let $e_n(\rho)$ denote the normalized result. That is,

$$\iint_{line-cross\ section} e_n(\rho) \cdot e_m(\rho)ds = \begin{cases} 1 & , \quad m = n \\ 0 & , \quad m \neq n \end{cases} \tag{3.25}$$

Therefore, we have to evaluate the normalizing constants P_n (where $e_n(\rho) = P_n f_n(\rho)$) such that

$$P_n^2 \int_0^{2\pi}\int_b^a \left[J_o(K^a_{\rho_n}b)N_1(K^a_{\rho_n}\rho) - N_o(K^a_{\rho_n}b)J_1(K^a_{\rho_n}\rho)\right]^2 \rho \ d\rho d\phi = 1 \tag{3.26}$$

Hence,

$$2\pi P_n^2 \int_b^a \left[J_o^2(K^a_{\rho_n}b)N_1^2(K^a_{\rho_n}\rho) + N_o^2(K^a_{\rho_n}b)J_1^2(K^a_{\rho_n}\rho)\right]\rho d\rho -$$
$$2\pi P_n^2 \int_b^a \left[2J_o(K^a_{\rho_n}b)N_o(K^a_{\rho_n}b)N_1(K^a_{\rho_n}\rho)J_1(K^a_{\rho_n}\rho)\right]\rho d\rho = 1 \ . \tag{3.27}$$

There are three integrals to be evaluated

$$I_1 = \int_b^a N_1^2(K_{\rho_n}^a \rho)\rho \, d\rho \qquad (3.28)$$

$$I_2 = \int_b^a J_1^2(K_{\rho_n}^a \rho) \, \rho d\rho \qquad (3.29)$$

and

$$I_3 = \int_b^a N_1(K_{\rho_n}^a \rho)J_1(K_{\rho_n}^a \rho)\rho \, d\rho d\phi \qquad (3.30)$$

The above integrals $(I_1, I_2$ and I_3) can be evaluated using the general formulas [56]

$$\int_b^a N_1^2(K\rho)\rho d\rho = \frac{\rho^2}{2}\left\{ N'^2_1(K\rho) + (1 - \frac{1}{K^2\rho^2})N_1^2(K\rho)\right\}_b^a \qquad (3.31)$$

$$\int_b^a J_1^2(K\rho)\rho d\rho = \frac{\rho^2}{2}\left\{ J'^2_1(K\rho) + (1 - \frac{1}{K^2\rho^2})J_1^2(K\rho)\right\}_b^a \qquad (3.32)$$

$$\int_b^a J_1(K\rho)N_1(K\rho)\rho d\rho = \frac{\rho^2}{2}\left\{ J'_1(K\rho)N'_1(K\rho) + (1 - \frac{1}{K^2\rho^2})J_1(K\rho)N'_1(K\rho)\right\}_b^a \qquad (3.33)$$

where the prime denotes differentiation with respect to the argument, or,

$$J'_1(K\rho) = J_o(K\rho) - \frac{1}{K\rho}J_1(K\rho) \qquad (3.34)$$

$$N'_1(K\rho) = N_o(K\rho) - \frac{1}{K\rho}N_1(K\rho) \; .$$ (3.35)

Using equations (3.28) - (3.35) the results of the integrals I_1, I_2 and I_3 are:

$$I_1 = \frac{a^2}{2}\left\{N_0^2(K_{\rho_n}a) - \frac{2}{K_{\rho_n}^a a}N_1(K_{\rho_n}^a a)N_o(K_{\rho_n}^a a) + N_1^2(K_{\rho_n}^a a)\right\}$$
$$- \frac{b^2}{2}\left\{N_o^2(K_{\rho_n}^a b) - \frac{2}{K_{\rho_n}^a b}N_1(K_{\rho_n}^a b)N_o(K_n\rho_n b) + N_1^2(K_{\rho_n}^a b)\right\}$$ (3.36)

$$I_2 = \frac{a^2}{2}\left\{J_0^2(K_{\rho_n}^a a) - \frac{2}{K_{\rho_n}^a a}J_1(K_{\rho_n}^a a)J_o(K_{\rho_n}^a a) + J_1^2(K_{\rho_n}^a a)\right\}$$
$$- \frac{b^2}{2}\left\{J_o^2(K_{\rho_n}^a b) - \frac{2}{K_{\rho_n}^a b}J_1(K_{\rho_n}^a b)J_o(K_n\rho_n b) + J_1^2(K_{\rho_n}^a b)\right\}$$ (3.37)

and

$$I_3 = \frac{a^2}{2}\left[J_0(K_{\rho_n}^a a)N_o(K_{\rho_n}^a a) + J_1(K_{\rho_n}^a a)N_1(K_{\rho_n}^a a)\right]$$
$$- \frac{a}{2K_{\rho_n}^a}\left[J_o(K_{\rho_n}^a a)N_1(K_{\rho_n}^a a) + J_1(K_{\rho_n}^a a)N_o(K_{\rho_n}^a a)\right]$$
$$- \frac{b^2}{2}\left[J_0(K_{\rho_n}^a b)N_o(K_{\rho_n}^a b) + J_1(K_{\rho_n}^a b)N_1(K_{\rho_n}^a b)\right]$$
$$+ \frac{b}{2K_{\rho_n}^a}\left[J_o(K_{\rho_n}^a b)N_1(K_{\rho_n}^a b) + J_1(K_{\rho_n}^a b)N_o(K_{\rho_n}^a b)\right] \; .$$ (3.38)

Therefore, the normalizing constants P_n can be evaluated by combining equations (3.27), (3.36) - (3.38) and carrying out some algebraic manipulations to simplify the resulting expression. The final result is

$$P_n = \frac{1}{\sqrt{\pi}}\;\frac{1}{\left[\alpha_n^2 - \beta_n^2\right]^{1/2}}$$ (3.39a)

where

$$\alpha_n = a\left[J_o(K^a_{\rho_n}b)N_1(K^a_{\rho_n}a) - N_o(K^a_{\rho_n}b)J_1(K^a_{\rho_n}a)\right] \qquad (3.39b)$$

$$\beta_n = b\left[J_o(K^a_{\rho_n}b)N_1(K^a_{\rho_n}b) - N_o(K^a_{\rho_n}b)J_1(K^a_{\rho_n}b)\right] \qquad (3.39c)$$

and hence,

$$e_n(\rho) = P_n\left[J_o(K^a_{\rho_n}b)N_1(K^a_{\rho_n}\rho) - N_o(K^a_{\rho_n}b)J_1(K^a_{\rho_n}\rho)\right] \quad , \quad for \ n > 0 \ . \qquad (3.40)$$

Redefining the constants in equations (3.21), (3.22):

$$E^a_\rho(M) = A_o e_o(\rho)e^{jK_o z} + \sum_{n=1}^{\infty} A_n e_n(\rho)e^{jK^a_{z_n} z} \qquad (3.41)$$

$$H^a_\phi(M) = -\frac{A_o}{\eta_o}e_o e^{jK_o z} - \sum_{n=1}^{\infty}\frac{A_n}{\eta_n}e_n(\rho)e^{jK^a_{z_n} z} \qquad (3.42)$$

where $e_n(\rho)$, $n > 0$ is given in equation (3.40), and $e_o(\rho)$ is given by

$$e_o(\rho) = \frac{1}{\rho\sqrt{2\pi \ln(b/a)}} \ . \qquad (3.43)$$

The tangential field components over the aperture (at $z = 0$), E^a_t and H^a_t are

$$E^a_t(M) = E^a_\rho|_{z=0} = A_o e_o(\rho)u_\rho + \sum_{n=1}^{\infty} A_n e_n(\rho)u_\rho \qquad (3.44)$$

and

$$H_t^a(M) = H_\rho^a|_{z=0} = -\frac{A_o}{\eta_o}e_o(\rho)u_\phi - \sum_{n=1}^{\infty}\frac{A_n}{\eta_n}e_n(\rho)u_\phi \ . \tag{3.45}$$

The coefficients A_o, A_n are evaluated by applying the remaining boundary condition, the tangential electric field over the aperture equals the magnetic current distribution on the aperture, or

$$M = u_z \times E_t^a \ . \tag{3.46}$$

Therefore, using equations (3.44) and (3.46)

$$M = A_o e_o u_\phi + \sum_{n=1}^{\infty}A_n e_n(\rho)u_\phi \ . \tag{3.47}$$

Note that M is in the direction of ϕ, i.e. $M = M_\phi u_\phi$. To solve for the coefficients, multiply both sides of equation (3.47) by e_m and integrate over the line cross section. By the orthonormality (3.25), all the terms of the summation are zero except the $m = n$ term. Hence,

$$A_n = 2\pi\int_b^a M_\phi e_n(\rho)\rho d\rho \quad , \quad n = 0, 1, 2, \ldots \tag{3.48}$$

Thus, the tangential magnetic field component over the aperture in region a ($H_t^a(M)$) is given in equation (3.45) with the coefficients defined by equation (3.48).

(2) The Cavity Region (Region (b)):

The scalar function Ψ^b appropriate for the derivation of $H^b_r(M)$ which also satisfies the boundary condition of zero tangential electric field at $z = d$ ($E^b_\rho|_{z=d}$) is

$$\Psi^b = \sum_{n=1}^{\infty} B_n J_o(K^b_{\rho_n}\rho) \cos K^b_{z_n}(z - d) \tag{3.49}$$

where

$$K^b_{z_n} = \left[\omega^2 \varepsilon^* \mu_o - (K^b_{\rho_n})^2\right]^{1/2}$$

and $\varepsilon^* = \varepsilon_r^* \varepsilon_o$, ε_r^* being the relative complex permittivity of the dielectric material in region (b). Thus by using equations (3.6) and (3.8) along with equation (3.49), the transversal field components are

$$E^b_\rho(-M) = \sum_{n=1}^{\infty} C_n J_1(K^b_{\rho_n}\rho) \sin K^b_{z_n}(z - d) \tag{3.50}$$

and

$$H^b_\phi(-M) = j\omega\varepsilon^* \sum_{n=1}^{\infty} \frac{C_n}{K^b_{z_n}} J_1(K^b_{\rho_n}\rho) \cos K^b_{z_n}(z - d) \tag{3.51}$$

where $C_n = \dfrac{K^b_{\rho_n} K^b_{z_n}}{j\omega\varepsilon^*} B_n$. The second boundary condition is that the tangential electric field at $\rho = R$ is zero ($E^b_z(-M)|_{\rho=R} = 0$). Consequently, from equations (3.7) and (3.49)

$$J_o(K^b_{\rho_n}R) = 0 \ . \tag{3.52}$$

Hence, if x_n^b denotes the zeros of the Bessel function $J_o(x)$ (that is $J_o(x_n^b) = 0$) then:

$$K_{\rho_n}^b = \frac{x_n^b}{R} \qquad (3.53)$$

The coefficients C_n can be evaluated by applying the remaining boundary condition

$$-M = -u_z \times E^b|_{z=0} \qquad (3.54)$$

Equations (3.50) and (3.54) yield

$$M_\phi(\rho) = -\sum_{n=1}^{\infty} C_n J_1(K_{\rho_n}^b \rho) \sin K_{z_n}^b d \qquad (3.55)$$

Note that $M = M_\phi u_\phi$ (in the direction of ϕ only) and also it is only defined for $b < \rho < a$ (that is $M_\phi = 0$ for $\rho < b$ or $\rho > a$). Therefore, to compute the coefficients C_n multiply both sides of equation (3.55) by $J_1(K_{\rho_m}^b \rho)$ and integrate over the cavity cross section to obtain

$$\int_0^{2\pi} \int_0^R M_\phi J_1(K_{\rho_m}^b \rho)\rho d\rho d\phi = -\int_0^{2\pi} \int_0^R \sum_{n=1}^{\infty} C_n \sin(K_{z_n}^b d) J_1(K_{\rho_n}^b \rho) J_1(K_{\rho_m}^b \rho)\rho d\rho d\phi \quad (3.56)$$

The limits of the integral on the left hand side of the above equation can be changed to be from b to a because, as mentioned earlier, the magnetic current M_ϕ equals zero for $\rho < b$ or $\rho > a$. Therefore, equation (3.56) becomes

$$2\pi \int_b^a M_\phi(\rho) J_1(K_{\rho_m}^b \rho)\rho d\rho = -2\pi \sum_{n=1}^{\infty} \int_0^R C_n \sin(K_{z_n}^b d) J_1(K_{\rho_n}^b \rho) J_1(K_{\rho_m}^b \rho)\rho d\rho \quad (3.57)$$

chapter 3

Because of the orthogonality of the Bessel functions, all the terms of the summation in the above equation are zero except the $m = n$ term giving

$$\int_b^a M_\phi(\rho) J_1(K^b_{\rho_m}\rho)\rho d\rho = - C_n \sin(K^b_{z_n}d) \int_0^R J_1^2(K^b_{\rho_n}\rho)\rho d\rho \ . \tag{3.58}$$

Using equation (3.32), the result of the integral on the right hand side of equation (3.58) is

$$\int_0^R J_1^2(K^b_{\rho_n}\rho)\rho d\rho = \frac{R^2}{2} J_1^2(K^b_{\rho_n}R) \ . \tag{3.59}$$

Therefore, combining equations (3.58), (3.59):

$$C_n = \frac{-2}{R^2 J_1^2(K_{\rho_n}R) \sin K^b_{z_n}d} \int_b^a M_\phi J_1(K^b_{\rho_n}\rho)\rho d\rho \ . \tag{3.60}$$

Thus, the tangential component of the magnetic field in region (b) over the aperture in terms of M is obtained from equation (3.51) as

$$H^b_t(M) = - H^b_\phi(-M)|_{z=0} = -j\omega\varepsilon^* \sum_{n=1}^\infty \frac{C_n}{K^b_{z_n}} J_1(K^b_{\rho_n}\rho) \cos(K^b_{z_n}d)u_\phi \tag{3.61}$$

where the coefficients C_n are given in equation (3.60).

(3) Method of Solution to Obtain M (Method of Moments):

Equation (3.4) is the exact equation for determining M which is rewritten for convenience

$$H_t^a(M) + H_t^b(M) = -2H_t^i \ . \tag{3.62}$$

In the previous two subsections, expressions for all the quantities in the above equation were obtained in terms of M (equations (3.10), (3.45) and (3.61)). It is impossible to solve equation (3.62) for M exactly. The method of moments is used to obtain an approximate solution. Define a set of expansion functions $\{M_n, \ n = 1,2, \ldots, N_1\}$ (must be an independent set) and a set of weighting functions $\{W_n, \ n = 1,2, \ldots, N_2\}$. Let

$$M = \sum_{n=1}^{N_1} V_n M_n \tag{3.63}$$

where the coefficients V_n are to be determined. Substituting (3.63) into (3.62) and using linearity

$$\sum_{n=1}^{N_1} V_n H_t^a(M_n) + \sum_{n=1}^{N_1} V_n H_t^b(M_n) = -2H_t^i \ . \tag{3.64}$$

Notational simplicity may be obtained by using the symmetric product defined as

$$<A,B> = \iint_{apert.} A \cdot B ds \ . \tag{3.65}$$

Taking the symmetric product of equation (3.64) with each W_n and using linearity of the symmetric product, one obtains

$$\sum_{n=0}^{N_1} V_n < W_m, H_t^a(M_n) > + \sum_{n=0}^{N_1} V_n < W_m, H_t^b(M_n) > = -2 < W_m, H_t^i > , \qquad (3.66)$$

$$m = 1, 2, \ldots , N_2$$

The solution of this set of linear equations determines V_n and thus M according to (3.63). Once M is known, the reflection coefficient, (S_{11}), can be computed as will be shown later.

Let's take the set of expansion functions to be the same as the set of weighting functions (i.e. $W_n = M_n$, $n = 1, 2, \ldots , N$), often called Galerkin's method. Hence, the above solution (equation (3.66)) can be put into matrix form as follows: Let $[Y^a]$ be an admittance matrix representing region (a) given by

$$[Y^a] = \left[< -M_m, H_t^a(M_n) > \right]_{N \times N} \qquad (3.67)$$

and let $[Y^b]$ be an admittance matrix for region (b) given by

$$[Y^b] = \left[< -M_m, H_t^b(M_n) > \right]_{N \times N} \qquad (3.68)$$

Define a source vector $\vec{I}^i$

$$\vec{I}^i = \left[2 < M_m, H_t^i > \right]_{N \times 1} \qquad (3.69)$$

and a coefficient vector $\vec{V}$

$$\vec{V} = [V_n]_{N \times 1} \qquad (3.70)$$

Thus, the matrix equation equivalent to equation (3.66) is of the form,

$$[Y^a + Y^b]\vec{V} = \vec{I}^i \qquad (3.71)$$

where the only unknown is the vector $\vec{V}$.

First we have to choose a set of expansion functions that best approximates the actual current distribution over the aperture (M). The modes of the transmission line region seems to be a good choice. Therefore, let

$$M_n = e_{n-1} \quad , \quad n = 1, 2, \dots, N \qquad (3.72)$$

where e_o is given in (3.43), while e_n $n > 0$ is defined in (3.40).

To compute the elements of the matrix equation (3.71), consider a single expansion function M_m across the aperture. The tangential magnetic field in region (a) over the aperture due to M_m is given by equation (3.45) where A_n must have a double subscript (A_{mn}) to account for the added subscript on M, i.e. equation (3.48) becomes

$$A_{mn} = 2\pi \int_b^a M_m e_n(\rho) \rho d\rho \quad , \qquad n = 0, 1, \dots, \quad m = 1, 2, \dots \qquad (3.73)$$

From equations (3.72), (3.73) and remembering the orthonormality (3.25):

$$A_{mn} = \begin{cases} 1 & , \quad n = m \\ 0 & , \quad n \neq m \end{cases} \qquad (3.74)$$

Therefore, using equations (3.67), (3.45), (3.72), (3.73), and (3.74) one can show that the elements of the of the admittance matrix $[Y^a]$ are given by,

$$Y_{mn}^a = \begin{cases} \dfrac{1}{\eta_{n-1}} & , \quad m = n \\ 0 & , \quad m \neq n \end{cases} \qquad (3.75)$$

The elements of the excitation vector $\vec{I}^i$ are easily obtained from equations (3.10), (3.25), (3.69) and (3.72)

$$\vec{I}_n^2 = \begin{cases} \dfrac{2}{\eta_o} & , \quad n = 1 \\[2mm] 0 & , \quad n > 1 \end{cases} \tag{3.76}$$

To compute the matrix elements of $[Y^b]$, the coefficients C_n must have a double subscript to account for the added subscript on M, i.e. equation (3.60) becomes

$$C_{mn} = \frac{-2}{R^2 J_1^2(K_{\rho_n}^b R) \sin K_{z_n}^b d} \int_b^a M_m J_1(K_{\rho_n}^b \rho) \rho \, d\rho \ . \tag{3.77}$$

Hence, using equations (3.61), (3.68), (3.72) and (3.77) the elements of $[Y^b]$ are

$$Y_{mn}^b = j\omega\varepsilon^* \sum_{l=1}^{\infty} \frac{C_{nl}}{K_{z_l}^b} \cos(K_{z_l}^b d) \, 2\pi \int_b^a M_m(\rho) J_1(K_{\rho_l}^b \rho) \rho \, d\rho \ . \tag{3.78}$$

Equation (3.78) can be rewritten as follows:

$$Y_{mn}^b = -j\omega\varepsilon^* \sum_{l=1}^{\infty} \frac{C'_{nl} C'_{ml}}{K_{z_l}^b} \frac{1}{\tan(K_{z_l}^b d)} \tag{3.79}$$

where

$$C'_{nl} = \frac{2\sqrt{\pi}}{R J_1(K_{\rho_l}^b R)} \int_b^a M_n J_1(K_{\rho_l}^b \rho) \rho \, d\rho \ . \tag{3.80}$$

In order to evaluate the integral in the above equation, the following general integral formulas [56] are useful:

$$\int_0^x J_1(r)dr = 1 - J_0(x) \qquad (3.81)$$

and

$$\int_b^a X_p(k_1 r)Z_p(k_2 r)rdr = \frac{1}{k_1^2 - k_2^2} \left\{ k_2 r X_p(K_1 r)Z'_p(k_2 r) - k_1 r X'_p(k_1 r)Z_p(k_2 r) \right\}_b^a \qquad (3.82)$$

where $X(k_1 r)$, $Z(k_2 r)$ are any Bessel functions. For $n = 1$, $M_1 = e_0$. Using equations (3.43), (3.80) and (3.81) C'_{1i} is

$$C'_{1i} = \frac{1}{\sqrt{2\pi \ln(b/a)}} \frac{2\sqrt{\pi}}{RJ_1(K^b_{\rho_i}R)} \frac{1}{K^b_{\rho_i}} \left\{ J_0(K^b_{\rho_i}b) - J_0(K^b_{\rho_i}a) \right\} \qquad (3.83)$$

For $n > 1$, the integral encountered in equation (3.80) can be evaluated using the general formula (3.82). Thus, using equations (3.40), (3.72), (3.80) and (3.82), the coefficients C'_{ni} can be computed. The result, after some algebraic manipulations to simplify the resulting expression, is

$$C'_{ni} = P_n \frac{2\sqrt{(\pi)}}{RJ_1(K^b_{\rho_i}R)} \frac{1}{(K^a_{\rho_n})^2 - (K^b_{\rho_i})^2} I_{ni} \qquad (3.84)$$

where P_n are defined in equation (3.39), and

$$I_{ni} = K^b_{\rho_i}a\, J_0(K^b_{\rho_i}a)\left\{ J_0(K^a_{\rho_n}b)N_1(K^a_{\rho_n}a) - N_0(K^a_{\rho_n}b)J_1(K^a_{\rho_n}a) \right\}$$
$$- K^b_{\rho_i}b\, J_0(K^b_{\rho_i}b)\left\{ J_0(K^a_{\rho_n}b)N_1(K^a_{\rho_n}b) - N_0(K^a_{\rho_n}b)J_1(K^a_{\rho_n}b) \right\}$$

which can be written as

$$I_{nl} = K_{\rho_l}^b \left[J_o(K_{\rho_l}^b a) \alpha_n - J_o(K_{\rho_l}^b b) \beta_n \right] \tag{3.85}$$

where α_n and β_n are defined in equations (3.39b) and (3.39c), respectively.

Once the coefficient vector $\vec{V}$ is computed, the magnetic current M can be obtained simply using equation (3.63). The reflection coefficient can be evaluated as follows: The tangential electric field over the aperture can be written as

$$E_\rho = (1 + S_{11})e_o(\rho) + \sum_{n=1}^{\infty} \Gamma_l e_n(\rho) \tag{3.86}$$

where S_{11} is the reflection coefficient, Γ_l are the amplitudes of the higher order modes generated at the aperture (unity incident power is assumed). Thus, the magnetic current $M = M_\phi u_\phi = u_z \times E|_{z=0}$ is given by

$$M_\phi = (1 + S_{11})e_o(\rho) + \sum_{n=1}^{\infty} \Gamma_l e_n(\rho) \tag{3.87}$$

Multiplying both sides by $e_o(\rho)$, then integrating over the aperture and using the orthonormality in (3.25), the following result is obtained:

$$S_{11} = \int_0^{2\pi} \int_b^a M_\phi e_o(\rho)\rho d\rho - 1 \tag{3.88}$$

Combining equations (3.63) and (3.88)

$$S_{11} = \sum_{n=1}^{N} V_n \int_0^\pi \int_b^a M_n e_o(\rho)\rho d\rho - 1 \tag{3.89}$$

But the expansion functions M_n are taken to be e_{n-1}, therefore, using the orthonormality in (3.25), S_{11} is given by

$$S_{11} = V_1 - 1 .$$

(3.90)

Similarly, the amplitudes of the higher order modes are obtained by multiplying both sides of (3.87) by $e_n(\rho)$, $n > 0$, integrating over the aperture and using orthonormality. The result is

$$\Gamma_n = V_n - 1 , \qquad n > 0 .$$

(3.91)

Later, in section 3.3, computer simulation results will be presented. The purpose of these experiments is to study the effect of varying the dimensions of the sample holder and the dielectric permittivity on the reflection coefficient. Hence, predictions can be made concerning the best choice of the dimensions as well as the bandwidth of this technique. The computer program code, written in Fortran language, is listed in appendix I.

3.2.2 Computation of ε^* Given S_{11} :

Equation (3.90) can be written as

$$S_{11} - V_1 + 1 = 0 .$$

(3.92)

The computation of ε^* is achieved by solving equation (3.92) along with the matrix equation (3.71). Since the elements of the matrix $[Y^a]$ are nonlinear functions of ε^*, the solution has to be achieved iteratively. The solution can be obtained by minimizing the following function:

$$f(\varepsilon^*) = |S_{11} - V_1 + 1|^2 \tag{3.93}$$

subject to the matrix equation (3.71). First, an initial guess for ε^* has to be assumed. Then, the V_n's are computed directly from the matrix equation (3.71) using Gaussian elimination. Only V_1 is needed to evaluate $f(\varepsilon^*)$ and, then, ε^* is updated using Powell's hybrid method [55]. Using the updated value of ε^*, again, the coefficients V_n's are obtained using Gaussian elimination and V_1 is used to evaluate $f(\varepsilon^*)$ and, hence, compute another updated value of ε^*. This iterative procedure is repeated until the value of $f(\varepsilon^*)$ is less than a desired tolerance.

The complete Fortran computer program is listed in appendix II.

3.3 Computer Simulation:

This section presents some computer simulation experiments aimed at studying the behavior of the reflection coefficient when some parameters of the sample (or the sample holder) are changed. These experiments are the following:

(a) Varying the diameter of the sample:

Figure (3.3) shows the effect of varying the diameter of the sample on the phase of the reflection coefficient. Three graphs are shown corresponding to diameters of 1cm, 2 cm and 3 cm. The permittivity is taken to be real ($\varepsilon''_r = 0$). Therefore, the magnitude of the reflection coefficient is unity. As shown in the figure, changing the diameter does not affect the phase except around resonance. This is expected because the fields are concentrated in the center and, therefore, the main effect of varying the radial dimension is on the resonant frequencies of the cavity. It is desirable to choose the diameter small to cause the first resonance to fall outside the bandwidth of interest.
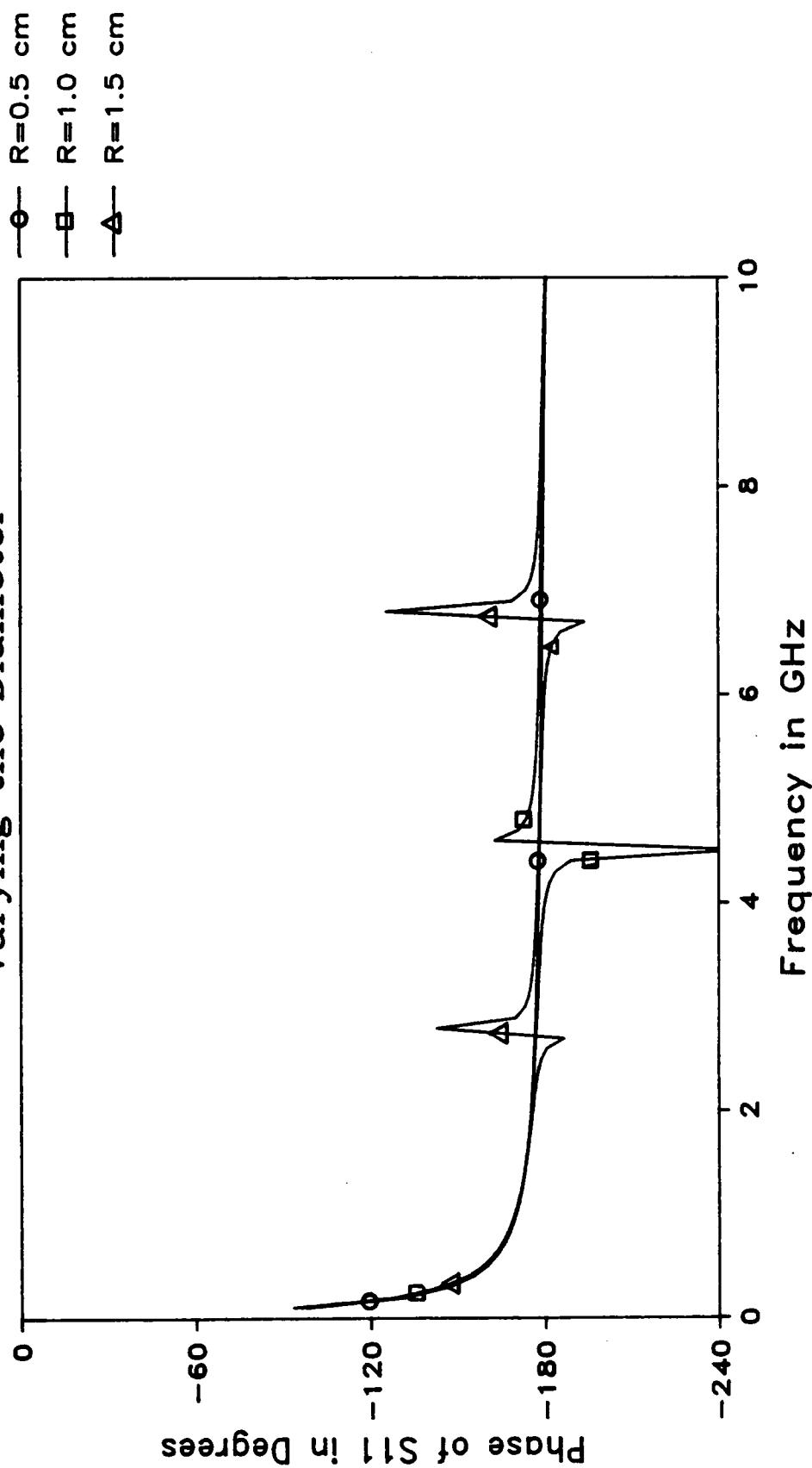
Figure 3.3: Effect of varying the diameter.

(b) Changing The thickness:

Figure (3.4) shows the effect of varying the sample thickness on the phase of the reflection coefficient. Again the material is assumed lossless. Three graphs are shown corresponding to thicknesses of 0.025 cm, 0.5 cm, and 0.75 cm. It is observed from the figure the thicker samples cause the phase to progress more slowly to $-180°$. This means that the bandwidth of the measurement is wider for thicker samples because when the phase approaches 180°, small errors in the reflection coefficient lead to significant errors in the computed permittivity. The resonance observed is due to the radial dimension, thus the three graphs have the same resonant frequencies. It is also concluded that the thickness has to be known precisely in order to get accurate results for the complex permittivity.

(c) Varying the dielectric constant (ε',):

Three graphs are shown in figure (3.5) corresponding to relative dielectric constants of 5,7 and 9. The loss is taken to be zero, consequently, the magnitude of the reflection coefficient is unity. It is observed that varying the dielectric constant changes the phase as well as the resonant frequencies of the cavity. Hence, the real part of the permittivity (ε') is mainly dependent on the reflection coefficient.

(d) Varying the dielectric loss (ε'',):

Figure (3.6) shows three graphs of the magnitude of the reflection coefficient corresponding to ε'', of 0.05, 0.5 and 5. The phase is shown in figure (3.7). From the figures, it is noticed that the effect on the phase is insignificant except around resonance. Thus, the loss information is mainly given by the magnitude of the reflection coefficient. As expected, for higher losses, the resonance diminishes. An important observation is that the change in the magnitude is not considerable if the losses are very low. Consequently,
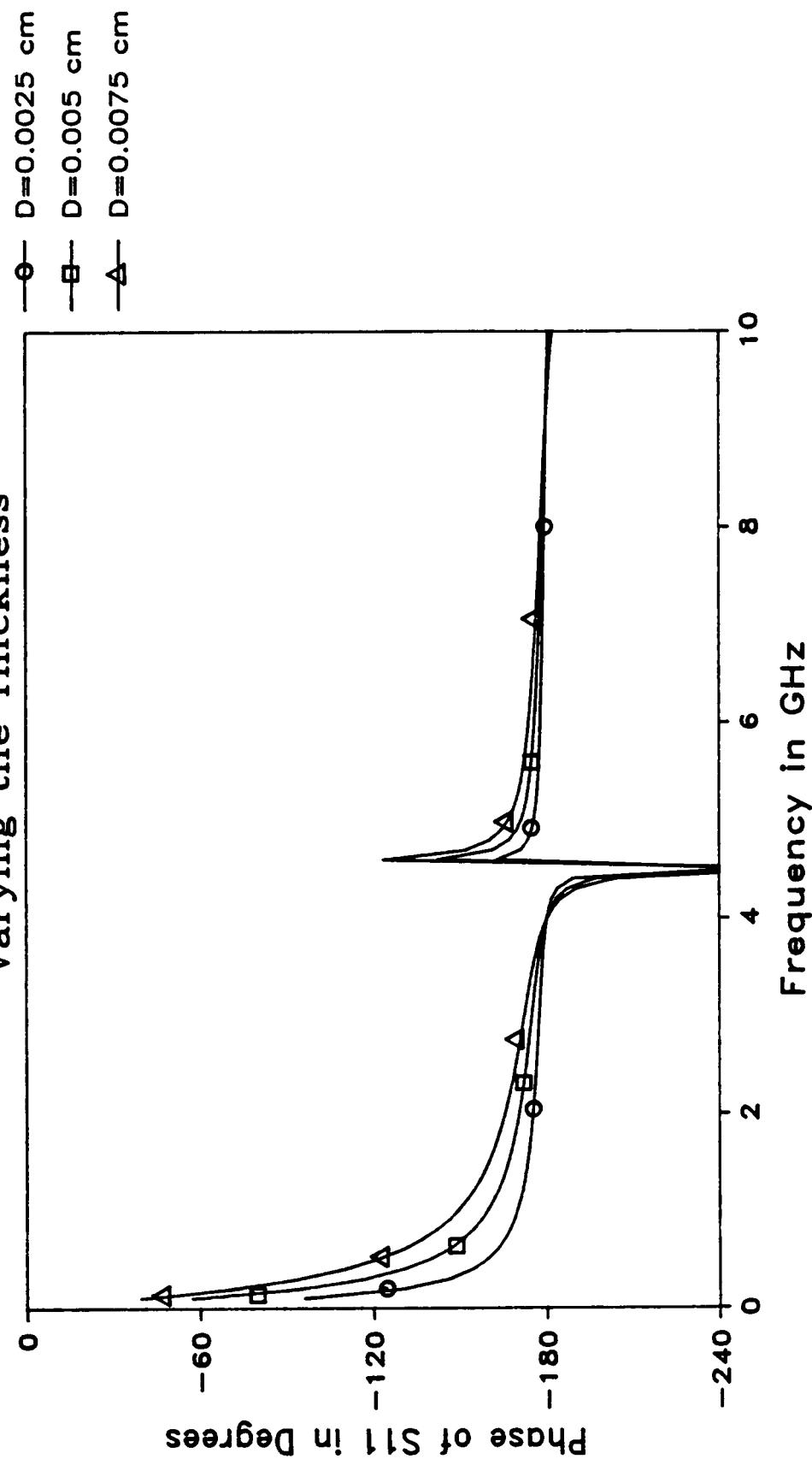
Figure 3.4: Effect of varyimg the thickness.
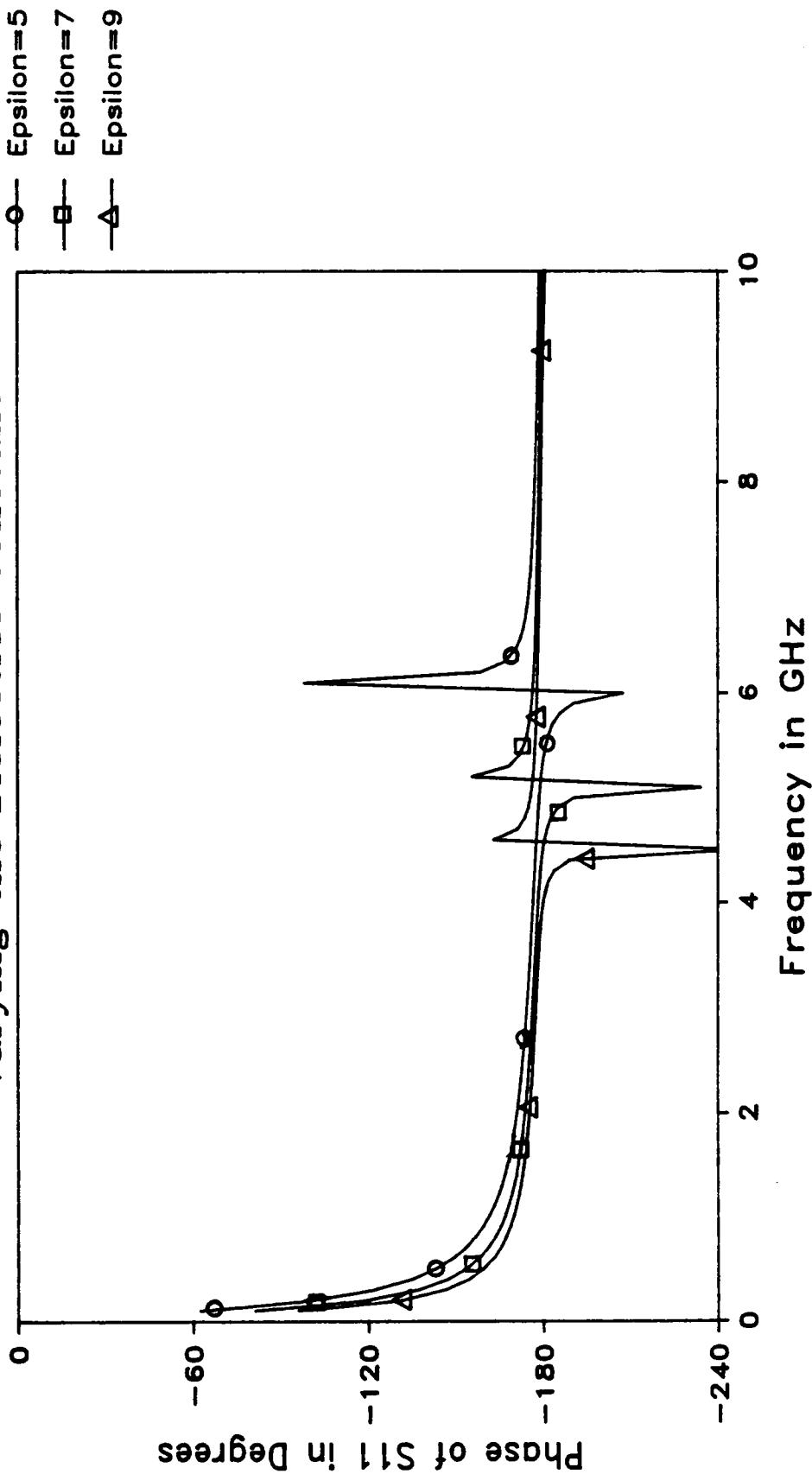
Figure 3.5: Effect of varying the dielectric constant.
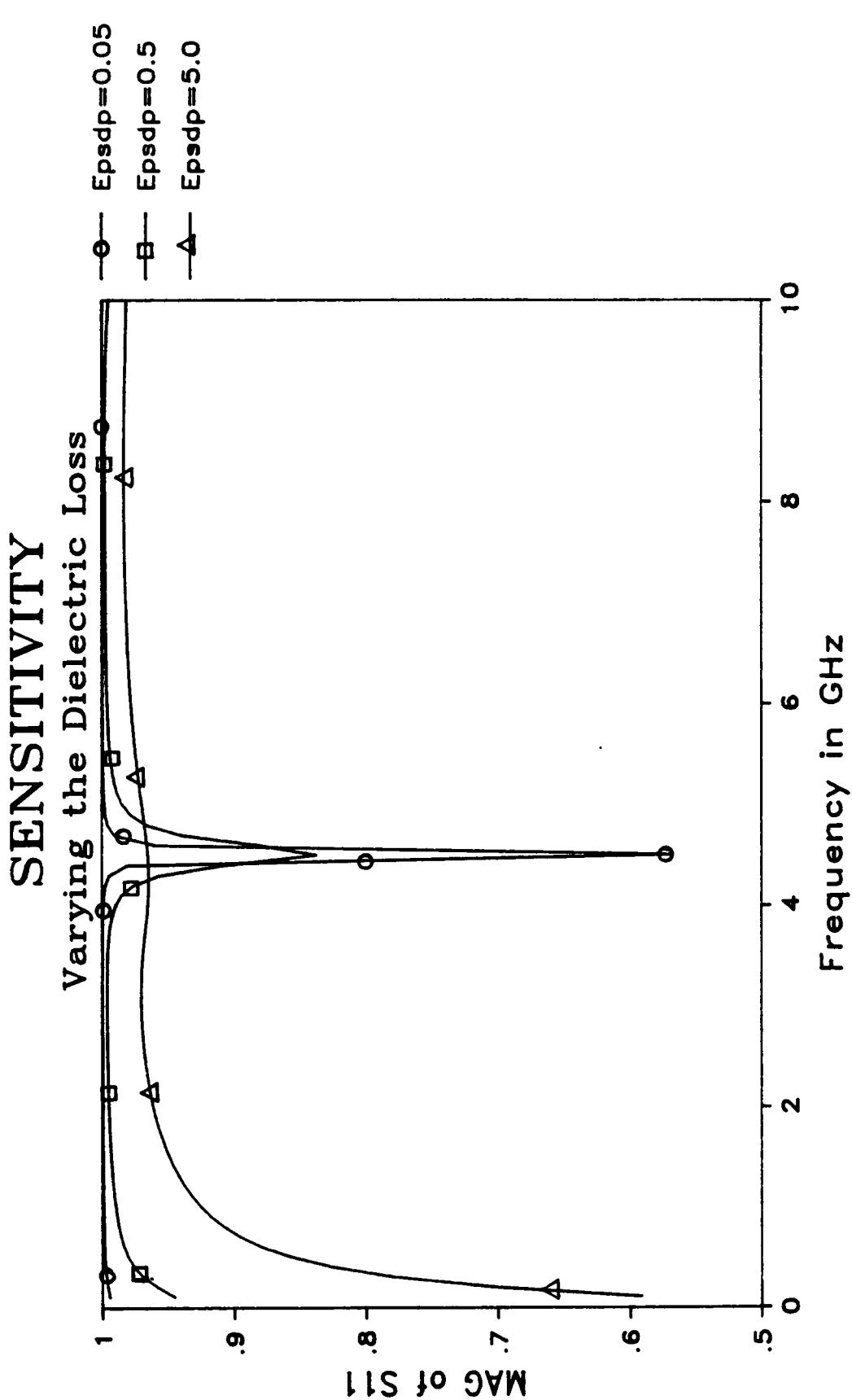
Figure 3.6: Effect of Varying the dielectric loss.
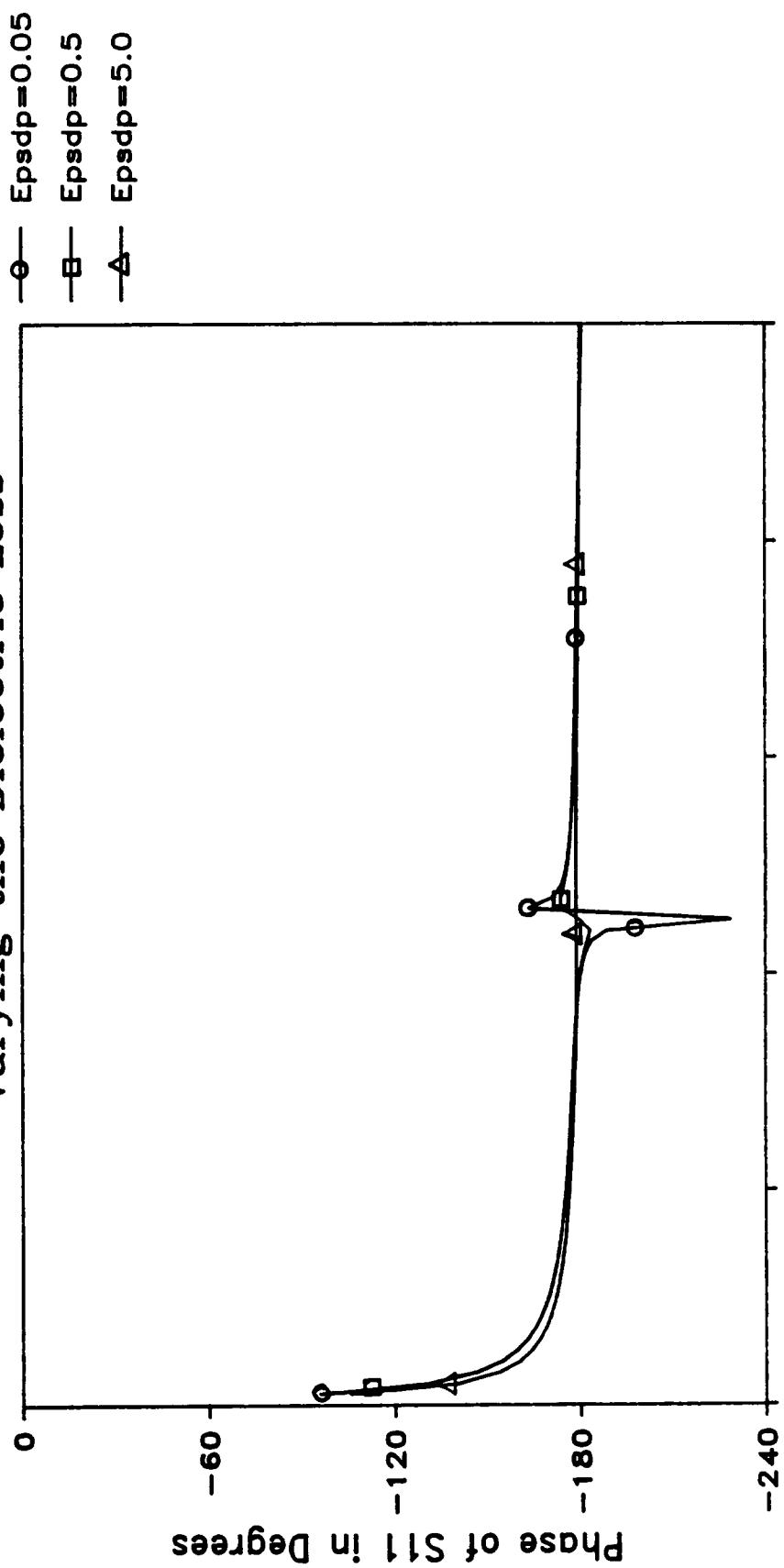
Figure 3.7: Effect of varying the dielectric loss.

when characterizing materials with very low losses, extreme precision in the measurements is necessary.

3.4 Time Domain Measurement Technique:

The experimental set up used in the time domain is that of a typical TDR system. Referring to figure (3.8), the set up consists of a pulse generator, a feed through sampler, a computer interfaced digital processing oscilloscope, and a transmission line terminated with the sample holder. The pulse generator generates a wideband step-like pulse which is launched down the reference line terminated by the WDFC. The feed through sampler provides means to detect the voltage waveforms in the reference line (both the incident and reflected). The digital processing scope digitizes the detected waveforms and forwards the digitized data to the computer for further data processing.
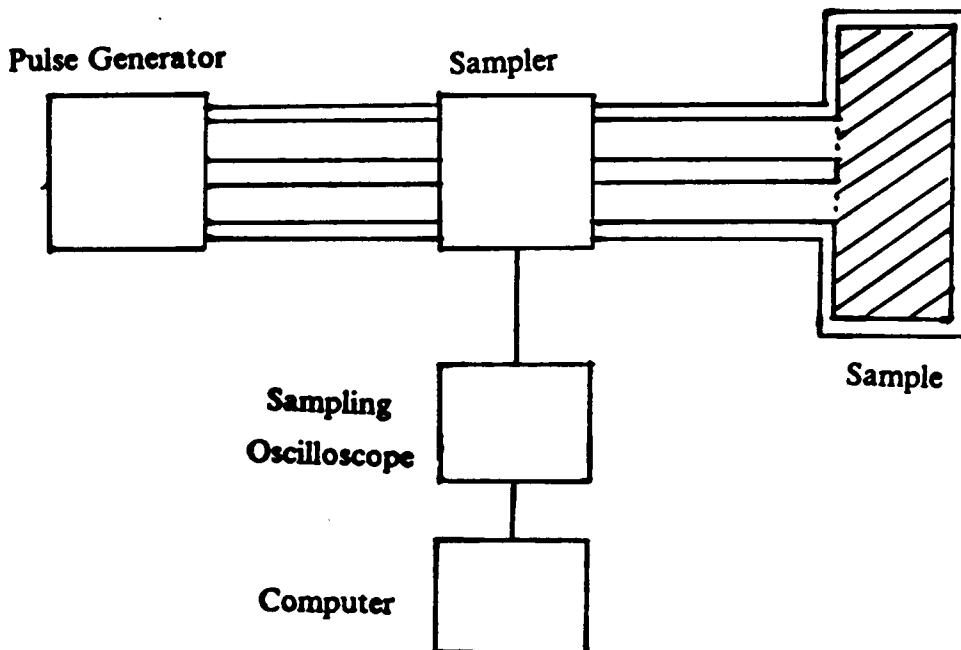
Figure 3.8: The time domain set-up.

From the information contained in the waveforms of the incident pulse and the reflection from the WDFC, the reflection coefficient $S_{11}(j\omega)$ of the WDFC can be computed. The method used to obtain the complex permittivity from $S_{11}(j\omega)$ was described in section 3.2.

To measure $S_{11}(j\omega)$, first the transmission line is terminated with a precision short to acquire the reference waveform, $v_{refr}(t)$. Then, the short is replaced by the WDFC and the response waveform, $v_{resp}(t)$, is acquired. Figures (3.9) and (3.10) show the reference and response waveforms of a sample measurement. The reflection coefficient is then computed by deconvolving $v_{refr}(t)$ from $v_{resp}(t)$ [61]. In this work, a simple division of the frequency domain forms was found to be adequate for the computation of $S_{11}(j\omega)$. The reflection coefficient is, therefore, given by

$$S_{11}(j\omega) = - \frac{V_{resp}(j\omega)}{V_{refr}(j\omega)} \tag{3.94}$$

where $V_{refr}(j\omega)$ and $V_{resp}(j\omega)$ are the Fourier transforms of $v_{refr}(t)$ and $v_{resp}(t)$, respectively. In this work, The complete fast Fourier transformation (CFFT) method [54] is used to compute the Fourier transforms since both $v_{refr}(t)$ and $v_{resp}(t)$ are step-like waveforms (the initial and final values are not equal). In its discrete form, $S_{11}(j\omega)$ is given by

$$S_{11}(k\Delta f) = - \frac{CFFT\{v_{resp}(n\Delta t)\}}{CFFT\{v_{refr}(n\Delta T)\}} \quad , \quad n = 0, 1, ..., N-1 \ , \ k = 0, 1, ..., 2N-1 \tag{3.95}$$

where Δf is the frequency resolution, ΔT is the time sampling interval, and $N\Delta T$ is the length of the time window. Δf and ΔT are related by:

$$\Delta f = \frac{1}{2N\Delta T} \tag{3.96}$$
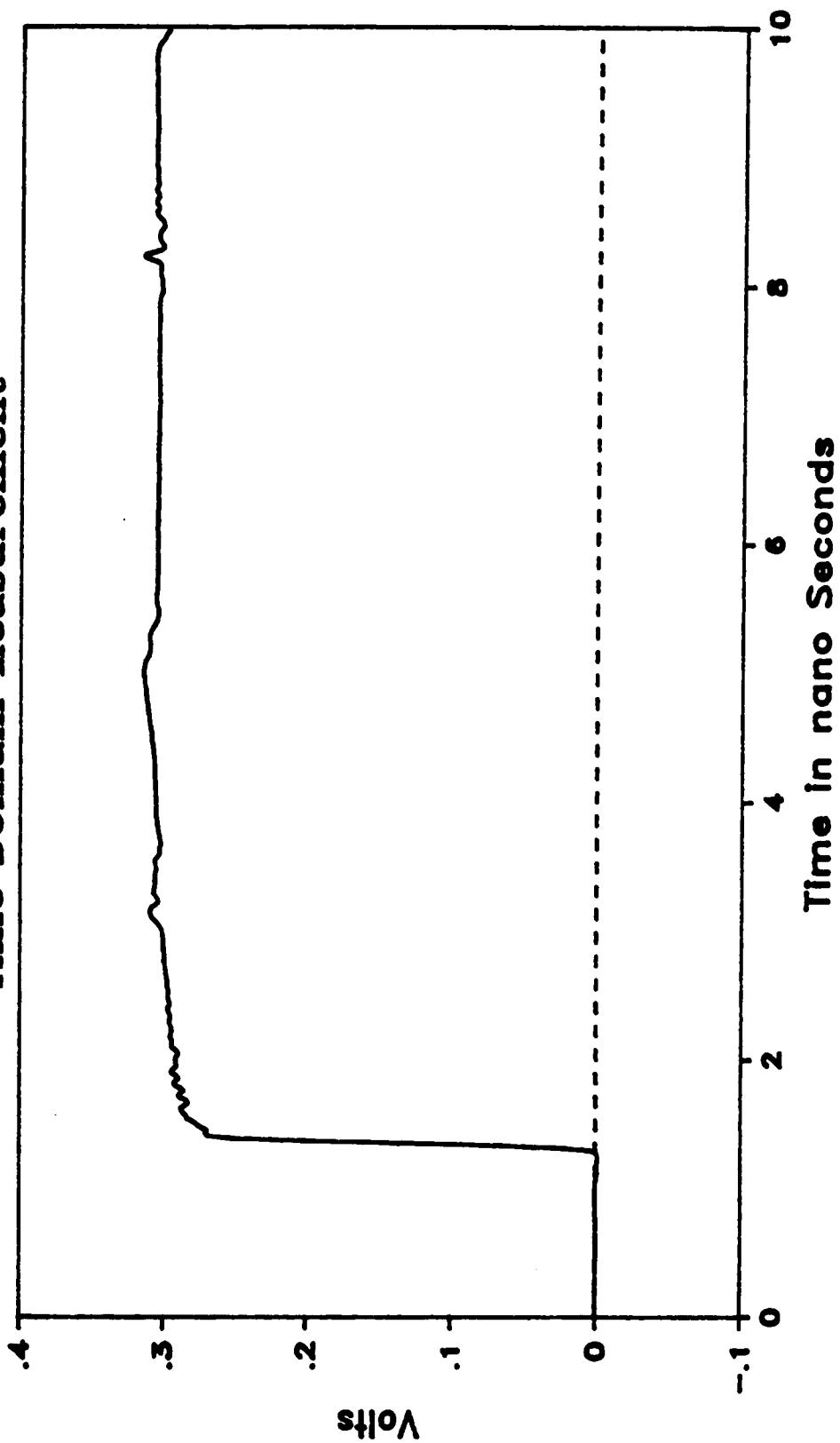
Figure 3.9: Reference waveform for a sample measurement.
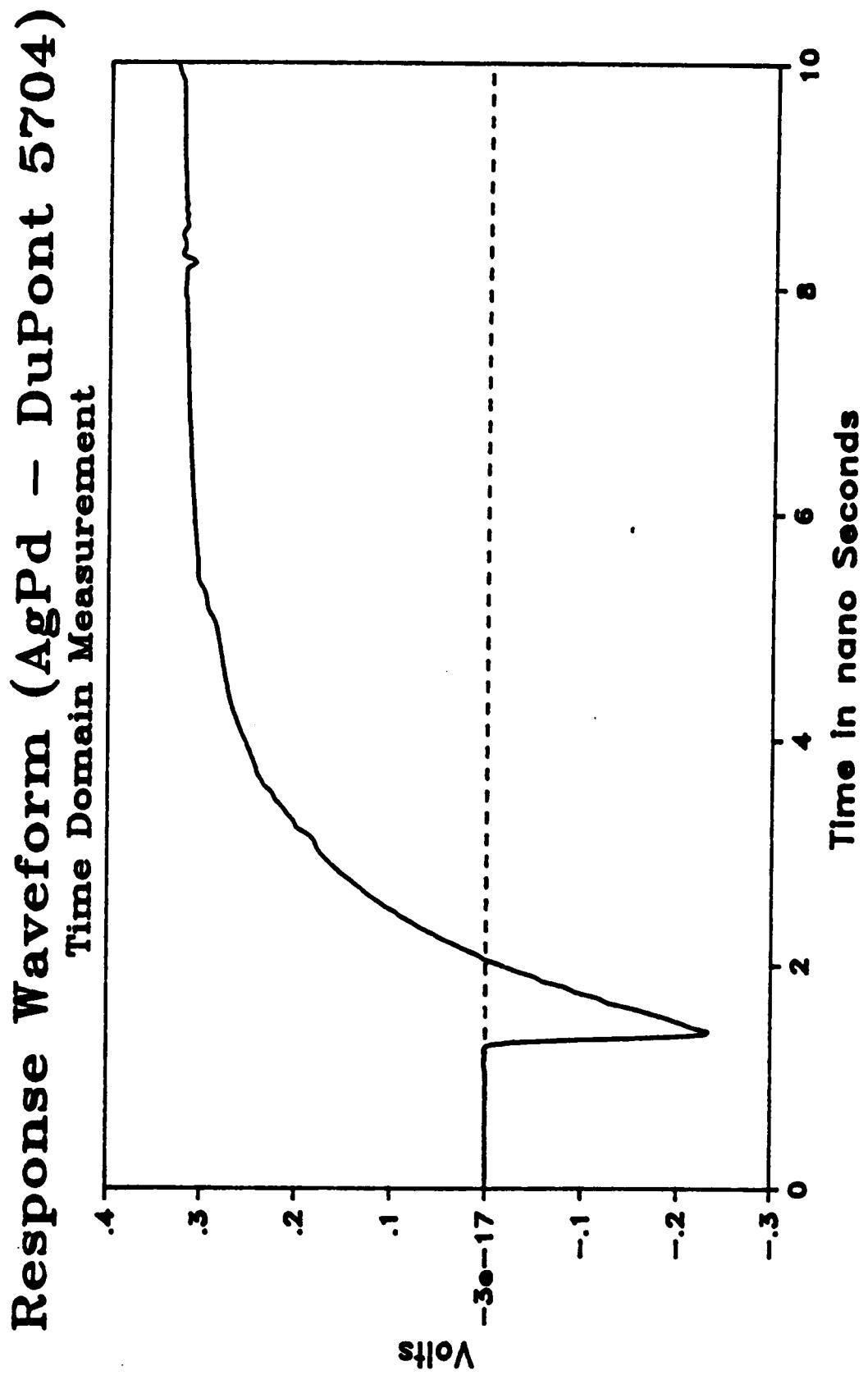
Figure 3.10: Response waveform for a sample measurement.

It is to be noticed that the CFFT technique produces 2N samples (double the resolution).

A computer program was written to enable data acquisition, to implement the complete FFT method, and to compute the reflection coefficient. This program in Tektronix SPS-Basic is listed in appendix VI. Figure (3.11) shows the phase of the reflection coefficient of a sample measurement. The magnitude is shown in figure (3.12).

Equipment used:

The following is a list of the equipment used in the setup:

1. Pulse generator: Picosecond Pulse Labs 4050A.

    - Note: The 4050A pulse generator was used because it has been found out that it is much less sensitive to loading than the Tektronix S52 tunnel diode pulse generator. In other words, the tunnel diode waveform suffers from both voltage and time offsets as the termination of the line is changed. The voltage offset can be corrected; However, the time offset transforms into a linear phase component in the reflection coefficient. If this linear phase component is not removed, serious errors will be introduced in the results. The removal of this linear component is not an easy task. Although the 4050A pulse generator covers a smaller bandwidth than the tunnel diode, it was adequate for the bandwidth of our measurements.

2. Sampler: Tektronix S6 feed through sampling head.

3. Scope: Tektronix 7704A digital processing oscilloscope.
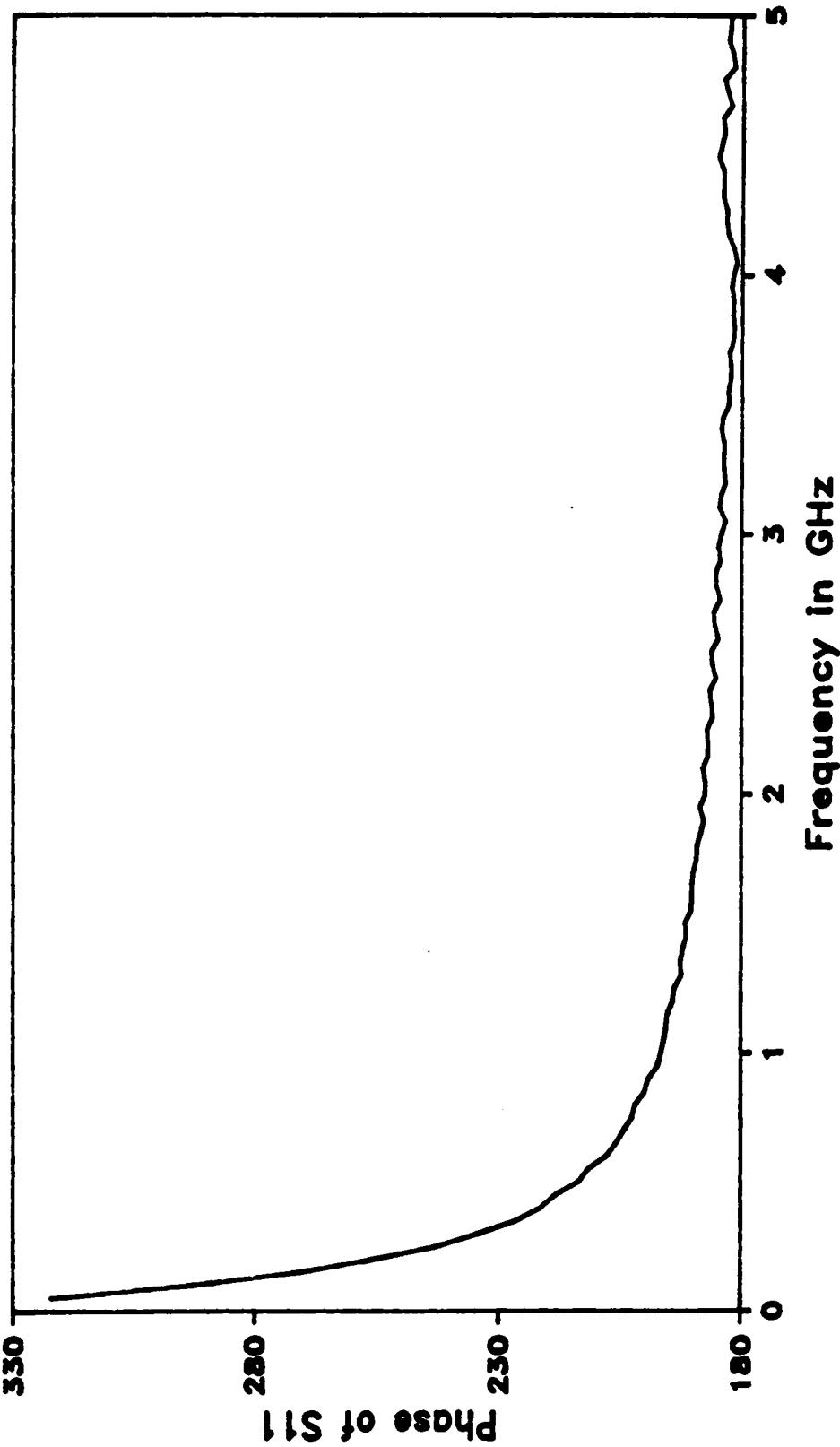
Figure 3.11: Phase of the reflection coefficient.
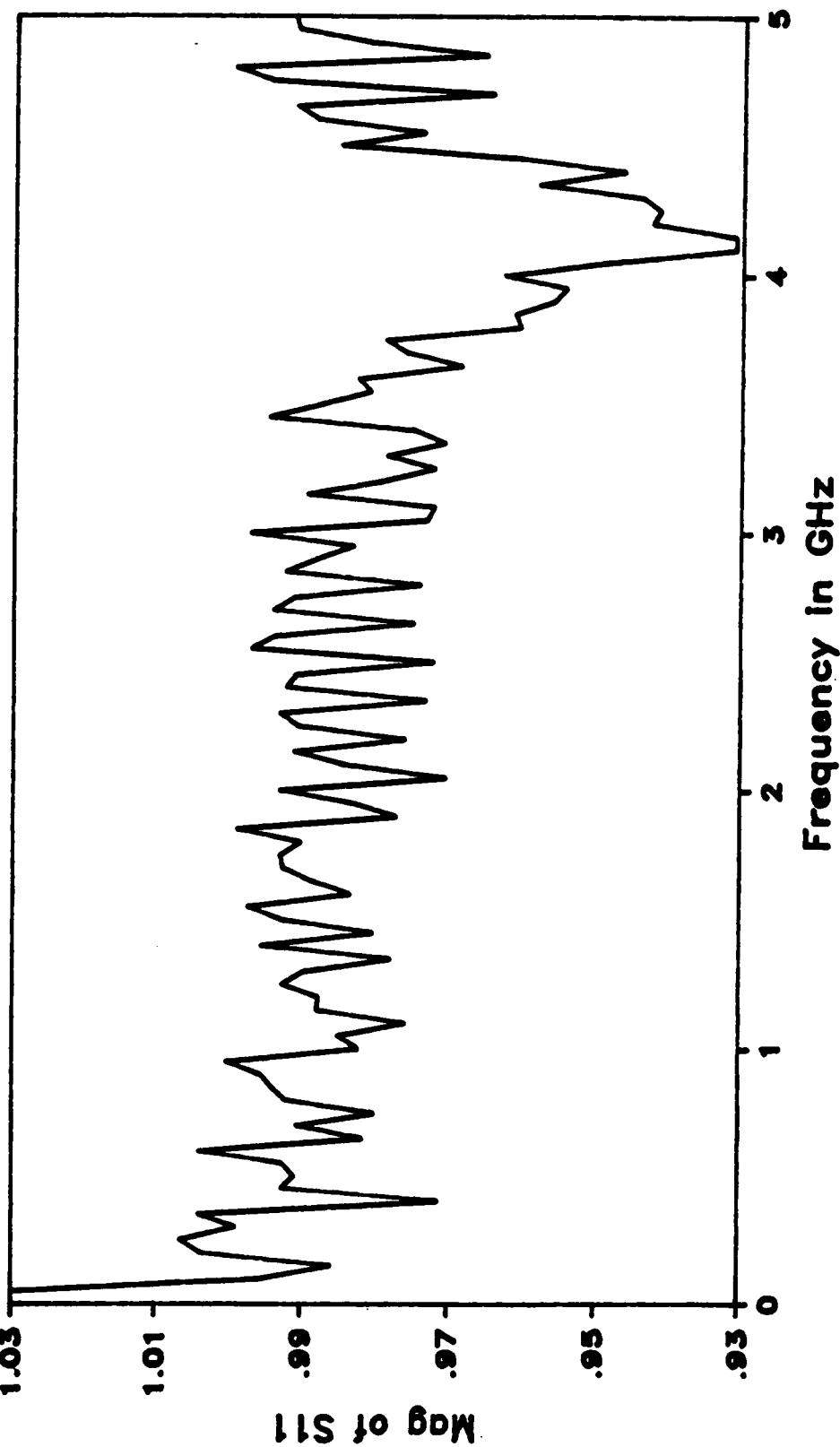
Figure 3.12: Magnitude of the reflection coefficient.

4.   Computer : PDP-11/34 minicomputer.

3.5 Experimental Results:

This section presents the results of experiments performed in both the time and frequency domain [60] for dielectric characterization using the WDFC technique. First, some experiments are performed using known materials in order to verify both the technique and as well as the used computer code. Another verification experiment using the resonances of the WDFC in determining the dielectric constant of the filling material was also performed. Following the verification, actual measurements are performed on two types of thick film dielectric pastes both made by DuPont; the DuPont 5704 thick film paste and the PCM dielectric paste. This section presents only the final results obtained from the analysis of the data collected from these experiments. The results are in the form of graphs of the complex permittivity versus frequency.

3.5.1 Verification:

Four verification experiments were performed. First, the capacitance of a standard (HP-OPEN) used in the calibration of the Network Analyzer is estimated using WDFC technique. The results are compared to the data provided by HP. The second experiment involves the characterization of a Quartz sample (fused silica) for which the dielectric constant is known to be 3.78. The third experiment uses a sample of teflon ($\varepsilon'_r = 2.1$). The last experiment uses the resonant frequencies of the cavity to estimate the dielectric constant. The dielectric constant obtained using the WDFC technique is compared to the dielectric constant estimated using the resonant frequencies of the

cavity. As will be seen later, the resonance method is capable of yielding results beyond the bandwidth obtained using the WDFC technique due to sample thickness and the measurement system precision. However, the resonance technique produces results only at the measured resonant frequencies (few GHz frequency intervals).

(1) HP-Open:

The HP-open is a standard "reference" open circuit termination made by Hewlett-Packard company and is typically used in the calibration of the network analyzer. As shown in figure (3.13), there is a piece of Polystirene in the middle to compress the spring loaded center conductor of the air line (or the APC-7 connector).
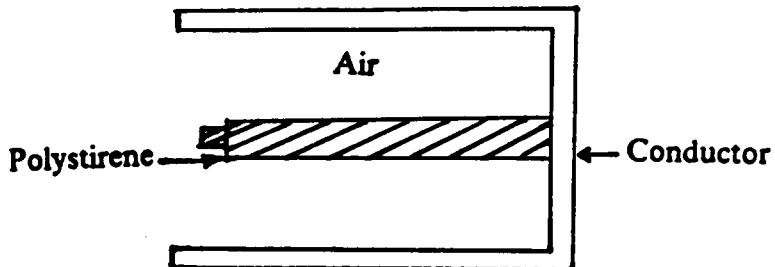
Figure 3.13: HP - Open

HP provides a formula from which the capacitance can be computed . The presence of the polystirene piece in the center, eliminates the possibility of computing the capacitance of the open precisely, using the developed model. But, the capacitance may be estimated assuming there is no polystirene, and also assuming the open is filled with polystirene, which has a dielectric constant of 2.56. The obtained results should bound the capacitance values given by the HP catalog. The program which computes the reflection coefficient for a given the permittivity was used to compute the capacitance for an air filled cavity and for a polystirene filled cavity. The cavity's dimensions are the
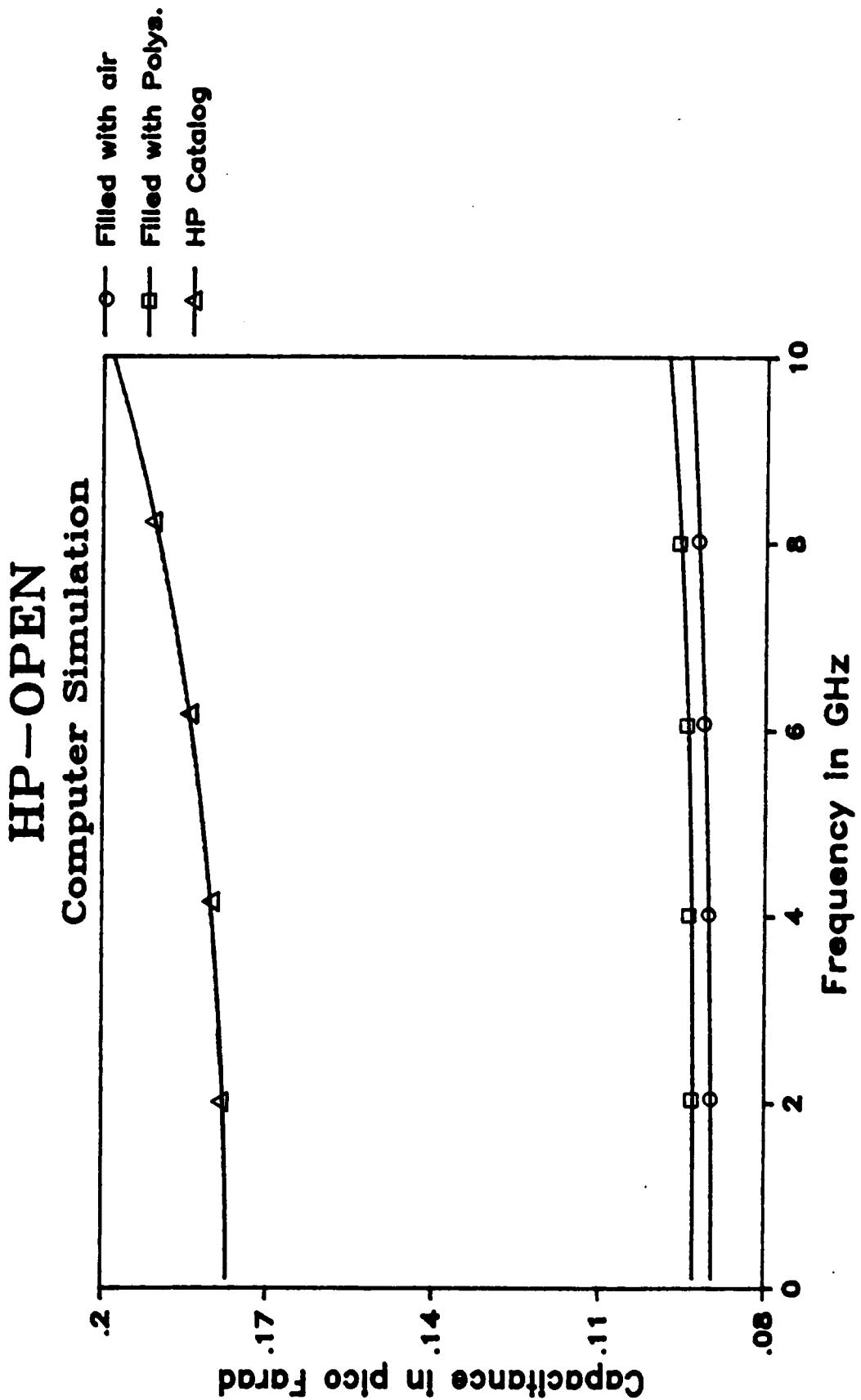
Figure 3.14: Capacitance of HP-Open.

proper dimensions of the HP-Open. The results are plotted in figure (3.14) and they are in good agreement with our predictions.

(2) Quartz Sample:

In this experiment, the permittivity of a disk of fused silica quartz is estimated. To construct a WDFC sample, the quartz disk was coated with a conductor which acted as the cavity walls. Aluminium was deposited on one side of the sample by using a sputtering unit. The disk edges as well as the backside were covered with silver epoxy and the backside was fixed to a supporting material for rigidity and handling. Fused Silica quartz is known to have a dielectric constant of 3.78. The main problem in performing the measurement is the proper alignment of the sample holder to the air line. This was the main source of error. The measurement was performed in the time domain and frequency domain. The calculated dielectric constant ε', is shown in figure (3.15). Figure (3.16) shows the loss ε'', . We notice that both the time domain and frequency domain measurements yield comparable results, which also agree with the actual value.

(3) Teflon Sample:

This experiment suffered from the problem of constructing the sample holder walls on the teflon disk. The reason for this problem is the difficulty encountered in finding a conductor material that adheres to teflon. Consequently, the conductor walls were constructed mechanically using copper. This resulted in air gaps between the teflon disk and the cavity walls. The measurement was performed in the time domain. The result is shown in figure (3.17). The dielectric constant of teflon is 2.1. The main source of error in our calculations is due to the presence of the air gaps.

(4) Using Resonance:

In this experiment, samples of DuPont 5704 thick film dielectric material were made.
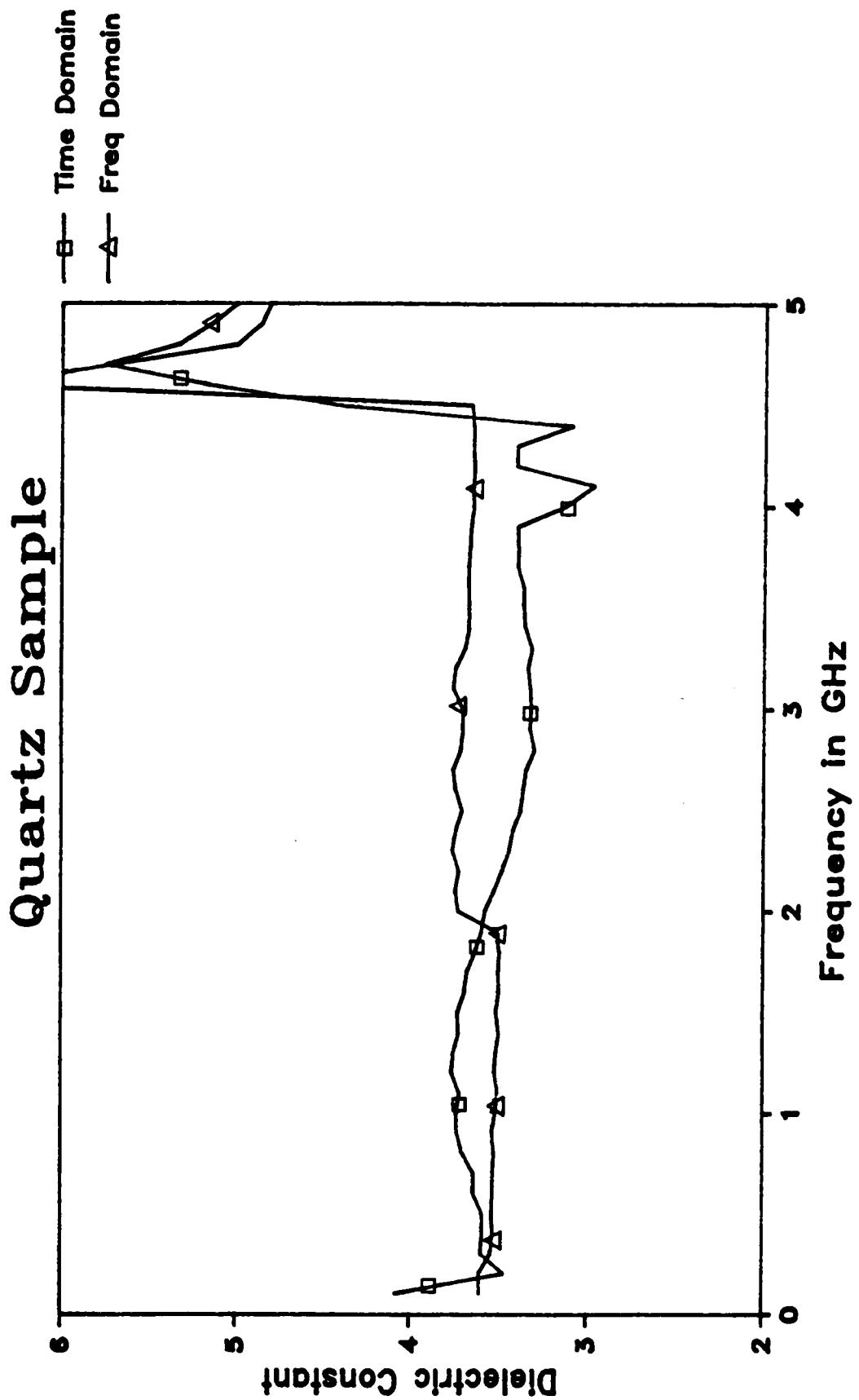
Figure 3.15: Dielectric constant of a quartz sample.
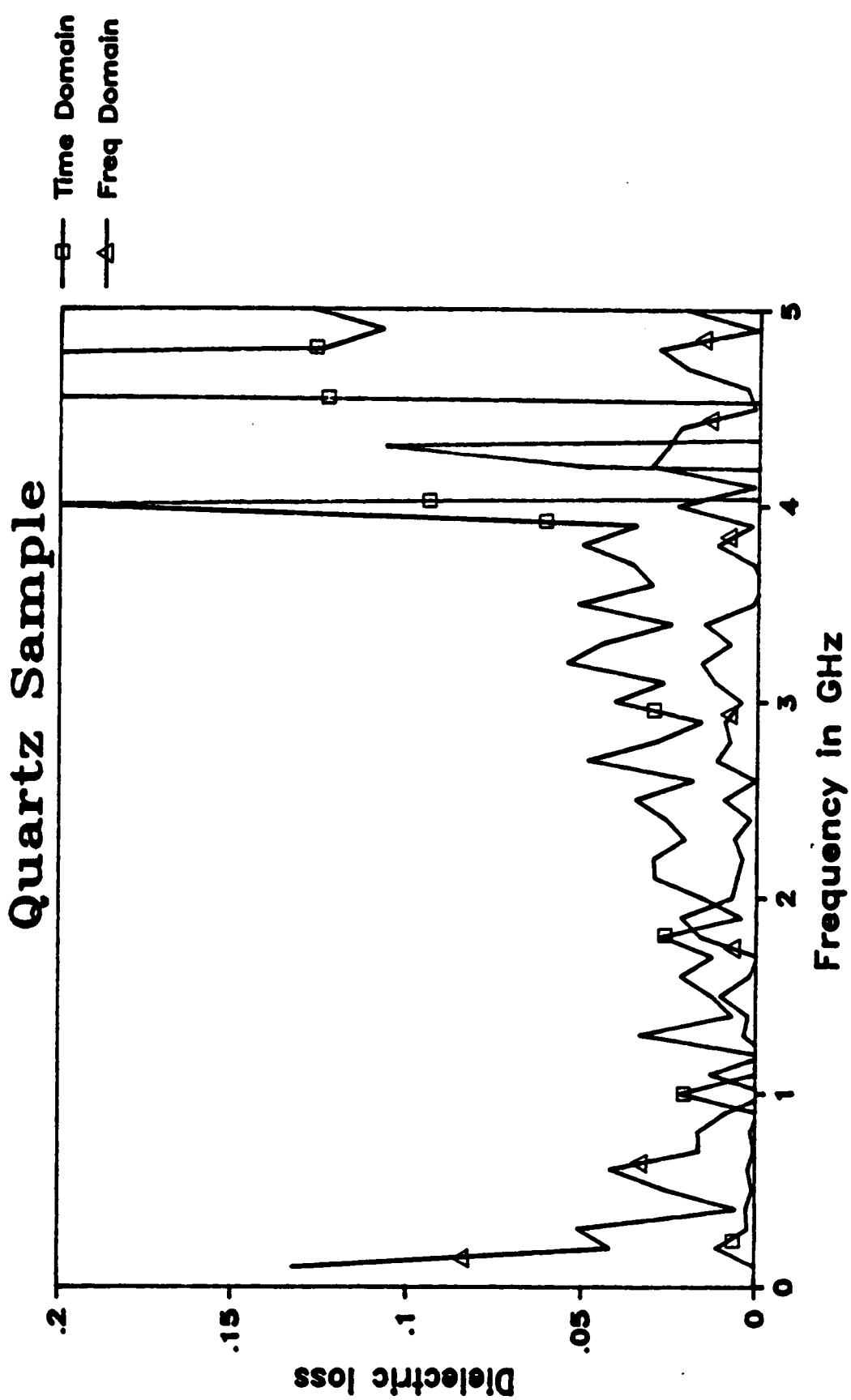
Figure 3.16: Dielectric loss of a quartz sample.
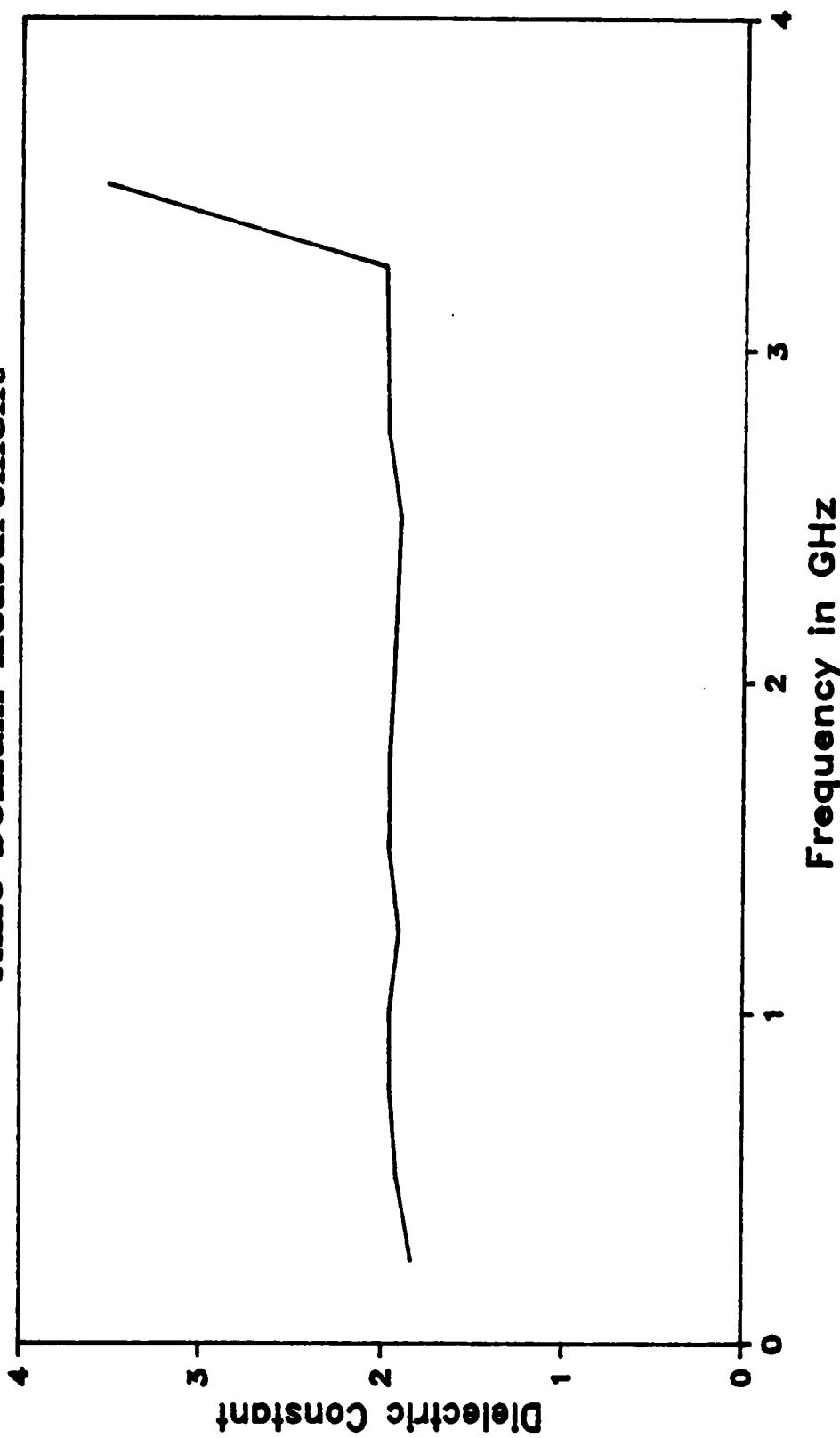
Figure 3.17: Dielectric constant of a teflon sample.

These samples have different diameters. The thickness of these samples is in the order of 30 microns. Therefore, the dominant resonances are given by

$$f_n = \frac{c}{\sqrt{2\pi\varepsilon_r}} \frac{x_{on}}{R} \qquad (3.97)$$

where x_{on} is the nth zero of the zero order Bessel function of the first kind, c is the speed of light and R is the radius of the sample holder. Neglecting the loss and thus assuming that the permittivity is real then the dielectric constant is given by

$$\varepsilon_r(f_n) = \left\{ \frac{c}{2\pi f_n} \frac{x_{on}}{R} \right\}^2 \qquad (3.98)$$

The measurements of these samples were performed in the frequency domain [60]. Figures (3.18) and (3.19) show the magnitude and phase of the reflection coefficient of a sample with 4 cm diameter. The resonances are easier to detect from the magnitude plot. From figure (3.18) and using equation(3.98), the resonant frequencies and the corresponding values of the estimated dielectric constant are given in table I. Figures (3.20) and (3.21) show the magnitude and phase of the reflection coefficient of a second sample with 6 cm diameter. Following the same procedure, the resonant frequencies and the corresponding values of the estimated dielectric constant are given in table II. As will be shown in section (3.5.2) these values agree fairly well with the values obtained using our technique. The reasons for the discrepancies are the following sources of error:

1. There is some error in the values of the measured resonant frequencies due to the frequency resolution used and also due to the quality factor of the cavity.

FREQUENCY DOMAIN MEASUREMENT
AgPd – DuPont 5704 Disk (Diameter = 4 cm)
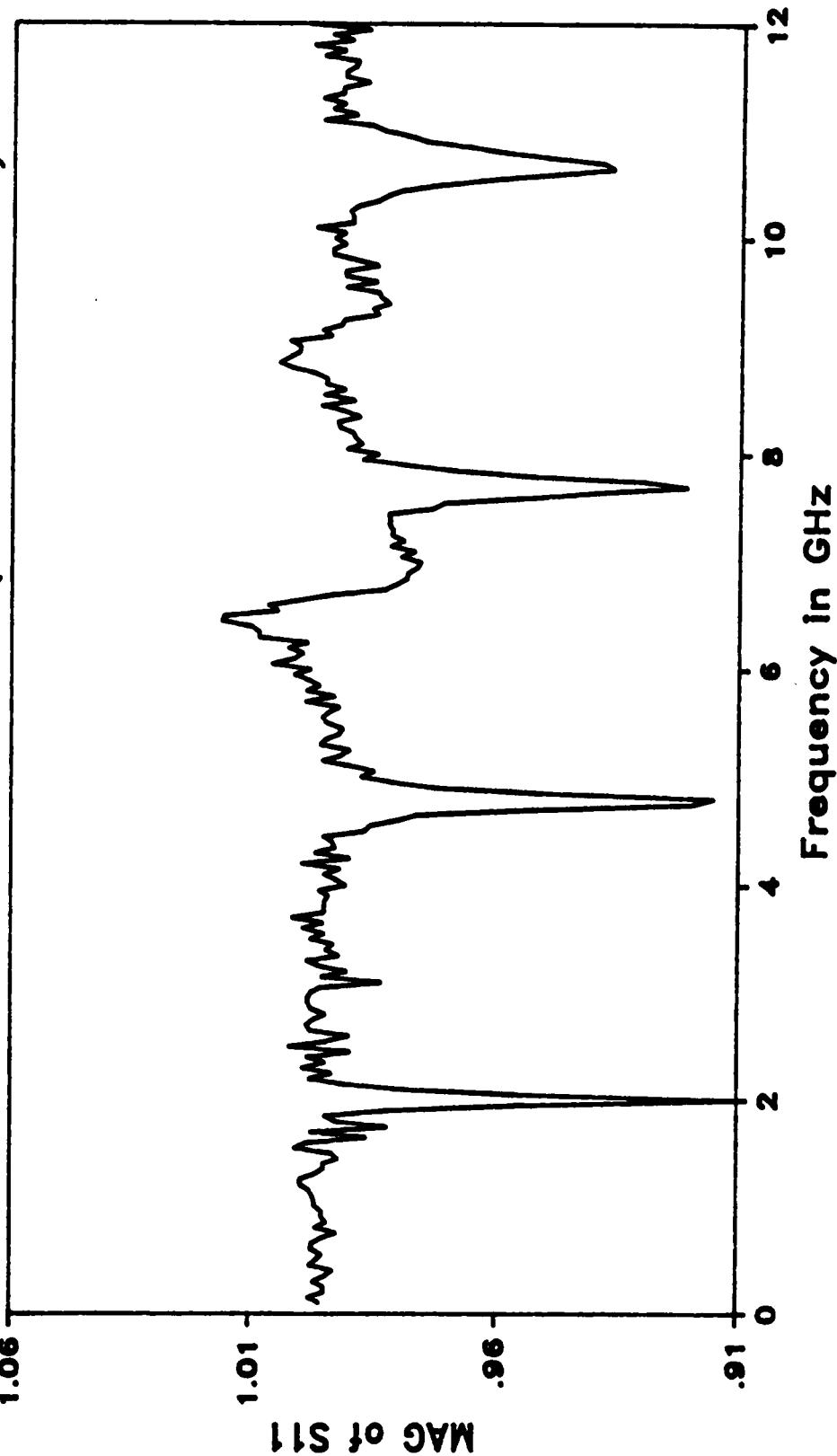
Figure 3.18: Magnitude of the reflection coefficient of a sample whose diameter is 4 cm.

FREQUENCY DOMAIN MEASUREMENT
AgPd – DuPont 5704 Disk (Diameter = 4 cm)
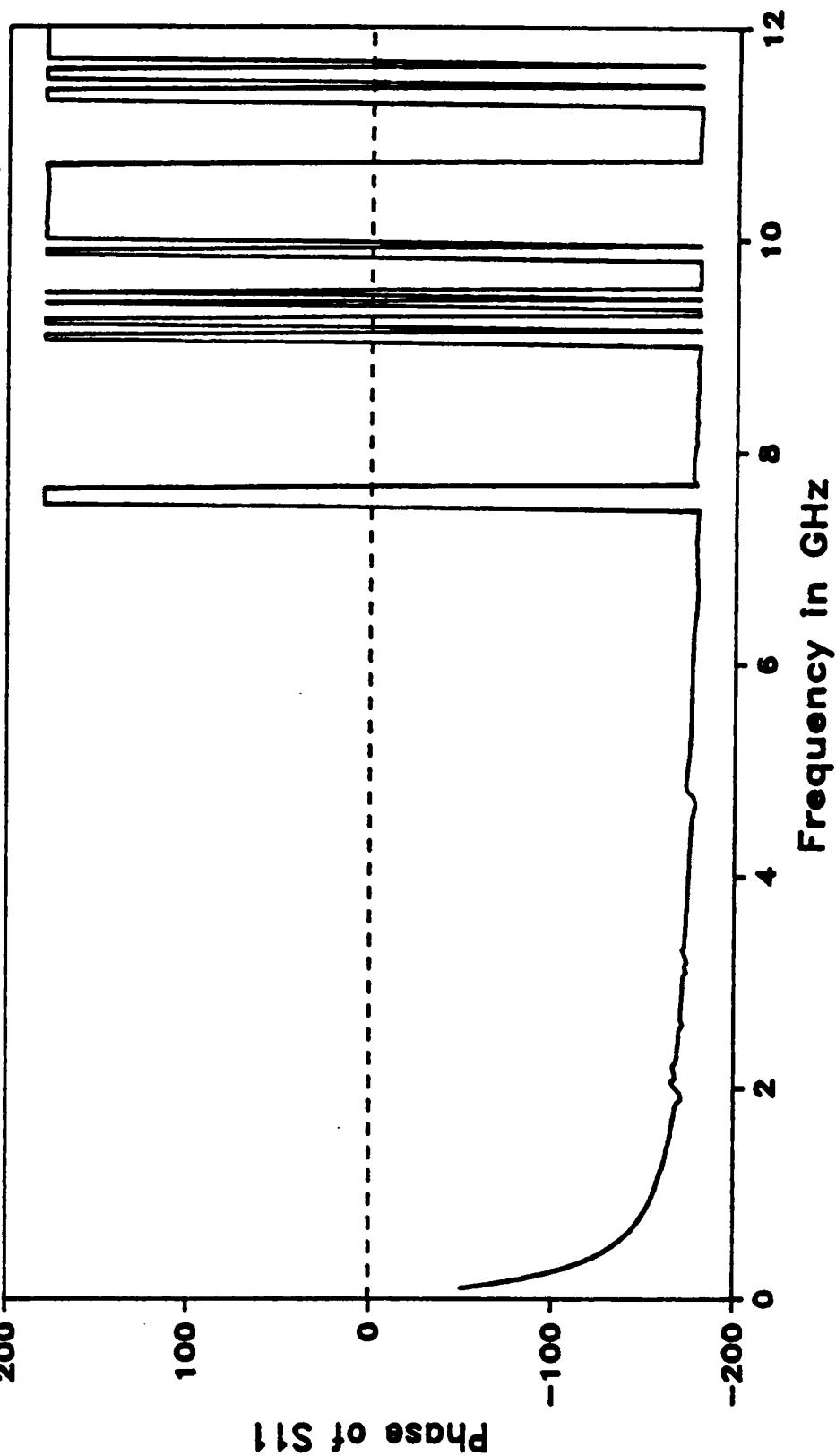
Figure 3.19: Phase of the reflection coefficient of a sample whose diameter is 4 cm.
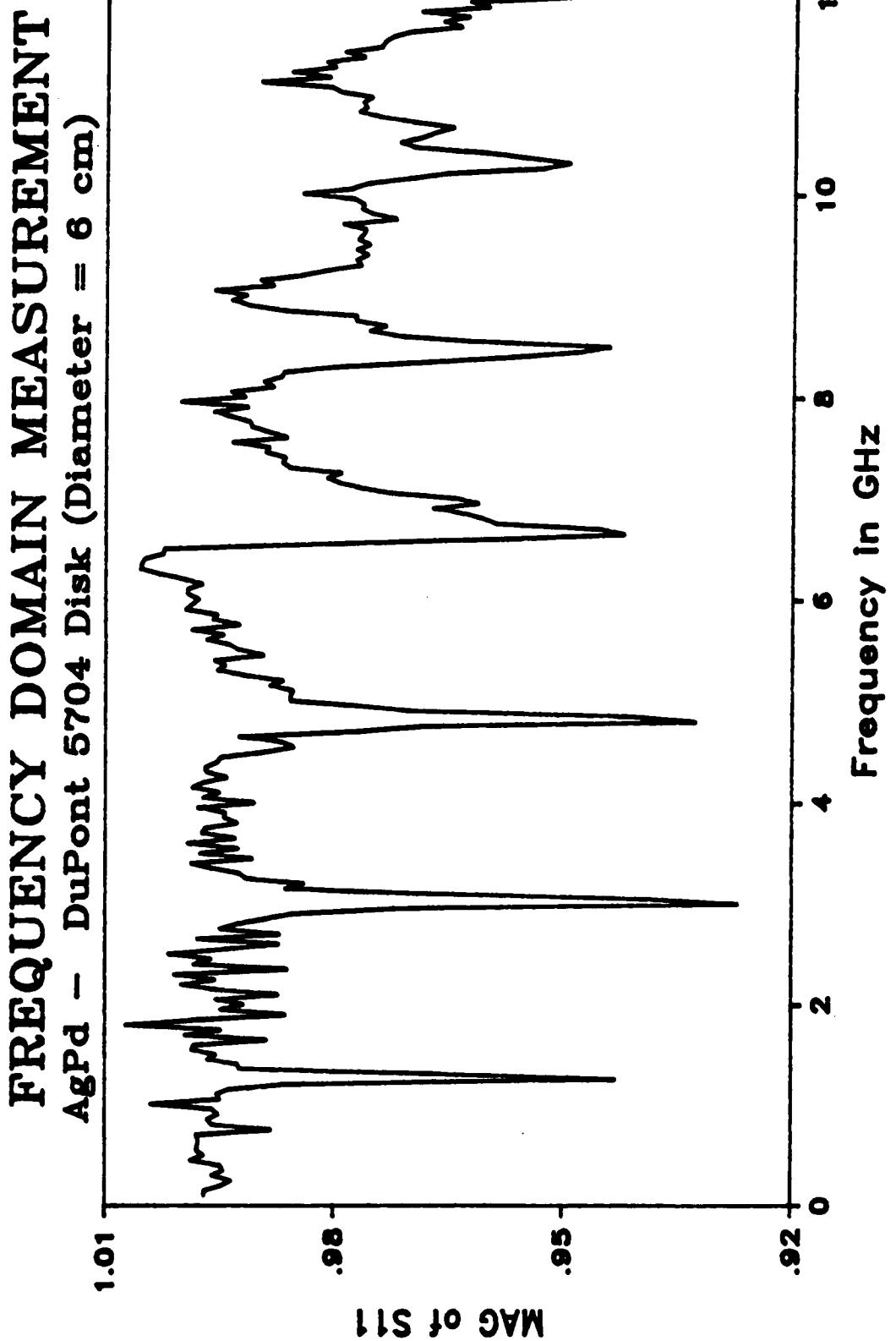
Figure 3.20: Magnitude of the reflection coefficient of a sample whose diameter is 6 cm.
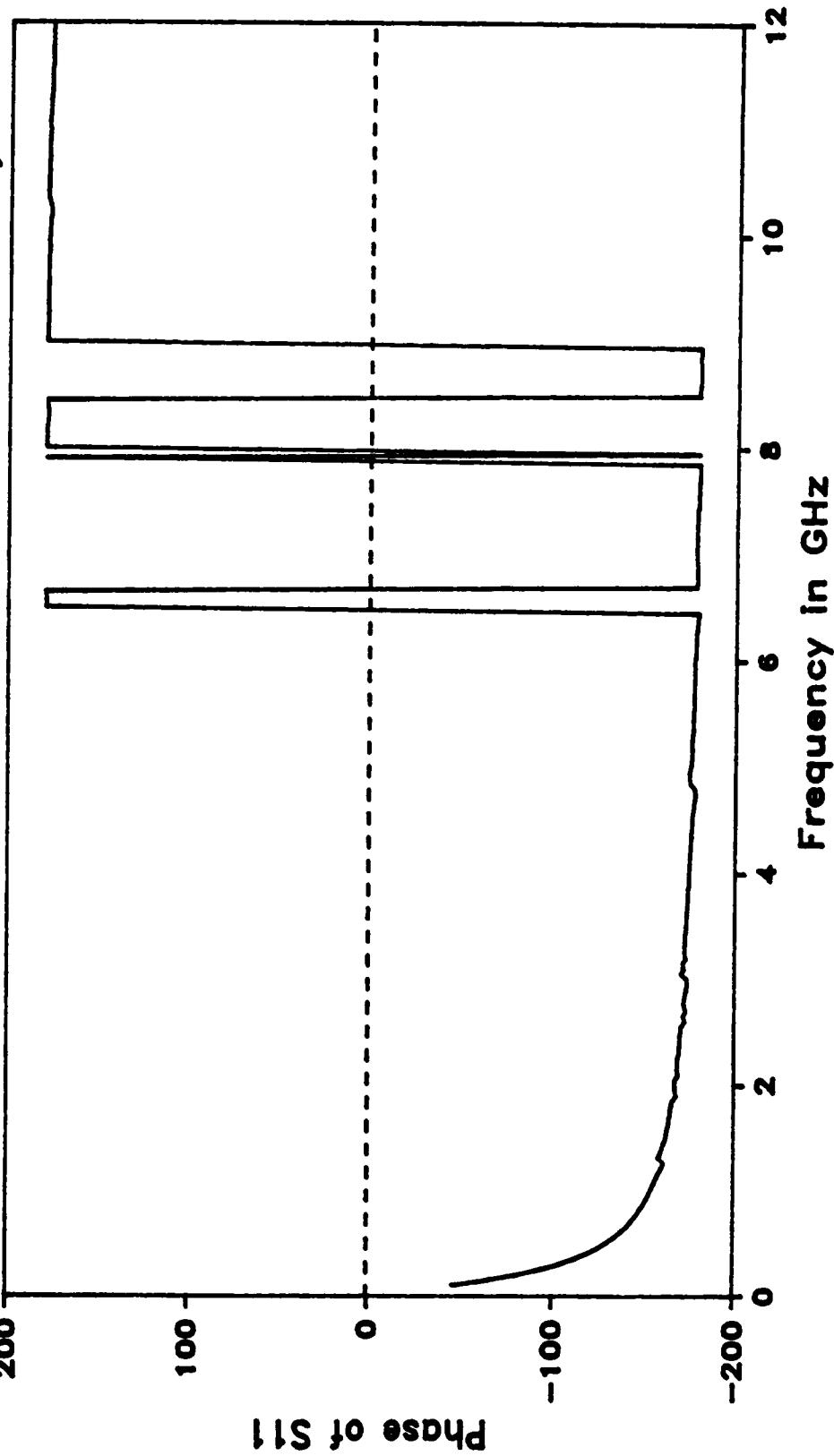
Figure 3.21: Phase of the reflection coefficient of a sample whose diameter is 6 cm.

Table I: Estimated dielectric constant using resonance for a 4 cm disk.

n	f(GHz)	dielectric constant
1	2	8.94
2	4.8	8.2
3	7.7	7.8
4	10.65	7.58

Table II: Estimated dielectric constant using resonance for a 6 cm disk.

n	f(GHz)	dielectric constant
1	1.25	9.69
2	3	8.87
3	4.8	8.51
4	6.65	8.23
5	8.5	8.08
6	10.3	8.01

2. The formula used to relate the resonant frequencies to the dielectric constant is for a closed cavity, and therefore, it is only approximate in our case because of the loading of the transmission line feeding the cavity.

3. Losses in the conductor walls forming the cavity as well as the dielectric loss degrade the quality factor, and hence, makes it harder to determine the accurate resonant frequencies.

3.5.2 Experiments on Some Thick Film Dielectric Materials:

This section presents results of some experiments performed in the frequency domain and the time domain on samples made of DuPont 5704 and DuPont PCM thick film dielectric materials. Figure (3.22) shows the dielectric constant $(\varepsilon',)$ obtained for DuPont 5704 sample while figure (3.23) shows the loss $(\varepsilon,'')$. The results for the PCM sample are shown in figures (3.24) and (3.25). As shown in all these plots, the time domain results agree with the frequency domain results. The loss results in figures (3.23) and (3.25) may have some errors for the following two reasons:

1. The conductor material used to form the walls of the cavity are not perfectly lossless. Therefore, the loss obtained is not only due to dielectric loss, but also has a contribution from the conductor losses. This is very significant if the dielectric materials have very low losses.

2. These materials may have very low losses, and thus very precise measurements of the reflection coefficient have to be performed. Our measurement systems are fairly precise but may not have the needed precision at present. Another source of error in this measurement is the alignment problem. The sample holder was attached to
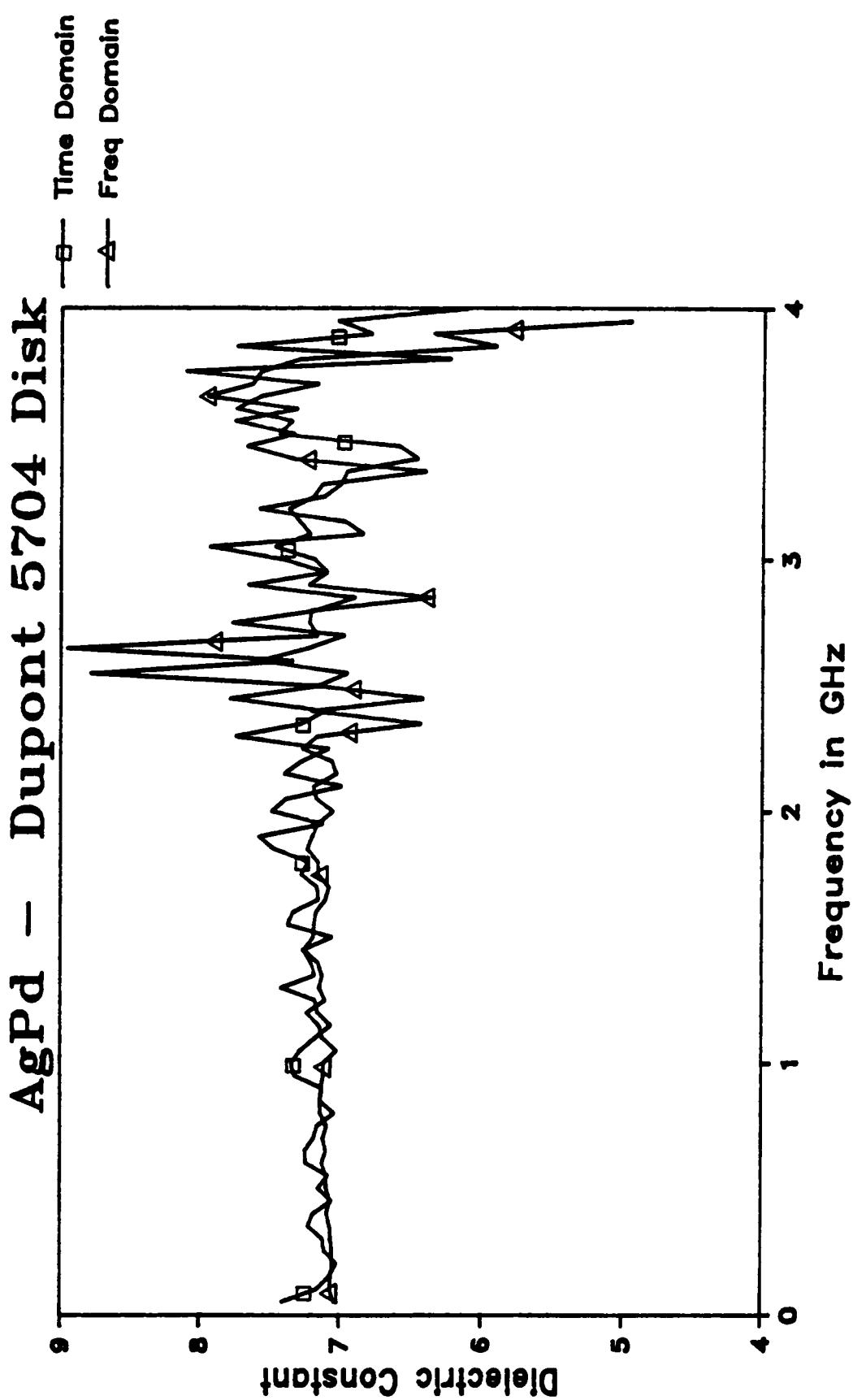
Figure 3.22: Dielectric constant of a DuPont 5704 thick film sample.

AgPd – Dupont 5704 Disk

Time Domain
Freq Domain

Dielectric loss

Frequency in GHz
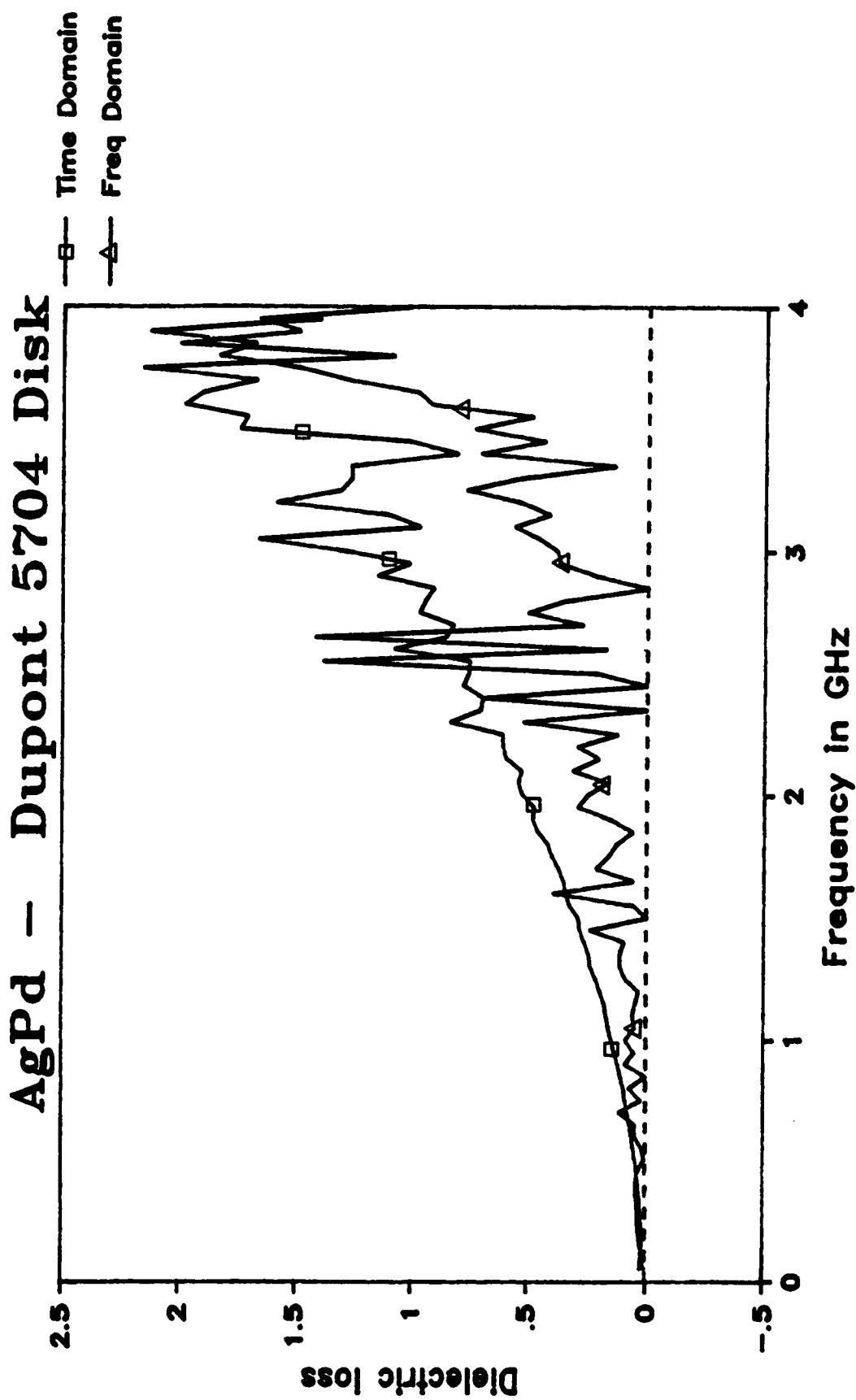
Figure 3.23: Dielectric loss of a DuPont 5704 thick film sample.
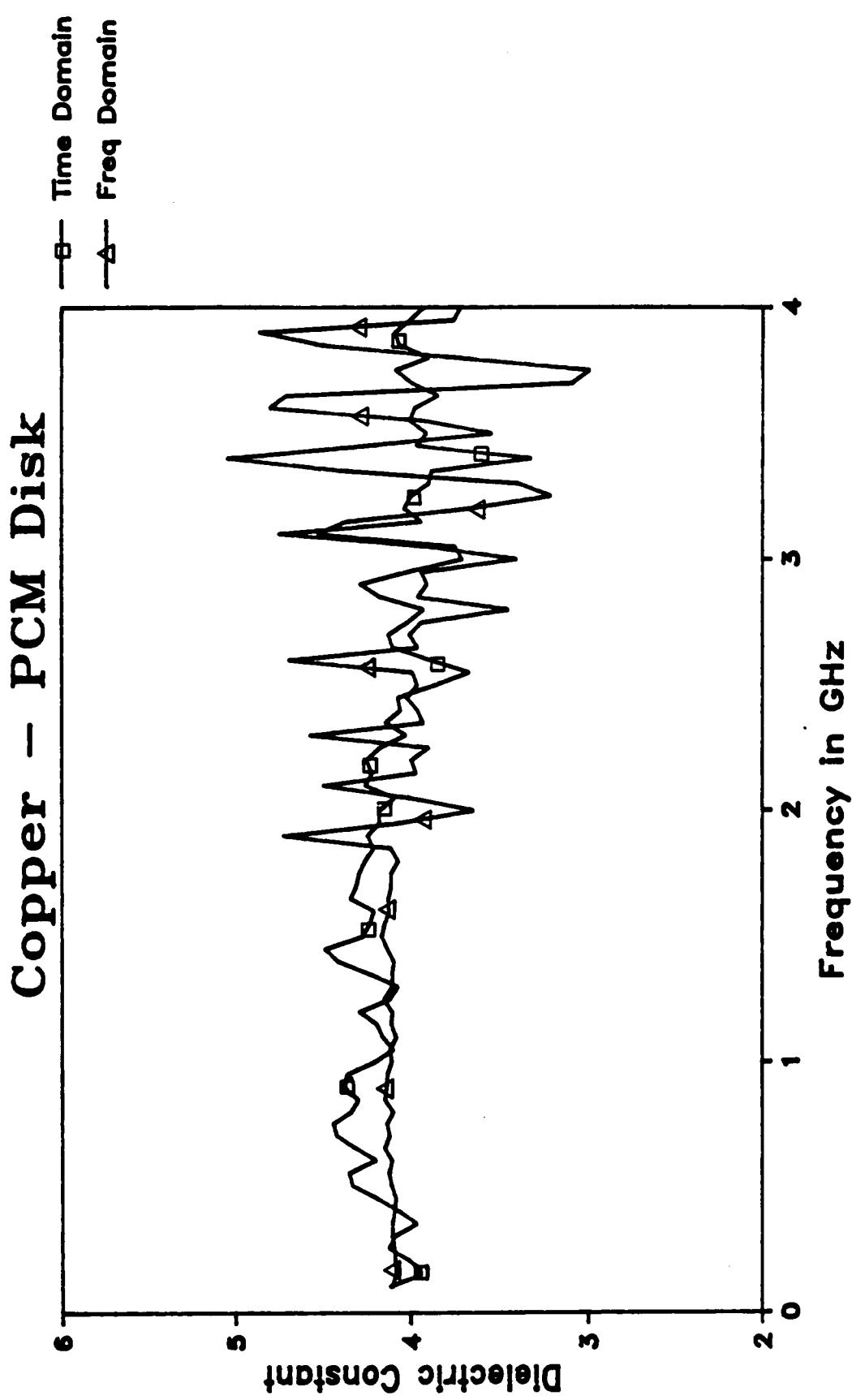
Figure 3.24: Dielectric constant of a DuPont PCM dielectric sample.
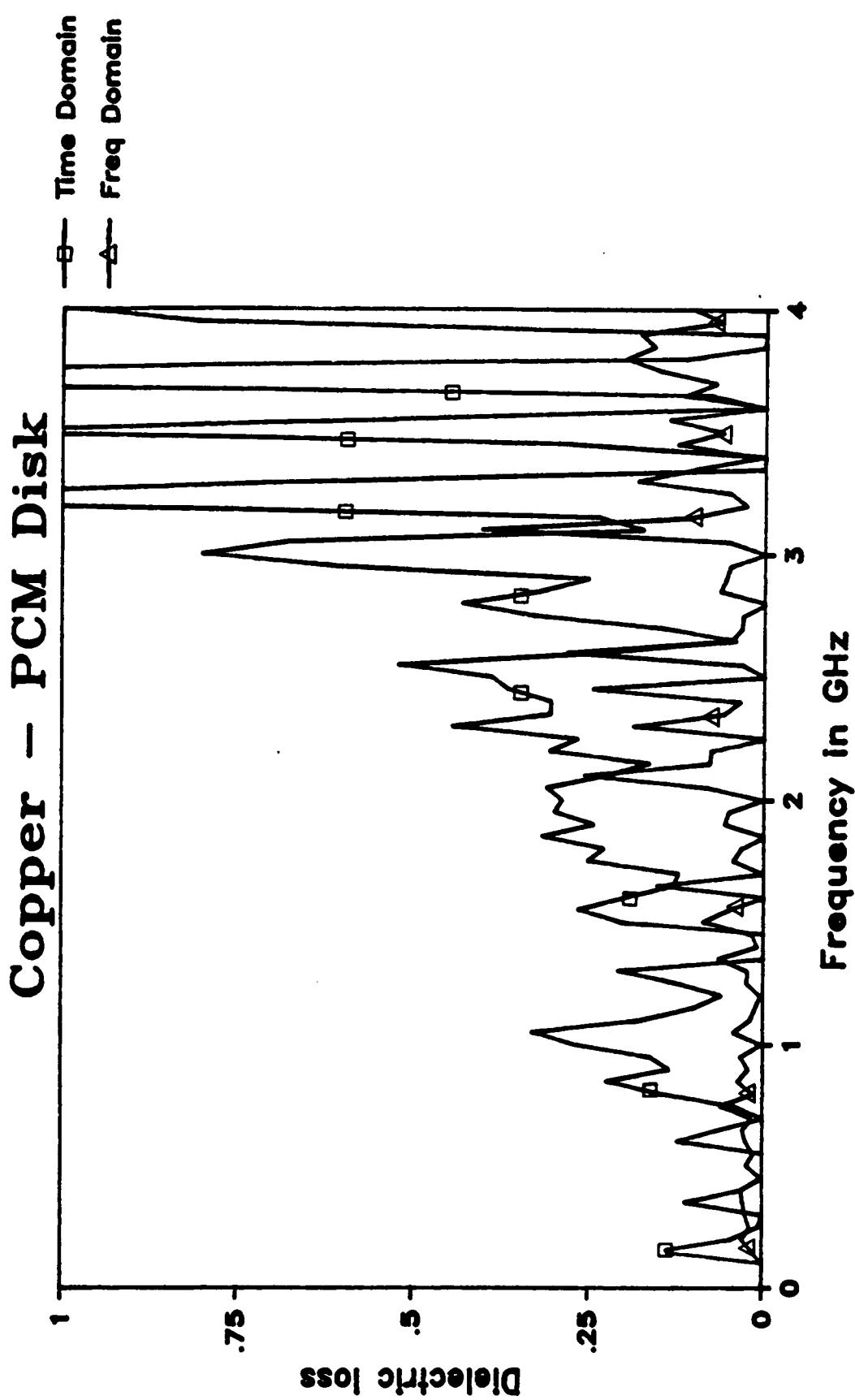
Figure 3.25: Dielectric loss of a DuPont PCM dielectric sample.

the end of the line manually and the alignment was done visually. To minimize this error, the acquisition of the reflected waveform from the sample was repeated several times and then averaged. A better solution would be to design a mechanical structure to hold the sample against the air line.

3.6 Conclusion:

In this chapter, the concept and analysis of a wideband dielectric filled cavity (WDFC) attached to the end of a transmission line was presented. The structure is to be used for the characterization of dielectric materials.

The results of some simulation experiments to test the technique and predict its performance were also presented. Based on these experiments, it was concluded that mainly the phase of the reflection coefficient yields the dielectric constant while the loss is derived from the magnitude of the reflection coefficient information. It was also concluded that the thickness of the dielectric sample must be known precisely to get accurate results for the complex permittivity. The thickness also affects the bandwidth of the measurement; thicker samples providing wider bandwidth. The diameter of the WDFC sample holder must be chosen such that the resonance due to the radial dimension is outside the bandwidth of interest.

The time-domain experimental setup as well as the procedure used to measure the reflection coefficient was described. The results of experiments performed in the time domain and the frequency domain for dielectric characterization using the WDFC technique were also presented. First, some experiments using known materials were performed for verification purposes. Then measurements were performed on two types of thick film dielectric materials: the DuPont 5704 and the DuPont PCM dielectric pastes. Satisfactory estimates for the dielectric constant were obtained. However, the loss re-

sults were not accurate because of two reasons: 1. the WDFC conductor walls were assumed ideal (lossless) 2. these materials have very low losses and, hence, very precise measurements of the reflection coefficient are required. Since the thick film samples have very small thicknesses ($\sim 30\mu m$), giving an upper frequency limit of about 4 GHz beyond which the results become noisy.

Chapter 4

WIDEBAND DIELECTRIC FILLED CAVITY

PLACED BETWEEN TWO

TRANSMISSION LINES

In this chapter, a wideband dielectric filled cavity (WDFC) placed between two transmission lines is described and analyzed. This arrangement enables the measurement of the reflection coefficient, $S_{11}(j\omega)$, as well as the measurement of the transmission coefficient, $S_{21}(j\omega)$. The complex permittivity can be computed from either the reflection coefficient or the transmission coefficient information. The availability of both the reflection and transmission coefficients may enable the computation of the complex permeability, μ^*, as well as the complex permittivity, ε^*. However, as will be shown in section 4.3 the computation of μ^* is very difficult in practice due to the fact that both $S_{11}(j\omega)$ and $S_{21}(j\omega)$ are rather insensitive to the variation in μ^*.

Section 4.1 discusses the concept of the proposed arrangement. In section 4.2, the full field analysis of this arrangement is carried out. Computer simulation experiments are presented in section 4.3. Section 4.4 describes the measurement technique and presents the result of an experiment involving the characterization of a teflon sample for verification (teflon is known to have a dielectric constant of 2.1). Finally, a conclusion is provided in section 4.5.

4.1 Concept:

The proposed arrangement is shown in figure 4.1. As shown in the figure, the WDFC is placed between two transmission lines. The walls of the WDFC sample holder may be deposited or molded on the dielectric sample to eliminate possible air gaps.
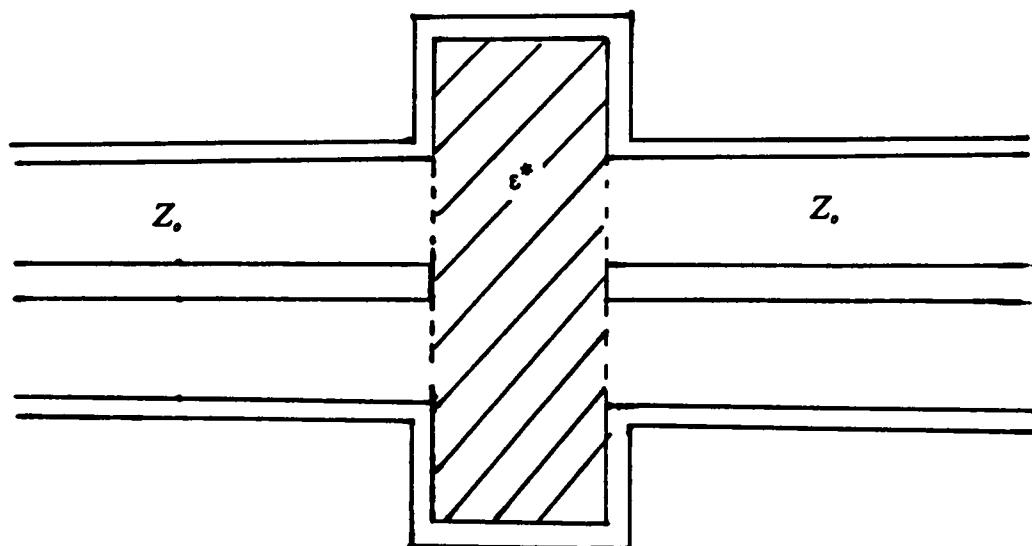
Figure 4.1: The proposed sample configuration

The complex permittivity of the dielectric sample is computed from either the reflection coefficient or the transmission coefficient. The measurement of the reflection coefficient and/or the transmission coefficient can be performed using a time-domain or a frequency-domain setup. In this work, a time-domain setup is used which will be described in section 4.4.

4.2 Analysis of the Proposed Structure:

Section 4.2.1 presents the analysis of the problem assuming that both the complex permittivity, ε^*, and the complex permeability, μ^*, of the dielectric sample are known; the unknown quantities being the reflection coefficient, $S_{11}(j\omega)$, and the transmission coefficient, $S_{21}(j\omega)$. In section 4.2.2, the inverse process is described, i.e. the determination of ε^* and/or μ^* given $S_{11}(j\omega)$ and/or $S_{21}(j\omega)$

4.2.1 Derivation of S_{11}, S_{21} given ε^* and μ^*:

Similar to what has been done in section 3.2.1, the proposed arrangement shown in figure 4.1 can be modeled as shown in figure 4.2 using the equivalence principle [59].
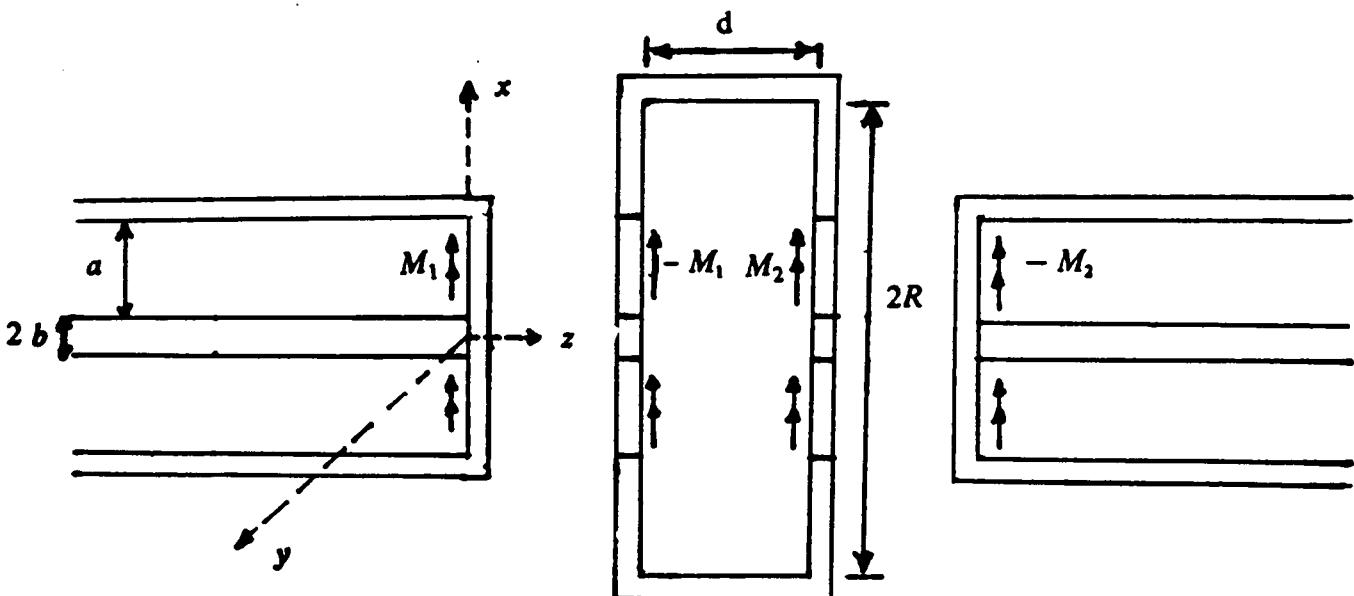
Figure 4.2: The equivalent problem.

The aperture between the first transmission line and the WDFC is replaced by a perfect electric conductor on which an equivalent magnetic current source M_1 is im-

posed. To ensure the continuity of the electric field across the first aperture, the equivalent magnetic current source must be M_1 in the first transmission line region (region (a)) and $-M_1$ in the WDFC region (region (b)). Similarly, the aperture between the WDFC and the second transmission line is replaced by a perfect electric conductor on top of which the magnetic current M_2 is imposed. Again, the magnetic current source must be M_2 in region (b) and $-M_2$ in the second transmission line region (region (c)) to ensure the continuity of the electric field across the second aperture. This is illustrated in figure 4.2.

The remaining boundary condition to be satisfied is the continuity of the magnetic field across both apertures. Let H^a, H^b, and H^c denote the magnetic fields in region (a), region (b), and region (c), respectively. Then, H^a can be decomposed as

$$H^a = H^i + H^r + H^a(M_1) \tag{4.1}$$

where H^i, H^r are the incident and reflected magnetic fields, respectively. $H^a(M_1)$ is the magnetic field due to the equivalent source M_1. The magnetic field in region (b) is

$$H^b = H^b_1(-M_1) + H^b_2(M_2) \tag{4.2}$$

While the magnetic field in region (c) is given by

$$H^c = H^c(-M_2) \tag{4.3}$$

To obtain the true solution for M_1 and M_2, the continuity of the tangential magnetic fields across both apertures needs to be satisfied. This yields two equations

$$H^a|_{z=0} = H^b|_{z=0} \tag{4.4}$$

$$H^b|_{z=d} = H^c|_{z=d} \tag{4.5}$$

Hence,

$$-H^a(M_1)|_{z=0} + H_1^b(-M_1)|_{z=0} + H_2^b(M_2)|_{z=0} = 2H^i|_{z=0} \qquad (4.6)$$

and

$$H_1^b(-M_1)|_{z=d} + H_2^b(M_2)|_{z=d} - H^c(-M_2)|_{z=d} = 0 \qquad (4.7)$$

Solving equations (4.6) and (4.7) simultaneously yields M_1 and M_2. An exact solution is impossible, therefore, an approximate solution will be obtained using the method of moments. First, we have to derive expressions for the field components in equations (4.6) and (4.7). This is achieved by solving the Helmoltz scalar equation (equation 3.5) in the three regions; the field components are then obtained using equations (3.6) - (3.9).

(1) Region (a):

The field components in this region were derived in Chapter 3 (section 3.2.1). The results will be rewritten here for convenience

$$H^i|_{z=0} = \frac{1}{\eta_o\sqrt{2\pi \ln(a/b)}} \; \frac{1}{\rho} u_\phi \qquad (4.8)$$

and

$$H^a(M_1)|_{z=0} = -\frac{A_o}{\eta_o}e_o(\rho)u_\phi - \sum_{n=1}^{\infty} \frac{A_n}{\eta_n}e_n(\rho)u_\phi \qquad (4.9)$$

with A_n given by equation (3.48) and $e_n(\rho)$ is given by equations (3.40) and (3.43).

(2) Region (b):

The scalar function ψ^b appropriate for the derivation of H^b is

$$\psi^b = \sum_{n=1}^{\infty} J_0(K_{\rho_n}^b \rho)\left[B_n \cos K_{z_n}^b(z - d) + C_n \cos K_{z_n}^b z \right] \tag{4.10}$$

where

$$K_{z_n}^b = \left[\omega^2 \varepsilon^* \mu^* - (K_{\rho_n}^b)^2 \right]^{1/2} \tag{4.11}$$

and $K_{\rho_n}^b$ is such that:

$$J_0(K_{\rho_n}^b R) = 0 \tag{4.12}$$

so that the tangential electric field at $\rho = R$ is zero. Thus, by using equation (3.6) and (3.8) along with equation (4.10), the transversal field components are

$$E_\rho^b = \sum_{n=1}^{\infty} J_1(K_{\rho_n}^b \rho)\left[D_n \sin K_{z_n}^b(z - d) + F_n \sin K_{z_n}^b z \right] \tag{4.13}$$

and

$$H_\phi^b = j\omega\varepsilon^* \sum_{n=1}^{\infty} \frac{1}{K_{z_n}^b} J_1(K_{\rho_n}^b \rho)\left[D_n \cos K_{z_n}^b(z - d) + F_n \cos K_{z_n}^b z \right] \tag{4.14}$$

where $D_n = \dfrac{K_{\rho_n}^b K_{z_n}^b}{j\omega\varepsilon^*} B_n$ and $F_n = \dfrac{K_{\rho_n}^b K_{z_n}^b}{j\omega\varepsilon^*} C_n$.

The coefficients D_n and F_n are evaluated by applying the following boundary conditions:

$$- u_z \times E^b|_{z=0} = - M_1 \tag{4.15}$$

$$u_z \times E^b|_{z=d} = M_2 \tag{4.16}$$

Equation (4.15) yields

$$M_1 = -\sum_{n=1}^{\infty} D_n J_1(K_{\rho_n}^b \rho) \sin K_{z_n}^b d \, u_\phi \tag{4.17}$$

while equation (4.16) yields

$$M_2 = \sum_{n=1}^{\infty} F_n J_1(K_{\rho_n}^b \rho) \sin K_{z_n}^b d \, u_\phi \ . \tag{4.18}$$

Note that both M_1 and M_2 are in the direction of ϕ and are functions of ρ only. Following the same procedure of Chapter 3, section 3.2.1 (2), equations (3.55) - (3.60), the coefficients D_n and F_n are given by

$$D_n = \frac{-2}{R^2 J_1^2(K_{\rho_n} R) \sin K_{z_n}^b d} \int_b^a M_1 J_1(K_{\rho_n}^b \rho) \rho d\rho \tag{4.19}$$

and

$$F_n = \frac{2}{R^2 J_1^2(K_{\rho_n} R) \sin K_{z_n}^b d} \int_b^a M_2 J_1(K_{\rho_n}^b \rho) \rho d\rho \tag{4.20}$$

Hence, the magnetic field in region (b) is given by

$$H^b = j\omega \varepsilon^* \sum_{n=1}^{\infty} \frac{1}{K_{z_n}^b} J_1(K_{\rho_n}^b \rho) \Big[D_n \cos K_{z_n}^b(z-d) + F_n \cos K_{z_n}^b z \Big] u_\phi \tag{4.21}$$

H^b can be written as:

$$H^b = H_1^b(-M_1) + H_2^b(M_2) \tag{4.22}$$

where

$$H_1^b(-M_1) = j\omega\varepsilon^* \sum_{n=1}^{\infty} \frac{D_n}{K_{z_n}^b} J_1(K_{\rho_n}^b \rho) \cos K_{z_n}^b(z-d)u_\phi \tag{4.23}$$

$$H_2^b(M_1) = j\omega\varepsilon^* \sum_{n=1}^{\infty} \frac{F_n}{K_{z_n}^b} J_1(K_{\rho_n}^b \rho) \cos K_{z_n}^b z u_\phi \tag{4.24}$$

D_n and F_n are defined in equations (4.19) and (4.20).

(3) Region (c):

The magnetic field in region (c) is due only to the magnetic source $-M_2$. This region is very similar to region (a). The appropriate scalar function for the derivation of the field components in this region is:

$$\Psi^c = (B_o + C_o \ln \rho)e^{-jK_o(z-d)} + \sum_{n=1}^{\infty} B_n g_n(\rho)e^{-jK_{z_n}^c(z-d)} \tag{4.25}$$

where

$$g(\rho) = N_o(K_{\rho_n}^a b)J_o(K_{\rho_n}^a \rho) - J_o(K_{\rho_n}^a b)N_o(K_{\rho_n}^a \rho)$$

Following the same procedure of section 3.2.1, the electric and magnetic fields are given by:

$$E^c(-M_2) = Q_o e_o(\rho)e^{-JK_o(z-d)}u_\rho + \sum_{n=1}^{\infty} Q_n e_n(\rho)e^{-JK_{z_n}^a(z-d)}u_\rho \qquad (4.26)$$

$$H^c(-M_2) = -\frac{Q_o}{\eta_o}e_o(\rho)e^{-JK_o(z-d)}u_\phi - \sum_{n=1}^{\infty}\frac{Q_n}{\eta_n}e_n(\rho)e^{-JK_{z_n}^a(z-d)}u_\phi \qquad (4.27)$$

where $e_o(\rho)$ and $e_n(\rho)$ are defined in equations (3.43) and (3.40).

To evaluate the coefficients, Q_n, apply the boundary condition

$$-M_2 = -u_z \times E^c|_{z=d} \qquad (4.28)$$

Therefore,

$$M_2 = \sum_{n=0}^{\infty} Q_n e_n(\rho)u_\phi = M_{2_\phi}u_\phi \qquad (4.29)$$

To solve for the coefficients, Q_n, multiply both sides of (4.29) by $e_m(\rho)$ and integrate over the aperture. By orthonormality (3.25), all the terms of the summation are zero except the $m = n$ term. Hence

$$Q_n = 2\pi \int_b^a M_{2_\phi}e_n(\rho)\rho d\rho \ , \qquad n = 0, 1, 2, \ldots \qquad (4.30)$$

Thus, $H^c(-M_2)|_{z=d}$ is given by

$$H^c(-M_2)|_{z=d} = -\sum_{n=0}^{\infty} \frac{Q_n}{\eta_n} e_n(\rho)u_\phi \qquad (4.31)$$

(4) Method of solution:

The method of moments explained in Chapter (4), section 4.2.1(3), is used to obtain approximate solutions for M_1 and M_2. Once M_1 and M_2 are solved for, the derivation of S_{11} and S_{21} is straight forward. Let the expansion functions be the same as the testing functions. These are the same expansion functions used in chapter 3, namely, $e_{n-1}(\rho)$. Hence, M_1 and M_2 are expressed as the linear combination of $e_{n-1}(\rho)$. That is

$$M_1 = \sum_{n=1}^{N} V_n M_n = \sum_{n=1}^{N} V_n e_{n-1}(\rho) \qquad (4.32)$$

and

$$M_2 = \sum_{n=1}^{N} U_n M_n = \sum_{n=1}^{N} U_n e_{n-1}(\rho) \qquad (4.33)$$

where the coefficients V_n and U_n are to be determined.

Substituting equation (4.32) in equation (4.6) and writing the result in matrix form, we obtain

$$\left[Y^a + Y_1^b \right]\vec{V} + Y_2^b \vec{U} = \vec{I} \qquad (4.34)$$

where

$$[Y_{ij}^a] = -\iint_{aperture} M_i \cdot H^a(M_j)|_{z=0} ds \qquad (4.35)$$

$$[Y_{1ij}^b] = \iint_{aperture} M_i \cdot H_1^b(-M_j)|_{z=0} ds \qquad . \qquad (4.36)$$

$$[Y_{2ij}^b] = \iint_{aperture} M_i \cdot H_2^b(M_j)|_{z=0} ds \qquad (4.37)$$

$$\vec{I}_j^i = 2\iint_{aperture} M_j \cdot H^i|_{z=0} ds \quad . \qquad (4.38)$$

$\vec{V}$ and $\vec{U}$ are the vectors containing the unknown coefficients V_n's and V_n's, respectively. Substituting (4.33) in equation (4.7) and writing the result in matrix form

$$B_1^b \vec{V} + [B_2^b + B^c]\vec{U} = 0 \qquad (4.39)$$

where:

$$[B_{1ij}^b] = \iint_{aperture} M_i \cdot H_{1ij}^b(-M_j)|_{z=d} ds \qquad (4.40)$$

$$[B_{2ij}^b] = \iint_{aperture} M_i \cdot H_2^b(M_j)|_{z=d} ds \qquad (4.41)$$

$$\left[B^c_{ij}\right] = \iint_{aperture} M_i \cdot H^c(-M_j)|_{z=d} ds \ . \tag{4.42}$$

Now, let's evaluate the elements of the above matrices.

The matrix $[Y^a]$ is identical to the admittance matrix $[Y^a]$ of Chapter 3 (see equations (3.67), (3.72) - (3.75)). Rewriting the result

$$Y^a_{mn} = \begin{cases} \dfrac{1}{\eta_{n-1}} & , \quad m = n \\ 0 & , \quad m \neq n \end{cases} \ . \tag{4.43}$$

Similarly, the elements of the excitation vector $\vec{I}$ are identical to those of Chapter 3 (equation (3.76))

$$\vec{I}_n = \begin{cases} \dfrac{2}{\eta_o} & , \quad n = 1 \\ 0 & , \quad n > 1 \end{cases} \ . \tag{4.44}$$

To compute the matrix elements of $[Y^b_1]$ and $[Y^b_2]$, the coefficients D_n and F_n defined in equations (4.19) and (4.20) must have double subscripts to account for the subscript on the basis function M_n and equations (4.19) and (4.20) become

$$D_{mn} = \frac{-2}{R^2 J_1^2(K_{\rho_n} R) \sin K^b_{z_n} d} \int_b^a M_m J_1(K^b_{\rho_n}\rho)\rho d\rho \tag{4.45}$$

and

$$F_{mn} = \frac{2}{R^2 J_1^2(K_{\rho_n} R) \sin K^b_{z_n} d} \int_b^a M_m J_1(K^b_{\rho_n}\rho)\rho d\rho \ . \tag{4.46}$$

Hence, using equations (4.23) and (4.36), the elements of $[Y_1^b]$ are

$$Y_{1mn}^b = j\omega\varepsilon^* \sum_{i=1}^{\infty} \frac{D_{ni}}{K_{z_i}^b} \cos(K_{z_i}^b d) \, 2\pi \int_b^a M_m(\rho) J_1(K_{\rho_i}^b \rho) \rho d\rho \quad . \tag{4.47}$$

Similarly, from equations (4.24) and (4.37), the elements of $[Y_2^b]$ are

$$Y_{2mn}^b = j\omega\varepsilon^* \sum_{i=1}^{\infty} \frac{F_{ni}}{K_{z_i}^b} \, 2\pi \int_b^a M_m(\rho) J_1(K_{\rho_i}^b \rho) \rho d\rho \quad . \tag{4.48}$$

Equations (4.47) and (4.48) can be written as follows (using equations (4.45) and (4.46))

$$Y_{1mn}^b = -j\omega\varepsilon^* \sum_{i=1}^{\infty} \frac{C'_{ni} C'_{mi}}{K_{z_i}^b} \, \frac{1}{\tan(K_{z_i}^b d)} \tag{4.49}$$

$$Y_{2mn}^b = j\omega\varepsilon^* \sum_{i=1}^{\infty} \frac{C'_{ni} C'_{mi}}{K_{z_i}^b} \, \frac{1}{\sin(K_{z_i}^b d)} \tag{4.50}$$

where

$$C'_{ni} = \frac{2\sqrt{\pi}}{R J_1(K_{\rho_i}^b R)} \int_b^a M_n J_1(K_{\rho_i}^b \rho) \rho d\rho \quad . \tag{4.51}$$

C'_{nl} as defined in (4.51) is identical to its definition in Chapter 3, section 3.2.1(3), equation (3.80). The evaluation of the integral in equation (4.51) was done in that section, equations (3.80) - (3.85). Rewriting the result

$$C'_{1l} = \frac{1}{\sqrt{2\pi}\,\ln(b/a)}\;\frac{2\sqrt{\pi}}{RJ_1(K^b_{\rho_l}R)}\;\frac{1}{K^b_{\rho_l}}\left\{J_o(K^b_{\rho_l}b) - J_o(K^b_{\rho_l}a)\right\} \qquad (4.52)$$

$$C'_{nl} = P_n\frac{2\sqrt{(\pi)}}{RJ_1(K^b_{\rho_l}R)}\;\frac{1}{(K^a_{\rho_n})^2 - (K^b_{\rho_l})^2}I_{nl}\;,\qquad n = 1,2,\ldots,N \qquad (4.53)$$

where P_n are defined in equation (3.39), and P_n is given in equation (3.85). The matrix elements of $[B^b_1]$ are evaluated by using equations (4.23) and (4.40)

$$B^b_{1mn} = j\omega\varepsilon^*\sum_{l=1}^{\infty}\frac{D_{nl}}{K^b_{z_l}}\,2\pi\int_b^a M_m(\rho)J_1(K^b_{\rho_l}\rho)\rho\,d\rho \qquad (4.54)$$

which can be rewritten as

$$B^b_{1mn} = -j\omega\varepsilon^*\sum_{l=1}^{\infty}\frac{C'_{nl}C'_{ml}}{K^b_{z_l}}\;\frac{1}{\sin(K^b_{z_l}d)} \qquad (4.55)$$

Comparing equations (4.55) with equation (4.50), we notice that

$$\left[B^b_1\right] = -\left[Y^b_2\right]. \qquad (4.56)$$

Similarly, equations (4.24) and (4.41), the elements of $[B^b_2]$ are given by

$$B_{2mn}^b = j\omega\varepsilon^* \sum_{l=1}^{\infty} \frac{F_{nl}}{K_{z_l}^b} \cos(K_{z_l}^b d)\ 2\pi \int_b^a M_m(\rho)J_1(K_{\rho_l}^b\rho)\rho d\rho \quad . \qquad (4.57)$$

Equation (4.57) can be rewritten as

$$B_{2mn}^b = j\omega\varepsilon^* \sum_{l=1}^{\infty} \frac{C'_{nl}C'_{ml}}{K_{z_l}^b} \frac{1}{\tan(K_{z_l}^b d)} \quad . \qquad (4.58)$$

Comparing equation (4.58) with equation (4.49), it is observed that

$$\left[B_2^b \right] = - \left[Y_1^b \right] \quad . \qquad (4.59)$$

To compute the matrix elements of $[B^c]$, the coefficients Q_n must have a double subscript to account for the subscript on the basis function M_n, i.e., equation (4.30) becomes

$$Q_{mn} = 2\pi \int_b^a M_m e_n(\rho)\rho d\rho \quad , \qquad n = 0, 1, 2, \ldots, N \qquad (4.60)$$

Since $M_m = e_{m-1}(\rho)$, and remembering the orthonormality defined in (3.25), equation (4.60) becomes

$$Q_{mn} = \begin{cases} 1 & , \quad n = m \\ 0 & , \quad n \neq m \end{cases} \quad . \qquad (4.61)$$

Therefore, using equations (4.31), (4.42), and (4.60), the elements of admittance matrix $[B^c]$ are given by

$$B_{mn}^c = \begin{cases} \dfrac{-1}{\eta_{n-1}} & , \quad m = n \\ 0 & , \quad m \neq n \end{cases} . \qquad (4.62)$$

Comparing equation (4.62) with (4.43), it is observed that

$$[B^c] = -[Y^a] . \qquad (4.64)$$

Therefore, the two matrix equations (4.34) and (4.39) which are needed to solve for the coefficients' vectors $\vec{U}$ and $\vec{V}$ become

$$[Y^a + Y_1^b]\vec{V} + Y_2^b\vec{U} = \vec{I} \qquad (4.65)$$

and

$$Y_2^b\vec{V} + [Y^a + Y_1^b]\vec{U} = 0 . \qquad (4.66)$$

Equations (4.65) and (4.66) can be augmented into one matrix equation

$$\begin{bmatrix} Y^a + Y_1^b & Y_2^b \\ Y_2^b & Y^a + Y_1^b \end{bmatrix} \begin{bmatrix} \vec{U} \\ \vec{U} \end{bmatrix} = \begin{bmatrix} \vec{I} \\ 0 \end{bmatrix} . \qquad (4.67)$$

Equation (4.67) can be solved to yield the coefficients' vectors $\vec{V}$ and $\vec{U}$. Once $\vec{V}$ and $\vec{U}$ are obtained, the reflection coefficient, S_{11}, and the transmission coefficient, S_{21}, can be evaluated easily. The evaluation of S_{11} is similar to the procedure described in Chapter 3. To reiterate, the magnetic current distribution over the first aperture can be written as

$$M_1 = u_z \times E^a|_{z=0} = (1 + S_{11})e_o(\rho)u_\phi + \sum_{n=1}^{\infty} R_i e_n(\rho)u_\phi = M_{1_\phi} u_\phi \qquad (4.68)$$

where R_i are the complex amplitudes of the higher order modes generated at the aperture (unity incident power is assumed). Multiplying both sides by $e_o(\rho)$, then integrating over the aperture and using orthonormality (3.25), the following result is obtained

$$S_{11} = \int_0^{2\pi} \int_b^a M_{1_\phi} e_o(\rho)\rho d\rho - 1 \ . \tag{4.69}$$

Combining equations (4.32) and (4.69)

$$S_{11} = \sum_{n=1}^N V_n \int_0^{2\pi} \int_b^a M_n e_o(\rho)\rho d\rho - 1 \ . \tag{4.70}$$

Replacing M_n by e_{n-1} and using orthonormality (3.25), S_{11} is given by

$$S_{11} = V_1 - 1 \ . \tag{4.71}$$

Similarly, the magnetic current distribution over the second aperture can be written as

$$M_2 = u_z \times E^b|_{z=d} = S_{21} e^{-jK_o d} e_o(\rho)u_\phi + \sum_{n=1}^\infty T_i e^{-jK_{zn}^a z} e_n(\rho)u_\phi = M_{2_\phi} u_\phi \ . \tag{4.72}$$

Following the same procedure used to obtain S_{11}, the transmission coefficient, S_{21} can be obtained

$$S_{21} = e^{jK_o d} \int_0^{2\pi} \int_b^a M_{2_\phi} e_o(\rho)\rho d\rho \ . \tag{4.73}$$

Combining equations (4.33) and (4.73)

$$S_{21} = e^{jK_o d} \sum_{n=1}^{\infty} U_n \int_o^{2\pi} \int_b^a M_n e_o(\rho) \rho d\rho \qquad (4.74)$$

Replacing M_n by e_{n-1} and using orthonormality (3.25)

$$S_{21} = U_1 e^{jK_o d} \,. \qquad (4.75)$$

A Fortran computer program implementing the formulas derived in this section was written to compute S_{11} and S_{21} given μ^* and ε^*. The computer code is listed in appendix III. Later, in section 4.3, the results of computer simulation experiments are presented. The purpose of these experiments is to test the sensitivity of the technique to various parameters and to predict its performance.

4.2.2 Computation of ε^* and/or μ^* given S_{11} and /or S_{21}:

As mentioned earlier, ε^* can be computed from either the reflection coefficient, $S_{11}(j\omega)$, or the transmission coefficient, S_{21}, if μ^* is known.

If $S_{11}(j\omega)$ is measured, then the complex permittivity is computed from equation (4.71) along with the matrix equation (4.67). The solution is obtained iteratively by minimizing the following function (see equation (4.71))

$$f_1(\varepsilon^*) = |S_{11} - V_1 + 1| \qquad (4.76)$$

subject to the matrix equation (4.67). An initial guess is assumed, then the coefficients V_n's and U_n's are computed directly by solving the matrix equation (4.67) using Gaussian elimination. Only V_1 is needed to compute $f_1(\varepsilon^*)$ and then to update the value of ε^* using Powell's hybrid method [55]. Using the updated value of ε^*, the coefficients V_n's and U_n's are again solved for by Gaussian elimination and V_1 is used to compute another

updated value of ε^*. This iterative process is repeated until the value of $f_1(\varepsilon^*)$ is less than the desired tolerance.

If S_{21} is to be used for the computation of ε^* given μ^*, the solution is obtained by minimizing the following objective function (see equation (4.75)):

$$f_2(\varepsilon^*) = |S_{21} - U_1 e^{jK_o d}| \tag{4.77}$$

subject to the matrix equation (4.67). The same iterative procedure described above is used to compute ε^*, however, here only U_1 is needed, not V_1.

If the goal is to compute μ^* assuming ε^* to be known, the same discussion above applies. However, now the iteration is performed on μ^* instead of ε^* and the above objective functions to be minimized are functions of μ^*, ε^*, because ε^* is now assumed to be known.

If a combined reflection - transmission measurement is performed, then, both S_{11} and S_{21} can be used to compute ε^* and μ^*. In this case, both equations (4.71) and (4.75) along with the matrix equation (4.67) must be used to solve for ε^* and μ^*. This can b achieved by minimizing the following objective function:

$$f_3(\varepsilon^*, \mu^*) = |S_{11} - V_1 + 1|^2 + |S_{21} - U_1 e^{jK_o d}|^2 \tag{4.78}$$

subject to the matrix equation (4.67). The same iterative process described earlier is used to compute ε^* and μ^* except ,now, the iteration is performed on both ε^* and μ^* and both U_1 and V_1 are needed to update the values of ε^* and μ^*. However, as will be demonstrated in the next section the practical computation of both ε^* and μ^* is very difficult since both the reflection and transmission coefficients are very insensitive to the variation in the permeability except around the resonant frequencies. In other words, varying the permeability considerably causes a very small variation in S_{11} and S_{21}. Consequently, the minimization process fails to converge to the global minimum for an ini-

tial guess unless that initial guess is extremely close to the actual values. Nevertheless, the assumption that the permeability of dielectric materials to be unity is a reasonable assumption. The main parameter which characterizes dielectric materials is the complex permittivity which can be computed from either S_{11} or S_{21}, as discussed above.

4.3 Computer Simulation:

In this section, the results of computer simulation experiments performed to test the sensitivity of the reflection and transmission coefficients to varying the dimensions of the WDFC sample holder and the dielectric material's properties. From the results of these experiments predictions concerning the performance of the WDFC can be made. These experiments are the following:

(1) Varying the diameter of the WDFC:

In this experiment, the effect of varying the diameter of the WDFC on the magnitude and phase of $S_{11}(j\omega)$ and $S_{21}(j\omega)$ is considered. Diameters of 1 cm, 2 cm, and 3 cm were used. The other parameters are as follows: thickness = 0.025 cm, $\varepsilon'_r = 5$, $\mu'_r = 1$, $\varepsilon''_r = \mu''_r = 0$. Figures (4.3) and (4.4) show the magnitude and phase of $S_{11}(j\omega)$ while figures (4.5) and (4.6) show the magnitude and phase of $S_{21}(j\omega)$. It can be noticed from the figures that varying the diameter mainly affects the resonance due to the radial dimension. It is desirable to choose the diameter of such that the radial resonance is outside the bandwidth of interest.

(2) Varying the thickness:

Figures (4.7) - (4.10) show the graphs of $S_{11}(j\omega)$ and $S_{21}(j\omega)$, magnitude and phase, demonstrating the effect of varying the thickness of the WDFC. Thickness values of
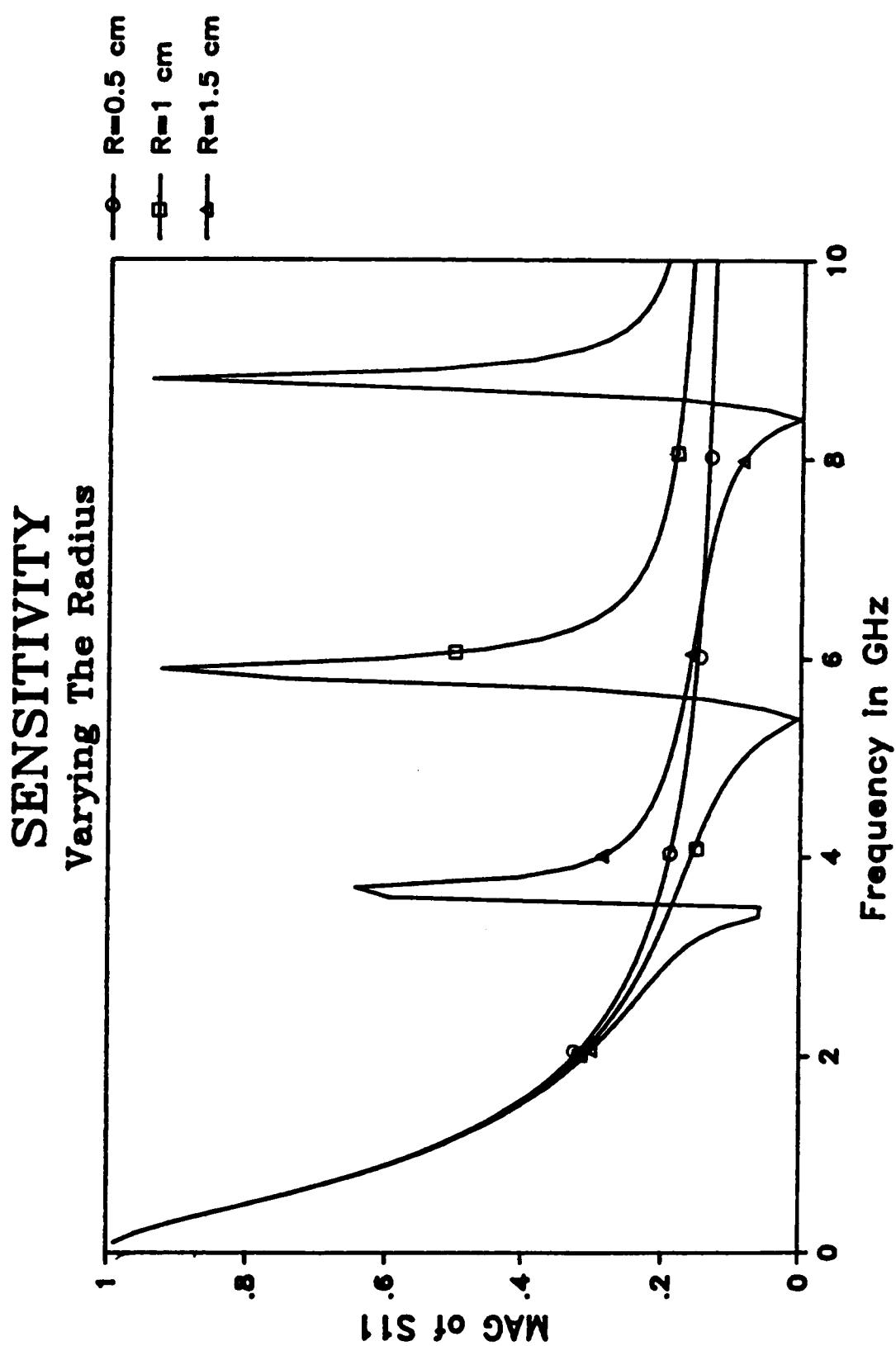
Figure 4.3: Effect of varying the diameter on the magnitude of S_{11}.
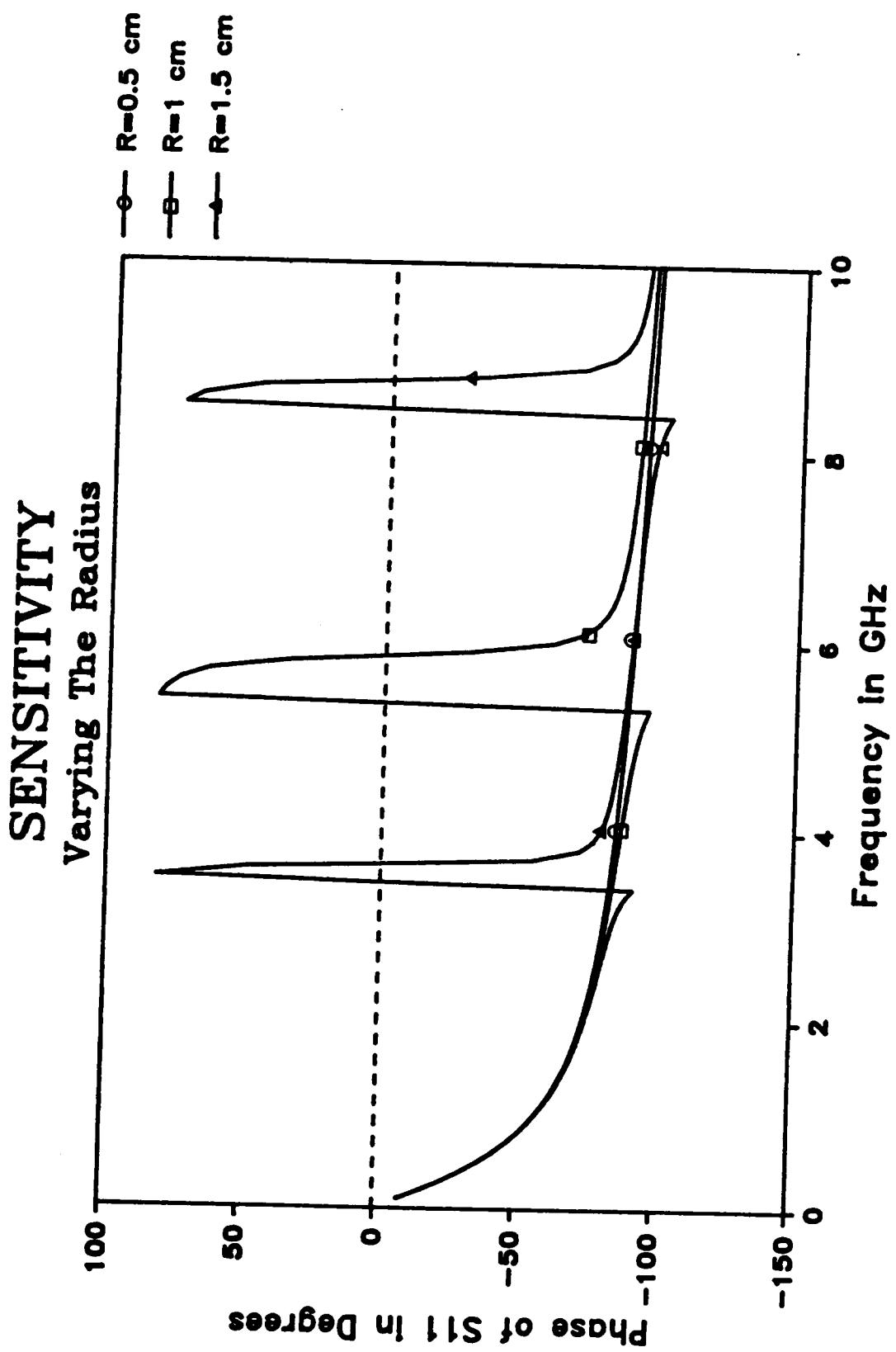
Figure 4.4: Effect of varying the diameter on the phase of S_{11}.
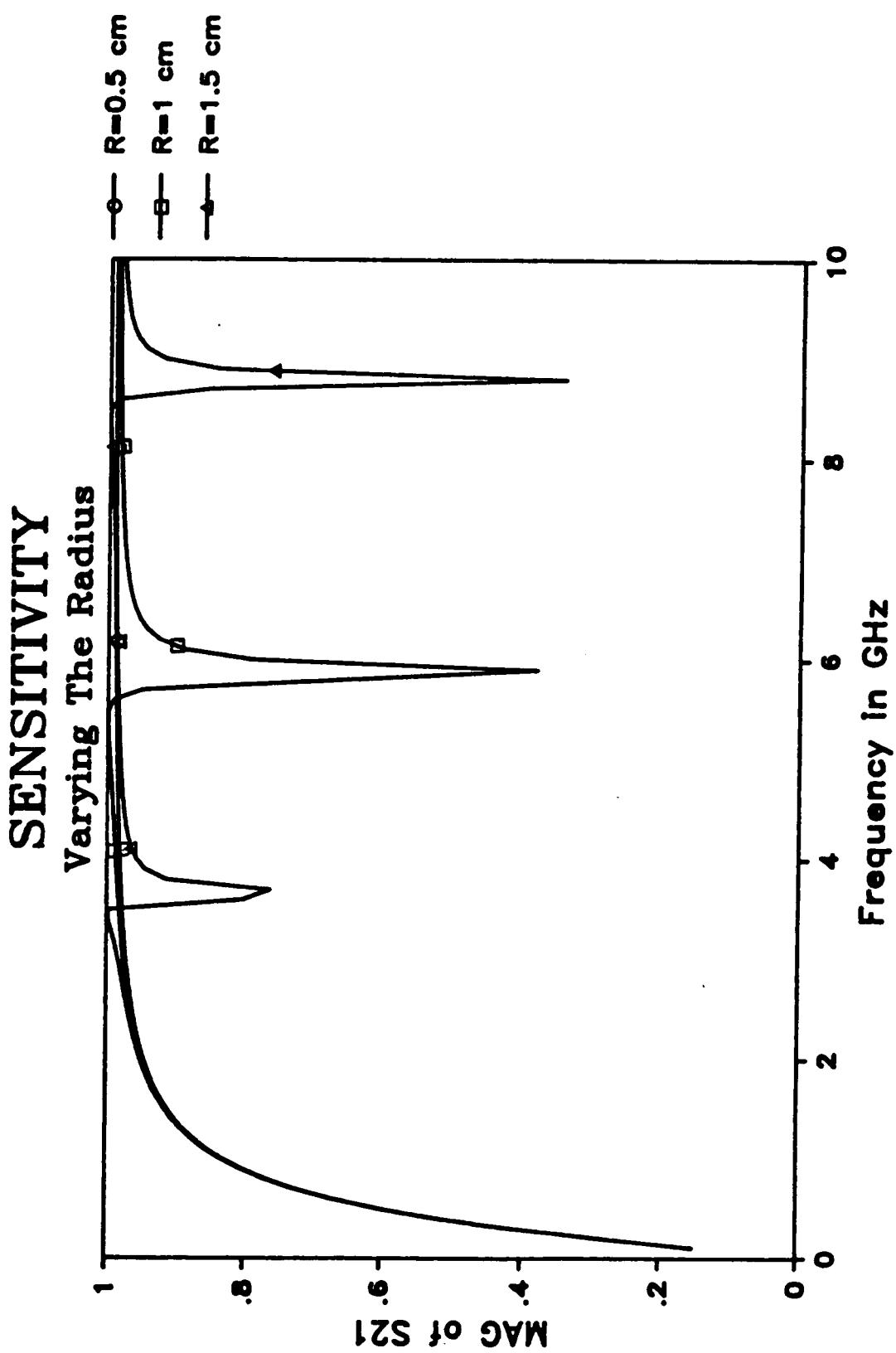
Figure 4.5: Effect of varying the diameter on the magnitude of S_{21}.
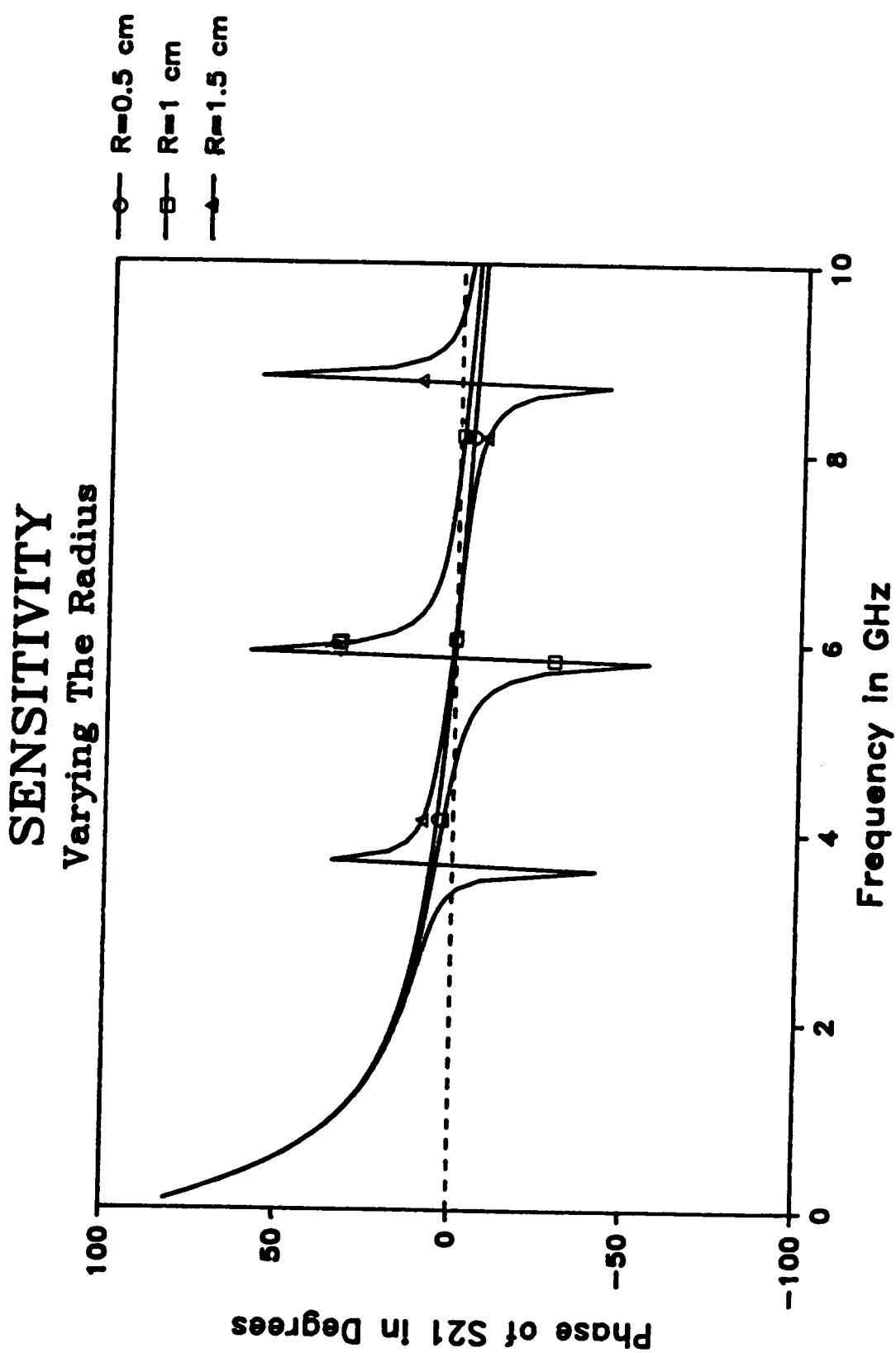
Figure 4.6: Effect of varying the diameter on the phase of S_{21}.
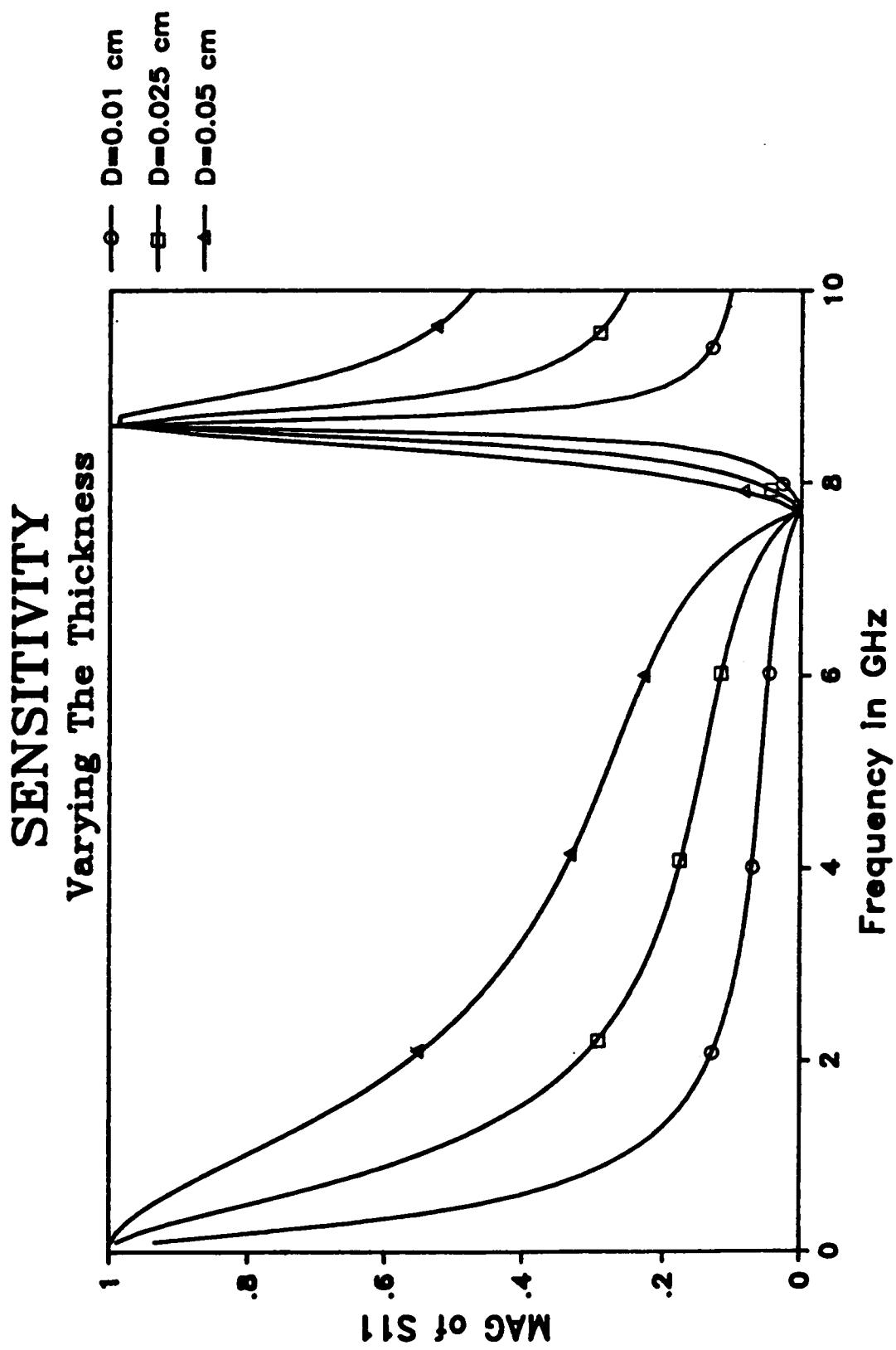
Figure 4.7: Effect of varying the thickness on the magnitude of S_{11}.
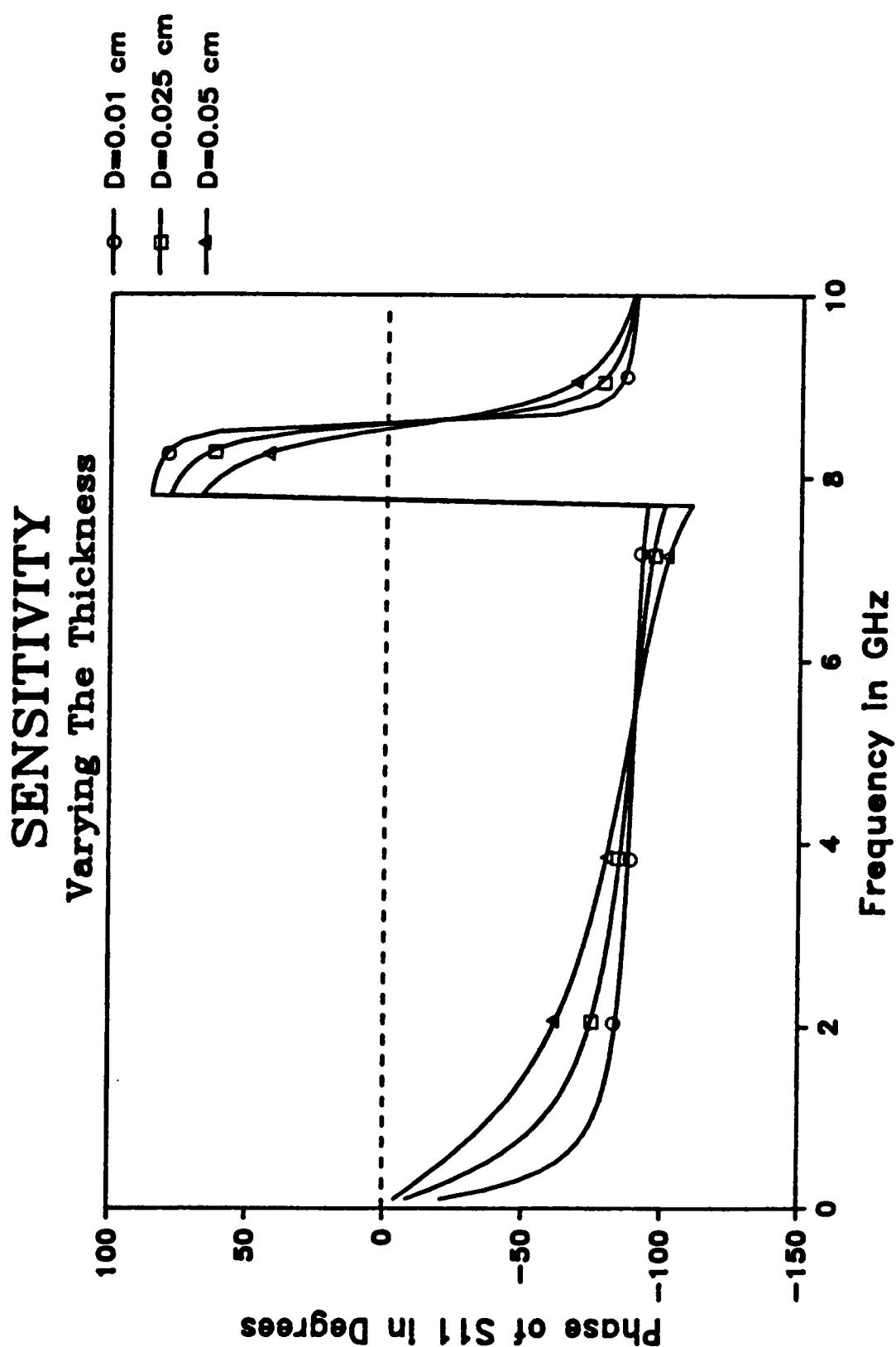
Figure 4.8: Effect of varying the thickness on the phase of S_{11}.
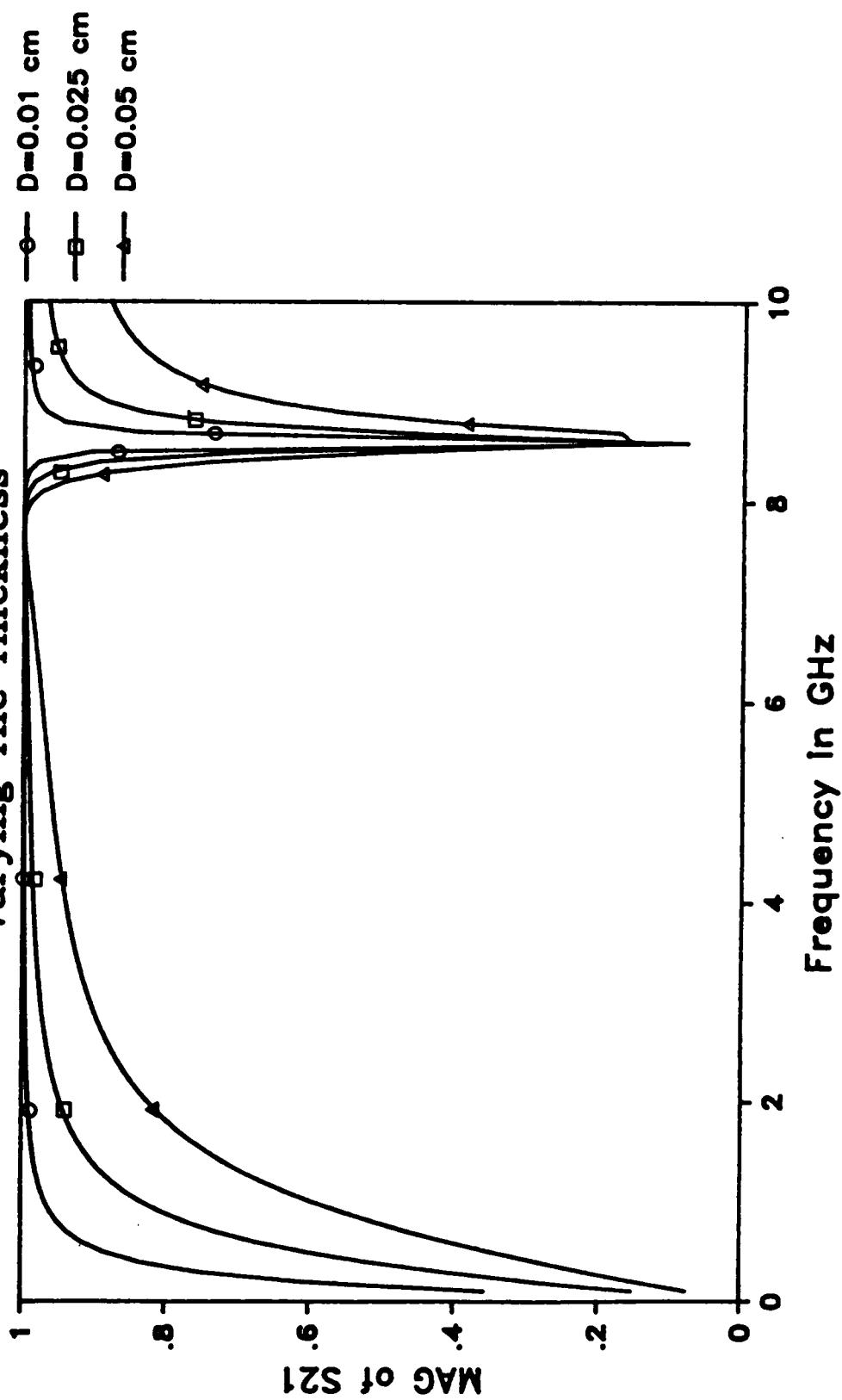
Figure 4.9: Effect of varying the thickness on the magnitude of S_{21}.
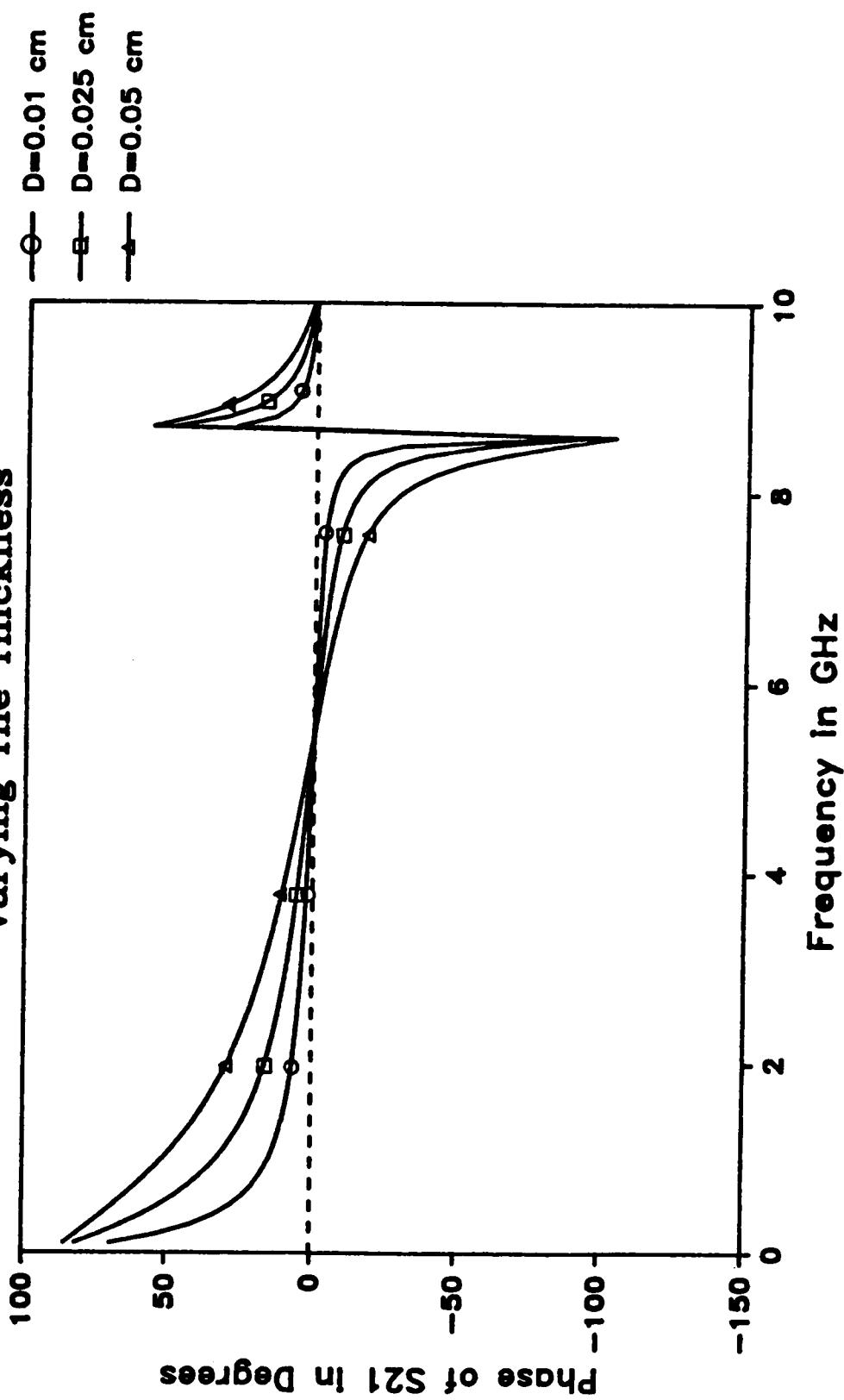
Figure 4.10: Effect of varying the thickness on the phase of S_{21}.

0.025 cm, 0.05 cm, and 0.075 cm were used. The other parameters were: diameter = 1 cm, $\varepsilon'_r = 5$, $\mu'_r = 1$, $\varepsilon''_r = \mu''_r = 0$. It is observed from the figures that both $S_{11}(j\omega)$ and $S_{21}(j\omega)$ change considerably if the thickness is changed. Therefore, the thickness must be known precisely in order to obtain accurate results.

(3) Varying the complex permittivity ε^*_r :

Figures (4.11) - (4.14) show the graphs of $S_{11}(j\omega)$ and $S_{21}(j\omega)$, magnitude and phase, corresponding to values of ε'_r of 3, 5, and 7; the other parameters of the WDFC being: diameter = 1 cm, thickness = 0.025 cm, $\mu'_r = 1$, $\varepsilon'' = \mu'' = 0$. It is observed that both S_{11} and S_{21} are sensitive to the change in the dielectric constant. It is further noticed that lower dielectric constants are easier to estimate over a wider bandwidth than higher dielectric constants. The reason is that the higher the dielectric constant, the faster the rate of change of S_{11} and S_{21} .

The effect of varying the dielectric loss is displayed in figures (4.15) - (4.18). As expected, the resonance diminishes with higher losses. An important observation is that the change in S_{11} and S_{21} are not considerable if the losses are very low. Consequently, when characterizing materials with very low losses, extreme precision in the measurement of $S_{11}(j\omega)$ and /or $S_{21}(j\omega)$ is necessary.

(4) Varying the complex permeability, μ^*_r :

The graphs of $S_{11}(j\omega)$ and $S_{21}(j\omega)$ corresponding to values of μ'_r of 3, 5, and 7 are shown in figures (4.19) - (4.22). The other WDFC parameters were chosen to be: $\varepsilon'_r = 5$, diameter = 1 cm, thickness = 0.025 cm, and $\varepsilon''_r = \mu''_r = 0$. The effect of varying the magnetic loss ($\mu''_r = 0.1$, 1, 3) is shown in figures (4.23) - (4.26), μ'_r was taken to be unity and the other parameters were the same as above. It is observed from these figures that neither S_{11} nor S_{21} is sensitive to varying the complex permeability. In other words, changing μ^*_r considerably causes a very small change in S_{11} and S_{21} except around the

Figure 4.11: Effect of varying the dielectric constant on the magnitude of S_{11}.

Figure 4.12: Effect of varying the dielectric constant on the phase of S_{11}.

SENSITIVITY

Varying The Dielectric Constant
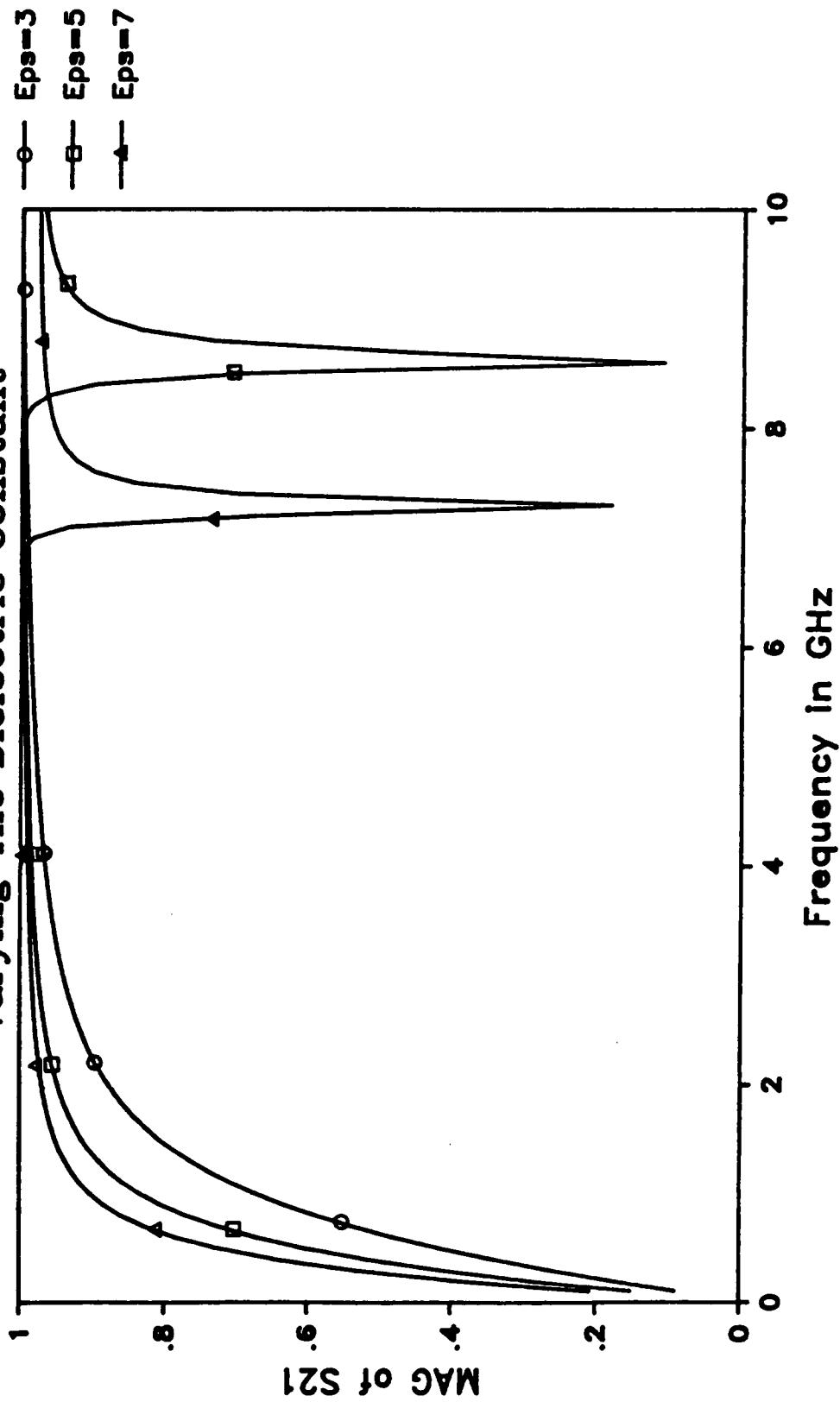
Figure 4.13: Effect of varying the dielectric constant on the magnitude of S_{21}.
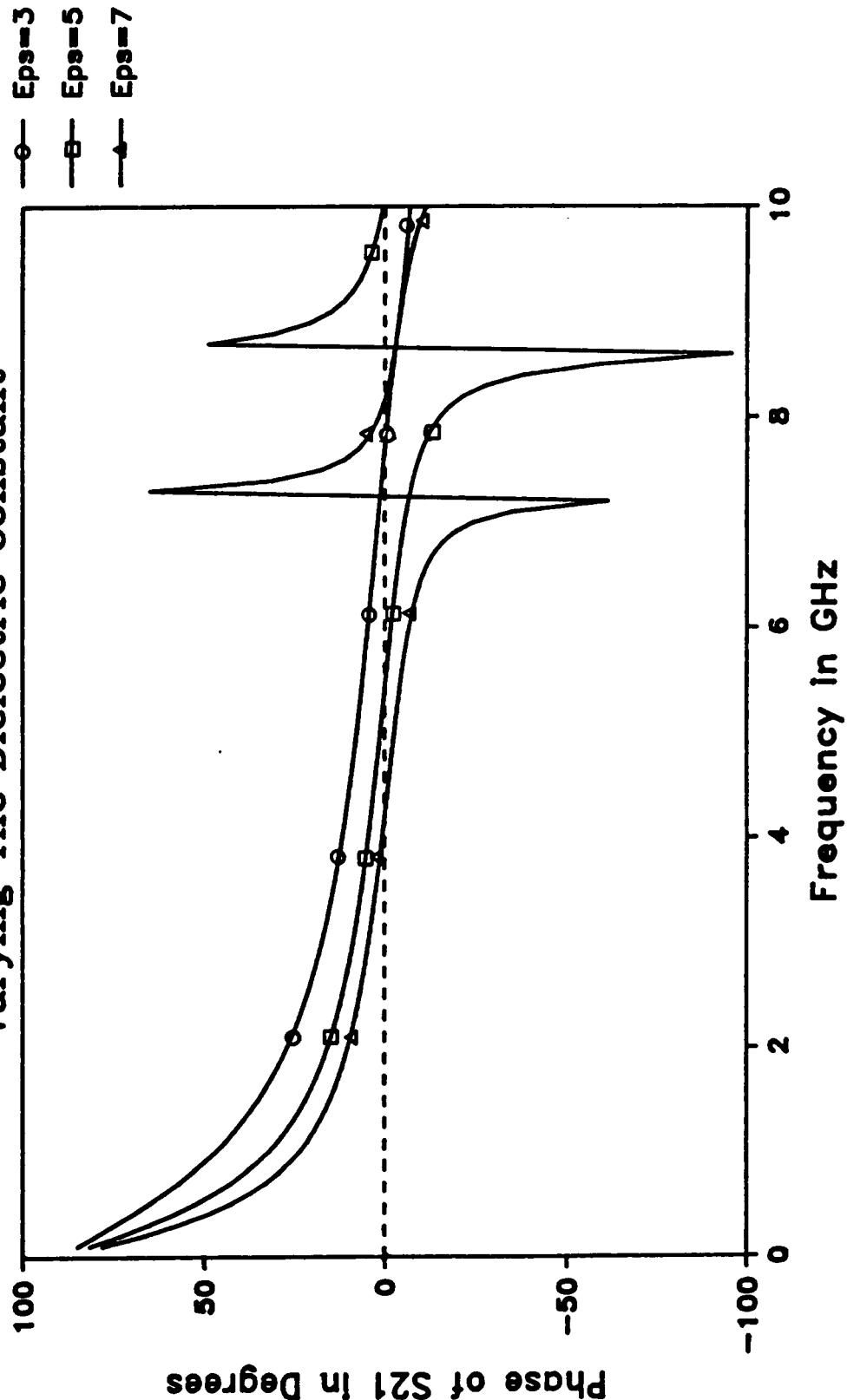
Figure 4.14: Effect of varying the dielectric constant on the phase of S_{21}.
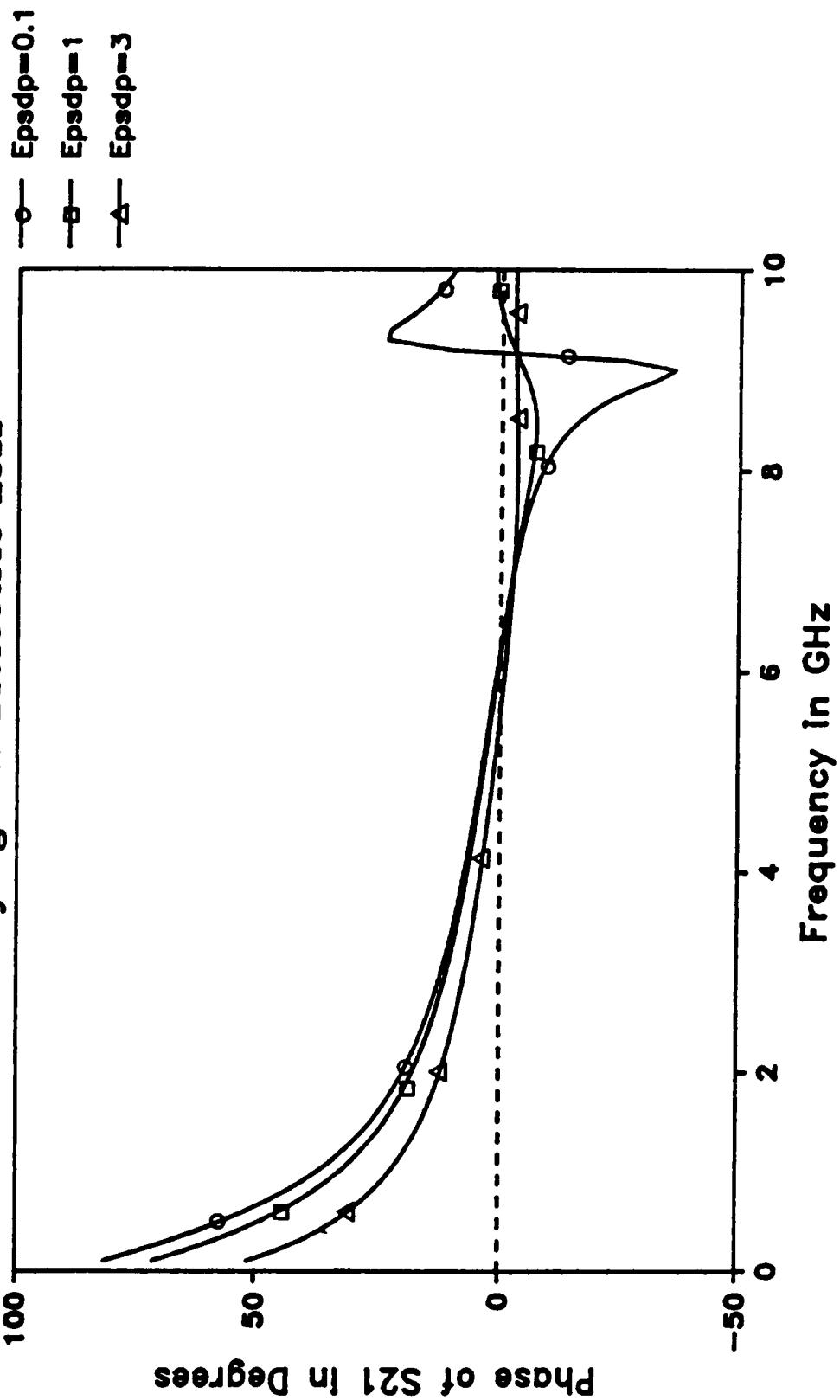
Figure 4.15: Effect of varying the dielectric loss on the magnitude of S_{11}.
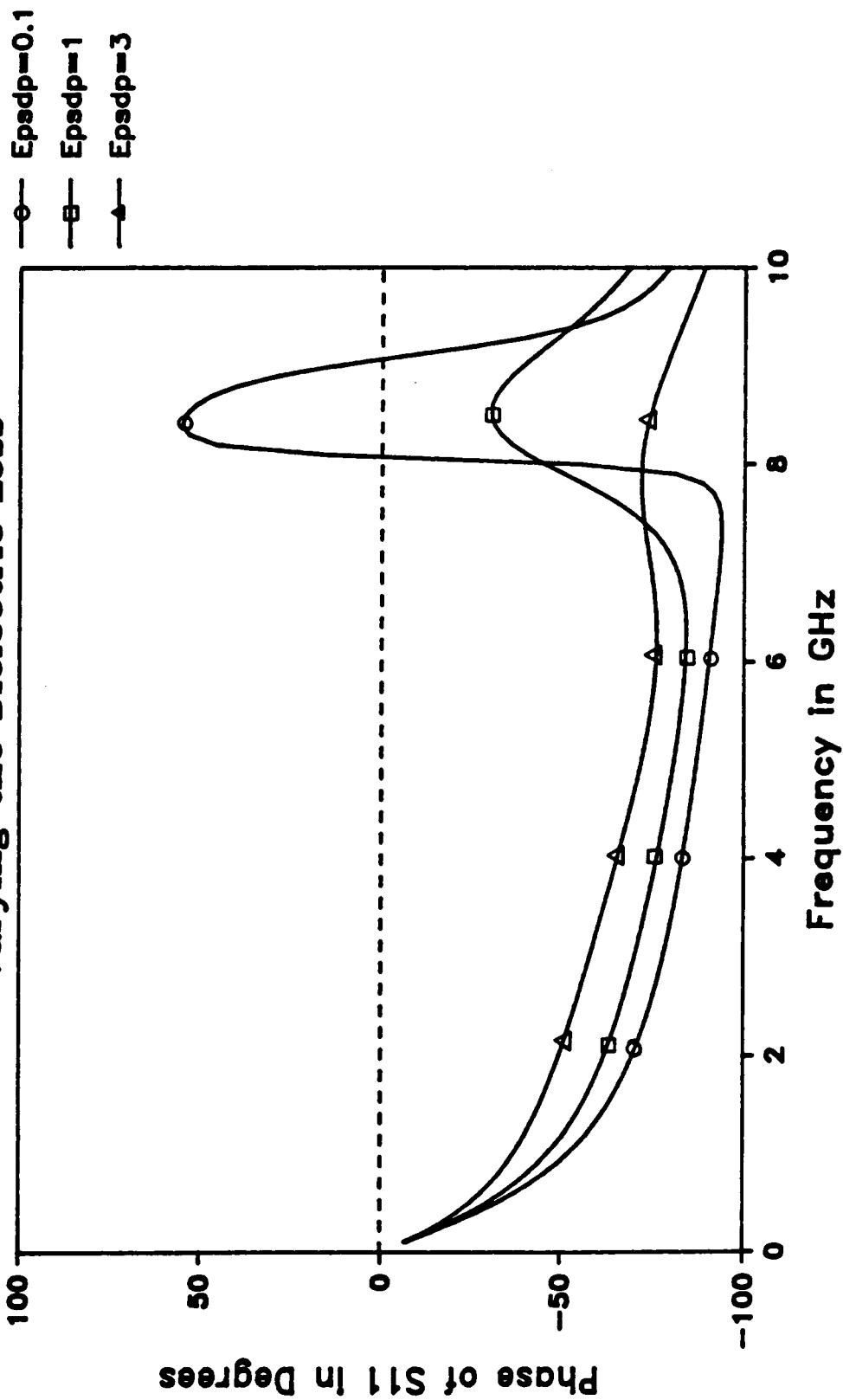
Figure 4.16: Effect of varying the dielectric loss on the phase of S_{11}.
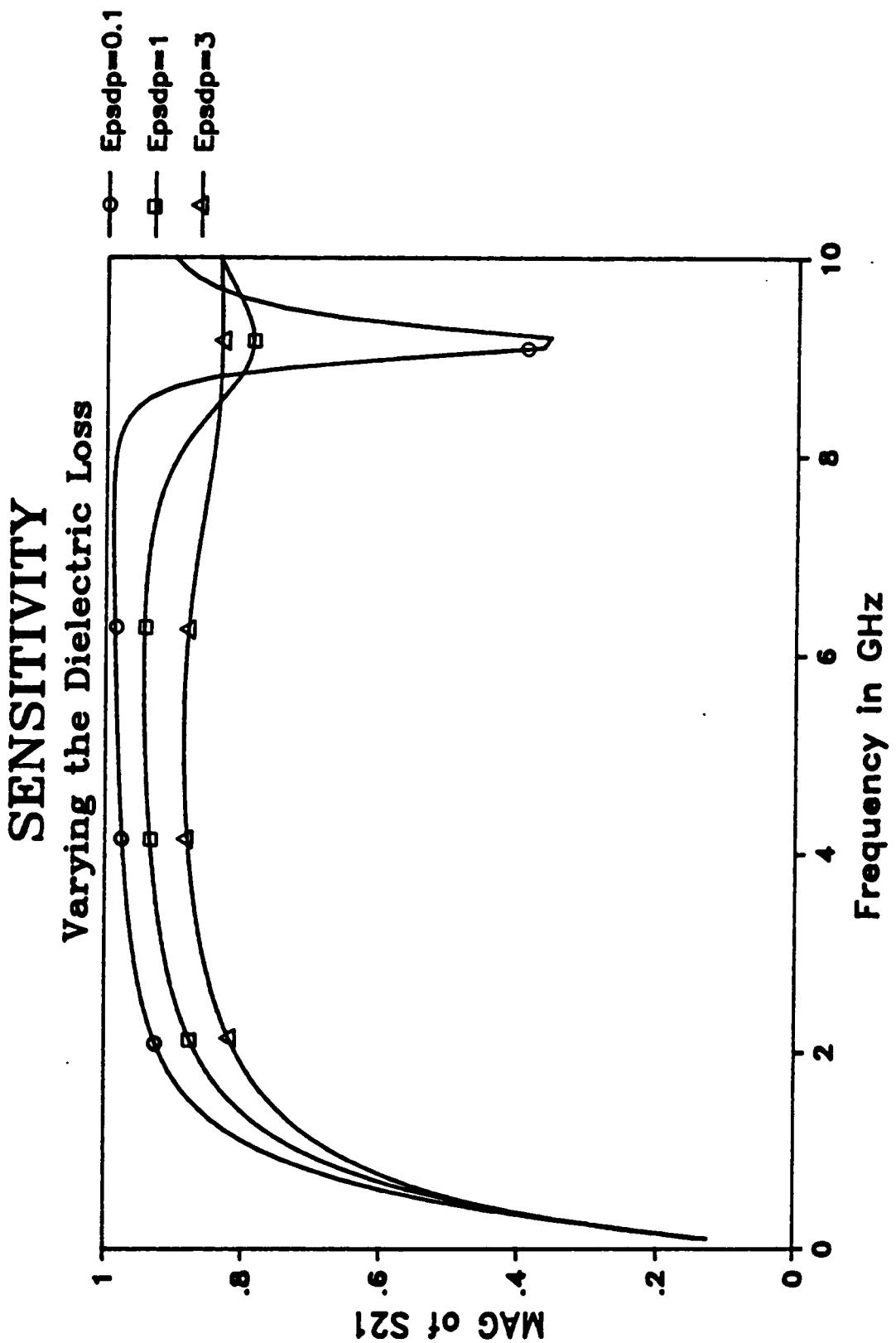
Figure 4.17: Effect of varying the dielectric loss on the magnitude of S_{21}.
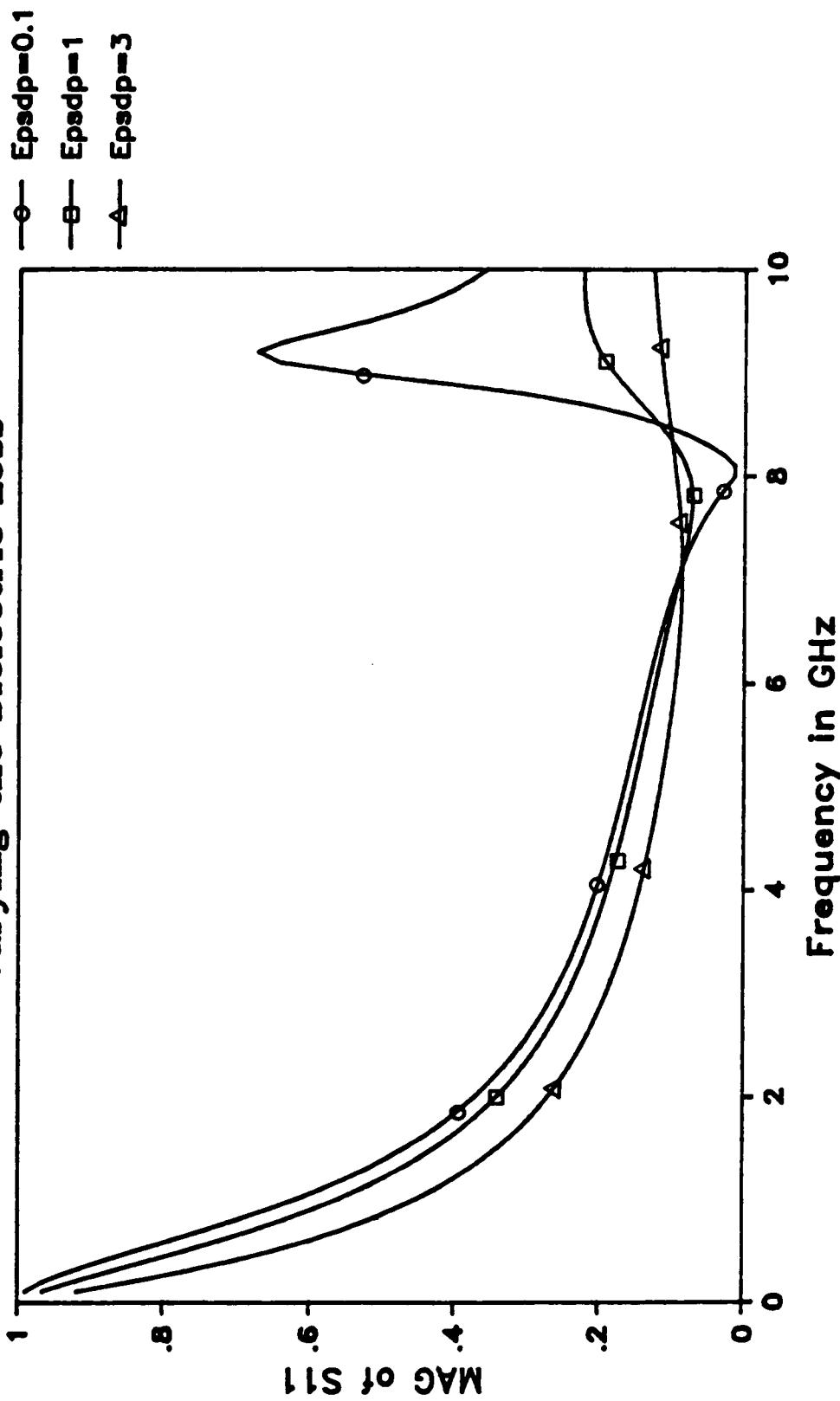
Figure 4.18: Effect of varying the dielectric loss on the phase of S_{2i}.
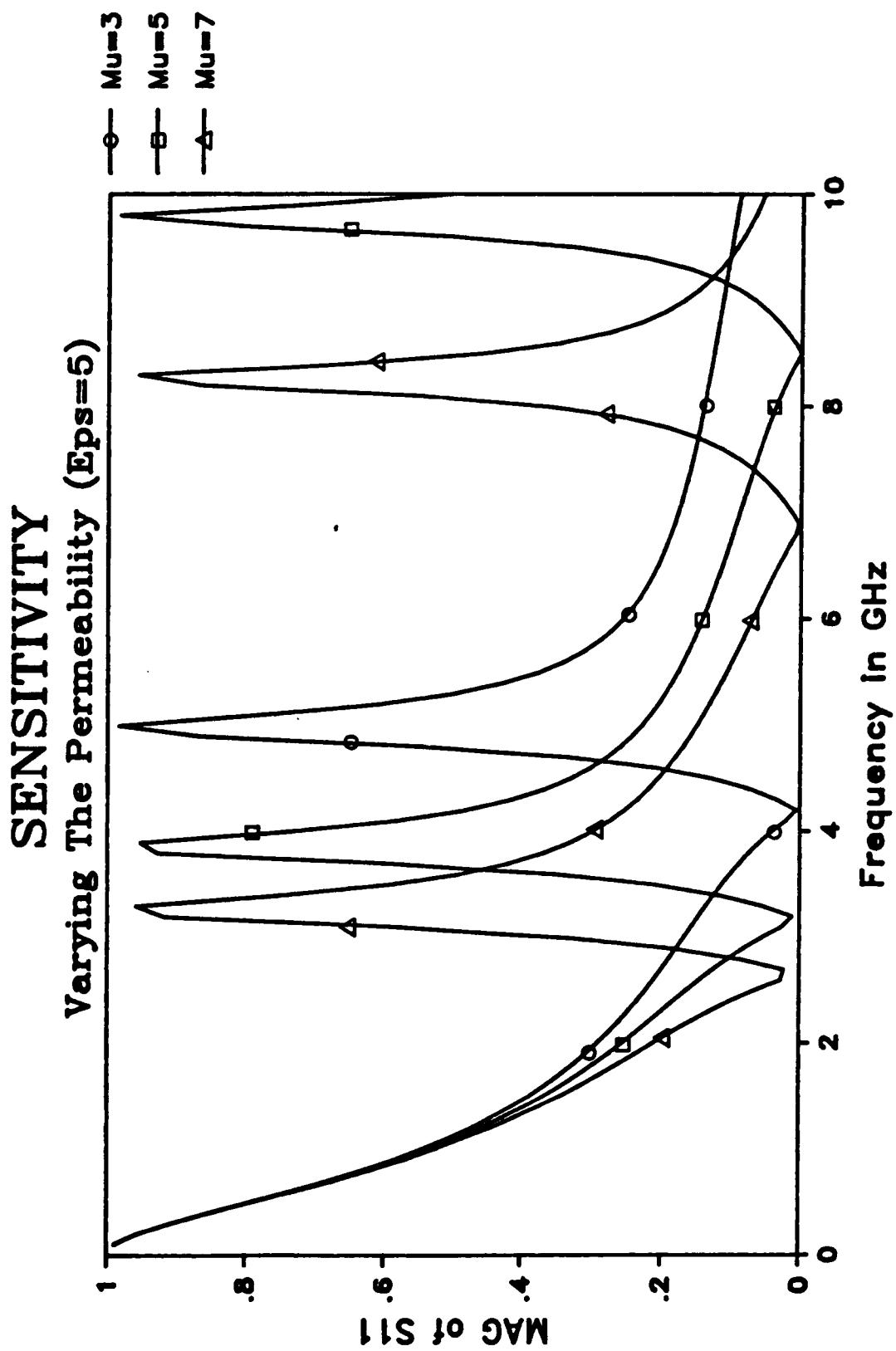
Figure 4.19: Effect of varying the permeability on the magnitude of S_{11}.
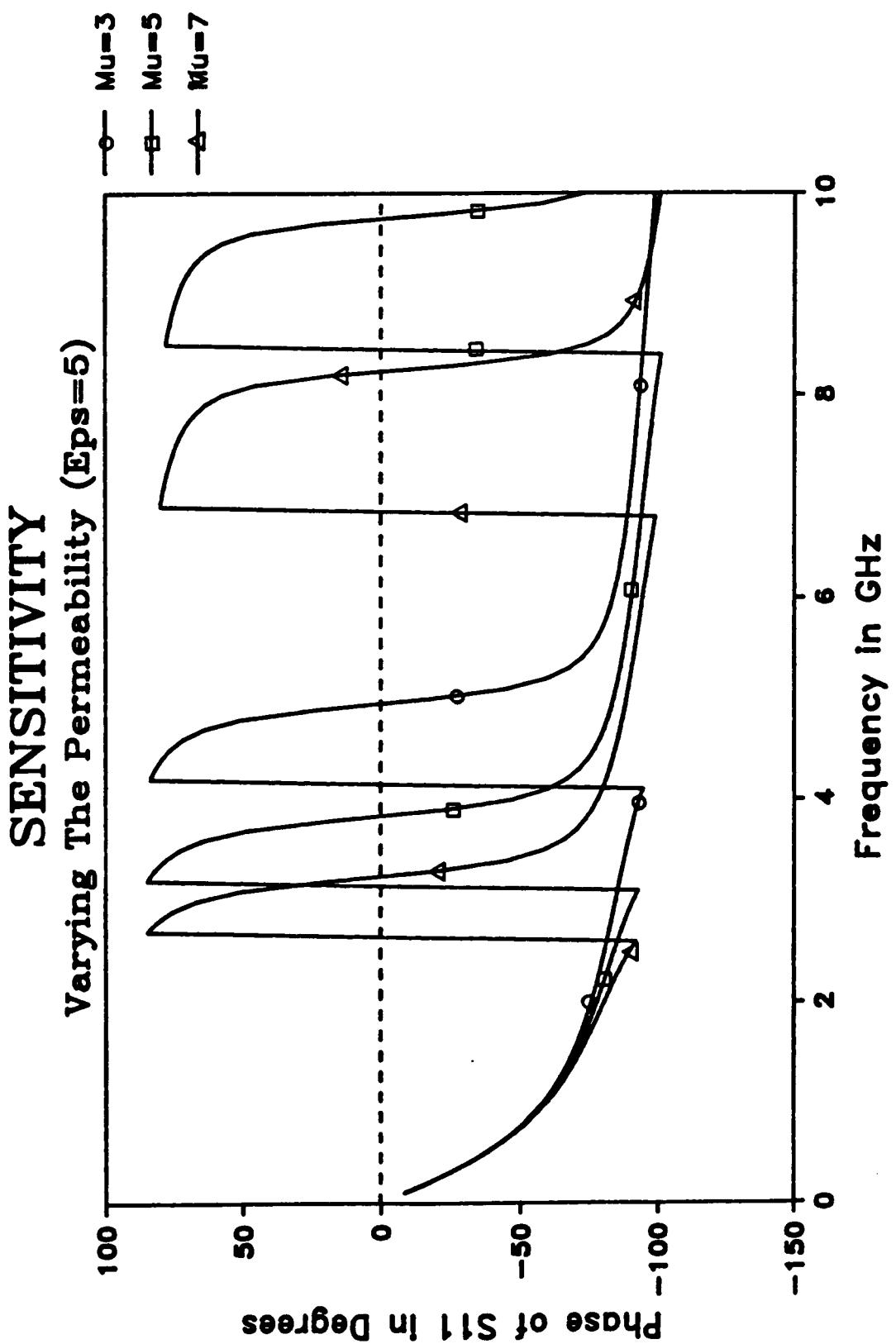
Figure 4.20: Effect of varying the permeability on the phase of S_{11}.
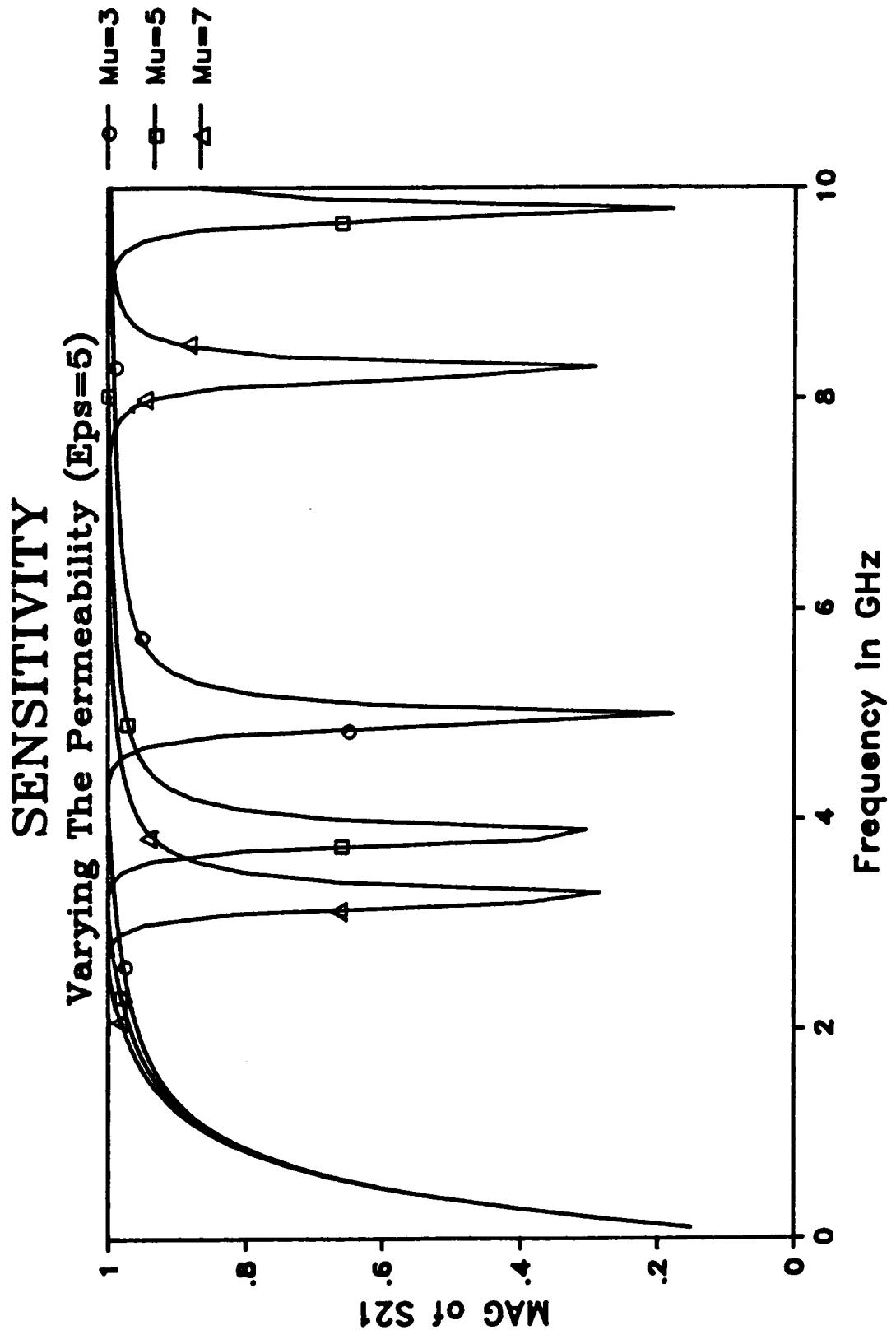
Figure 4.21: Effect of varying the permeabilty on the magnitude of S_{21}.
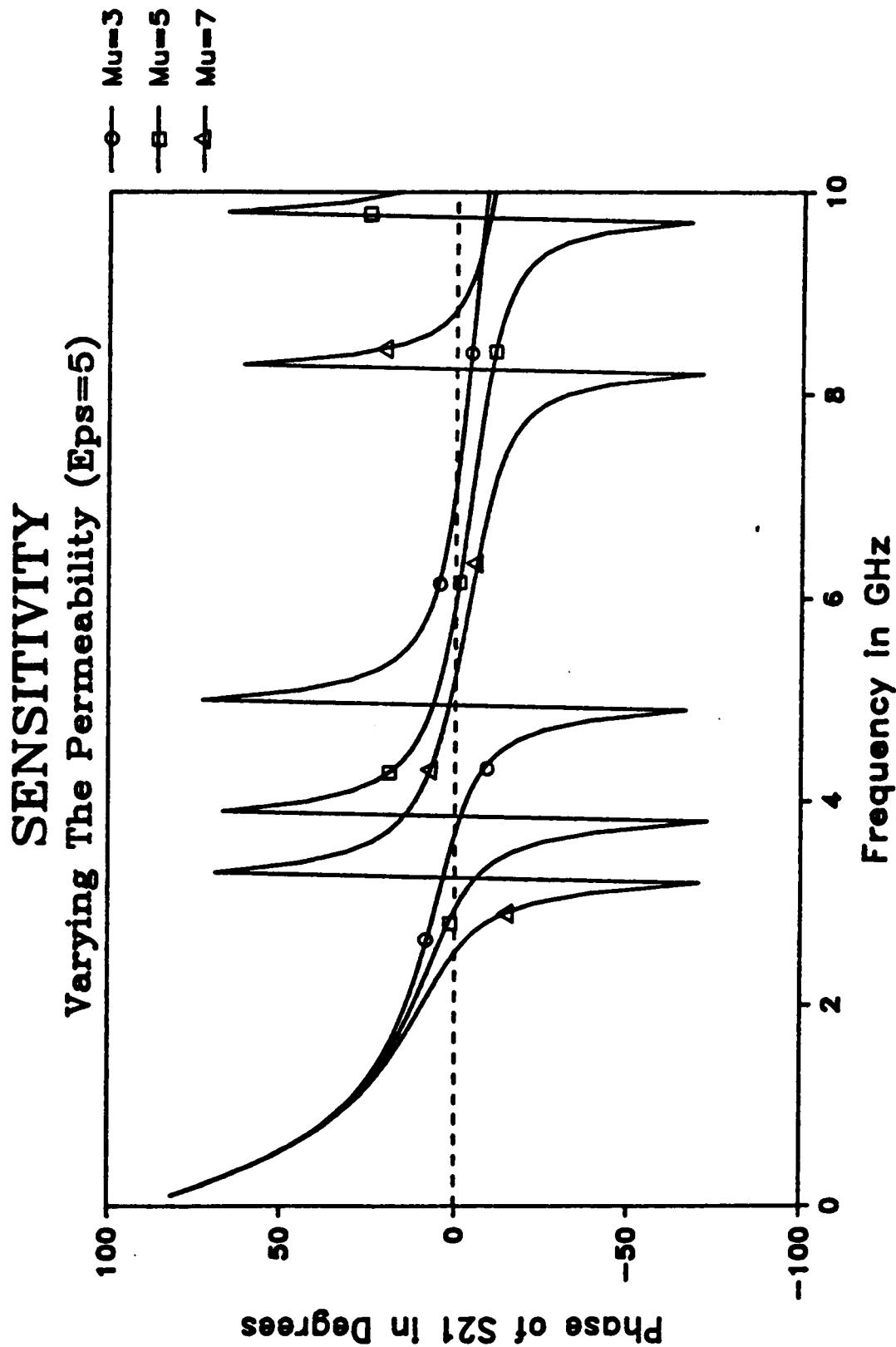
Figure 4.22: Effect of varying the permeability on the phase of S_{21}.
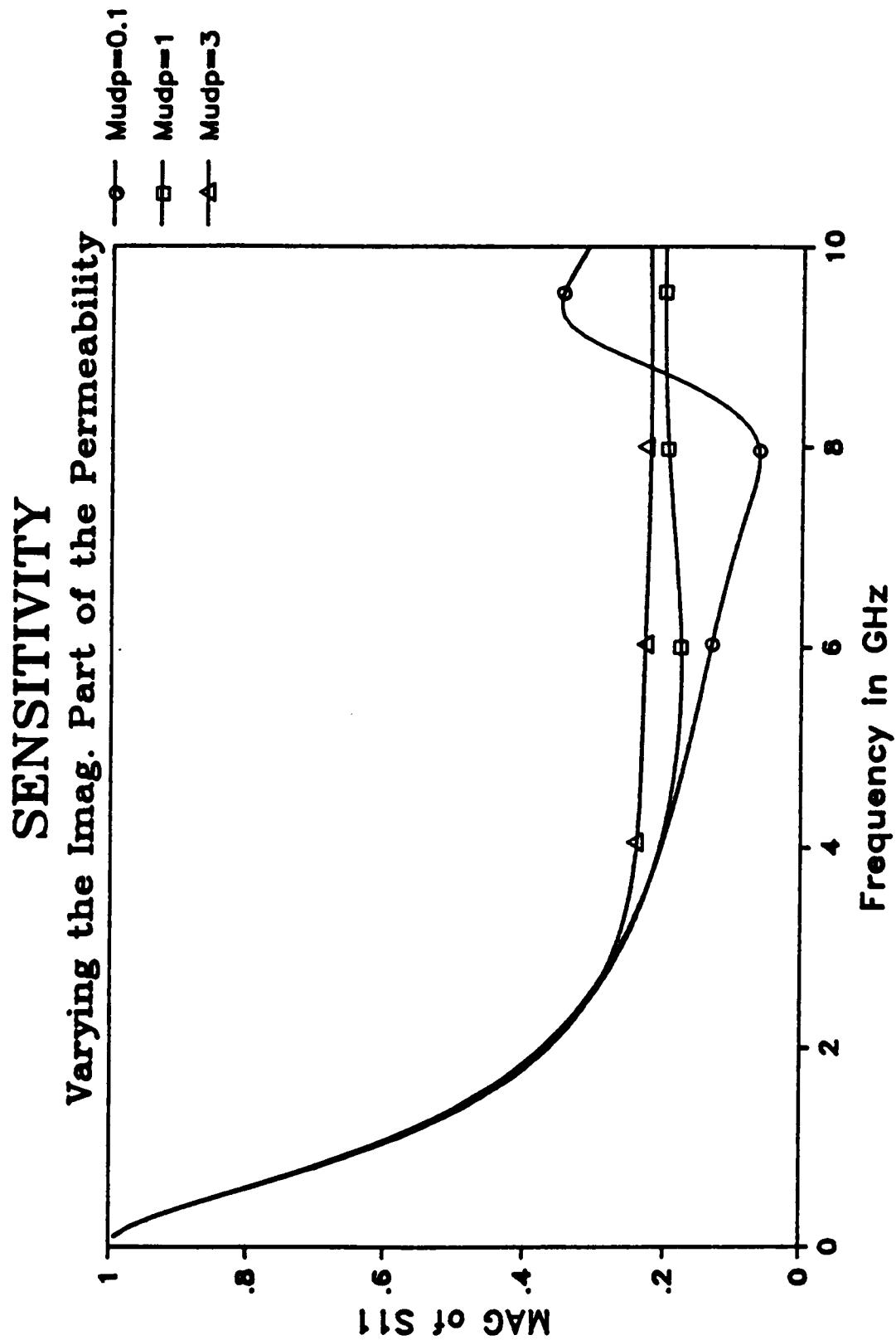
Figure 4.23: Effect of varying the magnetic loss on the magnitude of S_{11}.
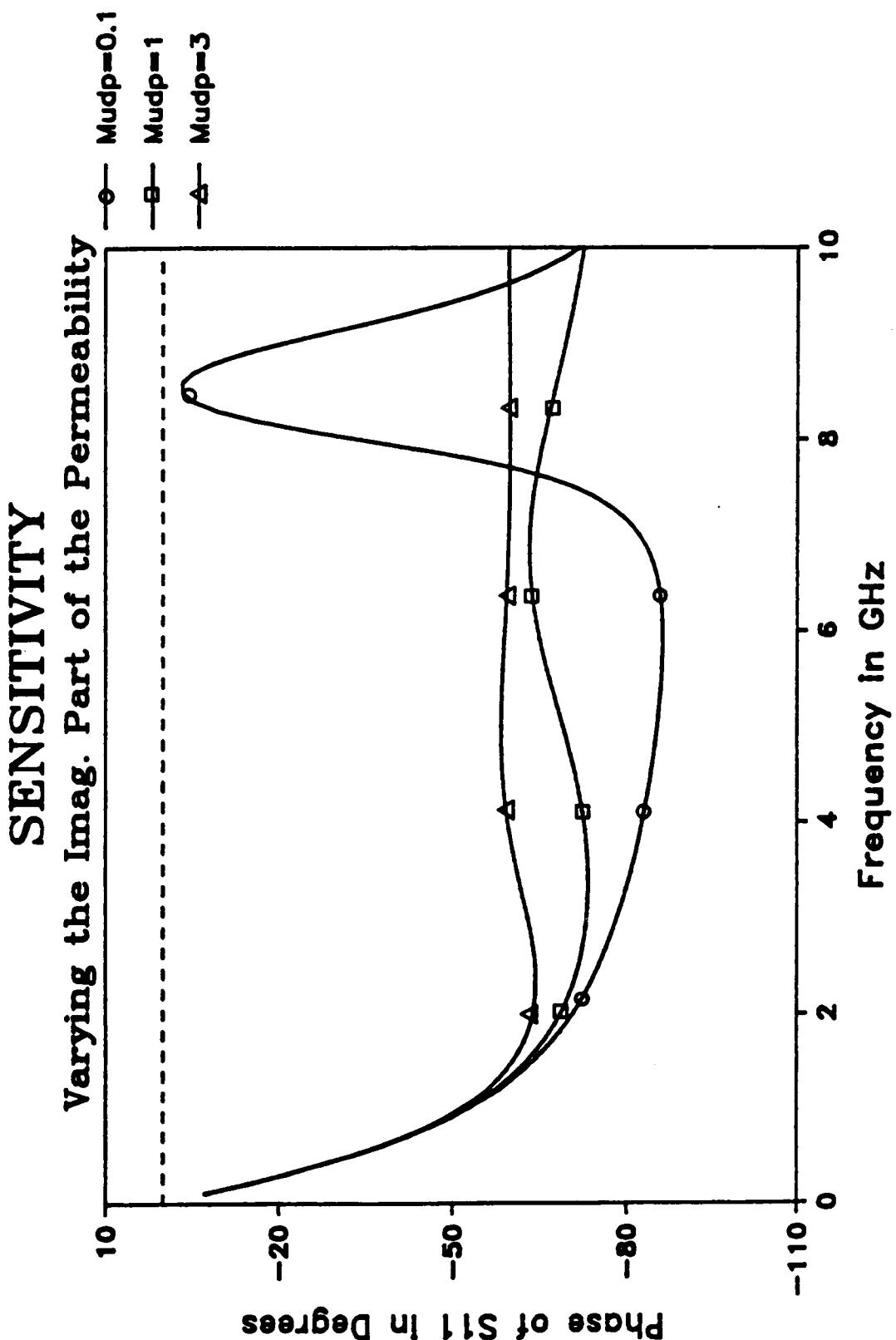
Figure 4.24: Effect of varying the magnetic loss on the phase of S_{11}.
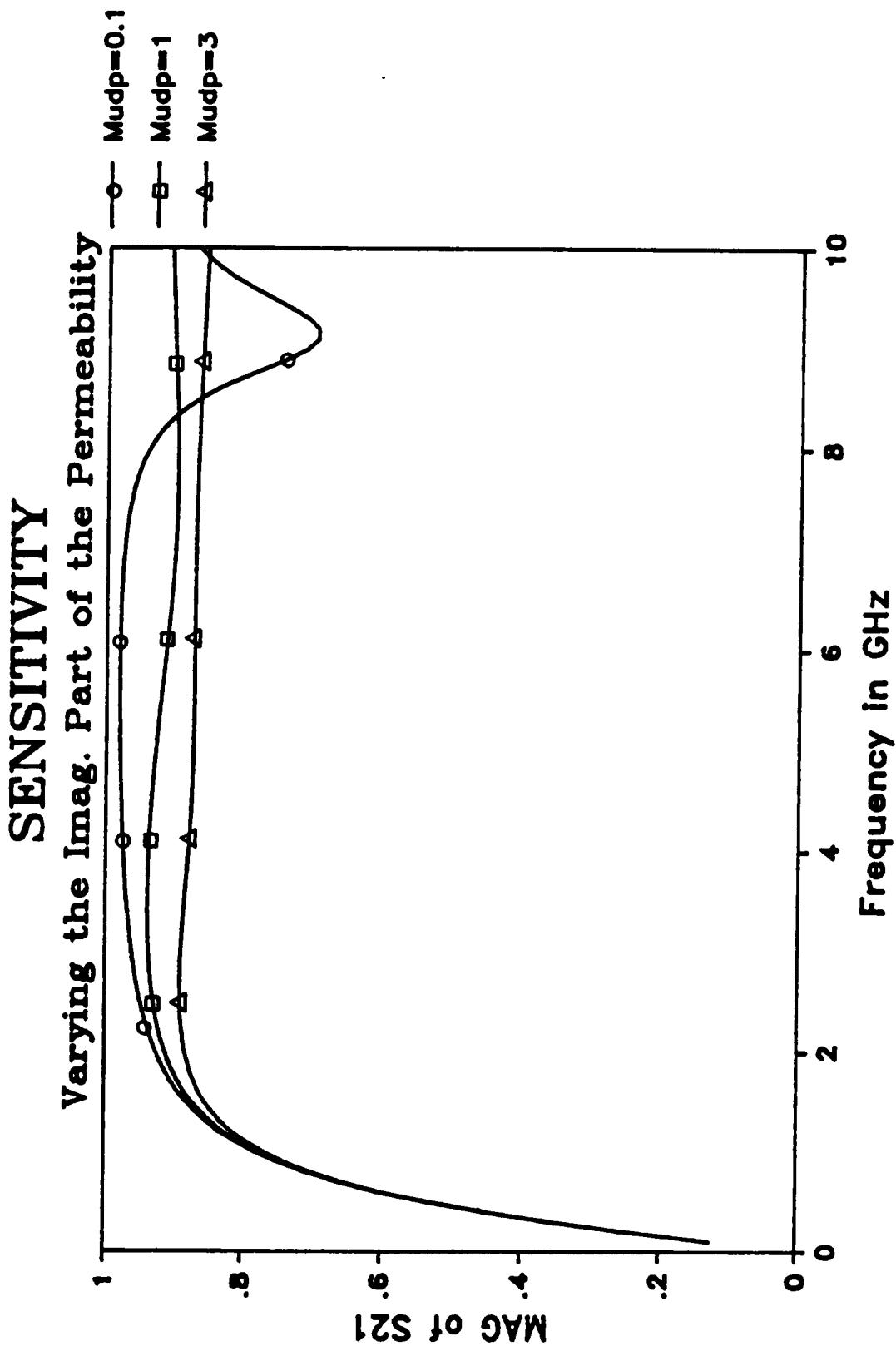
Figure 4.25: Effect of varying the magnetic loss on the magnitude of S_{21}.
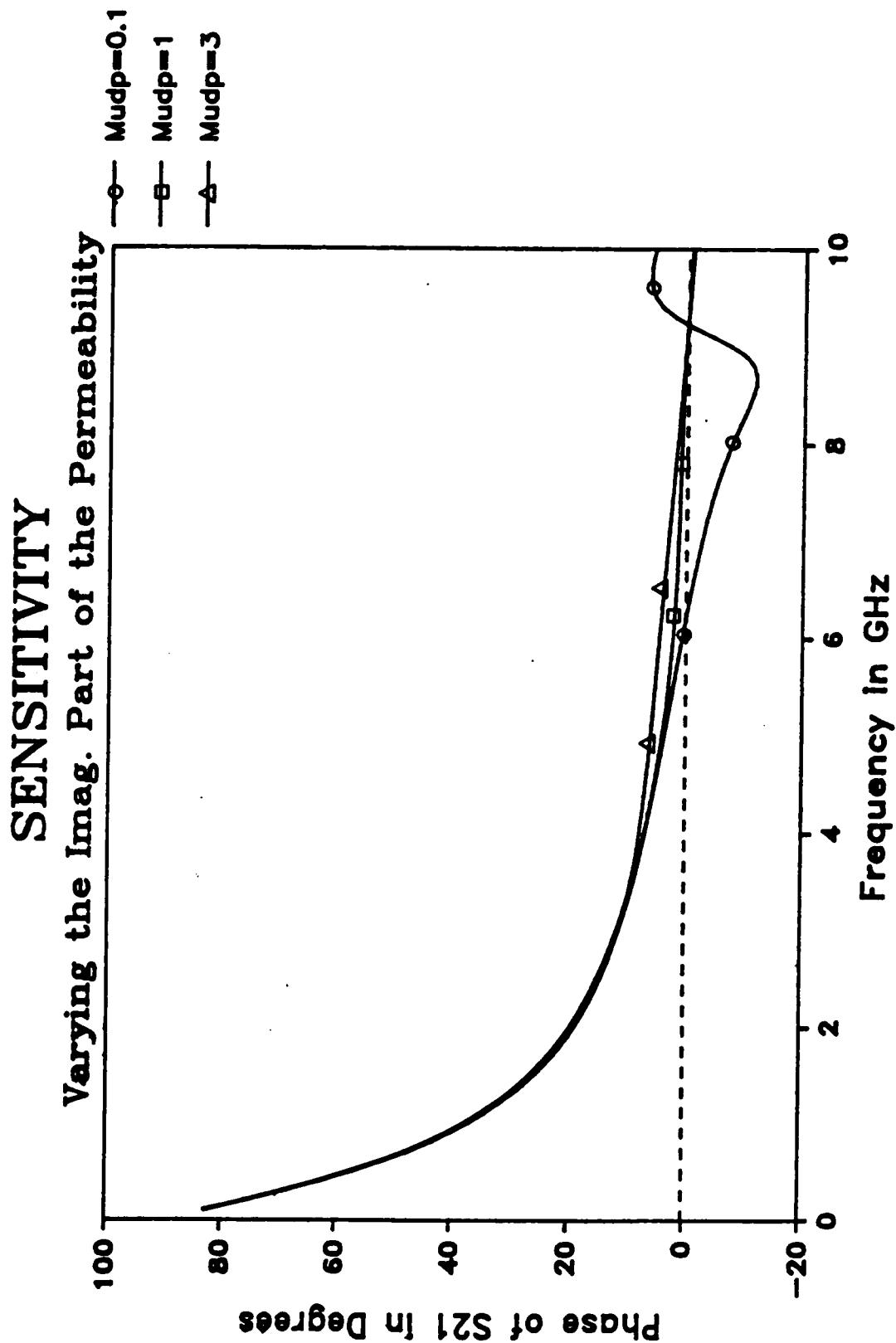
Figure 4.26: Effect of varying the magnetic loss on the phase of S_{21}.

resonance frequencies. Therefore, it is concluded that estimating the complex permeability using this configuration is very difficult.

4.4 Measurement Technique and Experimental Results:

The experimental setup used to measure S_{11} and S_{21} is the time domain setup shown in figure (4.27). The devices shown in the figure were described in Chapter 3, section 3.4.
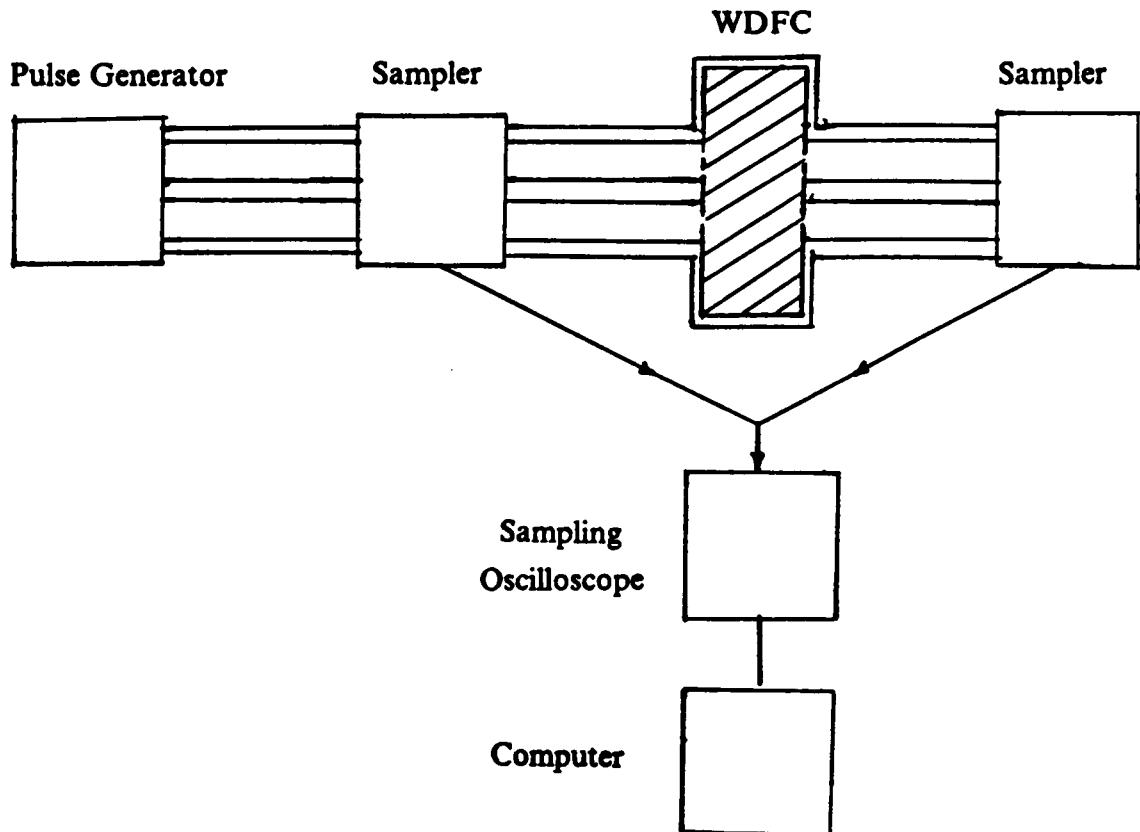
Figure 4.27: The experimental setup.

The procedure to measure the reflection coefficient, S_{11}, was presented in Chapter 3, section 3.4. Figure (4.28) shows the phase of S_{11} of a sample measurement while figure (4.29) shows the magnitude of S_{11}.

To measure the transmission coefficient, S_{21}, first, the WDFC is removed to acquire a reference waveform, $v_{refr}(t)$, as shown in figure (4.30a). Then, the response waveform, $v_{resp}(t)$, is acquired with the WDFC in its place as shown in figure (4.30b).
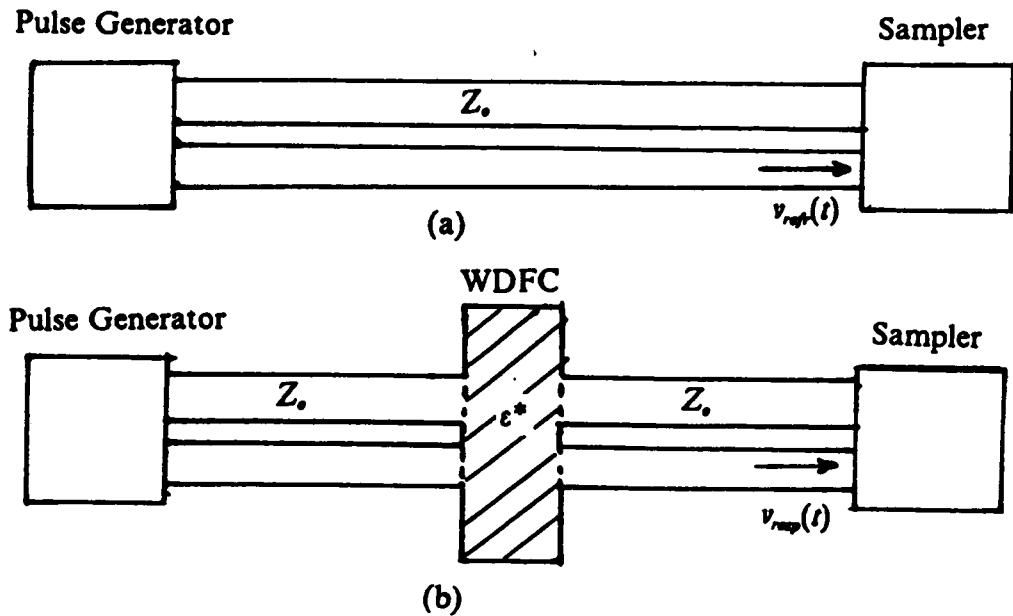
Figure 4.30: Measurement of reference and response waveforms to compute $S_{21}(j\omega)$

Figures (4.31) and (4.32) show the reference and response waveforms of a sample measurement. $S_{21}(j\omega)$ is then given by

$$S_{21}(j\omega) = \frac{V_{resp}(j\omega)}{V_{refr}(j\omega)}$$ (4.79)

where $V_{refr}(j\omega)$ and $V_{resp}(j\omega)$ are the Fourier transforms of $v_{refr}(t)$ and $v_{resp}(t)$, respectively. The complete fast Fourier transform (CFFT) method [54] is used to compute the Fourier

SAMPLE MEASUREMENT
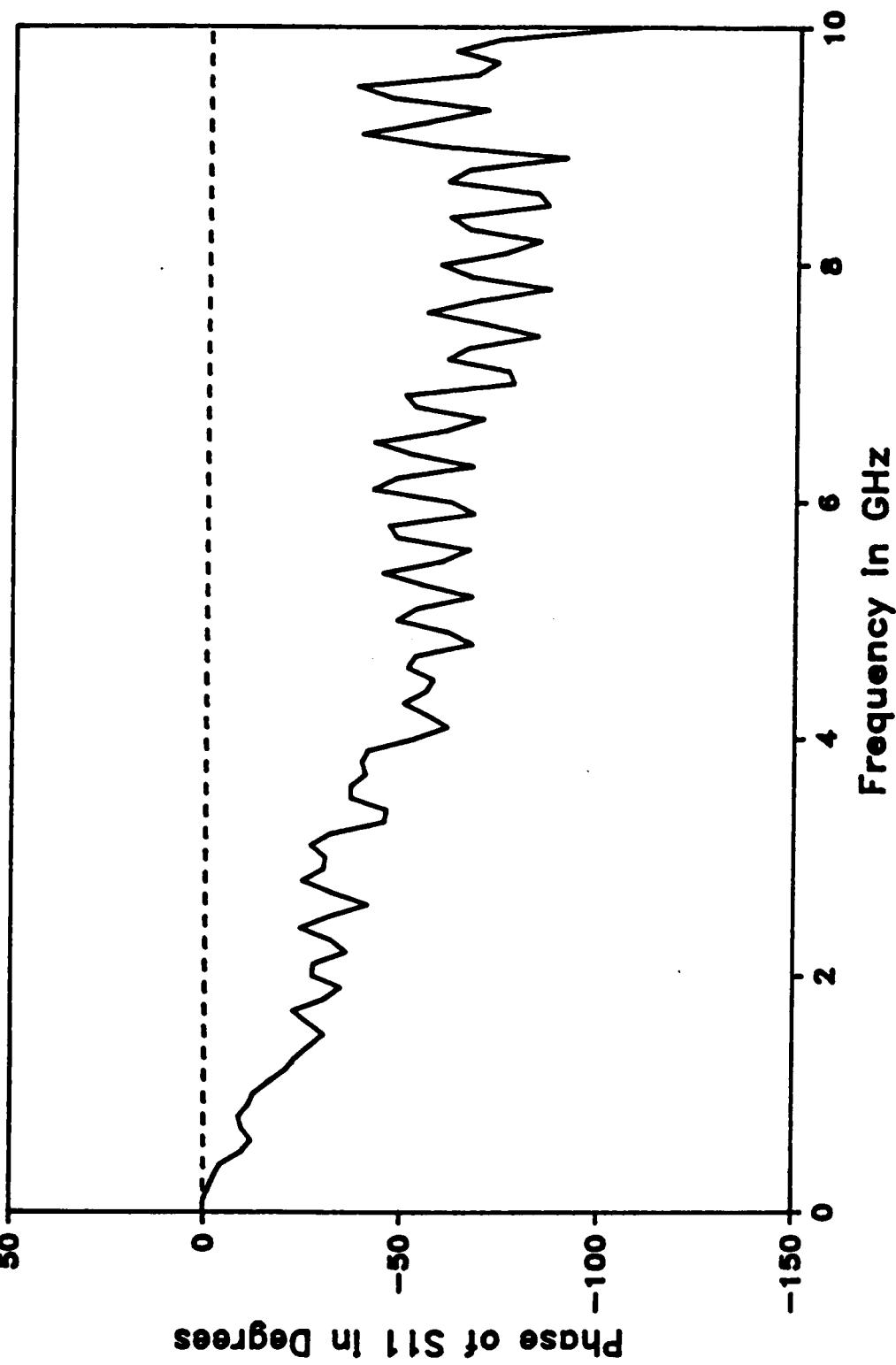
Figure 4.28: Phase of S_{11} of a sample measurement.
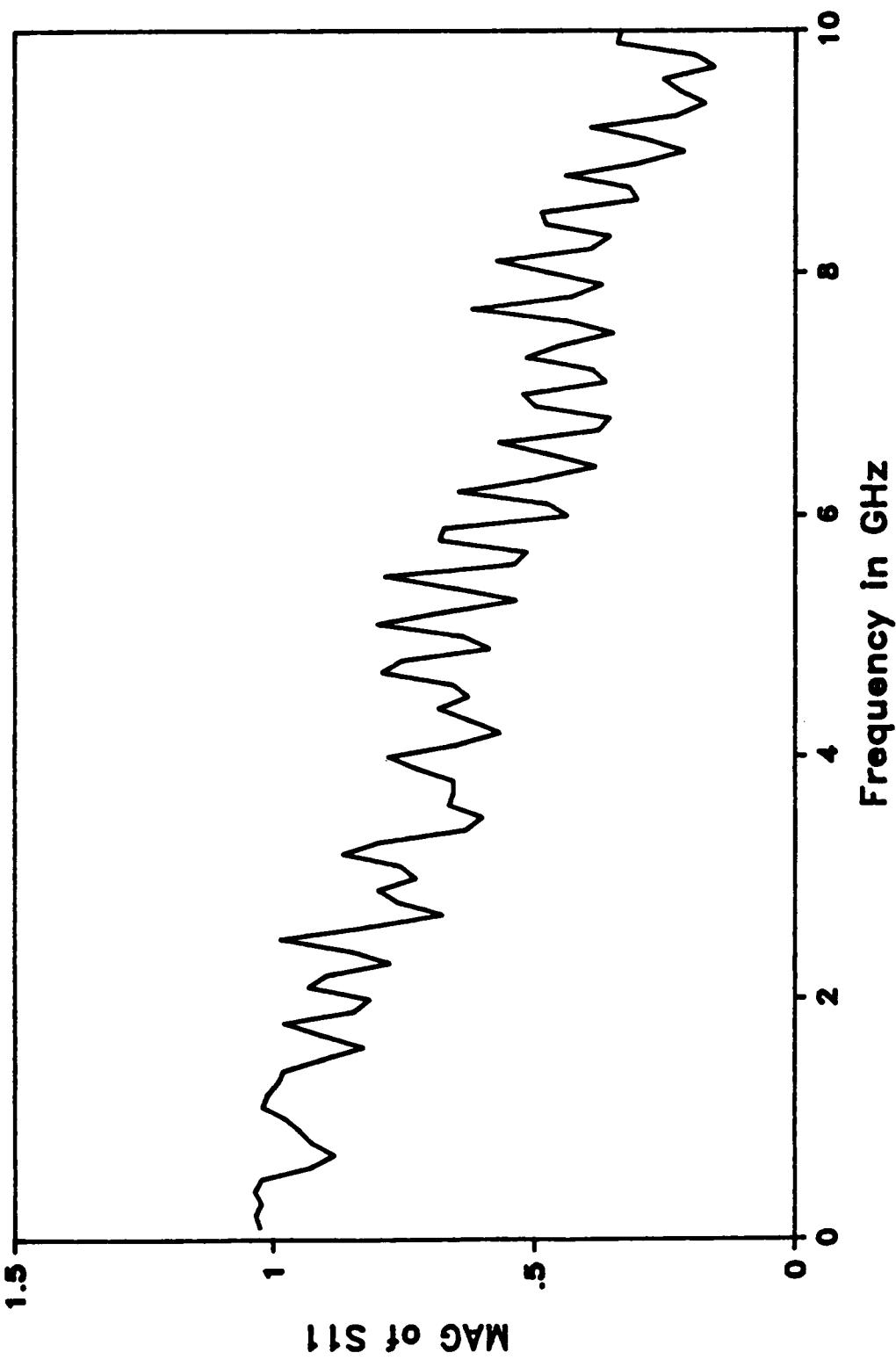
Figure 4.29: Magnitude of S_{11} of a sample measurement.
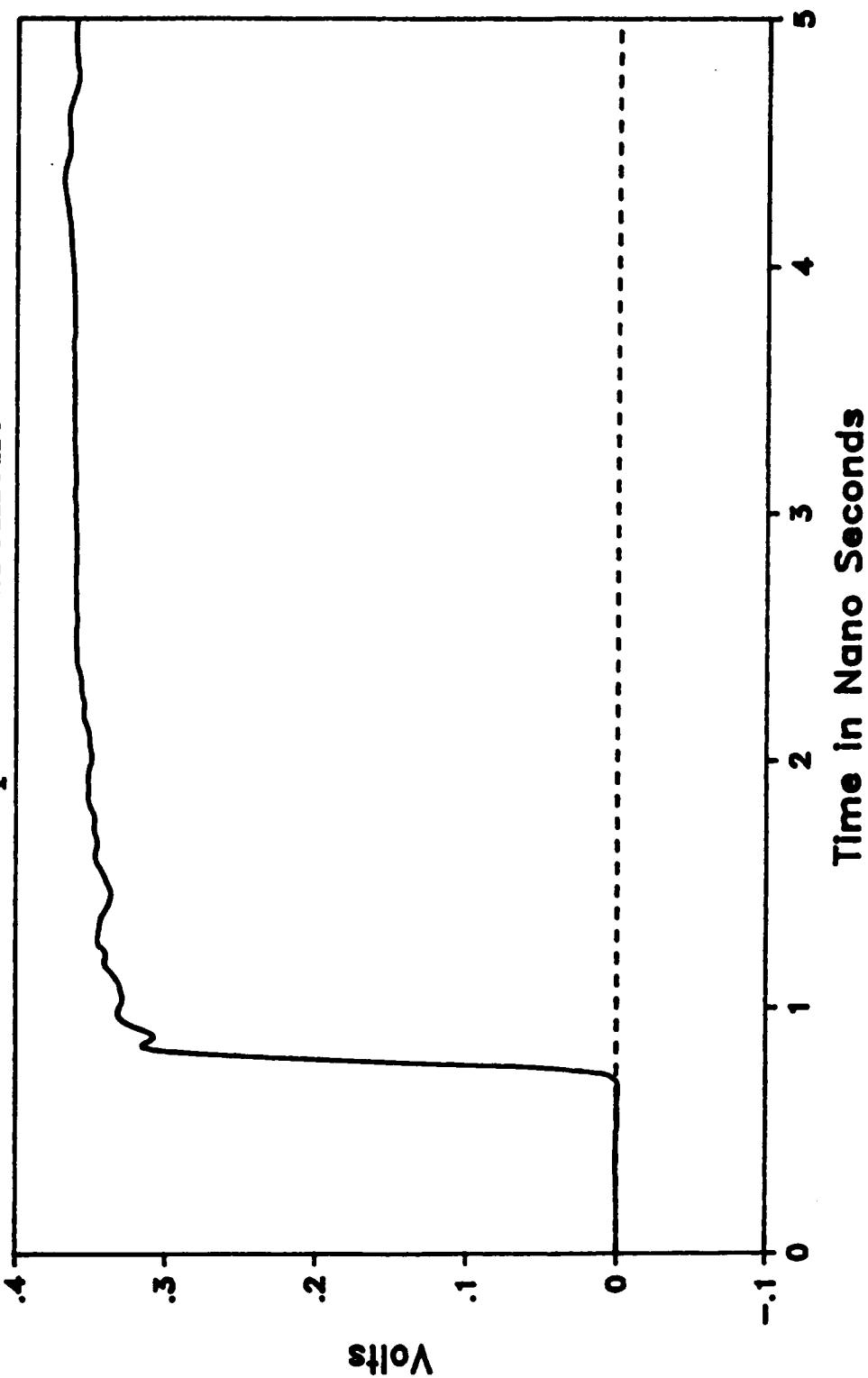
Figure 4.31: Reference waveform used for the computation of S_{21}.
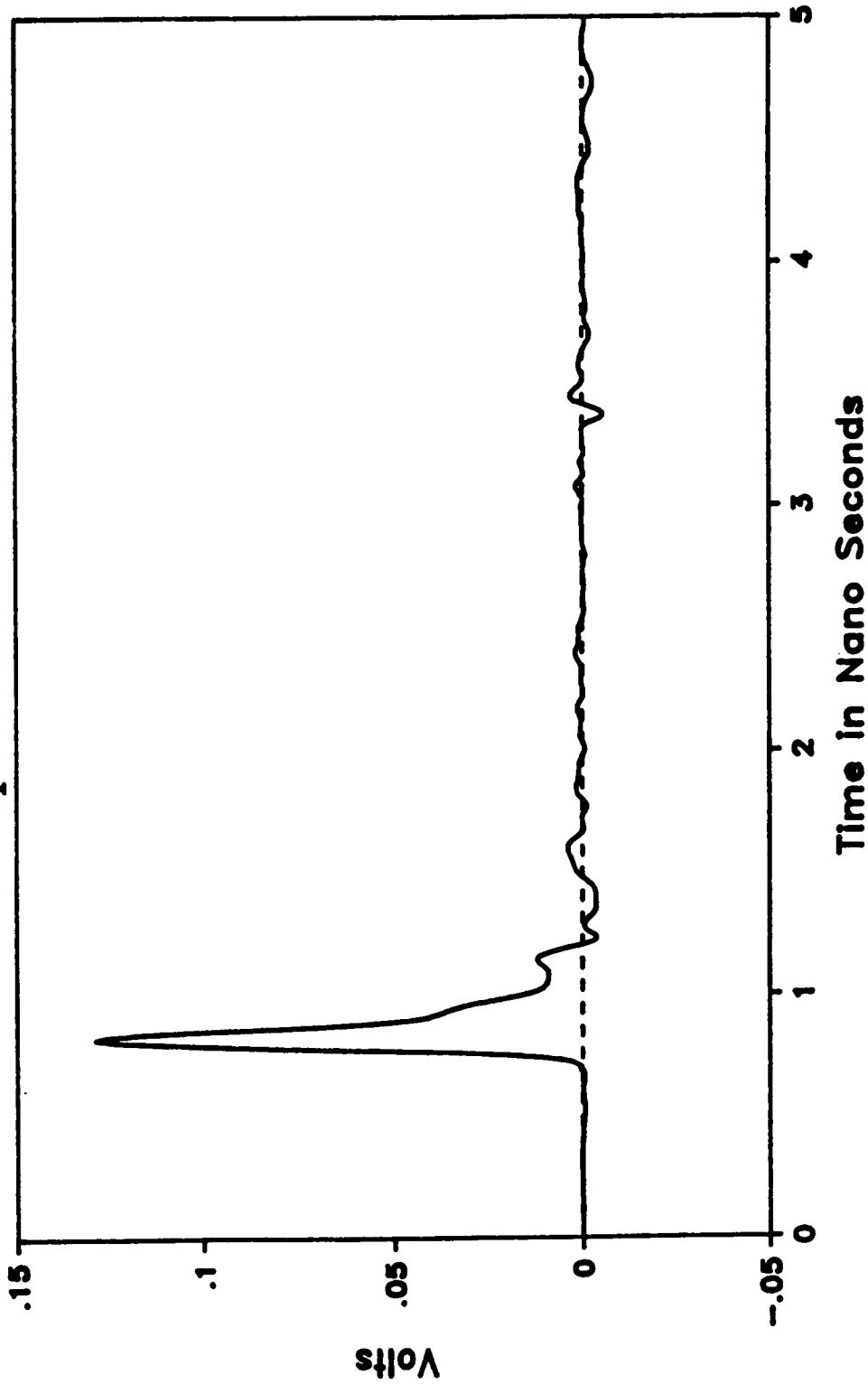
Figure 4.32: Response waveform used for the computation of S_{21}.

transforms since $v_{ref}(t)$ and $v_{resp}(t)$ are step - like waveforms. Figure (4.33) shows the phase of $S_{21}(j\omega)$ while figure (4.34) shows the magnitude for a sample measurement.

The Tektronix SPS-Basic computer program listed in appendix VI was used to enable the data acquisition and to compute S_{11} and S_{21}. An experiment was performed using teflon, which is known to have a dielectric constant of 2.1, to verify the technique. The experimental setup described above was used to measure both $S_{11}(j\omega)$ and $S_{21}(j\omega)$. Then, the computer program listed in appendix IV was used to compute the complex permittivity. The WDFC was formed by using a disk sample of the material to be characterized cut precisely to fit in between two APC-7 connectors. This only approximates the WDFC structure because of the presence of air gaps between the disk sample and the the walls of the APC-7 connectors forming the cavity. This source of error would be avoided if the cavity walls were molded or deposited on the sample. It has been assumed that $\mu^*_r = 1$ which is a reasonable assumption. Figure (4.35) shows the dielectric constant using $S_{11}(j\omega)$ and $S_{21}(j\omega)$ while figure (4.36) shows the loss ε''. It is observed that the computed dielectric constant using $S_{11}(j\omega)$ matches that obtained from $S_{21}(j\omega)$ which is close to the known value (2.1). The loss, ε_r'' shown in figure (4.36) is not accurate because of the same reasons discussed in Chapter 3, section 3.5.2; the main reason being that the conductor losses were not taken into account which are important when trying to measure the loss of very low loss materials.

Attempts were made to compute both the permittivity and the permeability simultaneously. However, as was expected in section 4.3, these attempts failed to yield good results. The reason being the insensitivity of $S_{11}(j\omega)$ and $S_{21}(j\omega)$ to variations in the permeability which makes it very difficult to obtain reliable results.
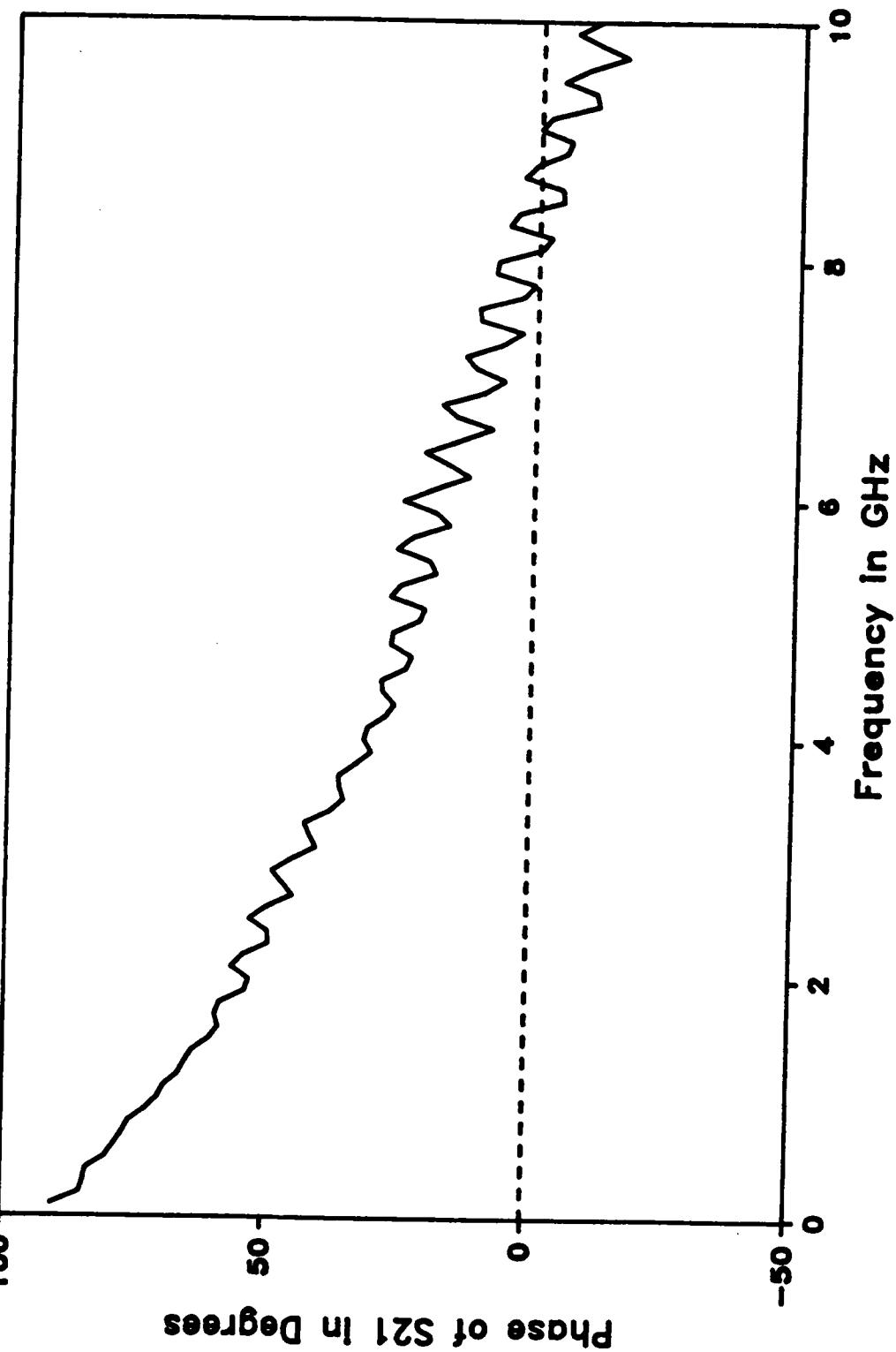
Figure 4.33: Phase of S_{21} of a sample measurement.
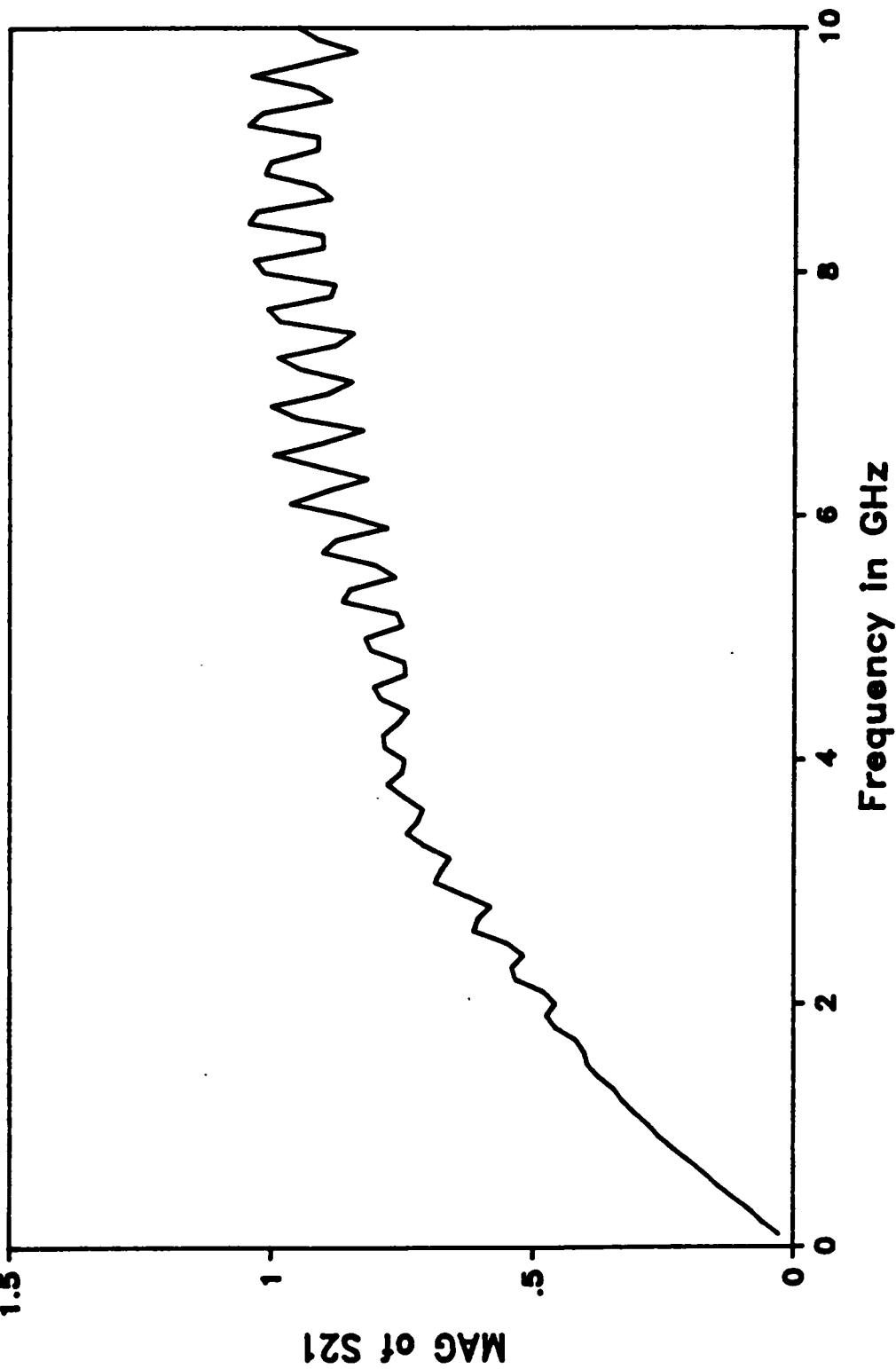
Figure 4.34: Magnitude of S_{21} of a sample measurement.
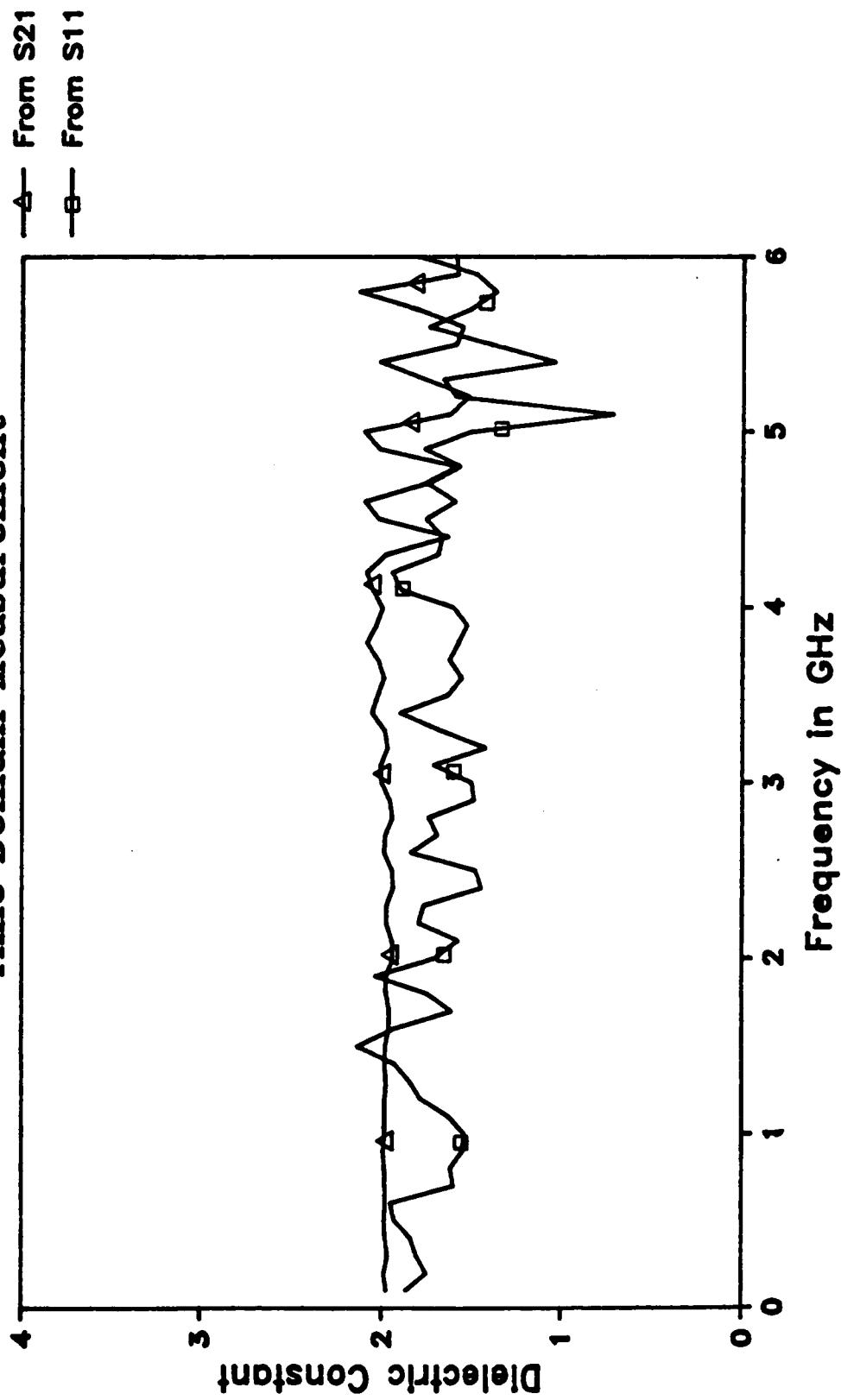
Figure 4.35: Dielectric constant of a teflon sample.
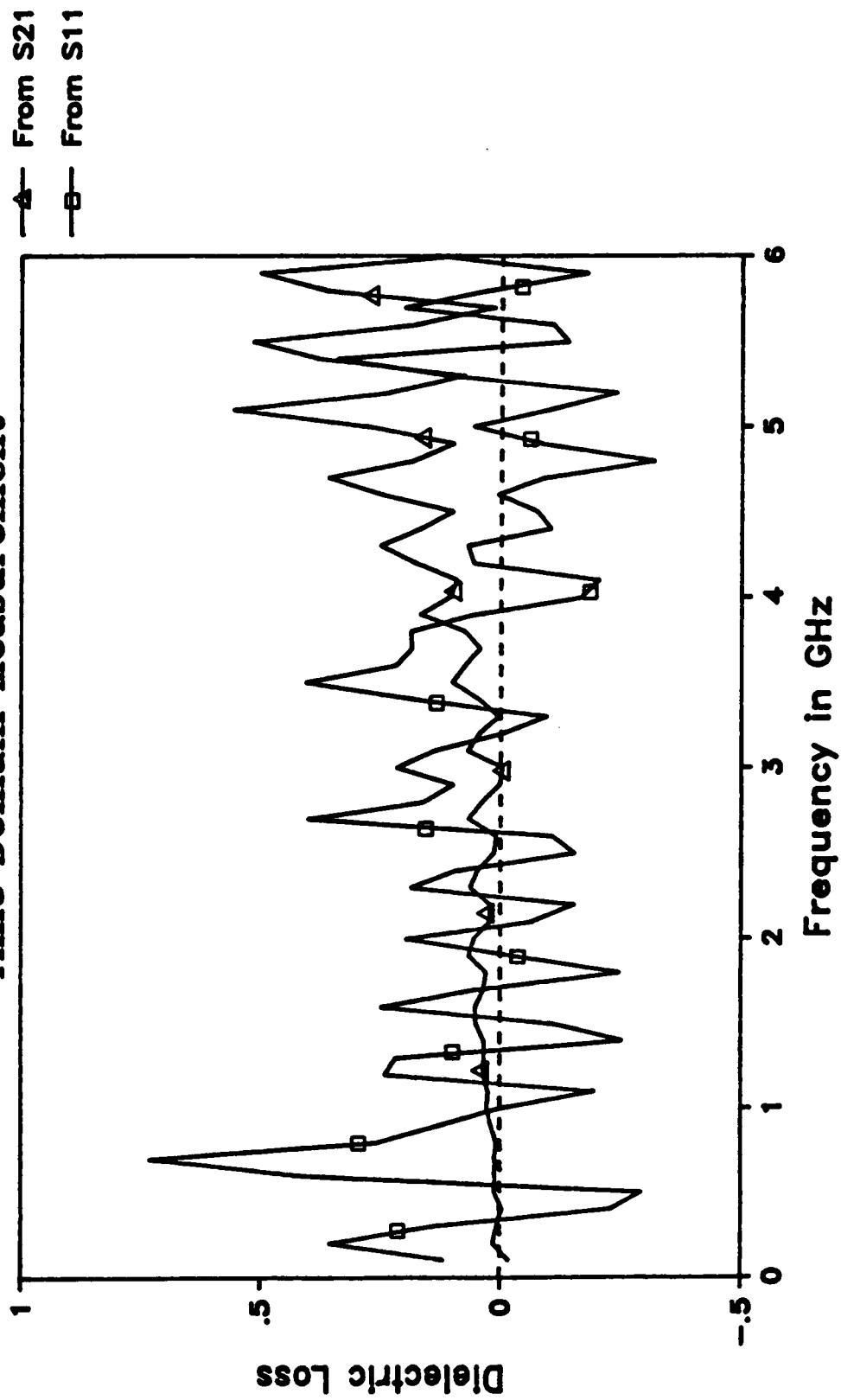
Figure 4.36: Dielectric loss of a teflon sample.

4.5 Conclusion:

This chapter presented the concept and analysis of a wideband dielectric filled cavity (WDFC) placed between two transmission lines to be used for dielectric characterization. This arrangement enables the measurement of both the reflection, $S_{11}(j\omega)$, and the transmission coefficient, $S_{21}(j\omega)$, from either of which the complex permittivity can be computed. In the analysis, higher order modes were taken into account and the solution was obtained using the method of moments.

The results of computer simulation experiments performed to test the sensitivity of the technique to various parameters of the WDFC as well as to test its performance were presented. It was concluded that even if a combined reflection-transmission measurement is performed, the computation of the complex permeability is very difficult. This is due to the fact that both the reflection and transmission coefficients are rather insensitive to variations in the permeability except around the resonance frequencies. As far as the dimensions of the WDFC are concerned, it is desirable to choose the diameter such that the first resonance due to the radial dimension is outside the bandwidth of interest.

The time-domain measurement set up used to measure $S_{11}(j\omega)$ and $S_{21}(j\omega)$ was described. The results of an experiment, performed in the time domain, to compute the complex permittivity of a teflon sample were also presented. The dielectric constant was computed successfully from both $S_{11}(j\omega)$ and $S_{21}(j\omega)$ However, the estimate of the loss (ε''_r) was inaccurate due to the fact that these materials have very low losses. Consequently, in order to obtain accurate results for ε''_r, the conductor losses must be taken into account, particularly, the losses in the cavity walls. Also, a very precise measurement setup must be used. The main source of error in these experiments is the presence of air gaps between the cavity walls, which was formed using two APC-7 connectors, and

the dielectric sample. This source of error can be avoided if the cavity walls are molded or deposited on the dielectric sample.

Chapter 5

CONCLUSION

This thesis summarized the work done towards developing a dielectric filled cylindrical cavity to be used for dielectric characterization over the frequency range 50 MHz - 15 GHz. This cavity structure was referred to as Wideband Dielectric Filled Cavity (WDFC). Two configurations were investigated:

1. The WDFC was adapted to the end of a transmission and the reflection coefficient was measured. The complex permittivity was then derived from the reflection coefficient information.

2. The WDFC was placed between two transmission lines. The complex permittivity is then derived from either the reflection coefficient, $S_{11}(j\omega)$, or the transmission coefficient, $S_{21}(j\omega)$.

The cavity walls can be molded or deposited on the dielectric sample to eliminate possible air gaps between the sample and the conductor walls of the cavity.

The full field analysis for these configurations was carried out to establish the relationship between the the complex permittivity and the reflection coefficient or the transmission coefficient. The solutions were obtained using the method of moments. Computer simulation experiments were performed to test the sensitivity of $S_{11}(j\omega)$ and $S_{21}(j\omega)$ to different parameters of the WDFC, and to predict the performance of each configuration. Furthermore, the time-domain experimental setups used to measure the

reflection and transmission coefficients were described. These configurations were used to characterize some known materials for verification purposes. The first configuration was also used to characterize two thick film materials: the DuPont 5704 thick film dielectric paste and the DuPont PCM dielectric paste.

The dielectric constant was estimated satisfactorily using both configurations. However, the dielectric loss estimates were not accurate because those materials were very low loss materials. Therefore, extreme precision in the measurement of the reflection and transmission coefficients is required to obtain reliable loss estimates for such materials. Moreover, the conductor losses must be taken into account in the analysis, particularly, the losses in the cavity walls.

Attempts were made to compute the permeability in addition to the permittivity using the second configuration by performing a combined reflection - transmission measurement. These attempts were not successful because of the insensitivity of the reflection and transmission coefficients to variations in the permeability, as was expected from the simulation experiments. Nevertheless, the assumption that the permeability of dielectric materials to be unity is valid and very reasonable.

APPENDICES

Appendix I provides the Fortran computer program listing used to compute the reflection coefficient of a wideband dielectric filled cavity (WDFC) adapted to the end of a transmission line assuming that the complex permittivity of the dielectric material is known (Program REFCAV).

Appendix II lists the Fortran computer program code used to compute the complex permittivity of a dielctric material using the WDFC adapted to the end of a transmission line from the reflection coefficient information (Program REFCAVOP).

Appendix III provides the Fortran computer program listing used to compute the reflection and transmission coefficients of the WDFC placed between two transmission lines given the complex permittivity and the complex permeability (Program TRCAV).

Appendix IV lists the Fortran computer code used to compute the complex permittivity and/or the complex permeability of a dielectric material using the WDFC placed between two transmission lines from the reflection coefficient and/or the transmission coefficient (Program TRCAVOP).

Appendix V lists the common subroutines being called by the programs in the above appendices.

Appendix VI provides the listing of the computer program written in Tektronix SPS-Basic to enable data acquition in the time domain setup and compute the reflection / transmission coefficient (Program ACQRFTR)

Appendix I: Program REFCAV

The following Fortran program implements the equations derived in Chapter (3) to compute the reflection coefficient of the WDFC which is adapted to the end of a transmission line assuming that the complex permittivity of the dielectric material is known.

```
      IMPLICIT REAL*8(A-H,O-Z)
      COMPLEX*16 Z,ZNUM,ZDEN,JSM,YA(50,50),YB(50,50),Y(50),
     *V(50)
      DIMENSION ROOTS(100),RKCS(50),CONSB(100),CONSM(50),
     *RESINT(100,50),ZEROS(100),ARRAY(3),ALP(50),BET(50), FARR(100),
     *SARR(100)
      OPEN(1,FILE = 'REFCAV.INP',STATUS = 'OLD')
      OPEN(6,FILE = 'REFCAV.OUT',STATUS = 'NEW')
C     OPEN(7,FILE = 'REFCAV.ERR',STATUS = 'NEW')
C READ THE ROOTS OF THE BESSEL-NEUMANN COMBINATION AND THE
C ROOTS OF ZERO ORDER BESSEL FUNCTION OF THE FIRST KIND
      DO 1 I = 1,100
        READ(1,*) ZEROS(I),ROOTS(I)
 1    CONTINUE
      PI = DACOS(-1.D0)
      A = 0.35D0
      B = 0.15D0
      C = A/B
      RADIUS = 1.0D + 00
      D = .0025D0
      NMODEA = 13
      NEXPFC = NMODEA
      NMODEB = 50
      EPS0 = 1.D0/((36.D + 11)*PI)
      AMU0 = PI*4.D-09
      SPLITE = DSQRT(EPS0*AMU0)
      Y0 = DSQRT(EPS0/AMU0)
      ARRAY(1) = 5.0D0
      ARRAY(2) = 7.0D0
      ARRAY(3) = 9.0D0
      DO 4 I = 1,NEXPFC
        XNA = ROOTS(I)
        RK1 = XNA/B
        ARG1 = RK1*A
        CALL BESSEL(0,XNA,RJ0KB)
        CALL BESSEL(1,ARG1,RJ1KA)
        CALL ANEUM(0,XNA,RN0KB)
        CALL ANEUM(1,ARG1,RN1KA)
        ALPHAN = A*(RJ0KB*RN1KA-RN0KB*RJ1KA)
        ALP(I) = ALPHAN
        ALPHA2 = ALPHAN*ALPHAN
        CALL BESSEL(1,XNA,RJ1KB)
        CALL ANEUM(1,XNA,RN1KB)
```

```
      BETAN = B*(RJ0KB*RN1KB-RN0KB*RJ1KB)
      BET(I) = BETAN
      BETA2 = BETAN*BETAN
      DEN = DSQRT(PI*(ALPHA2-BETA2))
      CONSM(I) = 1.D0/DEN
4    CONTINUE
     DO 13 I = 1,NMODEA
      RKCS(I) = ROOTS(I)*ROOTS(I)/(B*B)
13   CONTINUE
     DO 14 I = 1,NMODEB
      XMNB = ZEROS(I)
      CALL BESSEL(1,XMNB,FT)
      CONSB(I) = 2.D0*DSQRT(PI)/(RADIUS*FT)
14   CONTINUE
     CONS0 = 1.D0/DSQRT(2.D0*PI*DLOG(C))
     DO 2 I = 1,NMODEB
      XNB = ZEROS(I)
      RK2 = XNB/RADIUS
      ARG2A = RK2*A
      ARG2B = RK2*B
      CALL BESSEL(0,ARG2A,RJKBA)
      CALL BESSEL(0,ARG2B,RJKBB)
      FARR(I) = RJKBA
      SARR(I) = RJKBB
2    CONTINUE
     DO 17 I = 1,NMODEB
      RK2 = ZEROS(I)/RADIUS
      RESINT(I,1) = CONS0*CONSB(I)*(SARR(I)-FARR(I))/RK2
      DO 17 J = 2,NEXPFC
      RK1 = ROOTS(J)/B
      VAL = CONSM(J)*CONSB(I)/(RK1*RK1-RK2*RK2)
      RESINT(I,J) = VAL*RK2*(FARR(I)*ALP(J)-SARR(I)*BET(J))
17   CONTINUE
     DO 7 I = 1,NEXPFC
      Y(I) = 0.D0
7    CONTINUE
     Y(1) = 2.D0*Y0
     EPSP = 9.D0
     EPSDP = 0.D0
     WRITE(6,150) EPSP
150  FORMAT(2X,'EPSP = ',F10.3)
     DO 99 IW = 1,100
      W = 2.D0*PI*IW*100.D + 06
      FREQ = W*1.D-09/(2.D0*PI)
      WRITE(*,*) 'FREQUENCY (GHZ) = ',FREQ
      CALL REGA(Y0,SPLITE,W,EPS0,RKCS,NMODEA,NEXPFC,YA)
      CALL REGB(D,RADIUS,AMU0,EPS0,W,NMODEB,NEXPFC,
   *  ZEROS,YA,EPSP,EPSDP,RESINT,YB)
      CALL GAUSS(NEXPFC,YB,Y,V)
      R0R = DREAL(V(1))-1.D0
      R0I = DIMAG(V(1))
C COMPUTE THE CAPACITANCE
C     JSM = DCMPLX(0.D0,1.D0)
C     TR1 = 1.D0-R0R
C     TR2 = 1.D0 + R0R
C     ZNUM = DCMPLX(TR2,R0I)
C     ZDEN = DCMPLX(TR1,-R0I)
```

```
C     Z = ZNUM/ZDEN
C     ZREAL = Z
C     ZIMAG = -JSM*Z
C     ZMAG = 50.D0*DSQRT(ZREAL*ZREAL + ZIMAG*ZIMAG)
C     ZPHASE = DATAN2(ZIMAG,ZREAL)
C     ZPHASE = ZPHASE*180.D0/PI
C     CMAG = 1.D0/(ZMAG*W)
C     WRITE(6,97) FREQ,ZMAG,ZPHASE,CMAG
C97   FORMAT(4(2X,E15.8))
      RMAG = DSQRT(R0R*R0R + R0I*R0I)
      DUMMY = R0I/R0R
      PHASE = DATAN(DUMMY)
      PHASE = 180.D0*PHASE/PI
      IF(R0R.LT.0.D0) PHASE = 180.D0 + PHASE
      IF(R0R.GT.0.D0.AND.R0I.LT.0.D0) PHASE = PHASE + 360.D0
      WRITE(6,15) FREQ,RMAG,PHASE
 15   FORMAT(F12.5,2(2X,F12.5))
 99   CONTINUE
      STOP
      END
C
C *************************************************************************
C
C  THE FOLLOWING SUBROUTINE COMPUTES THE ELEMENTS OF
C  THE MATRIX REPRESENTING THE TRANSMISSION LINE REGION
C
C *************************************************************************
C
      SUBROUTINE REGA(Y0,SPLITE,W,EPS0,RKCS,NMODEA,NEXPFC,YA)
      IMPLICIT REAL*8 (A-H,O-Z)
      COMPLEX*16 JSM,SUM,YMN,RKMN,ARSQ,YA(50,50)
      DIMENSION RKCS(50)
      RK = W*SPLITE
      RKS = RK*RK
      YA(1,1) = Y0
      NA = NEXPFC-1
      IF(NMODEA.LT.NEXPFC) NA = NMODEA-1
      DO 1 I = 1,NA
        J = I + 1
        ARSQ = RKS-RKCS(I)
        RKMN = CDSQRT(ARSQ)
        YMN = W*EPS0/RKMN
        YA(J,J) = YMN
 1    CONTINUE
      RETURN
      END
C
C *************************************************************************
C
C  SUBROUTINE REGB EVALUATES THE MATRIX ELEMENTS REPRESENTING
C  THE CAVITY REGION.  IT ALSO COMPUTES THE MATRIX TO BE USED
C  IN THE GAUSSIAN ELIMINATION ROUTINE (SUBROUTINE GAUSS).
C
C *************************************************************************
C
      SUBROUTINE REGB(D,RADIUS,AMU0,EPS0,W,NMODEB,NEXPFC,
     *ZEROS,YA,EPSP,EPSDP,RESINT,YB)
```

```
      IMPLICIT REAL*8(A-H,O-Z)
      COMPLEX*16 JSM,KZD,EPSB,KDSQ,SUMB,ARR(100),
     *YA(50,50),YB(50,50)
      DIMENSION RESINT(100,50),ZEROS(100)
      JSM = DCMPLX(0.D0,1.D0)
      EPSB = DCMPLX(EPSP,-EPSDP)*EPS0
      KDSQ = W*W*EPSB*AMU0
      DO 1 I = 1,NMODEB
        XMNB = ZEROS(I)
        KZD = CDSQRT(KDSQ-((XMNB/RADIUS)*(XMNB/RADIUS)))
        ARR(I) = JSM*W*(EPSB*CDCOS(KZD*D)/(KZD*CDSIN(KZD*D)))
1     CONTINUE
      DO 2 I = 1,NEXPFC
      DO 2 J = 1,NEXPFC
       SUMB = 0.D0
       DO 3 L = 1,NMODEB
        SUMB = SUMB + ARR(L)*RESINT(L,I)*RESINT(L,J)
3     CONTINUE
       YB(I,J) = -SUMB
2     CONTINUE
      DO 4 I = 1,NEXPFC
      DO 4 J = 1,NEXPFC
       YB(I,J) = YA(I,J) + YB(I,J)
4     CONTINUE
      RETURN
      END
```

Appendix II: Program REFCAVOP

The following Fortran program implements the equations derived in chapter (3) to
compute the complex permittivity of a dielectric material using the WDFC which is
adapted to the end of a transmission line given the reflection coefficient.

```
      IMPLICIT REAL*8(A-H,O-Z)
      COMPLEX*16 Z,ZNUM,ZDEN,JSM,YA(25,25),YB(25,25),Y(25)
      COMMON / BLOCK / RESINT(100,25),ZEROS(100),Y0,YA,
     *D,R0R,R0I,RADIUS,AMU0,EPS0,NMODEB,NEXPFC,EPS
      COMMON / BLK / Y
      DIMENSION ROOTS(100),RKCS(25),CONSB(100),CONSM(25),
     *ALP(25),BET(25),FARR(100),SARR(100)
      OPEN(1,FILE = 'RFCAVEPS.INP',STATUS = 'OLD')
      OPEN(2,FILE = 'RFCAVEPS.S11',STATUS = 'OLD')
      OPEN(6,FILE = 'RFCAVEPS.EPS',STATUS = 'NEW')
      OPEN(7,FILE = 'RFCAVEPS.ERR',STATUS = 'NEW')
C     WRITE(*,*) 'ENTER THE RADIUS (IN CM) OF THE INNER CONDUCTOR'
C     READ(*,*) B
C     WRITE(*,*) 'ENTER THE RADIUS (IN CM) OF THE OUTER CONDUCTOR.'
C     READ(*,*) A
      WRITE(*,*) 'ENTER THE RADIUS (IN CM) OF THE SAMPLE HOLDER'
      READ(*,*) RADIUS
      WRITE(*,*) 'ENTER THE SAMPLE THICKNESS (IN CM)'
      READ(*,*) D
      WRITE(*,*) 'ENTER THE NUMBER OF DATA POINTS'
      READ(*,*) NP
      WRITE(*,*) 'ENTER AN ESTIMATE OF THE DIELECTRIC CONSTANT'
      READ(*,*) EPS
C READ THE ROOTS OF THE BESSEL-NEUMANN COMBINATION AND THE
C ROOTS OF ZERO ORDER BESSEL FUNCTION OF THE FIRST KIND
      DO 1 I = 1,100
        READ(1,*) ZEROS(I),ROOTS(I)
 1    CONTINUE
      PI = DACOS(-1.D0)
      A = 0.35D0
      B = 0.15D0
      C = A/B
      NMODEA = 13
      NEXPFC = NMODEA
C     NMODEB = NMODEA*(RADIUS/A)
      NMODEB = 50
      EPS0 = 1.D0/((36.D + 11)*PI)
      AMU0 = PI*4.D-09
      SPLITE = DSQRT(EPS0*AMU0)
      Y0 = DSQRT(EPS0/AMU0)
      DO 4 I = 1,NEXPFC
        XNA = ROOTS(I)
        RK1 = XNA/B
```

```
       ARG1 = RK1*A
       CALL BESSEL(0,XNA,RJ0KB)
       CALL BESSEL(1,ARG1,RJ1KA)
       CALL ANEUM(0,XNA,RN0KB)
       CALL ANEUM(1,ARG1,RN1KA)
       ALPHAN = A*(RJ0KB*RN1KA-RN0KB*RJ1KA)
       ALP(I) = ALPHAN
       ALPHA2 = ALPHAN*ALPHAN
       CALL BESSEL(1,XNA,RJ1KB)
       CALL ANEUM(1,XNA,RN1KB)
       BETAN = B*(RJ0KB*RN1KB-RN0KB*RJ1KB)
       BET(I) = BETAN
       BETA2 = BETAN*BETAN
       DEN = DSQRT(PI*(ALPHA2-BETA2))
       CONSM(I) = 1.D0/DEN
4    CONTINUE
     DO 13 I = 1,NMODEA
       RKCS(I) = ROOTS(I)*ROOTS(I)/(B*B)
13   CONTINUE
     DO 14 I = 1,NMODEB
       XMNB = ZEROS(I)
       CALL BESSEL(1,XMNB,FT)
       CONSB(I) = 2.D0*DSQRT(PI)/(RADIUS*FT)
14   CONTINUE
     CONS0 = 1.D0/DSQRT(2.D0*PI*DLOG(C))
     DO 2 I = 1,NMODEB
       XNB = ZEROS(I)
       RK2 = XNB/RADIUS
       ARG2A = RK2*A
       ARG2B = RK2*B
       CALL BESSEL(0,ARG2A,RJKBA)
       CALL BESSEL(0,ARG2B,RJKBB)
       FARR(I) = RJKBA
       SARR(I) = RJKBB
2    CONTINUE
     DO 17 I = 1,NMODEB
       RK2 = ZEROS(I)/RADIUS
       RESINT(I,1) = CONS0*CONSB(I)*(SARR(I)-FARR(I))/RK2
     DO 17 J = 2,NEXPFC
       RK1 = ROOTS(J)/B
       VAL = CONSM(J)*CONSB(I)/(RK1*RK1-RK2*RK2)
       RESINT(I,J) = VAL*RK2*(FARR(I)*ALP(J)-SARR(I)*BET(J))
17   CONTINUE
     N = 2
     DO 19 I = 2,NEXPFC
       Y(I) = 0.D0
19   CONTINUE
     Y(1) = 2.D0*Y0
     DO 99 IW = 1,NP
       READ(2,*) FREQ,RMAG,PHASE
       WRITE(*,*) 'FREQUENCY (GHZ) = ',FREQ
       W = 2.D0*PI*FREQ*1.D+09
       PHASE = PHASE*PI/180.D0
       R0R = RMAG*DCOS(PHASE)
       R0I = RMAG*DSIN(PHASE)
       CALL REGA(Y0,SPLITE,W,EPS0,RKCS,NMODEA,NEXPFC,YA)
       CALL EPSLN(N,W,EPSP,EPSDP,IER)
```

```
      WRITE(6,15) FREQ,EPSP,EPSDP
15    FORMAT(F15.8,2(2X,1PE16.6),I4)
99    CONTINUE
200   CONTINUE
      STOP
      END
C
C  ********************************************************************
C
C  THE FOLLOWING SUBROUTINE COMPUTES THE ELEMENTS OF
C  THE MATRIX REPRESENTING THE TRANSMISSION LINE REGION
C
C  ********************************************************************
C
      SUBROUTINE REGA(Y0,SPLITE,W,EPS0,RKCS,NMODEA,NEXPFC,YA)
      IMPLICIT REAL*8 (A-H,O-Z)
      COMPLEX*16 JSM,SUM,YMN,RKMN,ARSQ,YA(25,25)
      DIMENSION RKCS(50)
      RK = W*SPLITE
      RKS = RK*RK
      YA(1,1) = Y0
      NA = NEXPFC-1
      IF(NMODEA.LT.NEXPFC) NA = NMODEA-1
      DO 1 I = 1,NA
       J = I + 1
       ARSQ = RKS-RKCS(I)
       RKMN = CDSQRT(ARSQ)
       YMN = W*EPS0/RKMN
       YA(J,J) = YMN
1     CONTINUE
      RETURN
      END
C
C  ********************************************************************
C
C  THE FOLLOWING SUBROUTINE CALLS SUBROUTINE POWELL TO
C  MINIMIZE THE OBJECTIVE FUNCTION TO YIELD THE COMPLEX
C  PERMITTIVITY.
C
C  ********************************************************************
C
      SUBROUTINE EPSLN(N,OMEGA,EPSP,EPSDP,IER)
      IMPLICIT REAL*8(A-H,O-Z)
      COMPLEX*16 YA(25,25)
      COMMON / BLOCK / RESINT(100,25),ZEROS(100),Y0,YA,
     *D,R0R,R0I,RADIUS,AMU0,EPS0,NMODEB,NEXPFC,EPS
      DIMENSION X(2),F(2)
      X(1) = EPS
      X(2) = 1.D-05
      STEP = 0.01D0
      ACC = 1.D-15
      MAXFUN = 50
      DMAX = 10.D0
      CALL POWELL(N,OMEGA,X,F,STEP,DMAX,ACC,MAXFUN,IER)
      EPSP = X(1)
      EPSDP = X(2)
      RETURN
```

```
      END
C
C ***********************************************************************
C
C   SUBROUTINE REGB EVALUATES THE MATRIX ELEMENTS REPRESENTING
C   THE CAVITY REGION.  IT ALSO COMPUTES THE MATRIX TO BE USED
C   IN THE GAUSSIAN ELIMINATION ROUTINE (SUBROUTINE GAUSS).
C
C ***********************************************************************
C
      SUBROUTINE REGB(W,EPSP,EPSDP,YB)
      IMPLICIT REAL*8(A-H,O-Z)
      COMPLEX*16 JSM,KZD,EPSB,KDSQ,SUMB,ARR(100),
     *YA(25,25),YB(25,25)
      COMMON / BLOCK / RESINT(100,25),ZEROS(100),Y0,YA,
     *D,R0R,R0I,RADIUS,AMU0,EPS0,NMODEB,NEXPFC,EPS
      JSM = DCMPLX(0.D0,1.D0)
      EPSB = DCMPLX(EPSP,-EPSDP)*EPS0
      KDSQ = W*W*EPSB*AMU0
      DO 1 I = 1,NMODEB
        XMNB = ZEROS(I)
        KZD = CDSQRT(KDSQ-((XMNB/RADIUS)*(XMNB/RADIUS)))
        ARR(I) = JSM*W*(EPSB*CDCOS(KZD*D)/(KZD*CDSIN(KZD*D)))
1     CONTINUE
      DO 2 I = 1,NEXPFC
      DO 2 J = 1,NEXPFC
        SUMB = 0.D0
        DO 3 L = 1,NMODEB
          SUMB = SUMB + ARR(L)*RESINT(L,I)*RESINT(L,J)
3       CONTINUE
        YB(I,J) = -SUMB
2     CONTINUE
      DO 4 I = 1,NEXPFC
      DO 4 J = 1,NEXPFC
        YB(I,J) = YA(I,J) + YB(I,J)
4     CONTINUE
      RETURN
      END
C
C ***********************************************************************
C
C   SUBROUTINE FUNC EVALUATES THE VLUES OF THE ERROR FUNCTION.
C   IT CALLS SUBROUTINE REGB.
C
C ***********************************************************************
C
      SUBROUTINE FUNC(W,X,F)
      IMPLICIT REAL*8(A-H,O-Z)
      COMPLEX*16 YB(25,25),YA(25,25),EPSB,AMUB,Y(25),YX(25)
      COMMON / BLOCK / RESINT(100,25),ZEROS(100),Y0,YA,
     *D,R0R,R0I,RADIUS,AMU0,EPS0,NMODEB,NEXPFC,EPS
      COMMON / BLK / Y
      DIMENSION F(2),X(2)
      EPSP = X(1)
      EPSDP = X(2)
      CALL REGB(W,EPSP,EPSDP,YB)
      CALL GAUSS(NEXPFC,YB,Y,YX)
```

```
F(1) = DREAL(YX(1))-R0R-1.D0
F(2) = DIMAG(YX(1))-R0I
RETURN
END
```

Appendix III: Program TRCAV

The following Fortran program implements the equations derived in Chapter (4) to compute the reflection coefficient of the WDFC which is placed between two transmission lines assuming that the complex permittivity of the dielectric material is known.

```
      IMPLICIT REAL*8(A-H,O-Z)
      COMPLEX*16 YA(25,25),Y1B(25,25),Y2B(25,25),
     *AUG(50,50),V(50),Y(50),JSM
      DIMENSION ROOTS(100),RKCS(25),CONSB(100),CONSM(25),
     *RESINT(100,25),ZEROS(100),ARRAY(3),ALP(25),BET(25),FARR(100),
     *SARR(100)
      OPEN(1,FILE='TRANSCAV.INP',STATUS='OLD')
      OPEN(6,FILE='TRANSCAV.OUT',STATUS='NEW')
      OPEN(7,FILE='TRANSCAV.ERR',STATUS='NEW')
C READ THE ROOTS OF THE BESSEL-NEUMANN COMBINATION AND THE
C ROOTS OF ZERO ORDER BESSEL FUNCTION OF THE FIRST KIND
      DO 1 I=1,100
      READ(1,*) ZEROS(I),ROOTS(I)
1     CONTINUE
      ARRAY(1)=0.1D0
      ARRAY(2)=1.0d0
      ARRAY(3)=3.0D0
      PI=DACOS(-1.D0)
      JSM=DCMPLX(0.D0,1.D0)
      A=0.35D0
      B=0.15D0
      C=A/B
      RADIUS=0.75D+00
      D=.025D0
      NMODEA=10
      NEXPFC=NMODEA
C     NMODEB=NMODEA*(RADIUS/A)
      NMODEB=50
      EPS0=1.D0/((36.D+11)*PI)
      AMU0=PI*4.D-09
      SPLITE=DSQRT(EPS0*AMU0)
      Y0=DSQRT(EPS0/AMU0)
      DO 4 I=1,NEXPFC
      XNA=ROOTS(I)
      RK1=XNA/B
      ARG1=RK1*A
      CALL BESSEL(0,XNA,RJ0KB)
      CALL BESSEL(1,ARG1,RJ1KA)
      CALL ANEUM(0,XNA,RN0KB)
      CALL ANEUM(1,ARG1,RN1KA)
      ALPHAN=A*(RJ0KB*RN1KA-RN0KB*RJ1KA)
      ALP(I)=ALPHAN
      ALPHA2=ALPHAN*ALPHAN
```

```
        CALL BESSEL(1,XNA,RJIKB)
        CALL ANEUM(1,XNA,RNIKB)
        BETAN = B*(RJ0KB*RN1KB-RN0KB*RJIKB)
        BET(I) = BETAN
        BETA2 = BETAN*BETAN
        DEN = DSQRT(PI*(ALPHA2-BETA2))
        CONSM(I) = 1.D0/DEN
4    CONTINUE
     DO 13 I = 1,NMODEA
        RKCS(I) = ROOTS(I)*ROOTS(I)/(B*B)
13   CONTINUE
     DO 14 I = 1,NMODEB
        XMNB = ZEROS(I)
        CALL BESSEL(1,XMNB,FT)
        CONSB(I) = 2.D0*DSQRT(PI)/(RADIUS*FT)
14   CONTINUE
     CONS0 = 1.D0/DSQRT(2.D0*PI*DLOG(C))
     DO 2 I = 1,NMODEB
        XNB = ZEROS(I)
        RK2 = XNB/RADIUS
        ARG2A = RK2*A
        ARG2B = RK2*B
        CALL BESSEL(0,ARG2A,RJKBA)
        CALL BESSEL(0,ARG2B,RJKBB)
        FARR(I) = RJKBA
        SARR(I) = RJKBB
2    CONTINUE
     DO 17 I = 1,NMODEB
        RK2 = ZEROS(I)/RADIUS
        RESINT(I,1) = CONS0*CONSB(I)*(SARR(I)-FARR(I))/RK2
        DO 17 J = 2,NEXPFC
        RK1 = ROOTS(J)/B
        VAL = CONSM(J)*CONSB(I)/(RK1*RK1-RK2*RK2)
        RESINT(I,J) = VAL*RK2*(FARR(I)*ALP(J)-SARR(I)*BET(J))
17   CONTINUE
     N = 2*NEXPFC
     EPSP = 5
     AMUP = 1.D0
     AMUDP = 0.D0
     EPSDP = 0.d0
     DO 7 I = 2,N
        Y(I) = 0.D0
7    CONTINUE
     Y(1) = 2.D0*Y0
     DO 99 IW = 1,100
        W = 2.D0*PI*IW*100.D + 06
        FREQ = W*1.D-09/(2.D0*PI)
        WRITE(*,*) 'FREQUENCY (GHZ) = ',FREQ
        CALL REGA(Y0,SPLITE,W,EPS0,RKCS,NMODEA,NEXPFC,YA)
        CALL REGB(D,RADIUS,AMU0,EPS0,W,NMODEB,NEXPFC,
     *   ZEROS,EPSP,EPSDP,AMUP,AMUDP,RESINT,Y1B,Y2B)
        DO 18 I = 1,NEXPFC
        DO 18 J = 1,NEXPFC
          AUG(I,J) = YA(I,J) + Y1B(I,J)
          AUG(I,J + NEXPFC) = Y2B(I,J)
          AUG(I + NEXPFC,J) = -Y2B(I,J)
          AUG(I + NEXPFC,J + NEXPFC) = -AUG(I,J)
```

appendices   159

```
 18   CONTINUE
      CALL GAUSS(N,AUG,Y,V)
      S11R = DREAL(V(1))-1.D0
      S11I = DIMAG(V(1))
      V(1 + NEXPFC) = V(1 + NEXPFC)*CDEXP(JSM*W*SPLITE*D)
      S21R = DREAL(V(1 + NEXPFC))
      S21I = DIMAG(V(1 + NEXPFC))
      S11MAG = DSQRT(S11R*S11R + S11I*S11I)
      S21MAG = DSQRT(S21R*S21R + S21I*S21I)
      S11PHA = (DATAN2(S11I,S11R))*180.D0/PI
      S21PHA = (DATAN2(S21I,S21R))*180.D0/PI
      WRITE(6,15) FREQ,S11MAG,S11PHA,S21MAG,S21PHA
 15   FORMAT(F10.5,4(2X,1PE12.5))
 99   CONTINUE
 200  CONTINUE
      STOP
      END
C
C ********************************************************************
C
C   THE FOLLOWING SUBROUTINE COMPUTES THE ELEMENTS OF
C   THE MATRIX REPRESENTING THE TRANSMISSION LINE REGION
C
C ********************************************************************
C
      SUBROUTINE REGA(Y0,SPLITE,W,EPS0,RKCS,NMODEA,NEXPFC,YA)
      IMPLICIT REAL*8 (A-H,O-Z)
      COMPLEX*16 SUM,YMN,RKMN,ARSQ,YA(25,25)
      DIMENSION RKCS(25)
      RK = W*SPLITE
      RKS = RK*RK
      YA(1,1) = Y0
      NA = NEXPFC-1
      IF(NMODEA.LT.NEXPFC) NA = NMODEA-1
      DO 1 I = 1,NA
        J = I + 1
        ARSQ = RKS-RKCS(I)
        RKMN = CDSQRT(ARSQ)
        YMN = W*EPS0/RKMN
        YA(J,J) = YMN
 1    CONTINUE
      RETURN
      END
C
C ********************************************************************
C
C   SUBROUTINE REGB EVALUATES THE MATRIX ELEMENTS REPRESENTING
C   THE CAVITY REGION (Y1B AND Y2B).  IT ALSO COMPUTES THE
C   MATRIX TO BE USED IN THE GAUSSIAN ELIMINATION ROUTINE
C   (SUBROUTINE GAUSS).
C
C ********************************************************************
C
      SUBROUTINE REGB(D,RADIUS,AMU0,EPS0,W,NMODEB,NEXPFC,
     *ZEROS,EPSP,EPSDP,AMUP,AMUDP,RESINT,Y1B,Y2B)
      IMPLICIT REAL*8(A-H,O-Z)
      COMPLEX*16 JSM,KZD,EPSB,KDSQ,ARR1(100),ARR2(100),Y1B(25,25),
```

```fortran
     *Y2B(25,25),SUM1B,SUM2B,AMUB
      DIMENSION RESINT(100,25),ZEROS(100)
      JSM = DCMPLX(0.D0,1.D0)
      EPSB = DCMPLX(EPSP,-EPSDP)*EPS0
      AMUB = DCMPLX(AMUP,-AMUDP)*AMU0
      KDSQ = W*W*EPSB*AMUB
      DO 1 I = 1,NMODEB
        XMNB = ZEROS(I)
        KZD = CDSQRT(KDSQ-((XMNB/RADIUS)*(XMNB/RADIUS)))
        ARR2(I) = JSM*W*EPSB/(KZD*CDSIN(KZD*D))
        ARR1(I) = ARR2(I)*CDCOS(KZD*D)
1     CONTINUE
      DO 2 I = 1,NEXPFC
      DO 2 J = 1,NEXPFC
        SUM1B = 0.D0
        SUM2B = 0.D0
        DO 3 L = 1,NMODEB
          VAL = RESINT(L,I)*RESINT(L,J)
          SUM1B = SUM1B + ARR1(L)*VAL
          SUM2B = SUM2B + ARR2(L)*VAL
3     CONTINUE
      Y1B(I,J) = -SUM1B
      Y2B(I,J) = SUM2B
2     CONTINUE
      RETURN
      END
```

Appendix IV: Program TRCAVOP

The following Fortran program implements the equations derived in chapter (4) to compute the complex permittivity and/or the complex permeability of a dielectric material using the WDFC which is adapted to the end of a transmission line given the reflection coefficient.

```
      IMPLICIT REAL*8(A-H,O-Z)
      COMPLEX*16 YA(20,20),Y(40)
      COMMON / BLOCK / RESINT(100,20),ZEROS(100),Y0,YA,ISLCT,SPLITE,
     *D,R0R,R0I,RADIUS,AMU0,EPS0,NMODEB,NEXPFC,EPS,AMU,NAUG,T0R,T0I
      COMMON / BLK / Y
      DIMENSION ROOTS(100),RKCS(20),CONSB(100),CONSM(20),
     *ALP(20),BET(20),FARR(100),SARR(100)
      WRITE(*,30)
 30   FORMAT(1X,'IS IT A REFLECTION MEASUREMENT (ENTER 1)',/,
     *' A TRANSMISSION MEASUREMENT (ENTER 2)',/,
     *' OR A COMBINED REFLECTION-TRANSMISSION MEASUREMENT (ENTER 3)')
      READ(*,*) ISLCT
      WRITE(*,*) 'ENTER THE NUMBER OF DATA POINTS'
      READ(*,*) NP
      WRITE(*,*) 'ENTER SAMPLE THICKNESS'
      READ(*,*) D
      WRITE(*,*) 'ENTER SAMPLE RADIUS'
      READ(*,*) RADIUS
      WRITE(*,*) 'ENTER AN ESTIMATE FOR THE DIELECTRIC CONSTANT'
      READ(*,*) EPS
      WRITE(*,*) 'ENTER AN ESTIMATE FOR THE PERMEABILITY'
      READ(*,*) AMU
C  READ THE ROOTS OF THE BESSEL-NEUMANN COMBINATION AND THE
C  ROOTS OF ZERO ORDER BESSEL FUNCTION OF THE FIRST KIND
      DO 1 I = 1,100
        READ(1,*) ZEROS(I),ROOTS(I)
 1    CONTINUE
      PI = DARCOS(-1.D0)
      A = 0.35D0
      B = 0.15D0
      C = A/B
      NMODEA = 13
      NEXPFC = NMODEA
      NMODEB = 50
      EPS0 = 1.D0/((36.D + 11)*PI)
      AMU0 = PI*4.D-09
      SPLITE = DSQRT(EPS0*AMU0)
      Y0 = DSQRT(EPS0/AMU0)
      DO 4 I = 1,NEXPFC
        XNA = ROOTS(I)
        RK1 = XNA/B
        ARG1 = RK1*A
```

```fortran
      CALL BESSEL(0,XNA,RJ0KB)
      CALL BESSEL(1,ARG1,RJ1KA)
      CALL ANEUM(0,XNA,RN0KB)
      CALL ANEUM(1,ARG1,RN1KA)
      ALPHAN = A*(RJ0KB*RN1KA-RN0KB*RJ1KA)
      ALP(I) = ALPHAN
      ALPHA2 = ALPHAN*ALPHAN
      CALL BESSEL(1,XNA,RJ1KB)
      CALL ANEUM(1,XNA,RN1KB)
      BETAN = B*(RJ0KB*RN1KB-RN0KB*RJ1KB)
      BET(I) = BETAN
      BETA2 = BETAN*BETAN
      DEN = DSQRT(PI*(ALPHA2-BETA2))
      CONSM(I) = 1.D0/DEN
4     CONTINUE
      DO 13 I = 1,NMODEA
      RKCS(I) = ROOTS(I)*ROOTS(I)/(B*B)
13    CONTINUE
      DO 14 I = 1,NMODEB
      XMNB = ZEROS(I)
      CALL BESSEL(1,XMNB,FT)
      CONSB(I) = 2.D0*DSQRT(PI)/(RADIUS*FT)
14    CONTINUE
      CONS0 = 1.D0/DSQRT(2.D0*PI*DLOG(C))
      DO 2 I = 1,NMODEB
      XNB = ZEROS(I)
      RK2 = XNB/RADIUS
      ARG2A = RK2*A
      ARG2B = RK2*B
      CALL BESSEL(0,ARG2A,RJKBA)
      CALL BESSEL(0,ARG2B,RJKBB)
      FARR(I) = RJKBA
      SARR(I) = RJKBB
2     CONTINUE
      DO 17 I = 1,NMODEB
      RK2 = ZEROS(I)/RADIUS
      RESINT(I,1) = CONS0*CONSB(I)*(SARR(I)-FARR(I))/RK2
      DO 17 J = 2,NEXPFC
      RK1 = ROOTS(J)/B
      VAL = CONSM(J)*CONSB(I)/(RK1*RK1-RK2*RK2)
      RESINT(I,J) = VAL*RK2*(FARR(I)*ALP(J)-SARR(I)*BET(J))
17    CONTINUE
      NAUG = 2*NEXPFC
      N = 2
      IF(ISLCT.EQ.3) N = 4
      DO 25 I = 2,NAUG
      Y(I) = 0.D0
25    CONTINUE
      Y(1) = 2.D0*Y0
      DO 99 IW = 1,NP
      IF(ISLCT.EQ.3) THEN
      READ(2,*) FREQ,RMAG,RPHA,TMAG,TPHA
      W = 2.D0*PI*FREQ*1.D + 09
      RPHA = RPHA*PI/180.D0
      TPHA = TPHA*PI/180.D0
      TPHA = TPHA-W*SPLITE*D
      R0R = RMAG*DCOS(RPHA)
```

```fortran
      R0I = RMAG*DSIN(RPHA)
      T0R = TMAG*DCOS(TPHA)
      T0I = TMAG*DSIN(TPHA)
      ELSE
      READ(2,*) FREQ,RMAG,RPHA
      W = 2.D0*PI*FREQ*1.D+09
      RPHA = RPHA*PI/180.D0
      IF(ISLCT.EQ.2) RPHA = RPHA-W*SPLITE*D
      R0R = RMAG*DCOS(RPHA)
      R0I = RMAG*DSIN(RPHA)
      ENDIF
      WRITE(*,*) 'FREQUENCY IN GHz=',FREQ
      CALL REGA(Y0,SPLITE,W,EPS0,RKCS,NMODEA,NEXPFC,YA)
      CALL EPSLN(N,W,EPSP,EPSDP,AMUP,AMUDP,IER)
      IF(ISLCT.EQ.3) THEN
      WRITE(6,20) FREQ,EPSP,EPSDP,AMUP,AMUDP,IER
20    FORMAT(F10.5,4(2X,1PE12.5),2X,I2)
      ELSE
      WRITE(6,21) FREQ,EPSP,EPSDP,IER
21    FORMAT(F10.5,2(2X,1PE12.5),2X,I2)
      ENDIF
99    CONTINUE
      STOP
      END
C
C ************************************************************
C
C  THE FOLLOWING SUBROUTINE COMPUTES THE ELEMENTS OF
C  THE MATRIX REPRESENTING THE TRANSMISSION LINE REGION
C
C ************************************************************
C
      SUBROUTINE REGA(Y0,SPLITE,W,EPS0,RKCS,NMODEA,NEXPFC,YA)
      IMPLICIT REAL*8 (A-H,O-Z)
      COMPLEX*16 SUM,YMN,RKMN,ARSQ,YA(20,20)
      DIMENSION RKCS(20)
      RK = W*SPLITE
      RKS = RK*RK
      YA(1,1) = Y0
      NA = NEXPFC-1
      IF(NMODEA.LT.NEXPFC) NA = NMODEA-1
      DO 1 I = 1,NA
      J = I+1
      ARSQ = RKS-RKCS(I)
      RKMN = CDSQRT(ARSQ)
      YMN = W*EPS0/RKMN
      YA(J,J) = YMN
1     CONTINUE
      RETURN
      END
C
C ************************************************************
C
C  THE FOLLOWING SUBROUTINE CALLS SUBROUTINE POWELL TO
C  MINIMIZE THE OBJECTIVE FUNCTION TO YIELD THE COMPLEX
C  PERMITTIVITY.
C
```

```
C ************************************************************
C
      SUBROUTINE EPSLN(N,OMEGA,EPSP,EPSDP,AMUP,AMUDP,IER)
      IMPLICIT REAL*8(A-H,O-Z)
      COMPLEX*16 YA(20,20)
      COMMON / BLOCK / RESINT(100,20),ZEROS(100),Y0,YA,ISLCT,SPLITE,
     *D,R0R,R0I,RADIUS,AMU0,EPS0,NMODEB,NEXPFC,EPS,AMU,NAUG,T0R,T0I
      DIMENSION X(10),F(10)
      EPSP = EPS
      EPSDP = 1.D-05
      AMUP = AMU
      AMUDP = 1.D-05
      X(1) = EPS
      X(2) = EPSDP
      IF(ISLCT.EQ.3) THEN
        X(3) = AMUP
        X(4) = AMUDP
      ENDIF
      STEP = 0.0001D0
      ACC = 1.D-10
      MAXFUN = 70
      DMAX = 10.D0
      CALL POWELL(N,OMEGA,X,F,STEP,DMAX,ACC,MAXFUN,IER)
      EPSP = X(1)
      EPSDP = X(2)
      IF(ISLCT.EQ.3) THEN
        AMUP = X(3)
        AMUDP = X(4)
      ENDIF
      RETURN
      END
C
C ************************************************************
C
C  SUBROUTINE REGB EVALUATES THE MATRIX ELEMENTS
C  REPRESENTING THE CAVITY REGION (Y1B AND Y2B).
C  IT ALSO FORMS THE MATRIX TO BE USED IN THE
C  GAUSSIAN ELIMINATION ROUTINE (SUBROUTINE GAUSS).
C
C ************************************************************
C
      SUBROUTINE REGB(W,EPSP,EPSDP,AMUP,AMUDP,AUG)
      IMPLICIT REAL*8(A-H,O-Z)
      COMPLEX*16 JSM,KZD,EPSB,KDSQ,ARR1(100),ARR2(100),Y1B(20,20),
     *Y2B(20,20),SUM1B,SUM2B,AMUB,AUG(40,40),YA(20,20)
      COMMON / BLOCK / RESINT(100,20),ZEROS(100),Y0,YA,ISLCT,SPLITE,
     *D,R0R,R0I,RADIUS,AMU0,EPS0,NMODEB,NEXPFC,EPS,AMU,NAUG,T0R,T0I
      DIMENSION F(10),X(10)
      JSM = DCMPLX(0.D0,1.D0)
      AMUB = DCMPLX(AMUP,-AMUDP)*AMU0
      EPSB = DCMPLX(EPSP,-EPSDP)*EPS0
      KDSQ = W*W*EPSB*AMUB
      DO 1 I = 1,NMODEB
        XMNB = ZEROS(I)
        KZD = CDSQRT(KDSQ-((XMNB/RADIUS)*(XMNB/RADIUS)))
        ARR2(I) = JSM*W*EPSB/(KZD*CDSIN(KZD*D))
        ARR1(I) = ARR2(I)*CDCOS(KZD*D)
```

```
1   CONTINUE
    DO 2 I = 1,NEXPFC
    DO 2 J = 1,NEXPFC
      SUM1B = 0.D0
      SUM2B = 0.D0
      DO 3 L = 1,NMODEB
        VAL = RESINT(L,I)*RESINT(L,J)
        SUM1B = SUM1B + ARR1(L)*VAL
        SUM2B = SUM2B + ARR2(L)*VAL
3     CONTINUE
      Y1B(I,J) = -SUM1B
      Y2B(I,J) = + SUM2B
2   CONTINUE
    DO 4 I = 1,NEXPFC
    DO 4 J = 1,NEXPFC
      AUG(I,J) = YA(I,J) + Y1B(I,J)
      AUG(I,J + NEXPFC) = Y2B(I,J)
      AUG(I + NEXPFC,J) = -Y2B(I,J)
      AUG(I + NEXPFC,J + NEXPFC) = -AUG(I,J)
4   CONTINUE
    RETURN
    END
C
C ********************************************************************
C
C SUBROUTINE FUNC EVALUATES THE VLUES OF THE ERROR FUNCTION.
C IT CALLS SUBROUTINE REGB.
C
C ********************************************************************
C
    SUBROUTINE FUNC(W,X,F)
    IMPLICIT REAL*8(A-H,O-Z)
    COMPLEX*16 AUG(40,40),EPSB,AMUB,Y(40),YX(40),YA(20,20)
    COMMON / BLOCK / RESINT(100,20),ZEROS(100),Y0,YA,ISLCT,SPLITE,
   *D,R0R,R0I,RADIUS,AMU0,EPS0,NMODEB,NEXPFC,EPS,AMU,NAUG,T0R,T0I
    COMMON / BLK / Y
    DIMENSION F(10),X(10)
    AMUP = 1.D0
    AMUDP = 0.D0
    EPSP = X(1)
    EPSDP = X(2)
    IF(ISLCT.EQ.3) THEN
      AMUP = X(3)
      AMUDP = X(4)
    ENDIF
    CALL REGB(W,EPSP,EPSDP,AMUP,AMUDP,AUG)
    CALL GAUSS(NAUG,AUG,Y,YX)
    IF(ISLCT.EQ.1) THEN
      F(1) = DREAL(YX(1))-R0R-1.D0
      F(2) = DIMAG(YX(1))-R0I
    ENDIF
    IF(ISLCT.EQ.2) THEN
      F(1) = DREAL(YX(1 + NEXPFC))-R0R
      F(2) = DIMAG(YX(1 + NEXPFC))-R0I
    ENDIF
    IF(ISLCT.EQ.3) THEN
      F(1) = DREAL(YX(1))-R0R-1.D0
```

```
   F(2) = DIMAG(YX(1))-R0I
   F(3) = DREAL(YX(1 + NEXPFC))-T0R
   F(4) = DIMAG(YX(1 + NEXPFC))-T0I
ENDIF
RETURN
END
```

Appendix V: Common Subroutines

This appendix lists the common subroutines being called by the programs in the above appendices. These subroutines are: POWELL, GAUSS, BESSEL, ANEUM. Other routines called by the subroutines in this appendix are also listed.

```
C
C *********************************************************************
C
C  SUBROUTINE POWELL IMPLEMENTS POWELL'S HYBRID METHOD
C  TO SOLVE A NONLINEAR SYSTEM OF EQUATIONS BY MINIMIZING
C  AN ERROR FUNCTION.
C
C *********************************************************************
C
      SUBROUTINE POWELL(N,OMEGA,X,F,DSTEP,DMAX,ACC,MAXFUN,IER)
      IMPLICIT REAL*8(A-H,O-Z)
      COMMON / BLOCK / YAR(40,40),YAI(40,40),RESINT(100,40),EXCITR(40),
     *ZEROS(100),D,R0R,R0I,RADIUS,AMU0,EPS0,NCOL,NMODEB,NEXPFC
      DIMENSION X(82),F(82),AJINV(82,82),W(4000)
C SET VARIOUS PARAMETERS
      MAXC = 0
C MAXC COUNTS THE NUMBER OF CALLS OF FUNC
      NT = N + 4
      NTEST = NT
C NT AND NTEST CAUSE AN ERROR RETURN IF F(X) DOES NOT DECREASE
      DTEST = DFLOAT(N + N)-0.5D0
C DTEST IS USED TO MAINTAIN LINEAR INDEPENDENCE
      NX = N*N
      NF = NX + N
      NW = NF + N
      MW = NW + N
      NDC = MW + N
      ND = NDC + N
C THESE PARAMETERS SEPERATE THE WORKING SPACE ARRAY W
      FMIN = 0.D0
      DD = 0.D0
      DSS = DSTEP*DSTEP
      DM = DMAX*DMAX
      DMM = 4.D0*DM
      IS = 5
      TINC = 1.D0
  1   MAXC = MAXC + 1
      CALL REGB(N,OMEGA,X,F)
C TEST FOR CONVERGENCE
      FSQ = 0.D0
      DO 2 I = 1,N
      FSQ = FSQ + F(I)*F(I)
  2   CONTINUE
```

```
      IF(FSQ-ACC) 300,300,4
300   IER = 0
      WRITE(7,400) MAXC,FSQ
400   FORMAT(2X,I5,2X,E15.7)
3     RETURN
C TEST FOR ERROR RETURN BECAUSE F(X) DOES NOT DECREASE
4     GO TO (10,11,11,10,11),IS
10    IF(FSQ-FMIN) 15,20,20
20    IF(DD-DSS) 12,12,11
12    NTEST = NTEST-1
      IF(NTEST) 13,14,11
14    WRITE(*,16) NT
16    FORMAT(///,5X,'ERROR RETURN BECAUSE',I5,' CALLS OF FUNC FAILED TO
     *IMPROVE THE RESIDUALS')
      IER = 1
17    DO 18 I = 1,N
      X(I) = W(NX + I)
      F(I) = W(NF + I)
18    CONTINUE
      FSQ = FMIN
      GO TO 3
C ERROR RETURN BECAUSE A NEW JACOBIAN IS UNSUCCESSFUL
13    WRITE(*,19)
19    FORMAT(///,5X,'ERROR RETURN BECAUSE F(X) FAILED TO DECREASE USING
     * A NEW JACOBIAN')
      IER = 2
      GO TO 17
15    NTEST = NT
C TEST WHETHER THERE HAVE BEEN MAXFUN CALLS OF FUNC
11    IF(MAXFUN-MAXC) 21,21,22
21    WRITE(*,23) MAXC
23    FORMAT(///,5X,'ERROR RETURN BECAUSE THERE HAVE BEEN',I5,'CALLS
     *OF FUNC')
      IER = 3
      IF(FSQ-FMIN) 3,17,17
22    GO TO (27,28,29,87,30),IS
C STORE THE RESULT OF THE INITIAL CALL OF FUNC
30    FMIN = FSQ
      DO 31 I = 1,N
      W(NX + I) = X(I)
      W(NF + I) = F(I)
31    CONTINUE
C CALCULATE A NEW JACOBIAN APPROXIMATION AND SET THE
C DIRETION MATRIX
32    IC = 0
      IS = 3
33    IC = IC + 1
      X(IC) = X(IC) + DSTEP
      GO TO 1
29    K = IC
      DO 34 I = 1,N
      W(K) = (F(I)-W(NF + I))/DSTEP
      K = K + N
34    CONTINUE
      X(IC) = W(NX + IC)
      IF(IC-N) 33,35,35
C CALCULATE THE INVERSE OF THE JACOBIAN MATRIX
```

```
 35  K = 0
     DO 36 I = 1,N
       DO 37 J = 1,N
         K = K + 1
         AJINV(I,J) = W(K)
         W(ND + K) = 0.D0
 37    CONTINUE
       W(NDC + K + I) = 1.D0
       W(NDC + I) = 1.D0 + DFLOAT(N-I)
 36  CONTINUE
     CALL MATINV(N,AJINV,IFLAG)
     IF(IFLAG.EQ.1) THEN
       WRITE(*,100) IFLAG
100    FORMAT(2X,'THE JACOBIAN MARIX IS SINGULAR,  IFLAG= ',I4)
       IER = 4
       RETURN
     ENDIF
C  START ITERATION BY PREDICTING THE DESCENT AND NEWTON MINIMA
 38  DS = 0.D0
     DN = 0.D0
     SP = 0.D0
     DO 39 I = 1,N
       X(I) = 0.D0
       F(I) = 0.D0
       K = I
       DO 40 J = 1,N
         X(I) = X(I)-W(K)*W(NF + J)
         F(I) = F(I)-AJINV(I,J)*W(NF + J)
         K = K + N
 40    CONTINUE
       DS = DS + X(I)*X(I)
       DN = DN + F(I)*F(I)
       SP = SP + X(I)*F(I)
 39  CONTINUE
C  TEST WHETHER A NEARBY STATIONARY POINT IS PREDICTED
     IF(FMIN*FMIN-DMM*DS) 41,41,42
C  IF SO THEN RETURN OR REVISE JACOBIAN
 42  GO TO (43,43,44),IS
 44  WRITE(*,45)
 45  FORMAT(///,5X,'ERROR RETURN BECAUSE A NEARBY STATIONARY POINT OF
    *F(X) IS PREDICTED')
     IER = 5
     GO TO 17
 43  NTEST = 0
     DO 46 I = 1,N
       X(I) = W(NX + I)
 46  CONTINUE
     GO TO 32
C  TEST WHETHER TO APPLY THE FULL NEWTON CORRECTION
 41  IS = 2
     IF(DN-DD) 47,47,48
 47  DD = DMAX1(DN,DSS)
     DS = 0.25D0*DN
     TINC = 1.D0
     IF(DN-DSS) 49,58,58
 49  IS = 4
```

```
      GO TO 80
C  CALCULATE THE LENGTH OF THE STEEPEST DESCENT STEP
 48   K = 0
      DMULT = 0.D0
      DO 51 I = 1,N
       DW = 0.D0
       DO 52 J = 1,N
        K = K + 1
        DW = DW + W(K)*X(J)
 52    CONTINUE
       DMULT = DMULT + DW*DW
 51   CONTINUE
      DMULT = DS/DMULT
      DS = DS*DMULT*DMULT
C  TEST WHETHER TO USE THE STEEPEST DESCENT DIRECTION
      IF(DS-DD) 53,54,54
C  TEST WHETHER THE INITIAL VALUE OF DD HAS BEEN SET
 54   IF(DD) 55,55,56
 55   DD = DMAX1(DSS,DMIN1(DM,DS))
      DS = DS/(DMULT*DMULT)
      GO TO 41
C  SET THE MULTIPLIER OF THE STEEPEST DESCENT DIRECTION
 56   ANMULT = 0.D0
      DMULT = DMULT*DSQRT(DD/DS)
      GO TO 98
C  INTERPOLATE BETWEEN THE STEEPEST DESCENT AND THE
C  NEWTON DIRECTIONS
 53   SP = SP*DMULT
      ANMULT = (DD-DS)/((SP-DS) + DSQRT((SP-DD)**2 + (DN-DD)*(DD-DS)))
      DMULT = DMULT*(1.D0-ANMULT)
C  CALCULATE THE CHANGE IN X AND ITS ANGLE WITH FIRST DIRECTION
 98   DN = 0.D0
      SP = 0.D0
      DO 57 I = 1,N
       F(I) = DMULT*X(I) + ANMULT*F(I)
       DN = DN + F(I)*F(I)
       SP = SP + F(I)*W(ND + I)
 57   CONTINUE
      DS = 0.25D0*DN
C  TEST WHETHER AN EXTRA STEP IS NEEDED FOR INDEPENDENCE
      IF(W(NDC + 1)-DTEST) 58,58,59
 59   IF(SP*SP-DS) 60,58,58
C  TAKE THE EXTRA STEP AND UPDATE THE DIRECTION MATRIX
 50   IS = 2.D0
 60   DO 61 I = 1,N
      X(I) = W(NX + I) + DSTEP*W(ND + I)
      W(NDC + I) = W(NDC + I + 1) + 1.D0
 61   CONTINUE
      W(ND) = 1.D0
      DO 62 I = 1,N
      K = ND + I
      SP = W(K)
      DO 63 J = 2,N
       W(K) = W(K + N)
       K = K + N
 63   CONTINUE
      W(K) = SP
```

```
   62  CONTINUE
       GO TO 1
C  EXPRESS THE NEW DIRECTION IN TERMS OF THOSE OF THE DIRECTION
C  MATRIX, AND UPDATE THE COUNTS IN W(NDC+1) ETC.
   58  SP = 0.D0
       K = ND
       DO 64 I = 1,N
         X(I) = DW
         DW = 0.D0
         DO 65 J = 1,N
           K = K + 1
           DW = DW + F(J)*W(K)
   65    CONTINUE
         GO TO (68,66),IS
   66    W(NDC + I) = W(NDC + I) + 1.D0
         SP = SP + DW*DW
         IF(SP-DS) 64,64,67
   67    IS = 1
         KK = I
         X(1) = DW
         GO TO 69
   68    X(I) = DW
   69    W(NDC + I) = W(NDC + I + 1) + 1.D0
   64  CONTINUE
       W(ND) = 1.D0
C  REORDER THE DIRECTIONS SO THAT KK IS FIRST
       IF(KK-1) 70,70,71
   71  KS = NDC + KK*N
       DO 72 I = 1,N
         K = KS + I
         SP = W(K)
         DO 73 J = 2,KK
           W(K) = W(K-N)
           K = K-N
   73    CONTINUE
         W(K) = SP
   72  CONTINUE
C  GENERATE THE NEW ORTHOGONAL DIRECTION MATRIX
   70  DO 74 I = 1,N
         W(NW + I) = 0.D0
   74  CONTINUE
       SP = X(1)*X(1)
       K = ND
       DO 75 I = 2,N
         DS = DSQRT(SP*(SP + X(I)*X(I)))
         DW = SP/DS
         DS = X(I)/DS
         SP = SP + X(I)*X(I)
         DO 76 J = 1,N
           K = K + 1
           W(NW + J) = W(NW + J) + X(I-1)*W(K)
           W(K) = DW*W(K + N)-DS*W(NW + J)
   76    CONTINUE
   75  CONTINUE
       SP = 1.D0/DSQRT(DN)
       DO 77 I = 1,N
         K = K + 1
```

```
          W(K) = SP*F(I)
  77   CONTINUE
C  CALCULATE THE NEXT VECTOR X, AND PREDICT THE RIGHT HAND SIDES
  80   FNP = 0.D0
       K = 0
       DO 78 I = 1,N
         X(I) = W(NX + I) + F(I)
         W(NW + I) = W(NF + I)
         DO 79 J = 1,N
           K = K + 1
           W(NW + I) = W(NW + I) + W(K)*F(J)
  79     CONTINUE
         FNP = FNP + W(NW + I)**2
  78     CONTINUE
C  CALL FUNC USING THE NEW VECTOR OF VARIABLES
       GO TO 1
C  UPDATE THE STEP SIZE
  27   DMULT = 0.9D0*FMIN + 0.1D0*FNP-FSQ
       IF(DMULT) 82,81,81
  82   DD = DMAX1(DSS,0.25D0*DD)
       TINC = 1.D0
       IF(FSQ-FMIN) 83,28,28
C  TRY THE TEST WHETHER TO INCREASE THE STEP LENGTH
  81   SP = 0.D0
       SS = 0.D0
       DO 84 I = 1,N
         SP = SP + DABS(F(I)*(F(I)-W(NW + I)))
         SS = SS + (F(I)-W(NW + I))**2
  84   CONTINUE
       PJ = 1.D0 + DMULT/(SP + DSQRT(SP*SP + DMULT*SS))
       SP = DMIN1(4.D0,TINC,PJ)
       TINC = PJ/SP
       DD = DMIN1(DM,SP*DD)
       GO TO 83
C  IF F(X) IMPROVES STORE THE NEW VALUE OF X
  87   IF(FSQ-FMIN) 83,50,50
  83   FMIN = FSQ
       DO 88 I = 1,N
         SP = X(I)
         X(I) = W(NX + I)
         W(NX + I) = SP
         SP = F(I)
         F(I) = W(NF + I)
         W(NF + I) = SP
         W(NW + I) = -W(NW + I)
  88   CONTINUE
       IF(IS-1) 28,28,50
C  CALCULATE THE CHANGES IN F AND IN X
  28   DO 89 I = 1,N
         X(I) = X(I)-W(NX + I)
         F(I) = F(I)-W(NF + I)
  89   CONTINUE
C  UPDATE THE APPROXIMATIONS TO J AND TO AJINV
       K = 0
       DO 90 I = 1,N
         W(MW + I) = X(I)
         W(NW + I) = F(I)
```

```
         DO 91 J = 1,N
           W(MW + I) = W(MW + I)-AJINV(I,J)*F(J)
           K = K + 1
           W(NW + I) = W(NW + I)-W(K)*X(J)
91       CONTINUE
90    CONTINUE
      SP = 0.D0
      SS = 0.D0
      DO 92 I = 1,N
        DS = 0.D0
        DO 93 J = 1,N
          DS = DS + AJINV(J,I)*X(J)
93      CONTINUE
      SP = SP + DS*F(I)
      SS = SS + X(I)*X(I)
      F(I) = DS
92    CONTINUE
      DMULT = 1.D0
      IF(DABS(SP)-0.1D0*SS) 94,95,95
94    DMULT = 0.8D0
95    PJ = DMULT/SS
      PA = DMULT/(DMULT*SP + (1.D0-DMULT)*SS)
      K = 0
      DO 96 I = 1,N
        SP = PJ*W(NW + I)
        SS = PA*W(MW + I)
        DO 97 J = 1,N
          K = K + 1
          W(K) = W(K) + SP*X(J)
          AJINV(I,J) = AJINV(I,J) + SS*F(J)
97    CONTINUE
96    CONTINUE
      GOTO 38
      END
```

```
C
C  ******************************************************************
C
C  SUBROUTINE MATINV EVALUATES THE INVERSE OF
C  A REAL N*N MATRIX
C
C  ******************************************************************
C
      SUBROUTINE MATINV(N,A,IFLAG)
      IMPLICIT REAL*8(A-H,O-Z)
      DIMENSION A(82,82),AINV(82,82)
      TOL = 0.D0
      DO 50 I = 1,N
      DO 40 J = 1,N
       AINV(I,J) = 0.D0
  40  CONTINUE
      AINV(I,I) = 1.D0
  50  CONTINUE
C  BEGIN INVERSION PROCEDURE
      DO 180 L = 1,N
C  SEARCH FOR PIVOT IN COLUMN L
      P = TOL
      K = 0
      DO 60 I = L,N
       Q = DABS(A(I,L))
       IF(P.GE.Q) GO TO 60
       P = Q
       K = I
  60  CONTINUE
      IF(K.GT.0) GO TO 70
      IFLAG = 1
      RETURN
  70  IF(K.EQ.L) GO TO 100
C  INTERCHANGE ROWS K AND L, BRINGING PIVOT IN OLUMN L TO ROW L
      DO 80 J = L,N
       R = A(K,J)
       A(K,J) = A(L,J)
       A(L,J) = R
  80  CONTINUE
      DO 90 J = 1,N
       R = AINV(K,J)
       AINV(K,J) = AINV(L,J)
       AINV(L,J) = R
  90  CONTINUE
C  PERFORM ELIMINATION IN COLUMN L
 100    LP1 = L + 1
      R = A(L,L)
      A(L,L) = 1.D0
      IF(L.EQ.N) GO TO 120
      DO 110 J = LP1,N
       A(L,J) = A(L,J)/R
 110   CONTINUE
 120    DO 130 J = 1,N
       AINV(L,J) = AINV(L,J)/R
 130   CONTINUE
      DO 170 I = 1,N
       IF(I.EQ.L) GO TO 170
```

```
            R = A(I,L)
            A(I,L) = 0.D0
            IF(L.EQ.N) GO TO 150
            DO 140 J = LP1,N
             A(I,J) = A(I,J)-R*A(L,J)
140         CONTINUE
150         DO 160 J = 1,N
             AINV(I,J) = AINV(I,J)-R*AINV(L,J)
160         CONTINUE
170         CONTINUE
180    CONTINUE
       DO 200 I = 1,N
       DO 200 J = 1,N
        A(I,J) = AINV(I,J)
200    CONTINUE
       IFLAG = 0
       RETURN
       END
```

```
C
C  *****************************************************************
C
C    THIS ROUTINE SOLVES SYSTEMS OF EQUATIONS USING GAUSSIAN
C    ELIMINATION AND COMPUTES ERROR BOUNDS.  IT CALLS SUBROUTINE
C    FACTOR, SUBROUTINE SOLVE AND SUBROUTINE CONDNO.
C
C  *****************************************************************
C
      SUBROUTINE GAUSS(N,A,B,X)
      IMPLICIT REAL*8(A-H,O-Z)
      COMPLEX*16 A(40,40),B(40),X(40),RES(40),AA(40,40)
      DIMENSION IPIVOT(40),IC(40)
      CALL FACTOR(A,N,AA,IPIVOT)
      CALL CONDNO(A,AA,N,IPIVOT,CNDN,IC,AINV)
      CALL SOLVE(AA,N,B,IPIVOT,X)
      DO 70 I=1,N
        RES(I) = 0.0D0
70    CONTINUE
      DO 4 I=1,N
      DO 5 J=1,N
        RES(I) = RES(I) + A(I,J)*X(J)
5     CONTINUE
4     CONTINUE
      DO 6 I=1,N
        RES(I) = RES(I)-B(I)
6     CONTINUE
      ANORMR = 0.0D0
      ANORMB = 0.0D0
      DO 7 I=1,N
        ANORMB = ANORMB + CDABS(B(I))
        ANORMR = ANORMR + CDABS(RES(I))
7     CONTINUE
      REUB = CNDN*ANORMR/ANORMB
      RELB = ANORMR/(ANORMB*CNDN)
C     WRITE(7,12) RELB, REUB
C12   FORMAT(5X,'THE RELATIVE ERROR LOWER BOUND = ',D18.8,/,5X,'THE RELAT
C    *IVE ERROR UPPER BOUND = ',D18.8,/,60(1H-))
      RETURN
      END
```

```
C
C  ************************************************************
C
C  THE FOLLOWING SUBROUTINE IS CALLED BY SUBROUTINE
C  GAUSS TO PERFORM GAUSSIAN ELIMINATION.
C
C  ************************************************************
C
      SUBROUTINE FACTOR(A,N,AA,IPIVOT)
      IMPLICIT REAL*8(A-H,O-Z)
      COMPLEX*16 A(40,40),AA(40,40),TR
      DIMENSION IPIVOT(40),D(40)
      DO 27 I = 1,N
      DO 27 J = 1,N
       AA(I,J) = A(I,J)
27    CONTINUE
      IS = N-1
      DO 29 IP = 1,IS
       J = IP
       DO 20 I = IP,N
         AMAX = 0.0D0
         DO 21 LJ = IP,N
           RAA = CDABS(AA(I,LJ))
           IF(RAA.GT.AMAX) AMAX = RAA
21       CONTINUE
         SAA = CDABS(AA(I,IP))
         D(I) = SAA/AMAX
20     CONTINUE
       BMAX = 0.0D0
       DO 22 I = IP,N
         IF(D(I).LE.BMAX) GO TO 22
         BMAX = D(I)
         J = I
22     CONTINUE
       IPIVOT(IP) = J
       DO 23 I = IP,N
         TR = AA(IP,I)
         AA(IP,I) = AA(J,I)
         AA(J,I) = TR
23     CONTINUE
       NP = IP + 1
       DO 25 J = NP,N
         AA(J,IP) = -AA(J,IP)/AA(IP,IP)
         DO 25 I = NP,N
           AA(J,I) = AA(J,I) + AA(J,IP)*AA(IP,I)
25     CONTINUE
29    CONTINUE
      RETURN
      END
```

```
C
C **********************************************************************
C
C  THE FOLLOWING SUBROUTINE IMPLEMENTS THE BACK SUBSTITUTION
C  STEP IN SOLVING THE LINEAR SYSTEM OF EQUATIONS.
C
C **********************************************************************
C
      SUBROUTINE SOLVE(AA,N,B,IPIVOT,X)
      IMPLICIT REAL*8(A-H,O-Z)
      COMPLEX*16 AA(40,40),X(40),B(40),SB(40),BT,SUM
      DIMENSION IPIVOT(40)
      DO 130 LL=1,N
       SB(LL)=B(LL)
130   CONTINUE
      MM=N-1
      DO 40 I=1,MM
       J=IPIVOT(I)
       BT=SB(I)
       SB(I)=SB(J)
       SB(J)=BT
       KK=I+1
       DO 41 K=KK,N
        SB(K)=SB(K)+AA(K,I)*SB(I)
41     CONTINUE
40    CONTINUE
      X(N)=SB(N)/AA(N,N)
      DO 42 I=2,N
       SUM=0.0D0
       II=N+1-I
       IJ=II+1
       DO 43 J=IJ,N
        SUM=SUM+AA(II,J)*X(J)
43     CONTINUE
       X(II)=(SB(II)-SUM)/AA(II,II)
42    CONTINUE
      RETURN
      END
```

```
C
C *******************************************************************
C
C  THE FOLLOWING SUBROUTINE COMPUTES THE CONDITION
C  NUMBER OF A MATRIX.  IT IS CALLED BY SUBROUTINE GAUSS
C  GAUSS TO PROVIDE ERROR BOUNDS TO THE OBTAINNED SOLUTION.
C
C *******************************************************************
C
      SUBROUTINE CONDNO(A,AA,N,IPIVOT,CNDN,IC,AINV)
      IMPLICIT REAL*8(A-H,O-Z)
      COMPLEX*16 A(40,40),AA(40,40),Z(40),
     *Y(40),XX(40),SUM,ZT
      DIMENSION IPIVOT(40),IC(40)
      IC(1) = 1
      Z(1) = 1.D0/AA(1,1)
      DO 50 I = 2,N
        SUM = 0.0D0
        IJ = I-1
        DO 51 J = 1,IJ
          SUM = SUM + AA(J,I)*Z(J)
51      CONTINUE
        IF(CDABS(SUM).EQ.0.D0) THEN
          IC(I) = 1
        ELSE
          IC(I) = -SUM/CDABS(SUM)
        ENDIF
        Z(I) = (IC(I)-SUM)/AA(I,I)
50    CONTINUE
      KN = N-1
      DO 52 I = 1,KN
        II = N-I
        IJ = II + 1
        DO 53 K = IJ,N
          Z(II) = Z(II) + AA(K,II)*Z(K)
53      CONTINUE
        J = IPIVOT(II)
        ZT = Z(II)
        Z(II) = Z(J)
        Z(J) = ZT
52    CONTINUE
      CALL SOLVE(AA,N,Z,IPIVOT,XX)
      ANORMX = 0.0D0
      ANORMY = 0.0D0
      DO 54 I = 1,N
        ANORMX = ANORMX + CDABS(XX(I))
        ANORMY = ANORMY + CDABS(Z(I))
54    CONTINUE
      AINV = ANORMX/ANORMY
      ANORMA = 0.0D0
      DO 55 I = 1,N
        SUMR = 0.0D0
        DO 56 J = 1,N
          SUMR = SUMR + CDABS(A(J,I))
56      CONTINUE
        IF(SUMR.GT.ANORMA) ANORMA = SUMR
55    CONTINUE
```

```
CNDN = ANORMA*AINV
RETURN
END
```

```
C
C  ************************************************************************
C
C  SUBROUTINE BESSEL COMPUTES THE ZERO ORDER OR THE
C  FIRST ORDER BESSEL FUNCTION OF THE FIRST KIND.
C
C  ************************************************************************
C
      SUBROUTINE BESSEL(NORD,ARG,VALJ)
      IMPLICIT REAL*8(A-H,O-Z)
      IF(ARG.GT.20.D0) THEN
        X = 3.D0/ARG
        IF(NORD.EQ.0) THEN
        FF = .79788456D0-.00000077D0*X-.0055274D0*X*X-.00009512D0*(X**3)
         FS = + .00137237D0*(X**4)-.00072805D0*(X**5) + .00014476D0*(X**6)
         TH0 = ARG-.78539816D0-.04166397D0*X-.00003954D0*X*X
     *       + .00262573D0*(X**3)-.00054125D0*(X**4)-.00029333D0*(X**5)
     *       + .00013558D0*(X**6)
        F0 = FF + FS
        VALJ = F0*DCOS(TH0)/DSQRT(ARG)
        RETURN
       ENDIF
       IF(NORD.EQ.1) THEN
       F1 = .79788456D0+ .00000156D0*X+ .01659667D0*X*X+ .00017105D0*(X**3)
     *    -.00249511D0*(X**4)+ .00113653D0*(X**5)-.00020033D0*(X**6)
         TH1 = ARG-2.35619449D0+ .12499612D0*X+ .00005650D0*X*X
     *      -.00637879D0*(X**3)+ .00074348D0*(X**4)+ .00079824D0*(X**5)
     *      -.00029166D0*(X**6)
        VALJ = F1*DCOS(TH1)/DSQRT(ARG)
        RETURN
       ENDIF
      ELSE
       FT = (ARG/2.D0)**NORD
       SUM = 0.D0
       DO 1 I = 1,100
        J = I-1
        JNORD = J + NORD
        F11 = (-ARG/2.D0)**J
        F12 = (ARG/2.D0)**J
        RIF = 1.D0
        RIMFAC = 1.D0
        IF(J.EQ.0) GO TO 3
        DO 2 K = 1,J
         RIF = RIF*K
2       CONTINUE
3       IF(NORD.NE.0) GO TO 4
        RIMFAC = RIF
        GO TO 6
4       DO 5 K = 1,JNORD
         RIMFAC = RIMFAC*K
5       CONTINUE
6       F2 = (F11/RIF)*(F12/RIMFAC)
        IF(DABS(F2).LE.1.D-10) GO TO 7
        SUM = SUM + F2
1      CONTINUE
       IF(DABS(F2).GT.1.D-10) WRITE(7,8) F2
8      FORMAT(/,5X,'DESIRED ACCURACY IN CALCULATING A BESSEL FUNCTION
```

```
      *IS NOT OBTAINED.  THE LAST TERM OF THE SERIES ADDED  = ',F15.8)
7    VALJ = FT*SUM
     ENDIF
     RETURN
     END
```

```
C
C ********************************************************************
C
C  SUBROUTINE ANEUM COMPUTES THE ZERO ORDER OR THE
C  FIRST ORDER BESSEL FUNCTION OF THE SECOND KIND.
C
C ********************************************************************
C
      SUBROUTINE ANEUM(NORDER,ARG,VALN)
      IMPLICIT REAL*8(A-H,O-Z)
      IF(ARG.GT.20.D0) THEN
        X = 3.D0/ARG
        IF(NORDER.EQ.0) THEN
        F0F = .79788456D0-.00000077D0*X-.0055274D0*X*X-.00009512D0*(X**3)
         F0S = +.00137237D0*(X**4)-.00072805D0*(X**5)+.00014476D0*(X**6)
          TH0 = ARG-.78539816D0-.04166397D0*X-.00003954D0*X*X
     *     +.00262573D0*(X**3)-.00054125D0*(X**4)-.00029333D0*(X**5)
     *     +.00013558D0*(X**6)
         F0 = F0F + F0S
         VALN = F0*DSIN(TH0)/DSQRT(ARG)
         RETURN
        ENDIF
        IF(NORDER.EQ.1) THEN
        F1F = .79788456D0+.00000156D0*X+.01659667D0*X*X+.00017105D0*(X**3)
         F1S = -.00249511D0*(X**4)+.00113653D0*(X**5)-.00020033D0*(X**6)
          TH1 = ARG-2.35619449D0+.12499612D0*X+.00005650D0*X*X
     *     -.00637879D0*(X**3)+.00074348D0*(X**4)+.00079824D0*(X**5)
     *     -.00029166D0*(X**6)
         F1 = F1F + F1S
         VALN = F1*DSIN(TH1)/DSQRT(ARG)
         RETURN
        ENDIF
       ELSE
        PI = 4.D0*DATAN(1.D0)
        GAMMA = 0.5772156649D0
        C = 2.D0*DLOG(ARG/2.D0)/PI
        C1 = 2.D0*GAMMA/PI
        IF(NORDER.EQ.0) THEN
          CALL BESSEL(0,ARG,VALJ0)
          FT0 = (C + C1)*VALJ0
          SUM1 = 0.D0
          DSUM1 = 0.D0
          AFACQ = 1.D0
          DO 14 I = 1,100
            AFACQ = AFACQ*DFLOAT(I)
            AN1 = ((-1)**I)*((ARG/2.D0)**I)
            DSUM1 = DSUM1 + 1.D0/DFLOAT(I)
            TER = (AN1/AFACQ)*(DSUM1/AFACQ)*((ARG/2.D0)**I)
            IF(DABS(TER).LE.1.D-10) GO TO 15
            SUM1 = SUM1 + TER
14        CONTINUE
          IF(DABS(TER).GT.1.D-10)
     *    WRITE(7,21) TER
21        FORMAT(/,5X,'DESIRED ACCURACY IN CALCULATING NEUMANN FUNCTIONS
     *IS NOT OBTAINED. THE LAST TERMS OF THE SERIES ADDED =',2F15.8)
15        VALN = FT0-2.D0*SUM1/PI
          RETURN
```

```
      ENDIF
      IF(NORDER.EQ.1) THEN
      CALL BESSEL(1,ARG,VALJ1)
      FT1 = (C + C1)*VALJ1
      SUM2 = 0.D0
      DSUM2 = 0.D0
      AFACQ = 1.D0
      AFACQ1 = 1.D0
      DSUM1 = 0.D0
      DO 20 I = 1,100
        DSUM1 = DSUM1 + 1.D0/DFLOAT(I)
        DSUM2 = 2.D0*DSUM1 + 1.D0/(DFLOAT(I) + 1.D0)
        AFACQ = AFACQ*DFLOAT(I)
        AFACQ1 = AFACQ*(DFLOAT(I) + 1.D0)
        AN1 = ((-1)**I)*((ARG/2.D0)**I)
        TER = (AN1/AFACQ)*(DSUM2/AFACQ1)*(ARG/2.D0)*((ARG/2.D0)**I)
        IF(DABS(TER).LE.1.D-10) GO TO 22
        SUM2 = SUM2 + TER
20    CONTINUE
      ENDIF
      IF(DABS(TER).GT.1.D-10)
     *WRITE(7,16) TER
16    FORMAT(/,5X,'DESIRED ACCURACY IN CALCULATING NEUMANN FUNCTIONS
     *IS NOT OBTAINED.  THE LAST TERMS OF THE SERIES ADDED = ',2F15.8)
22    VALN = FT1-(ARG/2.D0 + SUM2)/PI-2.D0/(PI*ARG)
      ENDIF
      RETURN
      END
```

Appendix VI: Program ACQRFTR

The follwing program is written in Tektronix SPS-BASIC to compute the reflection co-efficient of a sample adapted to a transmission line. A 7704A Tektronix digital proc-essing scope interfaced to a PDP11/34 is used. First, a reference waveform is acquired by putting a short circuit in place of the sample. Then, the response waveform is ob-tained by acquiring the reflected waveform of the sample. The program computes their Fourier transforms using the complete FFT method. The reflection coefficient (transfer function) is then computed from the FFT's of the waveforms by division.

This program can also be used to compute the transmission coefficient of a sample inserted in a transmission line. In this case, line 330 must be deleted. Also, the reference waveform is the acquired waveform when the sample is removed from the line.

```
10 CLOSE ALL
20 DIM CC(512)
30 WAVEFORM WX IS BI(511),T,X$,Y$
40 WAVEFORM WI IS AI(511),T,X$,Y$
50 WAVEFORM WO IS AO(511),T,X$,Y$
60 WAVEFORM WS IS SS(511),T,X$,Y$
70 WS = 0
80 LOAD "DPO
90 ATTACH #1 AS DPO:
100 PRINT "CHOOSE THE TIME WINDOW, HIT ANY KEY WHEN READY";\WAIT\PRINT
110 X$ = "S"\Y$ = "V"
120 GET WX FROM #1,"A"
130 PRINT "DO YOU WANT TO SUBTRACT THE EFFECT OF THE CONNECTORS";
140 PRINT "FROM BOTH WAVEFORMS (Y/N)";\INPUT A$
150 IF A$ = "Y" THEN 160\IF A$ = "N" THEN 200\GOTO 130
160 PRINT "WHICH CHANNEL";\INPUT S$
170 PRINT "HOW MANY TIMES WOULD YOU LIKE TO AVERAGE IT";\INPUT NA$
180 AV$ = "AVE"&NA$&","&S$
190 GET WS FROM #1,AV$\SS = SS-MEA(SS(0:19))
200 PRINT "DO YOU WANT TO ACQUIRE REFERENCE WAVEFORM FROM DPO (D)";
210 PRINT "OR READ FROM A FILE (F)";\INPUT A$
220 IF A$ = "D" THEN 230\IF A$ = "F" THEN 430\GOTO 200
230 PRINT "WHICH MEMORY IS THE REFERENCE WAVEFORM STORED IN";\INPUT B$
240 PRINT "HOW MANY TIMES DO YOU WANT TO AVERAGE IT";\INPUT NA$
270 AV$ = "AVE"&NA$&","&B$
300 GET WI FROM #1,AV$
310 AI = AI-MEA(AI(0:19))
320 AI = AI-SS
330 AI = -AI
```

```
340 PAGE\GRAPH WI\WAIT\PAGE
350 PRINT "DO YOU WANT TO STORE IT IN A FILE (Y/N)";\INPUT A$
360 IF A$ = "Y" THEN 370\IF A$ = "N" THEN 420\GOTO 350
370 PRINT "ENTER FILE NAME (NO EXTENTION)";\INPUT F$
380 F$ = F$&".DAT"
390 OPEN #2 AS F$ FOR WRITE
400 WRITE #2,WI
410 CLOSE #2
420 GOTO 450
430 GOSUB 3500
440 WI = WX
450 PRINT "DO YOU WANT TO ACQUIRE THE RESPONSE WAVEFORM FROM DPO (D)";
460 PRINT "OR READ FROM A FILE (F)";\INPUT A$
470 IF A$ = "D" THEN 480\IF A$ = "F" THEN 660\GOTO 450
480 PRINT "WHICH MEMORY IS THE RESPONSE WAVEFORM STORED IN";\INPUT B$
490 PRINT "HOW MANY TIMES DO YOU WANT TO AVERAGE IT";\INPUT NA$
520 PRINT "HOW MANY TIMES WOULD YOU LIKE TO REPEAT THE MEASUREMENT";
521 INPUT M
522 FOR I = 1 TO M
523 PRINT "ALIGN THE SAMPLE PROPERLY, HIT ANY KEY WHEN READY";\WAIT
530 AV$ = "AVE"&NA$&","&B$
550 GET WX FROM #1,AV$
560 BI = BI-MEA(BI(0:19))
570 BI = BI-SS
572 AO = AO + BI
574 NEXT I
576 AO = AO/M
580 PAGE\GRAPH WO\WAIT\PAGE
590 PRINT "DO YOU WANT TO STORE IT IN A FILE (Y/N)";\INPUT A$
600 IF A$ = "Y" THEN 610\IF A$ = "N" THEN 680\GOTO 590
610 PRINT "ENTER FILE NAME (NO EXTENSION)";\INPUT F$\F$ = F$&".DAT"
620 OPEN #3 AS F$ FOR WRITE
630 WRITE #3,WO
640 CLOSE #3
650 GOTO 680
660 GOSUB 3500
670 WO = WX
680 PRINT "WAS THERE AN ATTENUATOR CONNECTED WHEN ACQUIRING THE";
690 PRINT "REFERENCE WAVEFORM (Y/N)";\INPUT A$
700 IF A$ = "Y" THEN 710\IF A$ = "N" THEN 730\GOTO 680
710 PRINT "ENTER AMOUNT OF ATTENUATION (IN DB)";\INPUT DB
720 RT = 10¢(DB/20)\WI = RT*WI
730 PRINT "WAS THERE AN ATTENUATOR CONNECTED WHEN ACQUIRING THE";
740 PRINT "RESPONSE WAVEFORM (Y/N)";\INPUT A$
750 IF A$ = "Y" THEN 760\IF A$ = "N" THEN 780\GOTO 730
760 PRINT "ENTER AMOUNT OF ATTENUATION (IN DB)";\INPUT DB
770 RT = 10¢(DB/20)\WO = RT*WO
780 DELETE WX,WS,SS,BI
790 DELETE 10,790
800 OVERLAY "COMFFT.BAS"
1990 DELETE 5000,5300\DELETE 10,1990
1995 OVERLAY "TRANSM.BAS"
2590 DELETE 10,2590
3500 PRINT "ENTER  WAVEFORM'S FILENAME TO READ FROM (NO EXTENSION)";
3510 INPUT F$
3520 F$ = F$&".DAT"
3530 OPEN #4 AS F$ FOR READ
```

```
3540 READ #4,WX
3550 CLOSE #4
3560 PAGE\GRAPH WX\WAIT\PAGE
3570 RETURN
4500 PI = 4*ATN(1)
4510 VL = CC(0)
4520 FOR I = 1 TO 512
4530 DL = CC(I)-VL
4550 IF DL > PI THEN CC(I) = CC(I)-2*PI
4560 IF DL < -PI THEN CC(I) = CC(I) + 2*PI
4565 VL = CC(I)
4570 NEXT I
4580 RETURN
10000 PRINT "ENTER PARAMETER FOR PHASE CONTINUATION (0-1)";\INPUT Q
10010 DIM CC(512),MP(512)
10020 PI = 4*ATN(1)
10030 VL = CC(0)
10040 MP = 0
10050 QQ = 0
10060 FOR I = 1 TO 512
10070 DL = CC(I)-VL
10080 IF DL > Q*PI THEN QQ = QQ-2*PI
10090 IF DL < -Q*PI THEN QQ = QQ + 2*PI
10100 MP(I) = MP(I) + QQ
10110 VL = CC(I)
10120 NEXT I
10130 CC = CC + MP
10140 RETURN


Subprogram "COMFFT"

1500 PRINT "DO YOU WANT TO COMPUTE THEIR FFT'S (Y/N)";\INPUT A$
1510 IF A$ = "Y" THEN 1520\IF A$ = "N" THEN 2200\GOTO 1500
1520 DIM A(1023)
1530 WAVEFORM XW IS XI(512),TX,XM$,YM$
1540 WAVEFORM PX IS XP(512),TX,XP$,YP$
1550 DIM B(511)
1560 FOR I = 0 TO 511
1570 A(I) = AI(I)
1580 NEXT I
1590 GOSUB 5000
1600 TX = TR
1610 LET XW = WG\LET PX = WH
1620 FOR I = 0 TO 511
1630 A(I) = AO(I)
1640 NEXT I
1650 WAVEFORM YW IS YI(512),TY,XM$,YM$
1660 WAVEFORM PY IS YP(512),TY,XP$,YP$
1670 GOSUB 5000
1680 TY = TR
1690 YW = WG\PY = WH
1700 DELETE A,MI,MP,WH,WI,WO,AI,AO
5000 EX = (A(511)-A(0))/512
5010 FOR I = 0 TO 511
5020 A(I + 512) = A(511)-A(I) + A(0)
5030 B(I) = A(I)-EX*I-A(0)
```

```
5040 NEXT I
5050 WAVEFORM W IS A(1023),T,X$,Y$
5060 WAVEFORM WM IS AM(512),TM,XM$,YM$
5070 WAVEFORM WP IS AP(512),TP,XP$,YP$
5080 WAVEFORM BB IS B(511),T,X$,Y$
5090 WAVEFORM CM IS BM(256),SM,XM$,YM$
5100 WAVEFORM CP IS BP(256),SP,XP$,YP$
5110 RFFT W,WM,WP
5120 RFFT BB,CM,CP
5130 WM = WM/2\WP = WP/2
5140 TR = TM\TI = TP
5150 WAVEFORM WG IS MI(512),TR,XM$,YM$
5160 WAVEFORM WH IS MP(512),TI,XP$,YP$
5170 MI(0) = AM(0)\MP(0) = AP(0)
5180 FOR I = 1 TO 256
5190 MI(2*I-1) = AM(2*I-1)\MI(2*I) = BM(I)
5200 MP(2*I-1) = AP(2*I-1)\MP(2*I) = BP(I)
5210 NEXT I
5220 POLAR WG,WH
5230 PAGE\GRAPH WG\WAIT\PAGE
5240 PAGE\GRAPH WH\WAIT\PAGE
5250 DELETE W,WM,WP,AM,AP
5260 DELETE BB,CM,CP,BM,BP
5270 RETURN
```

Subprogram "TRANSM"

```
2000 PRINT "DO YOU WANT TO EVALUATE THE TRANSFER FUNCTION (Y/N)";
2005 INPUT A$
2010 IF A$ = "Y" THEN 2030\IF A$ = "N" THEN 2200
2020 GOTO 2000
2030 WAVEFORM WH IS H(512),TH,XH$,YH$
2040 WH = YW/XW
2050 WAVEFORM WP IS HP(512),TP,XP$,YP$
2060 WP = PY-PX
2070 CC = HP
2080 GOSUB 10000
2090 HP = CC
2100 DELETE YI,XI,YP,XP,XW,PX,YW,PY
2110 PRINT "THE FOLLOWING GRAPH IS THE MAGNITUDE OF THE TRANSFER,";
2120 PRINT "FUNCTION HIT ANY KEY TO DISPLAY IT";\WAIT
2130 PAGE\GRAPH WH\WAIT\PAGE
2140 PRINT "DO YOU WANT TO STORE IT IN A FILE";\INPUT A$
2150 IF A$ = "Y" THEN 2160\IF A$ = "N" THEN 2200\GOTO 2140
2160 PRINT "ENTER FILENAME (NO EXTENSION)";\INPUT F$\F$ = F$&".DAT"
2170 OPEN #2 AS F$ FOR WRITE
2180 WRITE #2,WH
2190 CLOSE #2
2200 PRINT "DO YOU WANT TO SEND IT TO DPO (Y/N)";\INPUT A$
2210 IF A$ = "Y" THEN 2220\IF A$ = "N" THEN 2300\GOTO 2200
2220 LOAD "DPO
2230 ATTACH #1 AS DPO:
2240 PRINT "ENTER THE CHANNEL";\INPUT S$
2250 WAVEFORM DH IS DM(511),TH,XH$,YH$
2260 FOR I = 1 TO 511
2270 DM(I) = H(I)\NEXT I
```

```
2280 DM(0) = H(0)
2290 PUT DH INTO #1,S$
2300 DELETE DH,DM
2310 PRINT "THE FOLLOWING GRAPH IS THE PHASE OF THE TRANSFER FUNCTION,";
2320 PRINT "HIT ANY KEY TO DISPLAY IT";\WAIT
2330 PAGE\GRAPH WP\WAIT\PAGE
2340 PRINT "DO YOU WANT TO STORE IT IN A FILE";\INPUT A$
2350 IF A$ = "Y" THEN 2360\IF A$ = "N" THEN 2410\GOTO 2340
2360 PRINT "ENTER FILENAME (NO EXTENSION)";\INPUT F$
2370 F$ = F$&".DAT"
2380 OPEN #2 AS F$ FOR WRITE
2390 WRITE #2,WP
2400 CLOSE #2
2410 PRINT "DO YOU WANT TO SEND IT TO DPO (Y/N)";\INPUT A$
2420 IF A$ = "Y" THEN 2430\IF A$ = "N" THEN 2490\GOTO 2410
2430 PRINT "ENTER THE CHANNEL";\INPUT S$
2440 WAVEFORM ZZ IS PP(511),TP,XP$,YP$
2450 FOR I = 0 TO 511
2460 PP(I) = HP(I)\NEXT I
2470 PUT ZZ INTO #1,S$
2480 DELETE ZZ,PP
2490 WAVEFORM RR IS HR(512),TH,XH$,YH$
2500 WAVEFORM RI IS HI(512),TH,XH$,YH$
2510 RR = WH*COS(WP)
2520 RI = WH*SIN(WP)
```

REFERENCES:

1. H. F. Feldegg and E. F. Barnett, 'Reflection of a Voltage Step from a Section of Transmission Line Filled with a Polar Dielectric', J. Phys. Chem., V.74, No.9, 1970, pp. 1962-1965.

2. M. J. C. v. Gemert, 'High-Frequency Time-Domain Methods in Dielectric Spectroscopy', Philips Res. Reports, 28, Nov. 1973, pp. 530-572.

3. H. Loeb, G. Young, P. Quickenden and A. suggett, 'New Methods for Measurement of Complex Permittivity up to 13 GHz and their Application to the Study of Dielectric Relaxation of Polar Liquids Including Aqueous Solutions', Ber. Bunsenges. Phys. Chem., 75, 1971, pp. 1155-1165.

4. C. Gabriel, A. W. J. Dawkins, R. J. Sheppard and E. H. Grant, 'Comparison of the Single reflection and total reflection TDS Techniques', The Institute of Physics, 1984, pp. 513-516.

5. B. Gestblom and E. Noreland, 'a New Transmission Method in Dielectric Time Domain Spectroscopy', Chemical Phys. Letters, V.47, No.2, 1977, pp. 349-351.

6. H. F. Feldegg, 'a Thin-Sample Method for the Measurement of Permeability, Permittivity and Conductivity in the Frequency and Time Domain', J. Phys. Chem., Vol.76, No.15, 1972, pp. 2116-2122.

7. M. v. Gemert, 'Evaluation of Dielectric Permittivity and Conductivity by Time Domain Spectroscopy. Mathematical Analysis of Fellner-Feldegg's Thin Cell Method', J. chem. phys., Vol.60, No.10, 1974, pp. 3963-3974.

8. B. E. Springett and T. K. Bose, 'Thin Sample Time Domain Reflectometry for Nonideal Dielectrics', Can. J. Phys., Vol.52, 1974, pp. 2463-2468.

9. T. A. Claasen and M. v. Gemert, 'Approximate Solutions in Multiple Reflection Time Domain Spectroscopy', J. Chem. Phys., Vol.63, No.1, 1975, pp. 68-73.

10. R. H. Cole, 'Evaluation of Dielectric Behaviour by Time Domain Spectroscopy. I. Dielectric Response by Real Time Analysis', J. Phys. Chem., Vol.79, No.14, 1975, pp. 1459-1469.

11. R. H. Cole, 'Evaluation of Dielectric Behaviour by Time Domain Spectroscopy. II. Complex Permittivity', J. Phys. Chem., Vol.79, No.14, 1975, pp. 1469-1474.

12. M. v. Gemert. and A. Suggett, 'Multiple Reflection Time Domain Spectroscopy, II. a Lumped Element Approach Leading to an Analytical Solution for the Complex permittivity', J. Chem. Phys., Vol.62, No.7, 1975, pp. 2720-2726.

13. R. Chahine and T. K. Bose, 'Measurements of Dielectric Properties by Time Domain Spectroscopy', J. Chem. Phys., Vol.65, No.6, 1976, pp. 2211-2215.

14. R. H. Cole, 'Time-Domain Spectroscopy of Dielectric Materials', IEEE Trans. Inst. Meas., Vol. IM-25, No.4, 1976, pp. 371-375.

15. A. M. Nicolson and G. F. Ross, 'Measurement of the Intrinsic Properties of Materials by Time-Domain Techniques', <u>IEEE Trans. Inst. Meas.</u>, Vol. IM-19, No. 4, 1970, pp. 377-382.

16. H. M. Cronson, A. M. Nicolson and P. G. Mitchell, ' Extensions of Time Domain Metrology above 10 GHz to Materials Measurements', <u>IEEE Trans. Inst. Meas.</u>, Vol. IM-23, No.4, 1974, pp. 463-468.

17. S. S. Stuchly and M. Matuszewski, 'a Combined Total Reflection-Transmission Method in Application to Dielectric Spectroscopy', <u>IEEE Trans. Inst. Meas.</u>, Vol. IM-27, No.3, 1978, pp. 285-288.

18. A. Suggett, 'Microwave Dielectric Measurements Using Time Domain Spectroscopy: Note on Recent Technique Advances', <u>J. Phys. E: Scientific Instruments</u>, Vol.8, 1975, pp. 327-330.

19. A. M. Bottreau, Y. Dutuit and J. Moreau, 'On a Multiple Reflection Time Domain Method in Dielectric Spectroscopy: Application to the Study of Some Primary Alcohols', <u>J. Chem. Phys.</u>, Vol.66, No.8, 1977, pp. 3331-3336.

20. R. H. Cole, 'Time Domain Reflectometry', <u>Ann. Rev. Phys.</u>, 28, 1977, pp. 283-300.

21. M. F. Iskander and S. S. Stuchly, 'a Time Domain Technique for Measurement of the Dielectric Properties of Biological Substances', <u>IEEE Trans. Inst. Meas.</u>, Vol. IM-21, No. 4, 1972, pp. 425-429.

22. S. S. Stuchly, M. A. Rzepecka and M. Iskander, 'Permittivity Measurements at Microwave Frequencies Using Lumped Elements', IEEE Trans. Inst. Meas., Vol. IM-23, No.1, 1974, pp. 56-62.

23. M. A. Rzepecka and S. S. Stuchly, 'a Lumped Capacitance Method for the Measurement of the Permittivity and Conductivity in the Frequency and Time Domain - a Further Analysis', IEEE Trans. Inst. Meas., Vol. IM-24, No.1, 1975, pp. 27-32.

24. M. A. Rzepecka, S. S. Stuchly and B. Parisien, 'a Method for Measurement of Permittivity of Thin Samples', J. Microwave Power, 14(1), 1979, pp.7-13.

25. R. H. Cole, S. Mashimo, and Paul Winsor.IV, 'Evaluation of Dielectric Behavior by Time Domain Spectroscopy. 3. Precision Difference Methods', J. Phys. Chem., Vol.84, No.7, 1980, pp. 786-793.

26. R. Chahine and T. Bose, 'Measurement of Small Dielectric Loss by Time Domain Spectroscopy: Application to Water/Oil Emulsions', IEEE Trans. Inst. Meas., Vol. IM-32, No.2, 1983, pp. 360-363.

27. R. Chahine and T. Bose, 'Comparative Studies of Various Methods in Time Domain Spectroscopy', J. Chem. Phys., Vol.72, No.2, 1980, pp. 808-815.

28. B. R. Parisien and S. S. Stuchly, 'a Microprocessor Controlled Time Domain Spectrometer', IEEE Trans. Inst. Meas., Vol. IM-28, No.4, 1979, pp. 269-272.

29. T. K. Bose, A. m. Bottreau and R. Chahine, 'Development of a Dipole Probe for the Study of Dielectric Properties of Biological Substances in Radio Frequency and

Microwave Region with Time Domain Reflectometry', <u>IEEE Trans. Inst. Meas.,</u> Vol. IM-35, No.1, 1986, pp. 56-60.

30.   M. Iskander and S. Stuchly, 'Fringing Field Effect in the Lumped-Capacitance Method for Permittivity Measurements', <u>IEEE Trans. Inst. Meas.,</u> Vol. IM-27, No.1, 1978, pp. 107-109.

31.   M. Stuchly and S. stuchly, 'Coaxial Line Reflection Methods for Measuring Dielectric Properties of Biological Substances at Radio and Microwave Frequencies - Review', <u>IEEE Trans. Inst. Meas.,</u> Vol. IM-29, No.3, 1980, pp.176-183.

32.   E. Risley, Jr., 'Discontinuity Capacitance of a Coaxial Line Terminated in a Circular Waveguide', <u>IEEE Trans. on Microwave Power and Tech.,</u> Vol. MTT-17, No.2, 1969, pp. 86-92

33.   Von Hippel, <u>'Dielectric Materials and Applications',</u> John Wiley and Sons, 1954.

34.   E. H. Grant , R. J. Sheppard and G. P. South, <u>'Dielectric Behaviour of Biological Molecules in Solution',</u> Oxford University Press, 1978.

35.   Ronald Pethig, <u>'Dielectric and Electronic Properties of Biological Materials',</u> John Wiley and Sons, 1979.

36.   B. K. P. Scaife, <u>'Complex Permittivity: Theory and Measurement',</u> The English Universities Press Ltd, 1971.

37.   M. N. Afsar and G. W. Chantry, 'Precise Dielectric Measurements of Low-Loss Materials at Millimeter and Submillimeter Wavelengths', <u>IEEE Trans. Mic. Th. Tech.,</u> Vol. MTT-25, No.6, 1977, pp. 509-511.

38. M. N. Afsar, 'Dielectric Measurements of Millimeter-Wave Materials', <u>IEEE Trans. Mic. Th. Tech.</u>, Vol. MTT-32, No.12, 1984, pp. 1598-1609.

39. R. J. Cook, 'Microwave Cavity Methods', in <u>'High Frequency Dielectric Measurement'</u>, Edited by J. Chamberlain and G. W. Chantry, 1973, pp. 12-27.

40. S. Roberts and Von Hippel, 'a New Method for Measuring Dielectric Constant and Loss in the Range of Centimetre Waves', <u>J. App. Phys.</u>, 17, 1946, pp. 610.

41. G. Williams, 'The Measurement of Dielectric Constant and Loss Factor of Liquids and Solutions Between 250 Mc./Sec. by Means of a Coaxial Transmission Line', <u>J. Phys. Chem.</u>, 1959, 63, pp.534-537.

42. T. W. Dakin and C. N. Works, 'Microwave Dielectric Measurements', <u>J. App. Pys.</u>, 18, 1947, pp.789.

43. M. G. Corfield, J. Horzeleki and A. H. Price, 'Rapid Method for Determining VHF Dielectric Parameters for Liquids and Solutions Using Standing Wave Procedures', <u>Brit. J. App. Phys.</u>, 12, 1961, pp. 680-682.

44. R. Bennet and J. Calderwood, 'Measurement of VHF Complex Permittivity of Liquids by Means of an Adjustable Coaxial Line', <u>Proc. IEE</u>, Vol. 112, No.2, 1965, pp. 416-420.

45. G. H. Brydon and D. J. Hipplestone, 'Microwave Measurement of Permittivity and tan δ over the temperature range $20° - 700°c$ ', <u>Proc. IEE</u>, Vol.112, No.2, 1965, pp. 421-425.

46. P. J. B. Clarricoats, 'a New Waveguide Method for Measuring the Permittivity of Dielectric Slabs', Proc. IEE, No-504 E, Feb. 1962, pp. 401-405.

47. E. Fatuzzo and P. R. Mason, 'Precision Measurement of the Microwave Dielectric Constant of Liquids', J. App. Phys., 36, 1965, pp.427.

48. R. Van. Loon and R. Finsy, 'The Precise Microwave Permittivity Measurement of Liquids Using a Multipoint and Curve-Fitting Procedure', J. Phys. D: App. Phys., Vol.8, 1975, pp. 1232-1243.

49. W. B. Weir, 'Automatic Measurement of Complex Dielectric Constant and Permeability at Microwave Frequencies', Proc. IEEE, Vol.62, No.1, 1974, pp. 33-36.

50. T. Athey, M. Stuchly and S. Stuchly, 'Measurement of Radio Frequency Permittivity of Biological Tissues with an Open-Ended Coaxial Line: Part I', IEEE Trans. Mic. Th. Tech., Vol. MTT-30, No.1, 1982, pp. 82-86.

51. M. Stuchly, T. Athey, G. Samaras and G. Taylor, 'Measurement of Radio Frequency Permittivity of Biological Tissues with an Open-Ended Coaxial Line: Part II-Experimental Results', IEEE Trans. Mic. Th. Tech., Vol. MTT-30, No.1, 1982, pp. 87-92.

52. T. J. Buchanan and E. H. Grant, 'Phase and Amplitude Balance Methods for Permittivity Measurements Between 4 and 50 cm', Brit. J. App. Phys., 6, 1955, pp. 64-66.

53. L. P. Lighthart, 'a Fast Computational Technique for Accurate Permittivity Determination Using Transmission Line Methods', <u>IEEE Trans. Mic. Th. Tech.</u>, Vol. MTT-31, No.3, 1983, pp. 249-254.

54. A. M. Shaarawi and S. M. Riad, 'Computing the Complete FFT of a Step-Like Waveform', <u>IEEE Trans. Inst. Meas.</u>, Vol. IM-35, No. 1, March 1986, pp. 91-92.

55. M. J. D. Powell, 'a Hybrid Method for Nonlinear Equations', In <u>'Numerical Methods for Nonlinear Algebraic Equations'</u>, Edited by Phillip Rabinowitz, Gordon and Research Science Publishers, PP. 87-114.

56. R. A. Waldron, <u>'Theory of Guided Electromagnetic Waves'</u>, Van Nostrand Reinhold Company Ltd., London, 1969.

57. M. N. Afsar, J. Birch and R. Clarke, 'The Measurement of the Properties of Materials', <u>Proc. IEEE</u>, Vol. 74, No.1, 1986, pp.183-199.

58. Nora E. Hill, Worth E. Vaughan, A. H. Price and M. M. Davies, <u>'Dielectric Properties and Molecular Behaviour'</u>, The Van Nostrand Series in Physical Chemistry, 1969.

59. Roger F. Harrington, <u>'Time Harmonic Electromagnetic Fields'</u>, McGraw Hill, 1961.

60. The frequency domain measurements were performed by Professor William A. Davis, Department of Electrical Engineering, Virginia Polytechnic Institute and State University.

61. S. M. Riad, 'The Deconvolution Problem: an Overview', <u>Proceedings of the IEEE</u>, Vol. 74, No.1, pp. 82 - 85, 1986. pp. 896-898.